

***The War Against Pain: The Design,
Synthesis and Testing of Potential
COX-2 Selective Inhibitors.***

Cathryn A. Slabber

Submitted in fulfillment of the requirements for the degree of

Doctor of Philosophy

in the

School of Chemistry and Physics

College of Science & Agriculture

University of KwaZulu-Natal

Pietermaritzburg

November 2014

DECLARATION

I, Cathryn Anne Slabber, hereby certify that this experimental work and the discussion thereof is a result of my own investigation in the School of Chemistry and Physics of the University of KwaZulu-Natal (Pietermaritzburg), under the supervision of Professor R.S. Robinson

This work was carried out by me, and has not already been accepted in substance for any degree and is not being submitted in candidature for any other

Signed.....

C. A. Slabber

I hereby certify that this statement is correct.

Signed.....

Prof R. S. Robinson (Supervisor)

Nerd: One who's unbridled passion for something, or things, defines who they are as a person, without fear of other people's judgment.

Zachary Levi

Abstract

Much research has focused on the inhibition of the cyclooxygenase (COX) enzyme as this protein is responsible for the first step in the pain pathway in the conversion of arachidonic acid into prostaglandins and thromboxanes. The binding of curcumin and celecoxib, a known cyclooxygenase-2 (COX-2) selective inhibitor, was investigated computationally in order to identify important ligand-protein interactions which would need to be mimicked by a novel COX-2 selective compound. Initial investigations into the binding of curcumin identified the lesser diketone tautomer as having potential COX-2 selective activity.

Two novel COX-2 selective compounds were designed using moieties common amongst known COX-2 selective compounds and moieties found in curcumin. Initial docking and binding scores showed that these compounds interacted in a similar manner with the protein as did celecoxib. Modifications to these initial compounds yielded two classes of compounds which explored the impact of the substitutions on the docking and binding scores, the poses and the ligand-protein interactions. All modifications made resulted in enhanced binding towards COX-2, and in a number of cases a reduction in the binding scores for COX-1. Thirty of the 166 compounds designed were selected for synthesis and biological screening as these compounds exemplified the range of changes observed in the full complement of compounds.

Retrosynthesis yielded two potential synthetic pathways, and while the first path proved unsuccessful, the second route, which makes use of convenient reaction conditions, afforded the compounds in modest to good yields. Complete NMR spectroscopic analysis was carried out on all compounds, with Diffusion Ordered Spectroscopy used to determine the diffusion coefficients and hydrodynamic radii of two compounds and illustrated the dependence of these measurements on the properties of the medium. NMR Analysis of Molecular Flexibility In Solution (NAMFIS) analysis of one of the final compounds identified six conformers as existing in solution, based on the comparison of experimentally derived Nuclear Overhauser Enhancement (NOE) data with the results from a conformational analysis carried out *in silico*.

Four of the six poses are responsible for >95% of the solution population, with one pose comprising almost 50%. All but one of the poses show Root Mean Squared Deviation (RMSD) values of less than 2 Å when compared to the predicted pose, indicating that any of these poses could bind into the protein.

Initial inhibition screening results of the unsubstituted parent benzenesulfonate compound appeared to show three-fold selectivity of COX-2 over COX-1 at 100 nM. Testing of the substituted compounds revealed that these compounds are not COX-2 selective as desired, rather a number show promise as COX-1 selective compounds, with inhibition scores of over 40%, and several other compounds show potential as non-selective COX inhibitors. There is no obvious correlation between the inhibition results and either the Glide XP docking scores or the Prime binding scores, and as such, additional computational analysis as well as experimental testing is required to identify a correlation between the theoretical results and the experimental data, and illustrates that computational results cannot be the sole criterion on which selectivity is judged.

Table of Contents

<i>Acknowledgements</i>	VII
<i>List of Tables</i>	VIII
<i>List of Figures and Schemes</i>	X
<i>List of Abbreviations</i>	XVIII
1. Introduction	1
1.1. <i>The History of Medicine: From Antiquity to Modern Times.</i>	1
1.1.1. <i>Witchcraft and Wizardry: The Joys of the Dark Ages.</i>	3
1.1.2. <i>The Modern Era: The Government Gets Involved.</i>	7
1.1.3. <i>The Process of Drug Discovery: An Expensive Undertaking.</i>	9
1.1.4. <i>Designer Drugs: The Rise of Targeted Therapeutics.</i>	15
1.1.5. <i>The Bottom-Up Approach: Tackling the Problem from a Different Angle.</i>	21
1.2. <i>The Machines Are Taking Over: The Role of Computers in Drug Design.</i>	27
1.2.1. <i>Making Predictions: Modern Techniques for Modern Problems.</i>	34
1.2.2. <i>The First Step: Docking and Pose Evaluation.</i>	36
1.2.3. <i>Scoring Functions: The Maths Behind It All.</i>	39
1.2.4. <i>The Final Hurdle: The Role Of Post Processing in Computational Drug Design.</i>	44
1.2.5. <i>Finding The Diamonds In The Rough: Linking Theory and Practice through NMR Analysis of Molecular Flexibility In Solution (NAMFIS).</i>	47
1.3. <i>Indian Gold: The Story of Curcumin.</i>	51
1.3.1. <i>The Pleotropic Nature of Curcumin: A Simple Explanation.</i>	54
1.3.2. <i>There's Always a Downside: The Trouble with Curcumin.</i>	57

1.4. A World of Pain: The Role of Cyclooxygenase in How We Feel Pain.	60
1.4.1. Pain Management: What Really Happens.	62
1.4.2. Taking Responsibility: The Family of Molecules to Blame.	64
1.4.3. A Fork In the Road: Steroidal and Non-Steroidal Painkillers.	66
1.4.4. Inherent Selectivity: Small Differences Equal Large Changes.	70
1.4.5. Where To From Here: The Future Of Coxibs.	76
2. Aims and Objectives	77
3. Results and Discussion: Computational Design and Analysis of Potential COX-2 Selective Compounds	78
3.1. Exploring the Possibilities: Computational Analysis of Curcumin and Celecoxib.	78
3.2. In the Beginning: Initial Design and Analysis of a Novel COX-2 Selective Compound.	87
3.3. Expanding the Horizon: Design and Analysis of Sulfonate Analogs.	92
3.4. Always Have a Backup Plan: Design and Analysis of Sulfonamide Analogs.	99
3.5. A Word to the Wise: Selection of Candidates for Synthesis.	107
3.6. What We Never Knew We Needed to Know: A Review.	111
4. Results and Discussion: Synthesis of Target Benzenesulfonates	113
4.1. From the Bottom Up: Retrosynthesis and Initial Synthesis.	113
4.2. Assembling the Puzzle: Attempts towards the Synthesis of the Final Compounds.	119
4.3. Changing Directions: Pathway B as an Alternative Route.	123
4.4. What We Never Knew We Needed to Know: A Review.	132

5. Results and Discussion: Analysis and Identification of Compounds	134
5.1. <i>The Truth of the Matter: Structure Elucidation through NMR Spectroscopy.</i>	134
5.2. <i>Separate but Still Together: Diffusion-Ordered Spectroscopy as a Chromatography Technique.</i>	143
5.3. <i>Linking the Abstract with the Concrete: Putting NMR Analysis of Molecular Flexibility in Solution (NAMFIS) to Work.</i>	151
5.4. <i>What We Never Knew We Needed to Know: A Review.</i>	158
6. Results and Discussion: Inhibition Screening and Selectivity Determination	159
6.1. <i>When Worlds Collide: Theory Vs. Experiment.</i>	159
6.2. <i>An Unexpected Turn of Events: When Experiment and Theory Clash.</i>	162
6.3. <i>Gazing into the Crystal Ball: The Future of Isoform-Selective Coxibs.</i>	167
6.4. <i>What We Never Knew We Needed to Know: A Review.</i>	170
7. Conclusion	171
8. Future Work	175
9. Methods and Materials	178
10. References	214
11. Supplementary Information - CD	
11.1. <i>Complete Docking and Binding Scores.</i>	SI 1
11.2. <i>X-Ray Spectroscopy</i>	SI 8
11.3. <i>NAMFIS Data</i>	SI 9

Acknowledgements

"I am smart enough to know to work with smart people."

Idina Menzel

The work presented in this thesis would not have been possible without the support, help and encouragement of many people. I would like to thank my supervisor, Professor Ross Robinson for allowing me to follow my own path down an avenue that I found interesting, whether he found it interesting or not. I would like to thank Dr Dennis Liotta, Dr Jim Snyder and all of the members of their research group at Emory University in Atlanta, GA, for allowing me into their group, for imparting their knowledge of a field foreign to me, and for making me feel welcome. I would also like to thank the University of KwaZulu-Natal and the NRF for financial support throughout my Ph.D studies, and for allowing me the opportunity of attending Emory University.

I am eternally grateful to Mr. Craig Grimmer, for invaluable help with both standard and unusual NMR experiment requests, insights and suggestions for synthesis and for countless cups of tea, to Prof. Orde Munro (UKZN) and Ms. Varia Nikolayenko (University of Stellenbosch) for X-ray diffraction analysis and to Ms. C Janse Van Rensburg (UKZN) for assistance with Mass Spectrometry. I am also indebted to Ms. Lauren Eyssen (UKZN) for taking time away from her own project to assist me with the biochemical testing, and to Prof. Theresa Coetzer (UKZN) for allowing her to do so.

Finally I would like to thank everyone who supported me during the course of this project – to my family, friends, old and new, and my fellow research students, the support staff and the laboratory technicians, my sincerest thanks. This could not have been done without your help.

List of Tables

3. Results and Discussion: Computational Design and Analysis of Potential COX-2 Selective Compounds

Table 3.1. Glide XP and Prime scores for celecoxib and the two isomers of curcumin.	85
Table 3.2. Glide and Prime scores for celecoxib and compounds 3 and 4 .	88
Table 3.3. Glide XP and Prime scores for selected sulfonates.	94
Table 3.4. Glide XP and Prime scores for selected sulfonamides.	100
Table 3.5. Glide XP and Prime scores for selected sulfonate compounds for synthesis.	108

4. Results and Discussion: Synthesis of Target Benzenesulfonates

Table 4.1. Optimization of conditions for ether formation.	115
Table 4.2. Optimization of conditions for chalcone formation.	117
Table 4.3. Yields for formation of various chalcones.	120
Table 4.4. Yields for the formation of methoxy-substituted chalcones.	122
Table 4.5. Protection and Deprotection of 66 .	127
Table 4.6. Yields for the formation of protected (bromomethyl)tosylates.	128
Table 4.7. Yields for the formation of various 4-[2-(2-acetylphenyl)ethyl]benzenesulfonates.	130
Table 4.8. Yields for the formation of target molecules.	131

5. Results and Discussion: Analysis and Identification of Compounds

Table 5.1. DOSY-derived diffusion coefficients for compounds 126 and 6 at 30°C.	149
Table 5.2. DOSY-derived self-diffusion coefficients of solvents.	149
Table 5.3. Stokes Radii for compounds 126 and 6 .	150
Table 5.4. Experimental and calculated NOE distances for 6 .	153
Table 5.5. Population distribution and RMSD values of NAMFIS conformers.	153

6. Results and Discussion: Inhibition Screening and Selectivity Determination

Table 6.1. Concentration-dependent inhibition of COX-2 and COX-1.	161
Table 6.2. COX-2 inhibition values, Glide XP and Prime scores.	163
Table 6.3. COX-1 inhibition values, Glide XP and Prime scores.	166

11. Supplementary Information	SI
<i>SI Table 1. Complete Glide XP and Prime scores for benzenesulfonates.</i>	SI 1
<i>SI Table 2. Complete Glide XP and Prime scores for benzenesulfonamides.</i>	SI 5
<i>SI Table 3. Selected X-Ray spectroscopy results for 62.</i>	SI 8
<i>SI Table 4. Selected X-Ray spectroscopy results for 73.</i>	SI 9
<i>SI Table 5. Conformational analysis results for 6.</i>	SI 9

List of Figures and Schemes

1. Introduction

Figure 1.1. Mesopotamian clay tablet, circa 2500 B.C.E.	1
Figure 1.2. A section of the Ebers papyrus, written around 1550 B.C.E.	2
Figure 1.3. Cover plate of a <i>Historia Plantarum</i> edition dated 1644.	3
Figure 1.4. A copy of Ibn Sina's <i>Canon Medicinæ</i> from 1597.	4
Figure 1.5. A page of de Sahagun's <i>Historia de las Cosas de la Nueva Espana</i> detailing customs, dress and medical practices of pre-Colombian tribes.	5
Figure 1.6. A 19th century bottle containing laudanum.	6
Figure 1.7. Victorian era preparations of heroin, cocaine and cannabis.	7
Figure 1.8. Structure of <i>S</i> - and <i>R</i> -thalidomide. The <i>S</i> -enantiomer is teratogenic, while the <i>R</i> -enantiomer is a sedative.	9
Figure 1.9. The drug discovery "pipeline".	9
Figure 1.10. Structures of (clockwise from left) morphine, heroin, atropine, quinine, digitoxin and scopolamine.	11
Figure 1.11. The natural sources of salicylic acids - White willow (<i>Salix alba</i> , left) and European meadowsweet (<i>Filipendula ulmaria</i> , right).	12
Figure 1.12. 2D structures of salicin (left) and salicylic acid (right).	13
Figure 1.13. 2D structure of acetylsalicylic acid.	14
Figure 1.14. Aspirin bottle circa 1900.	14
Figure 1.15. 2D structures of (clockwise from left) aztreonam, vancomycin, erythromycin, nocardicin, and imipenem.	16
Figure 1.16. Pacific yew (<i>Taxus brevifolia</i>), source of the cancer drug Taxol®.	17
Figure 1.17. The "Top-down" approach to drug design. Many compounds are tested to identify hits, which are then further derivitized and optimized to generate a possible drug candidate.	18
Figure 1.18. 2D structure of sorafenib, the only compound developed through combinatorial chemistry to receive F.D.A. approval for use in renal carcinoma.	19
Figure 1.19. 2D structure of the novel oxazolidinone antibiotic Zyvox® (linezolid).	20

Figure 1.20. (a) Library screening vs. (b) fragment based drug design. Library screening attempts to fit a prebuilt molecule into a target, while FBDD identifies fragments which can be assembled into a complete molecule.	22
Figure 1.21. 2D structure of Zelboraf® (vemurafenib), designed using Fragment Based Drug Design techniques.	22
Figure 1.22. A molecular fragment library containing (a) simple carbocyclic and heterocyclic fragments and (b) simple drug scaffolds.	23
Figure 1.23. (a) Fragment growing and (b) fragment linking strategies for drug design.	24
Figure 1.24. Comparison of (a) fragment-growing and (b) fragment-linking techniques for the synthesis of a pantothenate synthetase inhibitor, adapted from Hung et al.	25
Figure 1.25. Application of computational methods to drug design.	28
Figure 1.26. (a) Fragment-growing, (b) fragment-linking and (c) fragment-scaffold merging techniques.	31
Figure 1.27. The pharmacophore model and resultant lead compound for inhibition of aldose reductase 2.	32
Figure 1.28. A schematic diagram of “Lock and Key” model for enzymes, where the active site is complementary to the structure of the native ligand.	35
Figure 1.29. A schematic diagram of the Induced-Fit model for the binding of a ligand into an active site.	35
Figure 1.30. The steps in modern docking processes.	37
Figure 1.31. Ideal method for the calculation of free energy, using the “Lock and Key” model for simplicity.	44
Figure 1.32. Gauche (left and center) and anti-Gauche (right) conformations.	48
Figure 1.33. The 2D structure of Taxol® (left) and the 3D structure of Taxol® bound in tubulin (right).	50
Figure 1.34. Botanical view of the turmeric (<i>Curcuma longa</i>) plant.	51
Figure 1.35. 2D structure of curcumin.	52
Figure 1.36. Keto-enol tautomerisation of curcumin.	55
Figure 1.37. The nociceptive pain pathway.	61
Figure 1.38. Sites of action of the various classes of painkillers.	62
Figure 1.39. 2D structures of (clockwise from left) PGE ₂ , PGD ₂ , TxA ₂ , PGI ₂ , and PGF _{2α}	64
Figure 1.40. An example of prostaglandin synthesis: the formation of PGE ₂ from arachidonic acid.	65

Figure 1.41. 2D structures of (clockwise from left) prednisone, prednisolone, dexamethasone , hydrocortisone and methylprednisolone	67
Figure 1.42. 2D structures of (clockwise from left) ibuprofen, naproxen, phenylbutazone indomethacin, diclophenac, and sulindac.	68
Figure 1.43. 2D structures of (left to right) the COX-2 selective compounds celecoxib, rofecoxib and valdecoxib.	69
Figure 1.44. Schematic overview of how the structural differences between the COX isoforms allow for selective inhibition of COX-2.	71
Figure 1.45. 2D structure of celecoxib, currently the only COX-2 selective compound with F.D.A. approval.	72
Figure 1.46. 2D structure of rofecoxib, the first COX-2 selective compound removed from the market due to safety concerns.	73
Figure 1.47. 2D structures of valdecoxib (l) and its pro-drug parecoxib (r) which is converted into valdecoxib in the liver.	73
Figure 1.48. 2D structure of etoricoxib, a second-generation coxib.	74
Figure 1.49. 2D structures of lumiracoxib and its parent molecule diclofenac.	74

3. Results and Discussion: Computational Design and Analysis of Potential COX-2 Selective Compounds

Figure 3.1. 2D structure of curcumin.	79
Figure 3.2. Keto-enol tautomerization of curcumin.	80
Figure 3.3. An example of prostaglandin synthesis: the formation of PGE ₂ from arachidonic acid.	80
Figure 3.4. 2D structures of the coxibs (clockwise from top left) celecoxib, rofecoxib, etoricoxib and lumiracoxib.	81
Figure 3.5. Ligand interaction diagram of celecoxib with COX-2 showing the interactions of the <i>p</i> -sulfonamide group of celecoxib with the secondary pocket present in COX-2, taken from the PDB file 3LN1. 13 The red line indicates the presence of a π -cation interaction between the ligand and the protein, the solid purple lines a presence of an H-bond between the ligand and the backbone of the protein, and the dashed purple line an H-bond interaction between the ligand and a side chain.	82

Figure 3.6. X-ray crystal structures of celecoxib (PDB file 3LN1), shown with green carbon atoms, and arachidonic acid (PDB file 3HS5), shown with blue carbon atoms.	83
Figure 3.7. The generated pose of celecoxib with carbon atoms shown in red overlapping with the pose of celecoxib bound to COX-2, shown with green carbon atoms (PDB file 3LN1).	83
Figure 3.8. The generated pose of celecoxib, carbon atoms shown in red, overlapping with the pose of celecoxib bound to COX-1, carbon atoms shown in green (PDB file 3KK6).	84
Figure 3.9. Ligand interaction diagram of 1 with COX-2 showing the interactions present between the protein and the ligand.	85
Figure 3.10. Ligand interaction diagram (left) of 2 with COX-2 and the overlap of the generated pose with the X-ray crystal structure of celecoxib in COX-2 (right).	86
Figure 3.11. General structure of a novel class of COX-2 selective compounds identifying the important structural features derived from the parent molecules. The blue portion is derived from curcumin, the purple portion from the 1,2-disubstituted central ring of coxibs and the red portion the common p-sulfuryl phenyl ring also from the coxibs.	87
Figure 3.12. Generic structures of 3 (X = OH) and 4 (X = NH ₂).	88
Figure 3.13. Ligand interaction diagram for 3 (left) and the docked pose of 3 (shown in blue) overlaid with the structure of celecoxib (carbon atoms shown in green) as found in the X-ray crystal structure of COX-2 (right).	89
Figure 3.14. Ligand interaction diagram for 4 (left) and the docked pose of 4 (blue) overlaid with the structure of celecoxib (carbon atoms shown in green) as found in the X-ray crystal structure of COX-2 (right).	90
Figure 3.15. Ligand interaction diagram of 3 in COX-1 highlighting the interactions formed between ligand and protein.	91
Figure 3.16. Ligand interaction diagram of 4 in COX-1 illustrating the contacts made between the protein and the docked ligand.	91
Figure 3.17. Ring identification and substituent placement for analogs of 3 and 4 .	93
Figure 3.18. Overlap of the poses generated for compound 5 with celecoxib and 3 , when docked into COX-2, showing the close clustering obtained. Celecoxib is shown with green carbon atoms, 3 in blue and 5 in red.	95
Figure 3.19. The "inversion" of the pose generated for compound 15 , shown in purple, as compared to the pose generated for the parent sulfonate 3 , shown in blue.	96
Figure 3.20. The rotation of the alkyl chain in the pose generated for 16 , shown in green, as compared	97

	<i>to the pose generated for the parent sulfonate 3, shown in blue.</i>	
Figure 3.21.	<i>Ligand interaction diagram for 22 with COX 2, showing the predicted protein-ligand interactions.</i>	98
Figure 3.22.	<i>Overlap of the poses generated for 26 (shown in pink) and 3 (shown in blue).</i>	99
Figure 3.23.	<i>Overlap of the poses generated for 4 (shown in blue) and 29 (shown in green) when docked into COX-2.</i>	101
Figure 3.24.	<i>Overlap of the poses generated for 4 (shown in blue) and 29 (shown in green) when docked into COX-1.</i>	101
Figure 3.25.	<i>Overlap of 4 (shown in blue) and 31 (shown in green) when docked into COX-2.</i>	102
Figure 3.26.	<i>Overlap of the poses of 4 (shown in blue) and 32 (shown in yellow) when docked into COX-2.</i>	103
Figure 3.27.	<i>Ligand interaction diagram for 32 showing the interactions formed between the ligand and COX-2.</i>	103
Figure 3.28.	<i>Ligand interaction diagram for 35 showing the interactions formed between the ligand and COX-1.</i>	104
Figure 3.29.	<i>Overlap of the poses generated for 4 (shown in blue) with compound 38 (shown in purple) when docked into COX-2.</i>	105
Figure 3.30.	<i>Overlap of the pose generated for 38 when docked into COX-2 (depicted in light blue) with the X-ray crystal structure of celecoxib (depicted in green).</i>	105
Figure 3.31.	<i>Overlap of the poses of 4 (shown in blue) with 40 (shown in green) when docked into COX-2.</i>	106
Figure 3.32.	<i>Ligand interaction diagram for 40 showing the interactions between the ligand and COX-1.</i>	106
Figure 3.33.	<i>Overlap of the poses of 24 (shown in purple) and 3 (shown in blue) when docked into COX-1.</i>	109
Figure 3.34.	<i>Ligand interaction diagram of 24 with COX 1.</i>	110
Figure 3.35.	<i>Ligand interaction diagram of 53 with COX-1.</i>	111

4. Results and Discussion: Synthesis of Target Benzenesulfonates	
Scheme 4.1. Retrosynthetic analysis of the target molecule showing two synthetic pathways.	114
Scheme 4.2. Synthesis of ether 62 .	115
Figure 4.1. ¹ H NMR spectrum of 62 showing the shift in the location of the methylene signals on formation of the ether bond.	116
Figure 4.2. An ORTEP view of 62 showing the perpendicular arrangement of the phenyl rings. Displacement of the non-hydrogen atoms are shown at the 50% probability level.	116
Scheme 4.3. Synthesis of chalcone 64 .	117
Figure 4.3. ¹ H NMR spectrum of 64 highlighting the signals corresponding to the double bond protons.	118
Scheme 4.4. Synthesis of sulfonamide 66 .	118
Figure 4.4. Sections of the ¹ H and 1D gHSQC ¹ H- ¹⁵ N NMR spectra of 66 showing the presence of amine protons.	119
Scheme 4.5. General synthetic approach for the formation of chalcones.	119
Figure 4.5. An ORTEP view of 73 showing the out-of plane rotation of the benzaldehyde-derived phenyl ring Displacement of the non-hydrogen atoms are shown at the 50% probability level.	121
Scheme 4.6. General scheme for the base-catalyzed flavanone formation	122
Figure 4.6. A portion of the ¹ H NMR spectrum of the flavanone product showing the characteristic aliphatic proton signals with both germinal and vicinal coupling.	123
Scheme 4.7. Synthesis of 111 through Pathway B.	124
Scheme 4.8. Addition of sulfonyl chloride to 62 .	124
Figure 4.7. 2D structures of 4-(bromomethyl)benzenesulfonyl chloride 112 and 4-(bromomethyl)benzenesulfonamide 113 .	125
Scheme 4.9. General scheme for the formation of tosylated 2'-hydroxyacetophenones.	126
Scheme 4.10. Formation of protected sulfonyl chlorides and subsequent deprotection .	126
Figure 4.8. 2D structures of 123 and 124	128
Scheme 4.11. Synthesis of benzenesulfonate 125 .	129
Scheme 4.12. General route for the synthesis of the target benzenesulfonates	130

5. Results and Discussion: Analysis and Identification of Compounds	
Figure 5.1. 2D structure of aquatolide and <i>Asteriscus aquaticus</i> .	134
Figure 5.2. Initial incorrect structure of aquatolide.	135
Scheme 5.1. NMR structure elucidation of 6 through analysis of precursors	136
Figure 5.3. ¹ H NMR spectrum and assignment of 62 .	137
Figure 5.4. 1D NOE spectrum of 62 with selective irradiation of the methylene protons.	138
Figure 5.5. ¹ H NMR spectrum and assignment of compound 125 .	139
Figure 5.6. 1D NOE spectrum of 125 with selective irradiation of the methylene protons.	139
Figure 5.7. ¹ H NMR spectrum and assignment for chalcone 69 .	141
Figure 5.8. 1D NOE spectrum of 69 with selective irradiation of the methane protons.	139
Figure 5.9. ¹ H NMR spectrum and assignment of 6 .	141
Figure 5.10. 2D NOE spectrum of 6 , showing connections between the various components.	142
Figure 5.11. Overlap of the methylene peaks of 112 (shown in red) and 125 (shown in blue) in DMSO-d ₆ . The second peak in the spectrum of 113 is a decomposition product due to the reaction of 113 with the water present in the NMR solvent.	144
Figure 5.12. Overlays of the methylene peak region from the ¹ H NMR spectra of 6 , showing the solvent-dependance of these peaks. The spectrum shown in blue was run in DMSO-d ₆ , the spectrum shown in green in a mixture of D ₂ O and DMSO-d ₆ (5:1), and the red spectrum in D ₂ O.	144
Figure 5.13. Spatial spin encoding and decoding in DOSY experiments.	146
Figure 5.14. NMR diffusion spectra of a three-component mixture of water, 2-ethoxyethanol and caffeine.	147
Figure 5.15. 2D DOSY spectrum of the caffeine, 2-ethoxyethanol and water mixture showing the separation of the three compounds present	148
Figure 5.16. Processes in NMR Analysis of Molecular Flexibility In Solution (NAMFIS) analysis.	151
Figure 5.17. 2D NOE spectrum and assignment of compound 6 for NAMFIS analysis.	152
Figure 5.18. Overlay of the top NAMFIS-derived conformers 6-602 (shown in purple) and 6-1360 (shown in red).	154
Figure 5.19. Overlay of the pose generated for 6 when docked into COX-2 (shown in blue) with the NAMFIS-derived conformer 6-602 (shown in purple).	154
Figure 5.20. Overlay of the pose generated for 6 when docked into COX-1 (shown in green) with the NAMFIS-derived conformer 6-602 (shown in purple).	155

Figure 5.21. Overlay of the pose generated for 6 when docked into COX-2 (shown in blue) with the NAMFIS-derived conformer 6-1360 (shown in red).	155
Figure 5.22. Overlay of the pose generated for 6 when docked into COX-1 (shown in green) with the NAMFIS-derived conformer 6-1360 (shown in red).	156
Figure 5.23. Overlay of the pose generated for 6 when docked into COX-2 (shown in blue) with the NAMFIS-derived conformer 6-2492 (shown in purple).	157
Figure 5.24. Overlay of the pose generated for 6 when docked into COX-1 (shown in green) with the NAMFIS-derived conformer 6-2492 (shown in purple).	157
6. Results and Discussion: Inhibition Screening and Selectivity Determination	
Scheme 6.1. COX screening using the conversion of ADHP into resorufin.	160
Figure 6.1. 2D structures of DuP-697 (left) and SC-560 (right).	161
Figure 6.1. Allosteric inhibition of proteins.	165
Figure 6.1. 2D structure of ketorolac.	167
Figure 6.1. 2D structure of Mofezolac®, a COX-1 selective analgesic.	168
8. Future Work	
Figure 8.1. Imine-based analogs.	175
Scheme 8.1. Potential synthetic routes to the propanamide-protected benzenesulfonamide.	176

List of Abbreviations.

(x)P	(Prostanoid) receptor
AA	Arachidonic acid
ACE	Analytical Continuum Electrostatic
ADHP	10-acetyl-3,7-dihydroxyphenoxazine
ADME	Absorption, Distribution, Metabolism and Excretion
ADME-Tox	Absorption, Distribution, Metabolism Excretion and Toxicity
AIDS	Acquired Immunodeficiency Syndrome
ALR2	Aldose reductase
Arg	Arginine
AT	Adenine-Thymine
B.C.E.	Before Common Era
BRICS	Breaking of Retrosynthetically Interesting Chemical Structures
Bz	Benzyl
C.E.	Common Era
cAMP	Cyclic adenosine monophosphate
CCDC	Cambridge Crystallographic Data Centre
COSY	Correlation Spectroscopy
COX	Cyclooxygenase
DABCO	1,4-diazabicyclo[2,2,2]octane
DAIM	Decomposition And Identification of Molecules
DBU	1,8-diazobicyclo[5,4,0]undecane
DEPT	Distortionless Enhancement of Polarization Transfer
DMF	Dimethyl formamide
DMSO	Dimethyl sulfoxide
DNA	Demethoxyribonucleic acid
DOS	Diversity Oriented Synthesis
DOSY	Diffusion-Ordered Spectroscopy
ER	Endoplasmic reticulum
Et	Ethyl
EtOAc	Ethyl Acetate

EtOH	Ethanol
F.D.A.	Food and Drug Administration
FBDD	Fragment-Based Drug Design
FMNR	full-matrix-Newton-Raphson
GBSA	Generalized Born Surface Area
gHSQC	Gradient Heteronuclear Single Quantum Coherence
Gln	Glycine
Glu	Glutamic acid
GPCR	G protein coupled receptor
HDL	High-density lipoproteins
His	Histidine
HIV	Human Immunodeficiency Virus
HMBC	Heteronuclear Multiple Bond Coherence
HRMS	High Resolution Mass Spectrometry
HSQC	Heteronuclear Single Quantum Coherence
HTS	High-Throughput Screening
i.p.	intraperitoneal
IFD	Induced Fit Docking
Ile	Isoleucine
ⁱ Pr	<i>iso</i> -Propyl
ISPA	Isolated spin pair approximation
LBVS	Ligand-Based Virtual Screening
LDL	Low-density lipoproteins
Leu	Leucine
Me ₂ CO	Acetone
MeCN	Acetonitrile
MLSD	Multiple Ligand Simultaneous Docking
MM	Molecular Mechanics
MM/GBSA	Molecular Mechanical/Generalized Born Surface Area
MM/PBSA	Molecular Meachanics/Poisson-Boltzmann Surface Area
MMFF	Merck Molecular Force Field
NAMFIS	NMR Analysis of Molecular Flexibility In Solution

NMR	Nuclear Magnetic Resonance
NOE	Nuclear Overhauser Enhancement
NOSY	Nuclear Overhauser Effect Spectroscopy
NPF	Natural Product Fragment
NSAID	Non-steroidal anti-inflammatory drug
OPLS-2005	Optimized Potentials for Liquid Simulations
OPLS-aa	Optimized Potentials for Liquid Simulations - all atoms
OTC	Over-the-counter
PDB	Protein Database
PG	Prostaglandin
PG(x)S	Prostaglandin (x) synthase
Ph	Phenyl
Phe	Phenylalanine
Phth	Phthalimide
PKC	Protein kinase C
QSAR	Quantitative Structure-Activity Relationship
QSPR	Quantitative Structure-Property Relationship
RECAP	Retrosynthetic Combinatorial Analysis Procedure
RMSD	Root Mean Square Deviation
RNA	Ribonucleic acid
RNAse	Ribonuclease
ROE	Rotating Frame Overhauser Enhancement
SAR	Structure-Activity Relationship
SBDD	Scaffold-Based Drug Design
SBVS	Structure-Based Virtual Screening
Ser	Serine
SP	Standard-Precision
SSD	Sum of Square Distanced
Succ	Succinamide
^t Bu	<i>tert</i> -Butyl
THF	Tetrahydrofuran
TNF- α	Tumor necrosis factor- α

TrxR	Thioredoxin reductase
Try	tryptophan
Tx	Thromboxane
Tyr	Tyrosine
Val	Valine
VS	Virtual Screening
XP	Extra-Precision

I. Introduction

1.1. The History of Medicine: From Antiquity to Modern Times.

“Study the past if you would define the future.”

Confucius

In the history of mankind, there have only been two reasons for man to explore and exploit nature: as a source of food, and as a source of medicines. Many ancient civilizations had comprehensive works on herbs or mixtures of them and how they could be used to treat various diseases. One of the earliest records of the use of natural products was found on cuneiform-covered clay tablets from Mesopotamia (Figure 1.1) dated to 2500 B.C.E (Before Common Era). These tablets document the use of oils from cypress (*Cupressus sempervirens*) trees, licorice (*Glycyrrhiza glabra*) root, poppy (*Papaver somniferum*) flowers and the resin from various myrrh (*Commiphora*) species as treatments for coughs, colds and inflammation, treatments which are still used today.¹⁻²

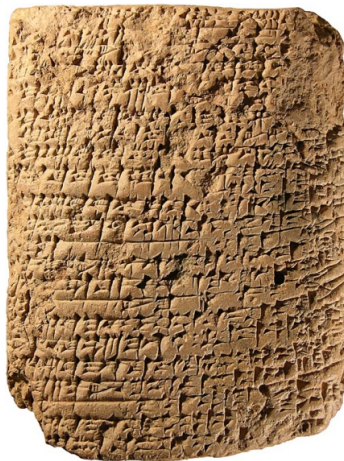


Figure 1.1. Mesopotamian clay tablet, circa 2500 B.C.E³

The Mesopotamians were not the only ancient culture to record medical information. Written around 1550 B.C.E., the Ebers Papyrus (Figure 1.2) is a record of over 700 plant-based prescriptions used in Ancient Egypt, ranging from ointments and pills to gargles and infusions.⁴ The Chinese *Materia Medica* (*Wu Shi Er Bing Fang*) from 1100 B.C.E, contains 52 prescriptions of natural products, the Shennong Herbal (~100 B.C.E) contains 365 drugs, and the Tang Herbal from 659 C.E contains 850.² The first written book on medical matters, *Shen Nong Ben Cao Jing*, describes the characteristics, processing and prescription of 250 plant-derived drugs, as well as 60 from animals and 50 related to minerals. Appearing in the first centuries B.C.E. and C.E, this is the earliest Chinese pharmacopoeia known and has

been extensively studied over the years.⁴ Chinese medicine reached its peak during the Ming dynasty (1368-1644), with the writing of *Pen Ts'ao Kang Mu* (*The Great Herbal*) by Li Shih Chen (1518-1593). The best known of the Chinese herbal texts, it encompasses 520 volumes and upwards of 11,000 prescriptions.^{4,5}

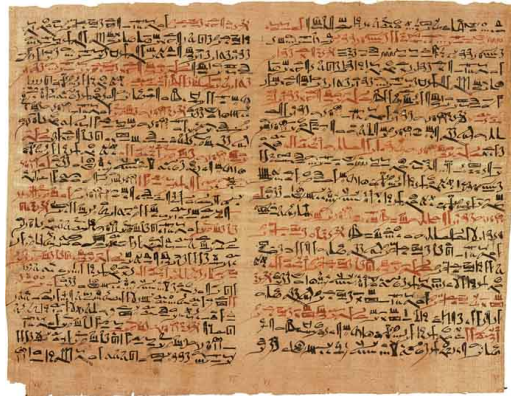


Figure 1.2. A section of the Ebers papyrus, written around 1550 B.C.E.⁶

Another source of ancient prescriptions is the Indian Ayurveda, dating back to 900 B.C.E. Literally translating as “the science and knowledge of life”, Ayurveda is based primarily on three texts – the *Sushruta Samhita*, the *Charaka Samhita* and the medical portions of the Bower Manuscript, also known as the *Bheda Samhita*. The *Sushruta Samhita* contains 184 chapters and the descriptions of 1,120 illnesses, 700 medicinal plants, 57 preparations from animal sources, and 64 mineral preparations.⁷ The Ayurvedic system formed the basis for the primary text of Tibetan medicine, *Gyu-Zhi* (Four Tantras),⁸ and is believed to be the basis for much of the North American Indian medicinal traditions as well. The similarities in the medicinal plants used by the North American Indians and the East Indian practitioners of Ayurveda is thought to be due to the migration of Asian Indians across the Bering Strait to Alaska and then south into the Americas, as the knowledge would have been carried along the journey.⁴

With regards to Western Medicine, the Greeks, greatly influenced by the Egyptians, contributed considerably to the development of the use of herbal drugs.⁴ Temples in ancient Greece were dedicated to Asklepios, the god of healing, and these temples became schools for physicians, such as the temple on the island of Kos. Under the leadership of Hippocrates, it is perhaps the most famous of medical schools in classical Greece, and it became a considerable influence on later medical schools, with the writings of the school, known as the *Hippocratic Corpus*, collected in the library of Alexandria around 280 B.C.E. The modern Hippocratic Oath is a compendium of medical and pharmaceutical ethics from this original body of work. In his *Historia Plantum* (Figure 1.3), Theophrastus (370-287 B.C.E)

documented the medicinal qualities of over 500 herbs, and noted that some characteristics could be changed due to cultivation.^{1,2} Friend and disciple of Aristotle, Theophrastus classified plants into trees, shrubs, subshrubs and herbs, a simple classification, but nonetheless the most rational until the Linnaean system was adopted in the 18th century. Even the words pharmacy and pharmacology have Greek origins – in the *Odyssey*, written in the 8th or 9th century B.C.E, Homer uses the word “*pharmakon*” to refer to a drug.



Figure 1.3. Cover plate of a *Historia Plantarum* edition dated 1644.⁹

1.1.1. Witchcraft and Wizardry: The Joys of the Dark Ages.

“Half of writing history is hiding the truth.”

Capt. Malcolm Reynolds, *Serenity*

With the decline and fall of the Roman Empire in the fourth century, Europe was plunged into the depths of the Dark Age, where the use of plants and plant-based treatments were viewed as witchcraft and sorcery.² Monasteries in European countries such as England, Ireland, Germany and France preserved what was left of this expertise, but it is the Arabs who are responsible for the conservation of the Greco-Roman knowledge, and for augmenting this knowledge base with their own traditions and those of the Chinese and Indian healers, knowledge which previously was unknown to the Greeks and

Romans.^{1-2,4} The Arabs were the first to establish privately owned drug stores,² and the Persian pharmacist, physician, philosopher and poet Ibn-Sina (Avicenna) influenced the sciences of pharmacy and medicine well into the 17th century as his work *Canon Medicinae* (Figure 1.4) was the standard medical text at medieval universities, and was recommended as a textbook in the universities of Montpellier and Leuven as late as 1650.¹⁰⁻¹¹ Completed in 1025, it is a clear, concise summary of all the medical knowledge of the time,¹² consisting of 5 volumes as compared to Galen's twenty.¹⁰ Ibn-Sina drew on many sources during the writing of his *Canon*, including the extensive pathology text, *Zhubing Yuanhuo Lun*, from the Chinese physician Chao Yuan-fang, which was written around 610 C.E, and the *Maijing*, a classic Chinese pulse diagnosis text by Wang Shu-hu, written ca. 310 C.E. *Canon Medicinae* is considered "the final codification of all Greco-Roman medicine."² Another important contributor to the field of medicine is the Arabic scientist Abulcasis, who wrote the medical encyclopedia *al-Tasrif*. A common text in European medical schools during the High Middle Ages, one part is devoted to surgery, with another section devoted to pharmaceutical practices. The 28th volume, *Liber Servitoris de Praeparatione Medicinarum Simplicum*, describes over 1,500 drugs, of which 400 are purely Arabic contributions.⁴



Figure 1.4. A copy of Ibn Sina's *Canon Medicinae* from 1597.¹³

A number of new drugs were introduced into what was then mainstream medicine with the discovery of America by the Spanish in 1492. Initial work on the medicinal plants of the Americas was not carried out by doctors or scientists, rather it was by monks, politicians and military men such as Fray Bernardino de

Sahagun, the Viceroy Fernandez de Oviedo and Pedro Cieza de Leon that much of the information on these plants was transmitted to Europe.⁴ Such was the flow of information that the physician Nicholas Monardes published a highly detailed book, "*Medicinal de las cosas que se traen de nuestras Indias Occidentales*" or "A book on the things brought from our West Indies that are used in medicine" without ever actually visiting the New World.¹⁴ The *Historia de las Cosas de la Nueva Espana*, written by Frey Bernardino de Sahagun and based on many years of anthropological, ethnological and ecological data collected from over 100 races and cultures, has been described as a magnificent work covering all aspects of pre-Columbian civilizations, including medicinal plants (Figure 1.5), and Pedro Cieza de Leon's *La Cronica del Peru*, published in 1533, is portrayed as a masterful account of the lifestyles and costumes of the Incas and other native Indians.⁴ The first scientific expedition of the modern era was carried out by the royal doctor Francisco Hernandez, on a commission from King Philip II of Spain. Sent to Mexico on a royal commission from 1571 to 1577, Hernandez devoted the time to a thorough study and description of over 4,000 medicinal plants found in New Spain's territory. While Hernandez died without seeing his work published, Nardo Antonio Rechi (Reccho) summarized the work and published it as *Rerum Medicarum Novae Hispaniae Thesaurus*, which only mentions 412 plants. Partially destroyed by a fire at the El Escorial Monastery library in 1671, the unaffected portion of Hernandez' work was published in 1790 as *Historia Plantarum Novae Hispaniae* and covered 2,900 plants.¹⁵



Figure 1.5. A page of de Sahagun's *Historia de las Cosas de la Nueva Espana* detailing customs, dress and medical practices of pre-Columbian tribes.¹⁶

During the height of the Renaissance, figures such as Vesalio and Copernicus arose and began to question thoughts, beliefs and teachings which had previously been accepted as truth. Vesalio, as chair of Surgery and Anatomy at Padua, used dissections as the primary teaching tool and carried out the

dissections himself, believing that hands-on experience was the only reliable source of information, rather than the classical texts of Galen, which at that point were over 1,000 years old.¹⁷ The field of toxicology was established by Paracelsus, who developed the concept of dose dependency for drug action and toxicity stating “*sola dosis facit venenum*” or “only the dose makes the poison.”¹⁸ Paracelsus is also credited for using laudanum, an analgesic preparation of opium containing morphine and codeine, as a painkiller, making him the first doctor to use a pharmacological agent against pain, however this remains speculation.¹⁹ A potent narcotic, laudanum was almost unknown until the 1670’s when Thomas Sydenham published *Medical Observations Concerning the History and Cure of Acute Diseases* in 1676, in which he promoted his own brand of laudanum, the contents of which differed greatly from the one encountered by Paracelsus.²⁰ By the 18th century, the properties of laudanum and opium were well-known (Figure 1.6) and used for almost every ailment until the early 20th century.²¹



Figure 1.6. A 19th century bottle containing laudanum.²²

1.1.2. The Modern Era: The Government Gets Involved.

"Bureaucracy is the art of making the possible impossible."

Javier Pascual Salcedo

The early 20th century brought greater understanding of the nature of the addictive properties of narcotics, including opium, and thus increased regulations were imposed on these substances. In the United States, the Food and Drug Act of 1906 required that certain drugs, including heroin, morphine, cocaine, cannabis and alcohol, be accurately labeled with contents and dosage, and many patent medications were affected as they had previously been sold with secret ingredients or with ambiguous labels. Britain passed similar laws limiting the narcotic content of medicines and revelation of these ingredients in 1906, as did Canada in 1908.²³ Despite the fact that drugs such as cocaine, cannabis and heroin could still be legally sold without prescriptions as long as they were labeled (Figure 1.7), it is estimated that the sale of opium-containing patent medications decreased by 33% after labeling became mandatory.²⁴



Figure 1.7. Victorian era preparations of heroin,²⁵ cocaine²⁶ and cannabis.²⁷

Prior to the 20th century, there were very few federal laws which regulated the sale and contents of food and pharmaceuticals. Due to journalists like Upton Sinclair in the United States, the public became interested in the potential hazards of food and pharmaceutical goods, and this led to more federal regulations for matters of public safety.²⁸ Prior to the 1906 Food and Drug Act which essentially established the Food and Drug Administration (F.D.A.), a Biologics Control Act was passed in 1902 after a tetanus-contaminated diphtheria antitoxin led to the deaths of thirteen children in St. Louis, Missouri.²⁸ The serum used to create the antitoxin had been collected from a horse named Jim, who had contracted

tetanus. Signed by President Roosevelt in June 1906, the Food and Drug Act prohibited, amongst other things, the interstate promotion of “adulterated” drugs, where the “standard of strength, quality or purity” of the active ingredients were either clearly declared on the label or listed in the *United States Pharmacopoeia* or the *National Formulary*.²⁹ By the 1930s, many groups were campaigning for the F.D.A. to have stronger regulatory authority, as a number of radioactive beverages, worthless cures for diabetes and tuberculosis and a brand of mascara which caused blindness had been granted approval under the 1906 law. After struggling to get passed in Congress for five years, the Food, Drug and Cosmetics Act (FD&C Act) was signed into law in 1938, due to the public backlash over the 1937 Elixir Sulfanilamide disaster, in which over 100 people died due to an untested solvent.³⁰ This new law mandated a pre-market review of the safety of all new drugs, as well as limiting the indications that a drug could be marketed for. The Durham-Humphrey Amendment of 1951 designated some drugs as “prescription-only,” and this act also allowed for post-marketing recalls of ineffective drugs by the F.D.A..³⁰

The Kefauver-Harris Amendment to the FD&C Act in 1962 symbolized a revolution in the regulatory authority of the F.D.A., as all new drug applications would not only have to demonstrate safety, but they would now have to show “substantial evidence” of the drugs’ activity in order to gain F.D.A. approval.³¹ This amendment was brought about by the thalidomide tragedy in Europe in 1959, where thousands of children were born with birth defects after their mothers were given thalidomide as an anti-nausea medication (Figure 1.8).³² The United States was for the most part spared the tragedy as Dr Frances Oldham Kelsey of the F.D.A. refused to authorize the sale of thalidomide until data suggesting severe side effects with long term use was explained.³³ Marking the start of the modern F.D.A. approval process, these reforms resulted in an increased amount of time needed before a drug could be brought to market. The AIDS epidemic has however raised concerns over the length of time required for drug approval, and in the mid- and late 1980s, the F.D.A. issued new rules aimed to expedite the approval of certain drugs for life threatening diseases and expanded the access of patients with limited treatment options to drugs which have passed Phase I clinical trials.³⁴⁻³⁵ In the face of the current Ebola epidemic, the F.D.A. has waived the pre-clinical testing requirement for GlaxoSmithKline’s Ebola vaccine,³⁶ and ZMapp, an experimental combination treatment from Mapp Biopharmaceutical and LeafBio, has been given to a small number of patients under the Expanded Access programme, despite not undergoing human safety trials.³⁷

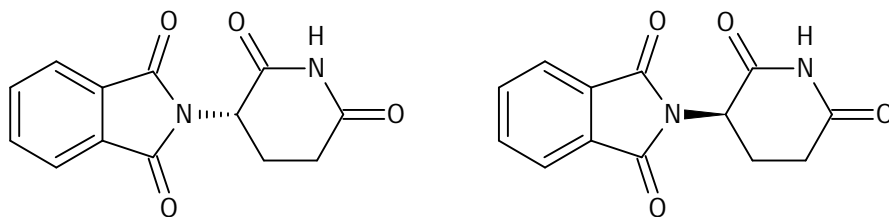


Figure 1.8. Structure of *S*- and *R*-thalidomide. The *S*-enantiomer is teratogenic, while the *R*-enantiomer is a sedative.

1.1.3. The Process of Drug Discovery: An Expensive Undertaking.

“The more original a discovery, the more obvious it seems afterwards.”

Arthur Koestler

The process of bringing a new drug to the shelf of a local pharmacy is a long, arduous, and expensive process. The Boston Consulting Group has estimated the average cost as \$1 billion over 15 years³⁸⁻³⁹ with both numbers fluctuating based on the disease being targeted, the nature of the drug being developed, and the type of clinical trials that the drug has to pass before being granted regulatory approval by bodies such as the F.D.A..³⁸ With only 5 out of 5,000 compounds that enter the preclinical phase surviving the rigours of testing to enter the human trials phase, and only one of these ultimately receiving approval, it is an enormous investment in terms of time, money and effort.⁴⁰ Often referred to as a “pipeline”, the process by which a drug is brought to market has a number of distinct stages (Figure 1.9), each of which requires the complex interaction of the members of the multidisciplinary teams responsible for that drug.^{38,41}



Figure 1.9. The drug discovery “pipeline”.

The Discovery and Basic Research stage is the initial stage, where new molecules are identified which have the potential to interact with biological systems, and these identified molecules are subjected to biological screening and pharmacological testing to explore the therapeutic potential of these compounds. Should a compound be identified with good therapeutic potential, it is then tested for

toxicology and safety in the Preclinical Testing phase. Dose formulation and stability is also carried out in the preclinical testing period. At this point, an application is made to the relevant regulatory authority to use the identified compound in human testing, and should approval be granted, the compound progresses to Phase I Clinical Trials. Absorption, distribution metabolism and excretion (ADME) patterns, tolerance and pharmacological effects are determined at this stage, often on a group of 20-80 healthy human volunteers. Phase II Clinical trials determine effectiveness in treating the targeted disease or medical condition in 100-300 patients, as well as any short term risks. Phase III Clinical Trials, which involve between 1,000 and 3,000 patients, determines the clinical benefit, if any, of the compound, and any adverse reactions which might occur. Process Development and Quality Control aims to establish the capacity of a company to produce the compound in large quantities in stable, uniform batches which meet the overall quality requirements. Prior to application for approval to market the new drug, Bioavailability Studies make use of healthy volunteers to establish that the product which is to be marketed is equivalent to the formulation used in the trials. Finally, Phase IV is carried out post-marketing in order to determine concealed adverse effects and the long term morbidity and mortality profile of the drug.³⁸

While the clinical trials stages of drug development contribute the most towards the overall cost of the development of new drugs – most sources estimate this proportion as 40% of the total development cost³⁸ - the second largest contribution comes from the initial discovery and basic research stage. This stage includes chemical synthesis and biological testing of thousands of compounds in order to identify hits, which are then further optimized into lead compounds and possibly new drug molecules.^{40,42} Traditional medicines and medicinal practices have formed the basis of the majority of early medicines,^{1,43-44} with the subsequent clinical, pharmacological and chemical studies carried out many years, in some cases centuries, after these treatments were introduced.^{1,45} Prime examples of this process are the well known compounds morphine, heroin, digitoxin, atropine, scopolamine, and quinine (Figure 1.10).

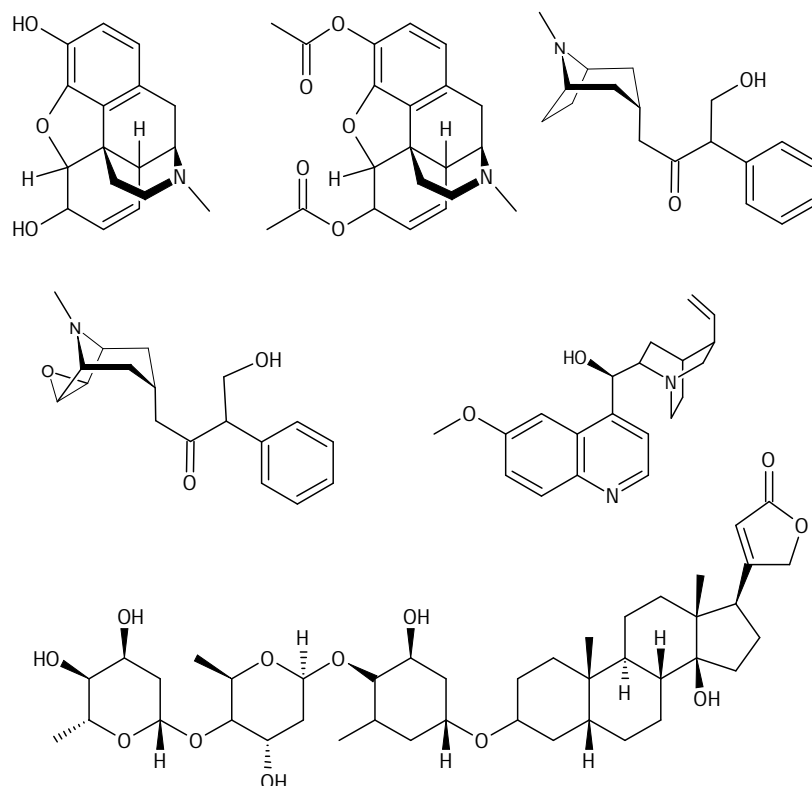


Figure 1.10. Structures of (clockwise from left) morphine, heroin, atropine, quinine, digitoxin and scopolamine.

The ancient Sumerians and ancient Greeks used extracts of the opium poppy (*Papaver somniferum*) medicinally, and the addictive effects of opium were documented by the Arabs, but morphine, one of the alkaloids present in the opium extracts, was not isolated until 1803, and heroin (diacetylmorphine) was not synthesized from crude morphine for another 70 years.^{1,46} Foxglove (*Digitalis purpurea*) has been used in Europe since the 10th century, but the compound responsible for the enhanced cardiac conduction observed was not identified as digitoxin until the 1700s.⁴⁶ Atropine and scopolamine, found in plants such as deadly nightshade (*Atropa belladonna*) and mandrake (*Mandragora officinarum*), have been used for thousands of years as an anesthetic or a sleeping agent, with ancient physicians such as Theophrastus and Dioscorides describing the use of these plants for these and other purposes.⁴⁷ Atropine was only prepared in pure form in 1833 by the German pharmacist Heinrich Mein,⁴⁸ and scopolamine was only isolated in 1880 by Albert Ladenburg.⁴⁶ The bark of several *Cinchona* tree species had been used for centuries by the Quechua peoples in South America for the treatment of malaria, indigestion, fever, mouth and throat diseases,⁴⁹ but formal use of the bark to treat malaria only began in the mid-1800's with the worldwide cultivation of this plant by the British and the Dutch,⁴⁶ and F.D.A. approval for quinine in the fight against malaria was only officially granted in 2005.⁵⁰

As the majority of the knowledge of the medicinal properties of plants comes as a result of trial and error by man over thousands of years,⁵¹⁻⁵² it is unsurprising that natural products, especially those of a plant-based origin, have been vitally important sources of potential drug leads,^{2,45,53-55} and still contribute greatly to the development of new drugs. A recent study of all drugs approved between 1980 and 2010 showed that almost 40% of these compounds are either natural products, or derived from natural products, and over 48% of the drugs approved in this time period for cancer treatment were either natural products or natural product derivatives.⁵⁶ The history of using natural products as a template for new drugs goes back to the late 19th century, with the development of acetylsalicylic acid, or aspirin, from salicylic acid. Plants such as the white willow (*Salix alba*) and meadowsweet (*Filipendula ulmaria*) (Figure 1.11) are rich in salicylate compounds, and portions of these plants have been used for thousands of years. The first specific reference to the use of these plants as painkillers and anti-inflammatories is found in the Ebers Papyrus, and references to these plants are found in the works of Hippocrates (5th century B.C.E.) and Dioscorides, and additional references can be found in Pliny the Elder's *Naturalis Historia* (77-79 CE) as well as in Celsus' *De Medicina* (ca. 30 C.E), and by the time Galen wrote his *Opera Omnia* in the second century CE, willow bark was commonly used throughout the Roman and Arab worlds.⁵⁷ Willow extract became recognized in the mid-18th century as a cure for fever, pain and inflammation when Edward Stone, an English chaplain, sent a letter to the Royal Society, relating the ability of this extract to cure a disease known then as ague, but known today to be the symptoms of malaria.⁵⁸ The common treatment for the ague was Peruvian bark, which was notoriously expensive, and once the cheaper willow extract was shown to have almost identical effects as the Peruvian bark, it became a popular substitute for Peruvian bark.⁵⁷ However, unlike the Peruvian bark which contained quinine, the willow extract relieved the symptoms of malaria rather than curing it.



Figure 1.11. The natural sources of salicylic acids - White willow (*Salix alba*, left)⁵⁹ and European meadowsweet (*Filipendula ulmaria*, right).⁶⁰

With the advent of the discipline of organic chemistry in the 19th century, many European scientists attempted to isolate, purify and identify the active compounds in the medicines used at that time, and the willow extract was not excluded from this scrutiny. In 1828, Joseph Buchner obtain reasonably pure salicin crystals, with Henri Leroux identifying a more productive extraction procedure for salicin from willow bark the following year.⁵⁷ A more potent acid form of the willow extract was obtained by Raffaele Piria in 1838, which he named salicylic acid. Work was also being carried out on extracts from the meadowsweet plant, and in 1834 Johan Pagenstecher isolated what he thought was a new pain-reducing substance. Karl Jacob Löwig, a German chemist working on identifying the meadowsweet extract in the early 1840's, discovered that it was the same salicylic acid as was identified by Piria in 1838.⁵⁷ The use of salicylate medicines, including salicin, salicylic acid and sodium salicylate (Figure 1.12), grew exponentially through the middle decades of the 19th century, as did the understanding of what these medications did – *i.e.* the reduction of fever, pain and inflammation. However, the side effects of these salicylate compounds seriously limited their value, and much research was carried out to reduce these side effects.⁵⁷

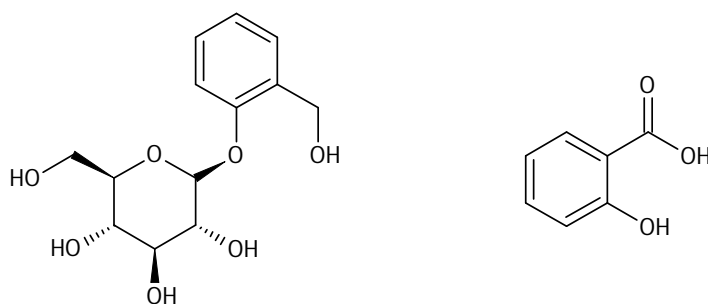


Figure 1.12. 2D structures of salicin (left) and salicylic acid (right).

Felix Hoffman, a member of the pharmaceutical group at Bayer, began work on a substitute for salicylic acid which did not have the same side effects, and based on work published by other scientists, he identified acetylsalicylic acid (Figure 1.13) as a potential replacement. Acetylsalicylic acid had first been prepared in 1853 by the French chemist Charles Frederic Gerhardt as a reaction of acetyl chloride and sodium salicylate, but as it was merely one of a number of reactions carried out for his paper on anhydrides, he did not investigate it any further.⁶¹ Von Gilm obtained analytically pure acetylsalicylic acid in 1859 from a reaction of salicylic acid and acetyl chloride,⁶² and Schröder, Prinzhorn and Kraut, by repeating both sets of reactions in 1869, concluded that the reactions of Gerhardt and Von Gilm yielded the same compound, and they were the first to correctly connect the acetyl group to the phenolic oxygen atom.⁶³

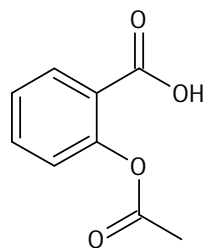


Figure 1.13. 2D structure of acetylsalicylic acid.

In 1897, Hoffman identified a superior method of synthesizing acetylsalicylic acid by heating salicylic acid with acetic anhydride at reflux,^{57,64} and the initial pharmacological testing results were promising, with none of the side effects of salicylic acid reported. Clinical trials for acetylsalicylic acid were delayed, in part due to the success of another of Hoffman's compounds, diacetylmorphine or heroin, but by 1899 Aspirin was being marketed (Figure 1.14) around the world by Bayer.⁵⁷ Aspirin's popularity as a painkiller declined with the release of paracetamol (acetaminophen) in 1956 and ibuprofen in 1969, but clinical trials and other studies from the 1960s to the 1980's showed that aspirin is an effective anti-clotting agent, and sales of aspirin recovered due to this new-found use preventing heart-attacks and strokes.⁵⁷



Figure 1.14. Aspirin bottle circa 1900.⁶⁵

1.1.4. Designer Drugs: The Rise of Targeted Therapeutics.

"I'm extremely disappointed. I send you out for exciting, new designer drugs, and you come back with tomato sauce."

Dr Gregory House, *House, M.D.*

As very little can be done to alter the structure of a drug once it has entered clinical trials, a huge amount of research goes into finding the optimal structure of a drug prior to this stage. Prior to the introduction of computer-aided drug design four decades ago, "Drug Discovery" involved identification of a compound or natural product, often based on traditional medicines. In the early part of the 20th century, bacterial infections of one form or another were responsible for a large percentage of deaths, and extensive studies were carried out in order to understand the microorganisms responsible. The discovery and isolation of penicillin from the *Penicillium notatum* fungus by Alexander Fleming in 1929⁶⁶ jump-started the search for new antibiotics from microorganisms as well as from natural products and other sources.⁶⁷⁻⁶⁸ While the "Golden Age of Antibiotics" is waning, a large number of important antibiotic compounds were identified during this period, including vancomycin, erythromycin, nocardicin, imipenem and aztreonam (Figure 1.15). Research into new antibiotics has not completely been abandoned – the development of drug-resistant microorganisms continues to fuel this area of research, and there are presently nine β -lactam antibiotic compounds either in clinical trials or undergoing drug registration, along with the glycolcyclines, a novel class of broad spectrum antibiotics.^{1,69}

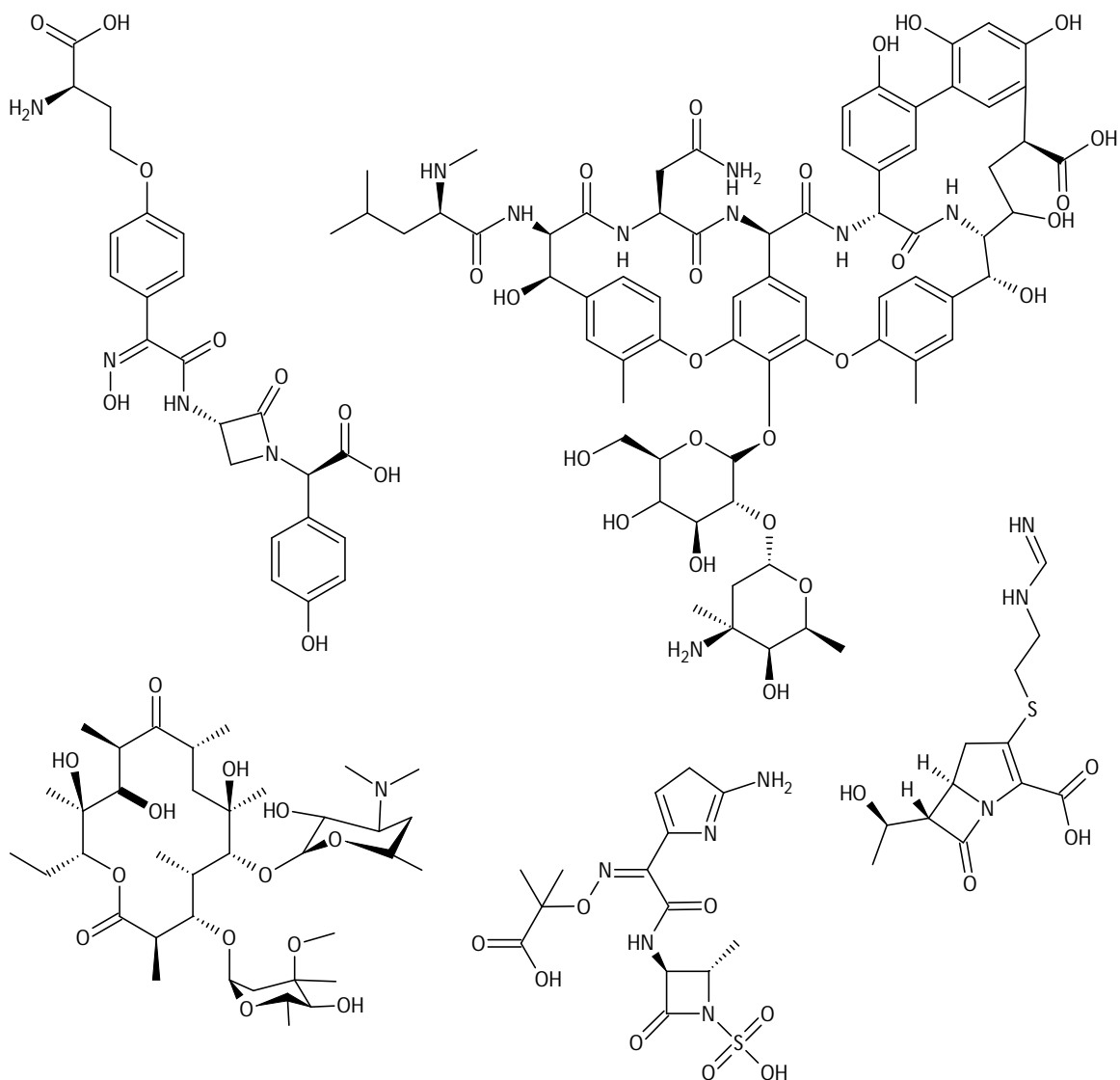


Figure 1.15. 2D structures of (clockwise from left) aztreonam, vancomycin, erythromycin, nocardicin, and imipenem.

During this “Golden Age”, many pharmaceutical companies commenced natural product discovery (NPD) projects, focusing not only on the development of antibacterial and antifungal agents, but also on infectious diseases and anti-cancer drugs. Paclitaxel, (Taxol® - Figure 1.16), the most widely used breast cancer drug, was isolated in 1962 from the bark of the Pacific yew (*Taxus brevifolia*) collected by the United States Department of Agriculture as part of the plant screening program carried out by the National Cancer Institute⁷⁰ and doxorubicin (Adriamycin®), which is used to treat acute leukemia, lung cancer, thyroid cancer, soft tissue and bone sarcomas as well as both Hodgkin’s and non-Hodgkin’s lymphomas, was isolated from a microbe found in a soil sample outside a castle in Italy in the

1950's.^{45,71-72} Drugs targeting microbial infections, hypercholesteremia and tissue rejection in organ transplantation were also developed during this period.⁷³⁻⁷⁴ The introduction of automated high throughput screening (HTS) during the 1990's and early 2000's resulted in countless pharmaceutical companies decommissioning their NPD programs,⁷⁵⁻⁷⁶ as biological testing and combinatorial testing were being touted as a better approach to creating drug-like compounds for HTS¹, which would produce lead topics by sheer weight of numbers.⁷⁷⁻⁷⁸ Traditional extract-based screening was thought to result in the constant rediscovery of previously isolated compounds, and many believed that both total synthesis and derivatization were required for the structural complexity of many natural products, both of which are often incredibly challenging and economically unviable.

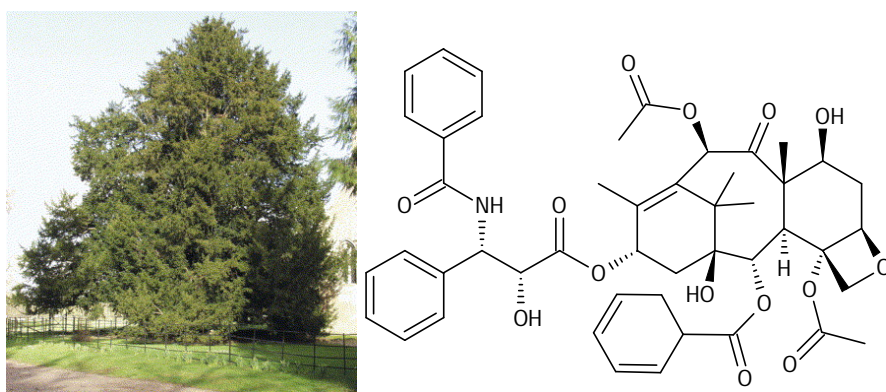


Figure 1.16. Pacific yew (*Taxus brevifolia*),⁷⁹ source of the cancer drug Taxol®.

HTS relies on combinatorial chemistry to produce large libraries containing thousands to millions of compounds, which are subjected to chemical, pharmacological or genetic tests using robotics and very sensitive detectors, in a “top-down” approach. In this “top-down” approach (Figure 1.17), complete molecules are tested for activity against a wide variety of targets, in the hope that one of the many compounds tested will show some form of activity against a target. HTS was intended to rapidly identify active compounds, known as “hits”, and these present the starting points for drug design. Hit compounds would then be derivatized and limited optimization carried out to yield potential drug-like compounds or “leads”. These leads, after further, more extensive optimization, would enter preclinical trials as possible drug candidates.⁸⁰⁻⁸² HTS was to deliver a greater number of lead compounds faster than traditional drug discovery techniques could, and without the intellectual property hassles often involved with natural products,^{45,83-86} and, not unexpectedly, natural product research was allocated a lower priority.

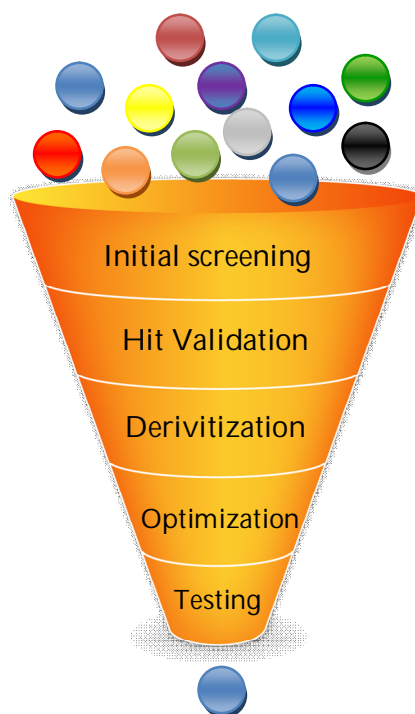


Figure 1.17. The “Top-down” approach to drug design. Many compounds are tested to identify hits, which are then further derivitized and optimized to generate a possible drug candidate.

However, combinatorial chemistry failed to deliver on its early promises, with only one compound, sorafenib, a completely synthetic kinase inhibitor (Figure 1.18), approved for use in renal carcinoma by the F.D.A. in 2005, despite almost 30 years of research.^{1,87} The usefulness of many large libraries generated by combinatorial chemistry was called in to question by the mid-1990's^{78,88-89} with Lipinski quoted as saying “The combinatorial libraries in the early years were so flawed that if you took the libraries across Pharma from 1992 to 1997 and stored them in dumpsters you would have improved productivity.”⁹⁰ Part of the reason for the inability of combinatorial chemistry to identify lead compounds from amongst the millions of compounds subjected to HTS is intrinsic to the way that HTS is carried out.^{81,91} In order to identify a small molecule which inhibits a protein, the entire library of compounds is analyzed using, for example, a protein binding assay; however, as protein binding does not necessarily indicate inhibition, the hits from the initial screen are subjected to a secondary functional screen to determine whether inhibition occurs. An alternate method would be to carry out functional screening initially to identify biological activity, followed by extensive characterization of the identified hits.⁹²

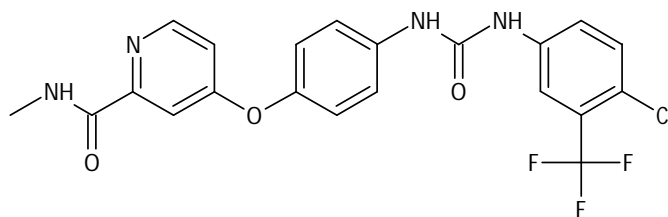


Figure 1.18. 2D structure of sorafenib, the only compound developed through combinatorial chemistry to receive F.D.A. approval for use in renal carcinoma.

After the initial hype surrounding combinatorial chemistry had died down, synthetic chemists realized that the combinatorial libraries, which contained huge numbers of compounds, lacked the inherent complexity of natural products.⁸⁷ The fact that natural products and the compounds in the combinatorial libraries essentially occupied different chemical space was proposed to be another reason that HTS had been unable to identify lead compounds.^{45,93-96} Some groups and companies have therefore begun to focus on “Diversity Oriented Synthesis” (DOS),⁹⁷⁻⁹⁹ where chemists focus on the synthesis of compounds which are similar to naturally-occurring compounds – “mimics” – or on compounds which have similar topology to natural products. As more emphasis in recent years has been placed on the quality of combinatorial libraries as well as the diversity of the libraries, natural products, which are well characterized in lists of “privileged structures” - molecular frameworks which are capable of providing useful ligands for more than one type of receptor or enzyme target by astute structural modifications¹⁰⁰ - have become ideal templates for new combinatorial libraries.^{45,95,101-108} A number of these compounds have been and currently are being tested in a wide variety of biological screens to determine possible activity, and some of these compounds are in various stages of clinical testing, and have received approval for use.⁸⁷ The antibiotic linezolid – sold under the name Zyvox® (Figure 1.19) was developed by chemists at Pharmacia (now part of Pfizer) starting from work carried out at DuPont Pharmaceutical on the mechanism of action and antibiotic activity of this novel oxazolidinone class of compounds.^{87,109-113} Derivatives of artemisinin, an anti-malaria drug isolated from the sweet wormwood (*Artemisia annua*) plant, are in development in Europe,^{2,71} and a synthetic trioxolane based on artemisinin is being tested in combination with another synthetic bisquinoline compound, piperazine, as an anti-malarial agent.¹¹⁴ There are at present three semi-synthetic erythromycin derivatives in clinical development as antibiotics– cethromycin (ABT, Restanza®), EP-420 (Enanta Pharmaceuticals) and BAL-19403 (Basilea),^{1,53} and the synthetic derivatives of tubocaurarine, a muscle relaxant isolated from the Amazonian *Chondrodendron tomentosum* plant, are now preferred over tubocaurarine due to its limited availability.^{1,71}

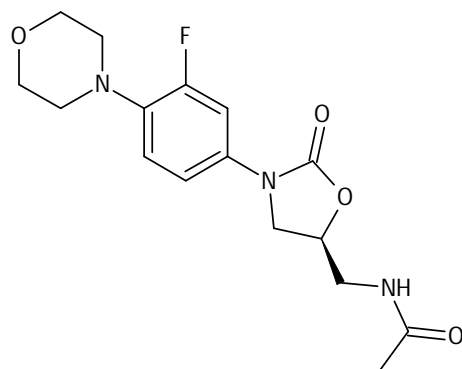


Figure 1.19. 2D structure of the novel oxazolidinone antibiotic Zyvox® (linezolid).

The chemical optimization of lead compounds into potential drug-like compounds has, however, led to some spectacular failures. Partially attributed to the reduced productivity of the pharmaceutical industry, an answer to the high failure rate was sought, and “Lipinski’s Rule of Five” was proposed as a guide to identify good lead compounds.¹¹⁵⁻¹¹⁷ While the rule describes properties important for pharmacokinetics in the human body, it does not predict whether a compound will be pharmacologically active. Characteristics identified as imperative to a promising compound include the maximum molecular weight of a compound (less than 500 Da), the total number of hydrogen bond donors and acceptors (5 and ten respectively) and an octanol-water partition coefficient ($c\text{Log}P$) not greater than 5. The weight limit of 500 Da came about with the realization of the connection between high molecular weight and poor solubility. Optimization of potent lead compounds with high molecular weight often results in compounds with even greater masses, and an associated reduction in solubility and poor pharmacokinetic properties.^{77,117} Attempts to improve predictions of “druglikeness” have resulted in extensions to this rule, such as the range for number of atoms (between 20 and 70), number of rotatable bonds (10 or less) and a polar surface area no greater than 140 \AA^2 . As with any rule, there are a number of exceptions – for example the 500 Da weight limit has been a matter of debate as a number of drugs, especially the naturally derived antibiotics, far exceed this. It has also been found that the polar surface area and the number of rotatable bonds are more important criteria in the identification of compounds with good bioavailability in rats.¹¹⁸

1.1.5. The Bottom-Up Approach: Tackling the Problem from a Different Angle.

“Bottom-up thinkers try to start from experience and move from experience to understanding. They don't start with certain general principles they think beforehand are likely to be true; they just hope to find out what reality is like.”

John Polkinghorne

An alternative to the “top-down” approach of HTS to drug design is the “bottom-up” or “knowledge-based” method, where the target of a compound, be it an active site in an enzyme, an area on the surface of a protein or a specific receptor protein, is used as a base for the design of a target compound. Techniques such as fragment-based drug design (FBDD), computational design and rational synthesis integrate existing structural or biochemical data of the target so that the compound which is designed or engineered has the best chance of showing the desired activity.¹¹⁹⁻¹²¹ An important distinction between FBDD and HTS is that the interaction of the fragments is predisposed towards a specific target, be it a protein receptor site, the active site of an enzyme or a patch on the surface of a protein which is functionally important.⁹² This concept was introduced in the early 20th century by John Newport Langley and Paul Ehrlich.¹²²⁻¹²³ Based on his observations of the responses to certain dyes, Ehrlich proposed the idea that different receptors exist in microorganisms, parasites and cancer cells,¹²⁴ and Langley, together with his collaborators, put forward the idea that receptors could be activated or inhibited by the binding of a ligand to a receptor in 1905,¹²⁵ with Joseph Clark using both of these theories as the basis for his study of drug action on cells in the 1930s.¹²⁶

As previously stated, the ability of a screen to identify lead compounds is still relatively poor.^{77,127} One of the problems alluded to lies in the nature of the hits identified by HTS. With the molecular weight of successful drugs in the World Drug index averaging in the low 300 Da,¹²⁸ identification of a hit compound with a similar mass from a “drug-like” corporate library, would, after optimization, result in a lead compound approaching 400 Da, and this compound would show significantly poorer pharmacokinetic properties due to this weight increase.¹¹⁷ As a solution, a number of research groups have proposed a “fragment-based” approach, where low molecular weight compounds (under 200 Da) target subpockets within the active site.^{115,129-134} Rather than trying to fit a prebuilt molecule into a target, as is the case with library screening through HTS, FBDD attempts to find the best fitting molecule

for a particular target by identifying building blocks that fit correctly, and then assembling these pieces into a complete molecule (Figure 1.20).

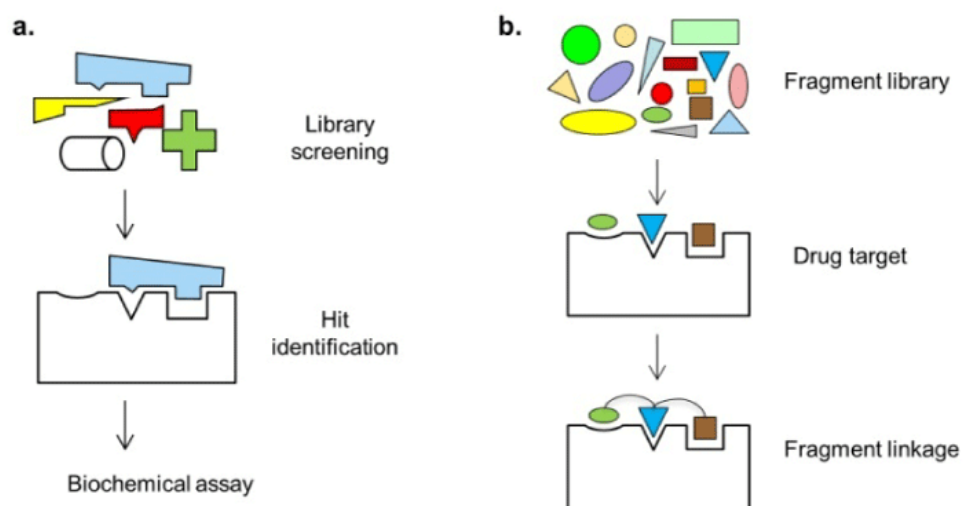


Figure 1.20. (a) Library screening vs. (b) fragment based drug design. Library screening attempts to fit a prebuilt molecule into a target, while FBDD identifies fragments which can be assembled into a complete molecule.⁹²

Initially proposed by Hol and co-workers in 1990¹³⁵ and again by Fesik and co-workers at Abbot Laboratories in 1994,¹³⁰ FBDD has become a well-known and widely applied strategy for the identification of novel hits in both industrial and academic settings,¹³⁶ with one F.D.A.-approved drug, vemurafenib (Zelboraf® - Figure 1.21), originating from this fragment screening and optimization approach, and several more in clinical trials.^{115,137-138}

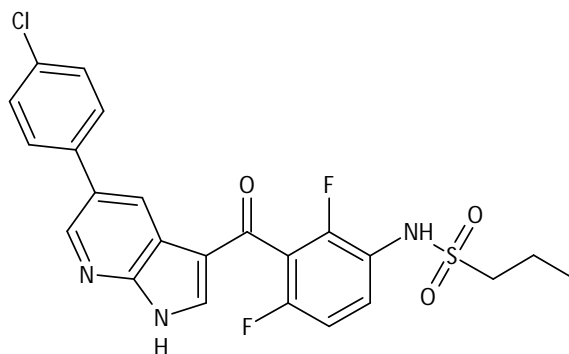


Figure 1.21. 2D structure of Zelboraf® (vemurafenib), designed using Fragment Based Drug Design techniques.

These fragments are defined as low molecular weight organic molecules which are lipophilic and highly soluble, and which typically bind to the target protein with low affinity (Figure 1.22).¹¹⁵ A “Rule of Three,” analogous to “Lipinski’s Rule of Five,” was proposed by Congreve and co-workers to define these fragments.^{115,139} The “Rule of Three” states that fragments should have a molecular weight under 300 Da, no more than three hydrogen bond donors or acceptors and a cLogP value of less than 3. Additional filters such as the maximum number of rotatable bonds (3) and a polar surface area of 60 Å² have also been indicated to aid in the identification of more desirable fragments. Of these widely accepted guidelines, the most flexible is the rule related to molecular weight, as fragments over 300 Da have been used to identify hits for a range of targets, including peroxisome proliferator-activated receptors (PPARs), phosphodiesterase type 4 (PDE-4) and the protein encoded by the mutant B-Raf-V600E (BRAF_{V600E}) gene.¹⁴⁰⁻¹⁴³ While these fragments have limited functionality and therefore weaker affinity, the hit fragments can either be optimized individually, or the fragments can be connected, yielding a bigger fragment which possesses the properties of each fragment.^{77,92,144}

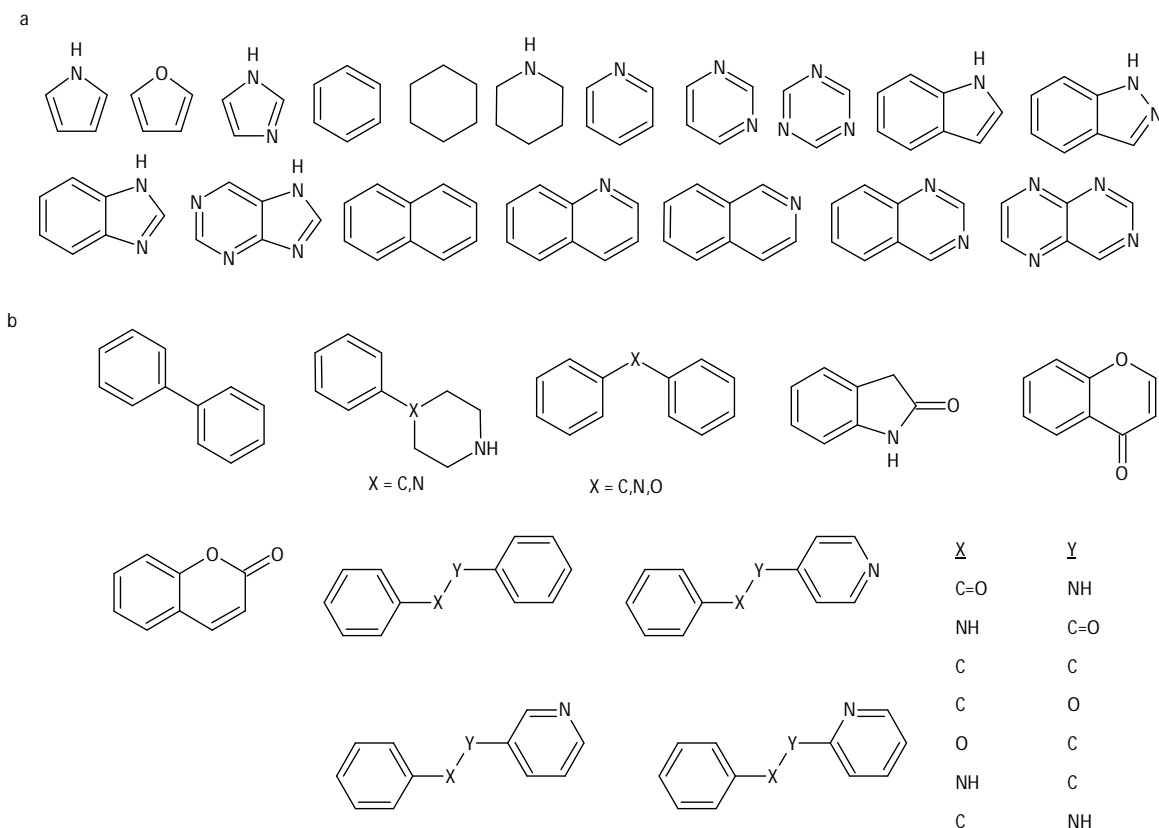


Figure 1.22. A molecular fragment library containing (a) simple carbocyclic and heterocyclic fragments and (b) simple drug scaffolds.⁷⁷

Optimization of fragment hits into lead compounds follows one of two paths (Figure 1.23) – “Fragment-growing” and “Fragment-linking.”⁴⁰ Fragment-growing is the stepwise addition of substituents or functional groups to a core fragment in order to maximize the interactions with the binding site, while fragment-linking approach involves the covalent linking of two or more fragments which are independently bound to the binding site with suitable linkers.^{115,145} Fragment-growing, the more common approach, conserves the initial binding mode of the initial fragment, and allows researchers to monitor the subtle changes in the binding mode that occur with each step in the optimization process.¹³⁶ Recent studies using fragment growing as the optimization strategy include the identification of Beta-site amyloid precursor protein cleaving enzyme 1 (BACE1),¹⁴⁶ matrix metalloproteins (MMPs),¹⁴⁷ phosphatidylinosito-3 kinase (PI3Ks) inhibitors¹⁴⁸ and acetylcholine-binding protein (AChBP).¹⁴⁹ Cheng *et al.* identified 2-aminoquinoline as an initial fragment hit from a library of 4,000 fragments screened against BACE1, and optimization using fragment growing improved the activity of the fragment by 10⁶ fold¹⁴⁶ and a 50-fold improvement was obtained after a single fragment growing optimization step was carried on a fragment identified as a hit for AChBP.¹⁴⁹

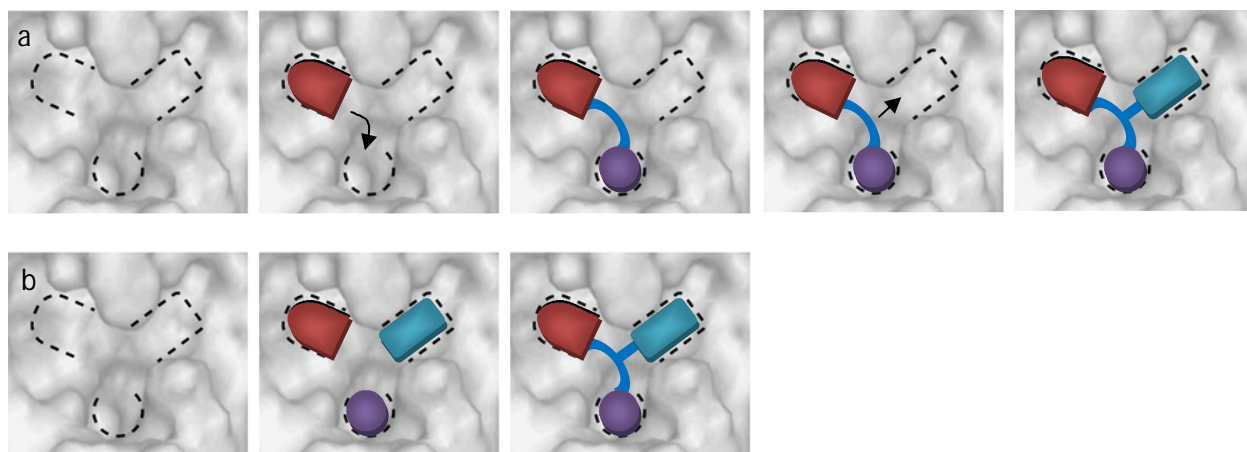


Figure 1.23. (a) Fragment growing and (b) fragment linking strategies for drug design.⁴⁰

While less common than the fragment-growing methodology, the fragment-linking approach has been used by a number of groups to obtain potent compounds from initial fragment hits.¹⁵⁰⁻¹⁵⁸ Fesik and co-workers¹³⁰ were the first to successfully demonstrate the applicability of fragment-linking, and Barker *et al.*¹⁵⁷ have established that linking two low affinity fragments can create a compound with 1,000 fold higher affinity than either fragment. In another study, Petros *et al.*¹⁵⁶ identified a B-cell lymphoma 2 (Bcl-2) inhibitor that was 1,000 fold more selective for Bcl-2 over B-cell lymphoma-extra large (Bcl-XL). Interestingly, *in situ* self assembly – where fragments in close proximity to each other assemble

themselves into one compound, has been described by Lewis *et al.*,¹⁵⁹ Hu *et al.*¹⁶⁰ and Suzuki *et al.*¹⁶¹ Lewis *et al.* demonstrated the acetylcholinesterase-mediated linkage of azides and alkynes into high potency inhibitors,¹⁵⁹ Hu *et al.* the self assembly of thio acids and sulfonyl azides in Bcl-XL into a “small molecule protein-protein interaction inhibitor” (SMPPH)¹⁶⁰ and Suzuki *et al.* described the formation of histone deacetylase inhibitors from an *in situ* reaction of hydroxamic-containing alkynes and azide fragments.¹⁶¹ The fragment-growing approach is more popular as it allows more freedom for multidimensional optimization as opposed to fragment-linking, which depends on being able to link adjacent fragments without altering the binding modes.¹¹⁵ A study by Hung *et al.*¹⁵⁰ in 2009 compared the two optimization methods by applying them to the same target protein – pantothenate synthetase from *Mycobacterium tuberculosis* (Figure 1.24). The fragments used were identified through biophysical techniques, and included an indole fragment for the growing approach, and an indole and a benzofuran fragment for the linking approach. After optimization was complete, the strategies resulted in similar structures with similar potencies, indicating that, at least in this case, there was no significant difference between the two strategies.^{115,150}

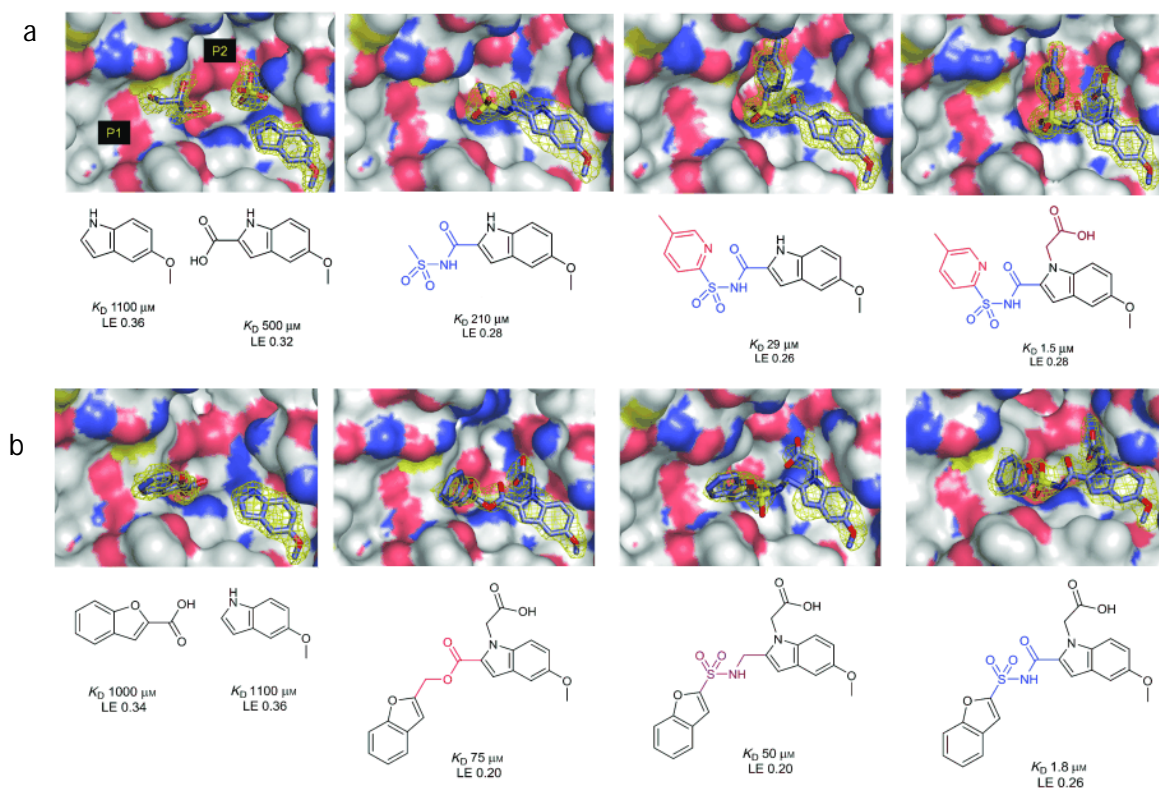


Figure 1.24. Comparison of (a) fragment-growing and (b) fragment-linking techniques for the synthesis of a pantothenate synthetase inhibitor, adapted from Hung *et al.*¹⁵⁰

While the list of benefits of FBDD over HTS is long and cannot be adequately covered here, the advantages that FBDD has over traditional HTS can be delineated into three main groups:

- The chemical diversity space is covered more completely with FBDD than with HTS, as smaller FBDD libraries can probe the chemical space more effectively and can generate the same amount of information as HTS.^{115-116,162-164}
- FBDD achieves higher hit rates than HTS, a fact which has been ascribed to the ability of fragments to bind to multiple sub-sites of a target as opposed to the larger, more functionalized molecules which show significantly more steric hindrance and electrostatic conflicts with the binding site.^{115,162,165}
- Lead compounds optimized from FBDD hits show higher binding efficiency per atom than those from HTS hits.¹¹⁵

FBDD does however have one major shortcoming – the affinity of the fragments used are often outside of normal detection limits, and therefore cannot routinely identified using standard bioassays.⁷⁷ While there has been some work on the sensitivity of bioassays, many researchers have used existing biophysical techniques such as X-ray crystallography and NMR spectroscopy to screen these low-affinity compounds.^{77,129-130,151} As “traditional” FBDD is not compatible with biochemical screening methods, FBDD has been expanded to include scaffold-based drug design (SBDD), where reoccurring chemical motifs from marketed drugs are used as templates for drugs.^{140,166} These scaffolds contain more functional groups than the fragments, and as such are able to provide a more substantial starting point for optimization. One of the key differences between FBDD and SBDD lies in the molecular weight limit imposed. In FBDD, the weight limit is around 200 Da per fragment; the limit for SBDD is 350 Da, with an average weight of 250 Da. This weight limit adjustment results in a bigger scaffold library (20,000 compounds as opposed to the 2,000 fragments used in FBDD), but these scaffolds are often able to bind to proteins at affinities which can be detected with biochemical assays.¹¹⁵ While the rate of false positives is high due to high compound concentration and low binding affinities, compounds are only selected as hits when activity is shown against multiple members of the same protein families.

Another difference between FBDD and SBDD is that only scaffolds with binding modes which will tolerate small substitutions are optimized further, leading to more accurate Structure-Activity Relationship (SAR) analyses and more efficient further optimization.¹¹⁵ While not often included in FBDD

or SBDD, fragments of natural products have also been used in drug design. Waldman and co-workers combined commercially available natural product fragments and some which were synthesized in a study which combined the chemical space-covering ability and binding ability of fragments with the chemistry and geometry of natural products.¹⁶⁷ Whilst some of the 193 natural product fragments (NPFs) tested resemble known chemotypes, some were novel scaffolds which showed good binding ability. By merging the techniques of FBDD and natural products, the authors were able to identify compounds which are biologically accessible and could potentially be the basis of novel, synthetic drug-like molecules which are also biologically optimized, in much the same way as food scientists at the Reese corporation were able to merge peanut butter and chocolate into peanut-butter cups, supposedly ending the culture war surrounding these ingredients.¹⁶⁶

1.2. The Machines Are Taking Over: The Role of Computers in Drug Design.

"I'm not afraid of computers taking over the world. They're just sitting there. I can hit them with a two-by-four."

Thom Yorke

One of the challenges facing drug designers is the vast amount of data generated from techniques such as FBDD and SBDD, as well as data generated from biophysical, biostructural and biochemical approaches. Playing an important role in the integration of data from various sources, computational methods are becoming increasingly more important in many drug discovery processes, with computer modeling and simulations estimated to account for 20% of pharmaceutical R&D expenditure by 2016.^{40,42} Computational drug design is involved in all stages of drug design (Figure 1.25), from target identification to fragment library generation to hit identification and lead optimization and even into the clinical trials phase. While a powerful tool in its own right, it has proven to be most useful when used in combination with experimental data.¹¹⁵ These *in silico* methods are cost effective, fast and can be applied to a wide range of biological targets.

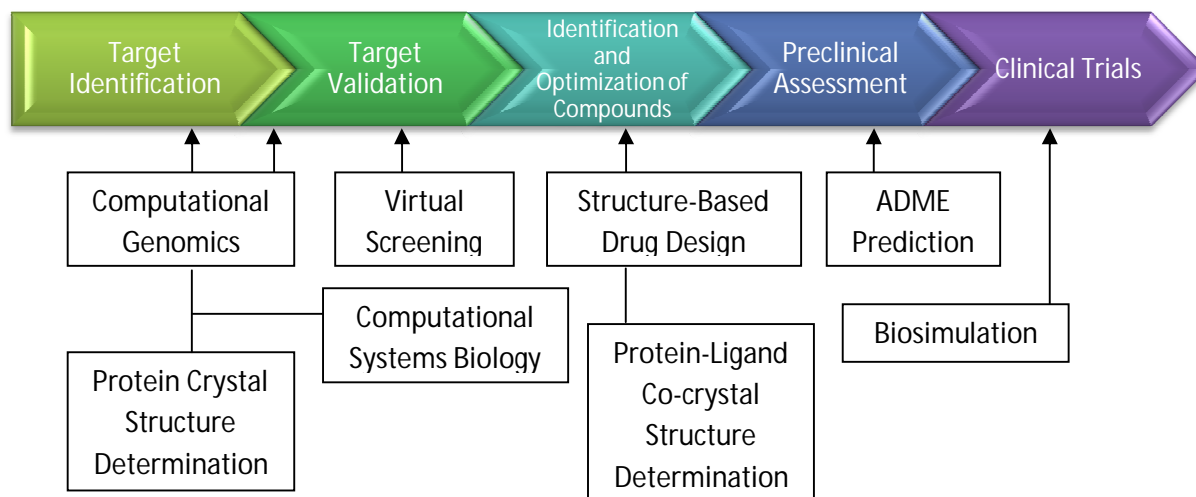


Figure 1.25. Application of computational methods to drug design.

The steps involved in *in silico* drug design mirror those found in *in vitro* drug design. A virtual library is designed and screened by another virtual approach, such as molecular docking, and prioritized fragments can then be virtually grown, linked or a combination of both into a virtual lead compound.¹¹⁵ As with all computational techniques regardless of the field of application, the adage “Garbage in, Garbage out” applies, and it is notoriously difficult to obtain a high quality, potent final compound without having a high quality fragment library. While a number of approaches have been developed to aid in the compilation of fragment libraries, the simplest and most commonly used technique to design a fragment library is the filtration of commercially available chemicals. A number of computational tools, such as the descriptor calculator plugins from ChemAxon,¹⁶⁸ the Chemistry Development kit (CDK),¹⁶⁹⁻¹⁷⁰ the sdfilter utility from MOE¹⁷¹ and QikProp from Schrödinger,¹⁷² can be used to filter libraries of drug-sized or lead-like compounds based on molecular properties including molecular weight, logP, number of rotatable bonds, number of H-bond acceptors or donors, and the polar surface area. With no fixed rules for filtering compounds, other filters such as molecular diversity, inclusion of common motifs and removal of chemically reactive elements have also been implemented.¹¹⁵

While the “Rule of Three” is often applied to guide the formation of a fragment library, as in the case *in vitro*, exceptions abound and different groups use different filters depending on the situation at hand. Fragment libraries have also been designed based on the computational retrosynthesis of compounds found on the World Drug Index. RECAP¹⁷³ (Retrosynthetic Combinatorial Analysis Procedure), designed by Lewell *et al.* was applied to 35,000 compounds on this list, and a number of biologically recognized

fragments and privileged scaffolds were identified. In 2006 Kolb and Caflish developed DAIM¹⁷⁴ (Decomposition And Identification of Molecules), a program which follows similar rules to RECAP to automatically break apart the compounds in small molecular libraries in order to generate fragments, and Degen *et al.* detailed an enhanced procedure for molecule decomposition using BRICS¹⁷⁵ (Breaking of Retrosynthetically Interesting Chemical Structures). This approach makes use of novel, more elaborate fragmentation rules and also maintains promising motifs through the fragmentation process. Comprehending the importance of *in silico* fragmentation in generating fragment libraries, many commercially available programs, such as CoLibri from BiosolveIT,¹⁷⁶ the sdfrag utility in MOE,¹⁷¹ Chomp from OpenEye¹⁷⁷ and the rule-based molecular fragmenting utility from Schrödinger¹⁷² are capable of carrying out fragmentation operations on small molecule libraries.¹¹⁵

Once a suitable fragment library has been compiled, the next step in the virtual drug design process is virtual screening (VS) of the fragments against a drug target, such as an enzyme or a protein receptor (Structure-based VS), so as to identify those fragments which are most likely to bind to the target.¹⁷⁸⁻¹⁸⁰ Structure-based VS (SBVS) involves the “docking” of a fragment into a target site of a protein or enzyme, and a subsequent application of a scoring function to estimate the probability of the fragment binding to the target site.¹⁸¹⁻¹⁸² The majority of these docking programs use hierarchical scoring schemes, where a simple shape-based scoring function applied to the entire library eliminates fragments which are sterically unsuited to the binding site, followed by progressively more intense scoring functions on the surviving fragments to yield, hopefully, a manageable list of compounds with good binding affinity scores.¹⁸³⁻¹⁸⁴ The binding affinity of a fragment is predicted by combining a number of different energetic contributions, such as electrostatic interactions, van der Waals interactions and hydrogen bonding interactions, however the contributions of entropy to the free energy of binding are difficult to estimate and are a source of large uncertainty in the values.⁹²

The initial fragment positioning methods, which in fact predate the experimental techniques,¹⁸⁵⁻¹⁹¹ were mostly force field-based methods and relied on protein-ligand interactions from molecular mechanics models to predict fragment positions. However, as computational drug design has improved and evolved, the positioning methods have made use of the more sophisticated force fields available. Examples which make use of these modern force fields include 3D-RISM, which generates the most likely binding mode for a given ligand and makes use of the 3D reference interaction site model solvation theory,¹⁹² and FTMap,¹⁹³ which generates a consensus site and uses a Fourier transform

correlation approach and the analytical continuum electrostatic (ACE) model to deal with solvation issues.

Computational screening methods such as molecular docking can be applied to a wide variety of targets if high quality structural data is available, and in the absence of experimental structures, 3D or homology models can be used. While already a proven technique in drug discovery when coupled with experimental validation,¹⁹⁴ molecular docking is believed to yield unreliable results due to promiscuous binding modes of the fragments, and the inability of a scoring function to separate native and irrelevant binding poses,¹⁹⁵⁻¹⁹⁶ as most of the docking programs and scoring methods are developed and optimized for more drug-like compounds with properties significantly different to those of fragments.^{115,145} A number of studies have been carried out to explore the performance of docking methods and scoring functions as virtual screens for fragment libraries, and these studies show that, as for docking in general, solvation is important but computationally expensive to carry out; that protein flexibility plays a role and that the accuracy of docking results is poorer for weakly-binding ligands.¹⁹⁷⁻¹⁹⁸ However, a number of studies have shown that the results from fragment docking are similar to those obtained for the docking of drug-like compounds in terms of enrichment.^{115,145}

Following the identification of hit fragment, the objective in drug discovery is then to design inhibitors using fragment-growing, fragment-linking or fragment-scaffold merging techniques, in much the same way as carried out *in vitro* (Figure 1.26). Although the theoretical basis for fragment connection was proposed in 1981,¹⁹⁹ computational connecting methods such as CAVEAT,²⁰⁰ HOOK,²⁰¹ and CONCERTS²⁰² emerged in the mid 1990s shortly after the first fragment positioning programs were released. While fragment-based design is conceptually simple, it proves to be a challenging problem in practice,²⁰³⁻²⁰⁴ as most *de novo* methods do not take into account the routes required for the synthesis of a compound, and can often identify a highly potent but synthetically unavailable compound. Modern programs attempt to solve this problem by limiting the combinatorial predicament when connecting fragments. The CONFIRM²⁰⁵ approach, for example, makes use of a database of bridge molecules derived from existing compounds, and by retaining the information about the connecting atom types for the bridges, increases the possibility of creating a molecule which can be synthesized, while ReCore²⁰⁶ uses recap synthesis rules to link or grow fragments into lead compounds. Common *de novo* design programs include BREED,²⁰⁷ GANDI,²⁰⁸ AlleGrow,²⁰⁹ BROOD,²¹⁰ GROWMOL²¹¹ and FOG.²¹² BREED, developed by Vertex Pharmaceuticals, has been used to create new inhibitors of cyclin-dependent kinase 2 (CDK2),

P38 mitogen-activated protein kinase and HIV protease,²⁰⁷ and Ligbuilder, a program combining both fragment growing and linking functionalities, has been used to design two potent Cyclophilin A inhibitors from an acylurea seed fragment.²¹³

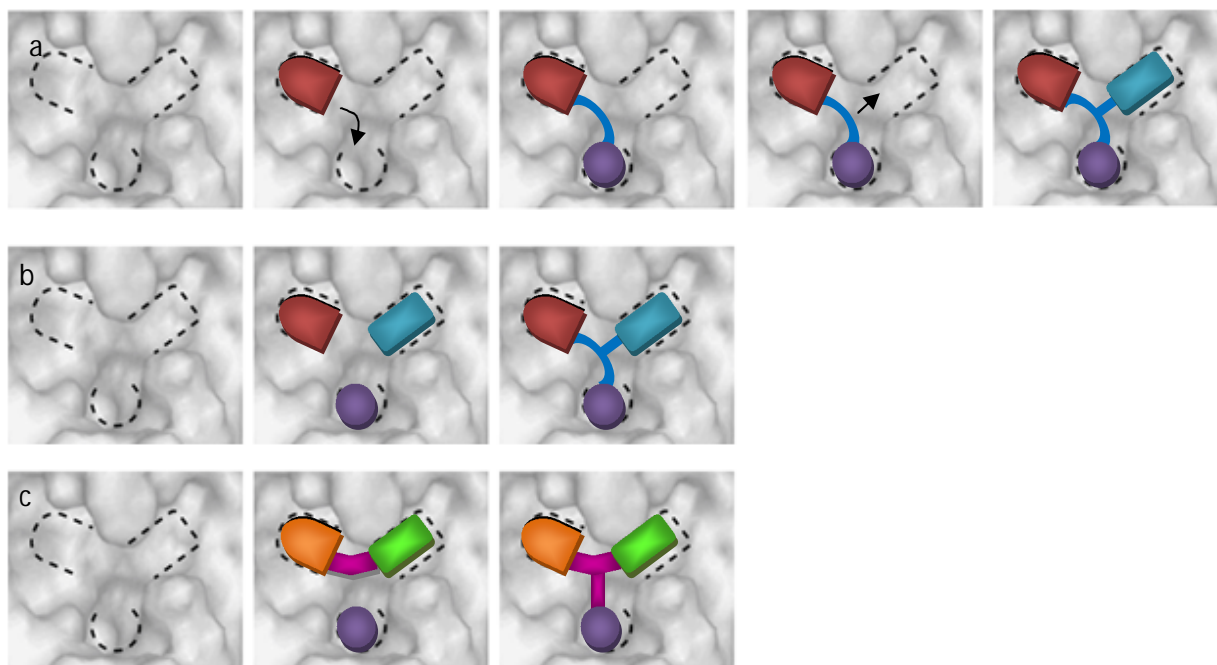


Figure 1.26. (a) Fragment-growing, (b) fragment-linking and (c) fragment-scaffold merging techniques.

An interesting case of a novel drug discovery method and computational fragment-based drug design was presented by Li *et al.* in 2011²¹⁴ when they used the MLSL (Multiple Ligand Simultaneous Docking) program²¹⁵ to simultaneously dock privileged scaffolds into hotspot regions of a cancer target, the transcription factor STAT3. In this study, the top fragments were selected for *in silico* linking, using different bridges such as amines, amides, ethers and olefins, and 15 virtual compounds were created. These 15 compounds were then used in a similarity search against the Drugbank²¹⁶ where celecoxib, a COX-2 inhibitor, was identified as a novel STAT3 inhibitor. Synthesis of a celecoxib derivative and one of the *in silico* linked hits confirmed this method as these compounds showed good potency against STAT3 *in vitro*. *In silico* drug development can also significantly reduce the time required to develop a drug, as demonstrated by Becker and co-workers, who used computational drug design and development to create a 5-hydroxytryptamine receptor (5-HT_{1A}) agonist for the treatment of anxiety and depression. The selective agonist was designed, optimized and carried to clinical trials in under 2 years, and required less

than 6 months of optimization and the synthesis of only 31 compounds, whereas without computational input, this process takes anywhere from 5 to 10 years.²¹⁷

While SBVS has proven to be an important design route for new drugs, the downside to this approach is that high-quality protein structure data is required, either from X-ray crystallography of the protein, or from other biophysical techniques. As getting this high-quality data is challenging at the best of times, there are a number of target proteins where the structure of the active site is not definitively known. Ligand-based VS (LBVS) occurs when a pharmacophore, a “conceptual description of the molecular features necessary for the interaction of a ligand to a target molecule,” is used as the benchmark against which the fragments are judged.²¹⁸⁻²¹⁹ A good pharmacophore model takes into account the common chemical motifs, and is able to explain how structurally diverse compounds are able to interact with a common receptor or active site.²²⁰⁻²²⁴ It highlights the important structural elements required for activity (Figure 1.27) and can be used to identify novel compounds which bind to the same receptor.²²⁵⁻²²⁸ Pharmacophore modeling has become an established screening technique,²²⁹ and has been used to identify a human dihydro-ototate dehydrogenase (DHODH) inhibitor,²³⁰ and a potent and selective neuronal nitric oxide synthase (nNOS) inhibitor.²³¹

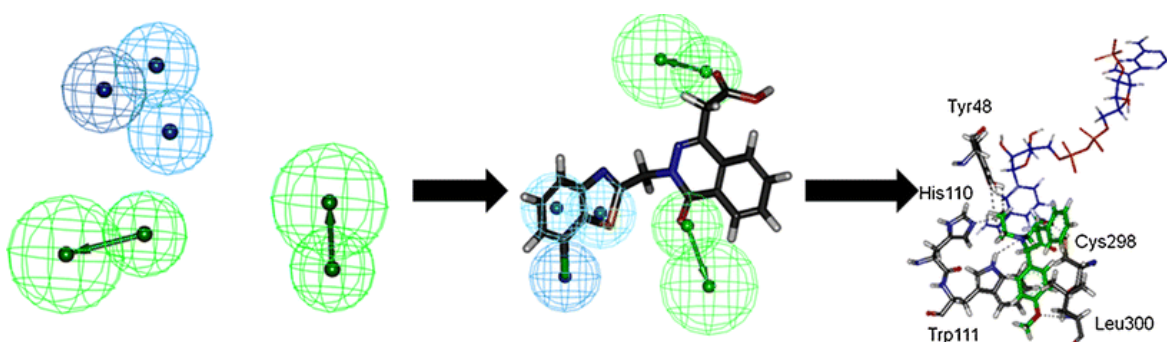


Figure 1.27. The pharmacophore model and resultant lead compound for inhibition of aldose reductase 2.²³²

Despite the fact that many lead compounds have been identified through either SBVS or LBVS, perhaps the most ideal situation arises when both approaches are used in tandem. When SBVS is used, the hit compounds or fragments should, by definition, be able to bind to the conformation of the protein, and when LBVS is used, the results will, as expected, show chemical similarity.¹⁴⁵ During the development of a histamine H1 inhibitor, Leurs *et al.*²³³ used structure-based docking techniques together with specific information obtained from known ligands to identify fragment hits with high binding affinities, including one with the highest affinity for a G protein-coupled receptor yet identified through SBVS.^{217,234}

As with all things, there are drawbacks to computational fragment-based screening. Perhaps the most serious are the relatively low prediction accuracy and the rapid accumulation of errors in the calculations. In general, experimental FBDD methods have greater accuracy than computational methods, and this difference has been ascribed to imperfect energy functions used to assess the ligand-protein interactions, as well as problems in sampling the conformational space completely.¹¹⁵ Computational methods which are fast are less accurate as they tend to make approximations during conformer searching, as well as during the calculations of energetic terms during the simulations, and the more accurate methods, which carry out more complete conformational searches and include protein flexibility, are much slower. A commonly adopted strategy to overcome these issues is to use a “layered” approach, where large libraries are screened with a fast method, and the resulting smaller collection of compounds is then further screened with a slower, more accurate method. While computer-based methods such as docking or molecular dynamics can be carried out on a homology model of a protein, the errors from this computationally-derived structure, added to the screening errors, can significantly lower the dependability of the hits identified through virtual screening. In spite of these disadvantages, the virtual screening of fragments can result in lead identification, although the most effective use of computational methods is in conjunction with experimental methods to both validate and guide the following computational steps. By focusing on small molecules which bind to a specific location, FBDD integrates relevant molecular information into the design of selective inhibitors with high affinities, and while this process appears slow, including this detailed interaction information into a drug design process is thought to facilitate the discovery of higher affinity binders that work through a known mechanism. The integration of experimental techniques with computational methods has become an indispensable tool for any drug discovery program.

1.2.1. Making Predictions: Modern Techniques for Modern Problems.

“Trying to predict the future is like trying to drive down a country road at night with no lights while looking out the back window.”

Peter Drucker

The art of prediction plays a fundamental role in the pharmaceutical industry, be it a biologist attempting to predict the effect of target inhibition on cell behavior, a doctor worried about the side effects of a drug, or a manager trying to predict future returns on an investment.²³⁵ Prediction in drug design relies on the knowledge of the three-dimensional (3D) structure of a specific macromolecule, such as a protein or enzyme, as the function of a macromolecule is as dependent on the 3D structure of the macromolecule as it is on the string of components which make up its primary structure. These 3D structures are vitally important to medicinal chemists striving to design compounds which inhibit these macromolecules, and many computational methods and techniques, such as molecular docking, *de novo* design, molecular dynamics and free energy calculations are available which aid in the design of novel inhibitors. As there are a number of programs and packages available, each with their own unique attributes, a review of all of these programs is impractical, and as such, the brief review of computational methods which follows will focus on the Schrödinger suite of software so as to better understand the results obtained during the design process.

Molecular docking uses known 3D coordinates of the site of interest to orient a ligand into a favored conformation within that site, and uses an empirical scoring function to predict the activity of a ligand based on the interactions between the ligand and the binding site. Modern structural drug design owes its beginning to the “Lock and Key” model for enzymes (Figure 1.28), proposed by Nobel laureate Dr Emil Fischer in 1894.²³⁶ This model, which describes how the active site of an enzyme is complementary to the structure of the native substrate, is still an important part of the molecular docking algorithms used in modern computational software.

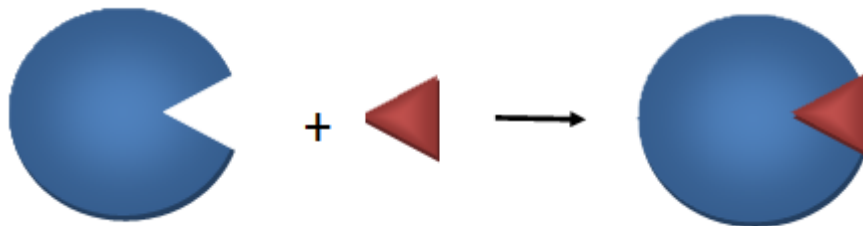


Figure 1.28. A schematic diagram of “Lock and Key” model for enzymes, where the active site is complementary to the structure of the native ligand.

The “Lock and Key” model is used to describe the binding process, which takes into account the solution structures of the ligand and the receptor separately as well as involving the conformations of the complex. While docking algorithms can be simplified by considering the receptor and ligands as rigid molecules, which has led to the successful prediction and reproduction of experimentally-determined structures of complexes,²³⁷⁻²⁴⁰ a rigid model is not suited to the majority of receptors and ligands, and the structural flexibility of both the receptor and ligand needs to be taken into account during the docking process.²⁴¹ With the increase in computing power and resources, more refined docking algorithms and methods have been developed which also take into account advances in our understanding of flexible molecular recognition with regards to the receptor and ligand. In particular, the Induced-Fit binding model, which suggests that an enzyme will attempt to assume a different conformation upon ligand binding in order to maximize the interactions between the protein and the ligand (Figure 1.29).²⁴²

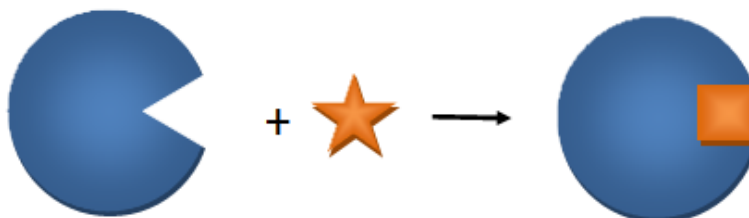


Figure 1.29. A schematic diagram of the Induced-Fit model for the binding of a ligand into an active site.

Released in 1982, DOCK made use of rigid spheres as representations of the atoms in the receptor and ligands, and removed all internal degrees of freedom.²⁴⁰ This first docking software portrayed the receptor as a collection of spheres in pockets and grooves within the binding site rather than depicting the individual receptor atoms. The 1986 release of DOCK introduced an algorithm which accounted for

the flexibility of the ligand by splitting the ligand into fragments, and then docking those fragments into the binding site, with the flexibility of the ligand incorporated into the connections between the fragments upon reassembly.²⁴³

While the developers of DOCK were tackling the problem of ligand flexibility, other software developers were attacking the problem from the other side by working on creating grid files which contained both chemical and physical information about the receptor. These grid files pre-calculate information which is reused for each ligand, and so increase the efficiency of the docking methods. The program GRID pre-calculated the potential energy of receptor-ligand interactions with various functional groups¹⁸⁵ and DOCKER made use of the grid files to extend the Van der Waals radii of the receptor atoms.²⁴⁴ Including approximations to directly calculate the protein-ligand interactions by combining the Van der Waals, Coulombic and hydrogen bonding contributions greatly improved these grids, and thus set the standard for the use of automated grid file in future docking programs.²⁴⁵⁻²⁴⁶

1.2.2. The First Step: Docking and Pose Evaluation.

“Science is fun. Science is curiosity. We all have natural curiosity. Science is a process of investigating. It’s posing questions and coming up with a method. It’s delving in.”

Sally Ride

Modern docking procedures generally involve four main steps – the creation of a receptor grid, generation of ligand conformations, docking of these conformations, and finally assigning a score to the docked ligand poses (Figure 1.30), although the specifics of each depend on the software used as well as docking method. The majority of docking software packages make use of receptor grid files containing structural and chemical information about the receptor, as well as including potential interactions with the ligand, and these grid files contains the coordinates and charges of the receptor atoms within a distinct binding area. The protein-ligand interaction energies are usually pre-computed and included in a table contained within the grid file, along with the location and dimensions of the binding site, obtained either through prior knowledge of the protein structure or through the use of binding site prediction software.²⁴⁷⁻²⁵⁰ This pre-calculation of data saves a large amount of computational time, especially when virtual screens containing millions of compounds are performed, as the energy calculations are not performed for every docking procedure. This grid can also be altered depending on the final goal of the

docking procedure – a small grid is used when trying to reproduce a crystal structure conformation, while a larger grid is used for the screening of new inhibitors as the binding mode and size of the new ligand might vary significantly.²⁵¹



Figure 1.30. The steps in modern docking processes.

The flexibility of the receptor is taken into consideration by a number of methods, with the first method making the atoms of the receptor “soft” by reducing the Van der Waals repulsion of overlapping atoms²⁵² and this method is still used today.²⁵³⁻²⁵⁴ Explicit protein flexibility was put into practice a few years later by exploring the flexibility of the rotatable bonds on the protein side chains.²⁵⁵⁻²⁵⁷ Different receptor structures are created by identifying rotatable bonds and systematically sampling the torsions of those bonds. Simple methods consider only the rotation of polar hydrogen atoms on receptor side chains, while more complex methods can include all possible rotatable bonds of specified side chains.

The most complex algorithms however, involve the simultaneous optimization of the ligand and the active site during the docking process,²⁵⁸⁻²⁶⁰ such as the Induced Fit Docking (IFD) protocol employed by the Schrödinger program suite.¹⁷² Under this protocol, ligands are docked into a receptor structure with a soft van der Waals potential, and the protein is relaxed iteratively until the structure of the protein is constant.²⁵³ Molecular dynamics can also be used to sample the conformations of proteins, and structures from these simulations can be used in ensemble-based docking methods, such as the relaxed complex scheme.²⁶¹⁻²⁶⁴ These ensemble-based schemes deal with the flexibility of the protein as a whole, either with or without a ligand present, while only localized protein flexibility is addressed with the rotation of side chains.²⁵¹

As ligands are significantly simpler than receptors, ligand conformation generators are employed more widely than the methods utilizing flexible receptors, and this is particularly the case when the binding mode of a ligand is unknown. Docking programs create a variety of different ligand conformations using a number of processes; however in most cases the bond distances are not varied. Docking protocols have come a long way from the 1986 version of DOCK, where the ligand was fragmented, the fragments

docked, and then the fragments reassembled into the complete ligand again.²⁴³ Recent docking methods include the use of energy optimization techniques, where the docked structure is minimized in order to maximize protein-ligand interactions²⁶⁵⁻²⁶⁶ while the most common approaches involve the use of genetic algorithms to generate possible ligand conformations.

Initially proposed by Judson *et al.*,²⁶⁷ and used by programs such as DARWIN,²⁶⁸ GOLD²⁶⁹ and AutoDock²⁷⁰ amongst others,²⁷¹⁻²⁷³ genetic algorithms use evolutionary ideas to find solution to search and optimization problems, such as determining the best binding mode for a ligand in an active site. With a genetic algorithm approach, a range of ligand conformations are generated and docked into the receptor site, before the coordinates and torsions of the lowest energy structures are used to generate a new pool of structures.²⁵¹ This process is repeated for a specified number of generations in order to determine the lowest energy binding modes for each ligand, with “mutations” randomly added to create new torsion and/or coordinate values, which ensures the diversity of the ligand conformations. As genetic algorithm methods are stochastic in nature, different ligand poses are generated through the use of random numbers to vary the internal torsions, rotations and translations of the rotatable bonds, and the results from docking programs, such as Schrödinger’s LigPrep program¹⁷², will differ from one run to another regardless of the input ligand structure.²⁷⁴ AutoDock²⁷⁵ and other similar stochastic programs perform energy minimization calculations on the structures, followed by an evaluation of the Metropolis criterion²⁷⁶ using Monte Carlo²⁷⁷ methods in order to determine which ligand conformations will give rise to the next generation of ligands.²⁷⁸

On the other hand, deterministic docking programs, such as CHARMM²⁷⁹ use a systematic approach – molecular dynamics and energy minimization - which leads to identical results if the same calculation is carried out on the same processor repeatedly, but even these results can vary depending on the coordinates of the input ligands, especially for conformer generation algorithms that use structure minimization methods.²⁸⁰ The downside to these deterministic methods is that they often get stuck in an energy “rut” – the energy barrier is too large for the algorithm to overcome, and the ligand is trapped in an energy minimum. As this prevents all the conformations from being sampled accurately, some molecular dynamics algorithms have implemented the use of biasing potentials in order to lower these energy barriers^{279,281-282} and sampling at higher temperatures has also been used to improve the docking results.²⁸³⁻²⁸⁴

Glide, the docking program from Schrödinger,²⁸⁵ is unique in the fact that the docking process employed is a combination of both deterministic and stochastic methods. An exhaustive search of torsion angle space generates ligand conformations, followed by a quick initial screening of all the generated poses. Promising poses are then minimized within the active site using the standard molecular mechanics “Optimized Potentials for Liquid Simulations - all atoms” (OPLS-aa) force field, which is combined with a distance-dependant dielectric model.²⁸⁶ A post-minimization Monte Carlo procedure applied to the internal dihedral angles of between three and six of the best poses allows for the optimization of the structure within the binding site by sampling the local torsional minima present present.²⁵¹

1.2.3. Scoring Functions: The Maths Behind It All.

“Today's scientists have substituted mathematics for experiments, and they wander off through equation after equation, and eventually build a structure which has no relation to reality.”

Nikola Tesla

Regardless of how good a docking algorithm is, if it cannot predict the binding affinity of the ligand poses then those poses are worthless. While more sophisticated calculations, such as free energy perturbation²⁸⁷ or thermodynamic integration²⁸⁸ exist, molecular docking programs use a simplified equation or set of equations – a “scoring function” – to approximate a binding score. These scoring functions allow for the calculations of large numbers of protein-ligand binding affinities quickly and efficiently, as would be the case in a HTVS of millions of potential drug candidates. Each docking program uses a slightly different scoring function, one matched to the docking algorithm used, however, in general, scoring functions can be separated into one of three categories – Force-field based, Knowledge-based or Empirical.²⁸⁹

The most computationally expensive scoring functions, force-field-based scoring functions are designed on first-principles, and correspond to non-bonded interactions, such as electrostatic and van der Waals interactions. The electrostatic interactions are predicted using a Coulombic interaction term, which is based on the distance and the charge between two atoms, with the distance assigned a cut-off point to reduce the computational requirements. The van der Waals contribution are described by a

Lennard-Jones potential function²⁹⁰ (Equation 1), where ϵ is the depth of a potential well, σ the finite distance where particle-particle potential is zero, r the distance between particles and r_m the distance where the potential is at a minimum. This equation is designed to approximate both the repulsive and attractive non-polar interactions present. Several force-field based programs, including GOLD,²⁹¹ AutoDock²⁷⁰ and DOCK²⁹² include functional forms of other energy terms in their scoring functions to account for the contributions of hydrogen bonding, entropy and solvation energies.²⁵¹

$$V_{LJ} = 4\epsilon \left[\left(\frac{\sigma}{r} \right)^{12} - \left(\frac{\sigma}{r} \right)^6 \right] = \epsilon \left[\left(\frac{r_m}{r} \right)^{12} - 2 \left(\frac{r_m}{r} \right)^6 \right] \quad (1)$$

The frequencies of specific atom-atom interactions in known protein-ligand complexes form the basis of knowledge-based scoring functions. In this approach, the interactions of experimental protein-ligand structures are analyzed for distance and frequency, and the more often that a particular interaction occurs, the more favorable that interaction is considered. The contact populations are converted into a scoring function, where the attractive interactions are favoured over the repulsive reactions. Knowledge-based scoring functions, including DrugScore,²⁹³ PMF score,²⁹⁴ and SMOG,²⁹⁵ are simple, fast and computationally inexpensive, and are usually limited by the set of protein-ligand structures chosen as the test set, but they can be expanded to include specific interactions, such as π -stacking and interactions with phosphorus, sulfur, halogens or metal atoms.²⁵¹

Empirical scoring functions, such as those found in FlexX,²⁹⁶ LUDI,¹⁸⁷ and ChemScore,²⁹⁷ are also simple and cheap from a computational infrastructure point of view. These equations can be separated into discrete energy terms, such as solvation free energies, hydrogen bonding, ionic interactions, entropic contributions, and non-polar interactions, but they do not reflect classical non-bonded interaction functional.²⁵¹ In the case of the ChemScore equation (Equation 2), the constants, C , are determined from a set of test complexes, the first two summation terms cover all hydrophobic and hydrogen-bonding interactions for all the atom-atom pairs and the final summation term covers any and all pairwise contacts between metal atoms in the receptor and the ligand atoms. The functions f , g and h are distance (r) and/or angle (α) dependant functions with the subscripts lr and lm denoting ligand-receptor or ligand-metal distances or angles. The final term, $C_{rotb}H_{rotb}$, accounts for the inflexibility of ligand bonds by applying an entropic penalty to the frozen bonds, which are defined as a rotatable bond where atoms on either side of a bond are in contact with the receptor.²⁵¹ Empirical scoring functions are

based on the premise of fitting data from receptor-ligand complexes with known binding affinities, and, while quick to evaluate, the accuracy of these functions is dependent on the set of complexes used to determine the coefficients used in the equations. If the test set has problems, for example not containing enough or a wide enough variety of complexes, the accuracy of the scoring function is negatively affected when a complex not in the test set is included.²⁵¹

$$\Delta G_{bind} = C_0 + C_{lipo} \sum f(r_{lr}) + C_{hb} \sum g(\Delta r)h(\Delta\alpha) + C_{metal} \sum f(r_{lm}) + C_{rotb}H_{rotb} \quad (2)$$

The two scoring functions present in Glide – Standard-Precision (SP)²⁸⁵ and Extra-Precision (XP)²⁹⁸ – make use of empirical methods which are based on the ChemScore function (Equation 2 above), however each of these Glide functions makes use of an expanded equation. The SP function (Equation 3) expands the summations found in the ChemScore function into more specific categories in order to improve the enrichment of results, especially those associated with the docking of diverse ligands.²⁹⁹

$$\begin{aligned} \Delta G_{bind} = & C_{lipo-lipp} \sum f(r_{lr}) + C_{hb,nn} \sum g(\Delta r)h(\Delta\alpha) + C_{hb,nc} \sum g(\Delta r)h(\Delta\alpha) \quad (3) \\ & + C_{hb,cc} \sum g(\Delta r)h(\Delta\alpha) + C_{max,mi} \sum f(r_{lm}) + C_{rotb}H_{rotb} \\ & + C_{pol,phob}V_{pol,phob} + C_{coul}E_{coul} + C_{vdw}E_{vdw} + solvation \end{aligned}$$

In Equation 3, the first term, which accounts for lipophilic or hydrophobic interactions is unchanged from the original ChemScore equation, but the single hydrogen bonding term is expanded into three individually weighted terms. This takes into account the different hydrogen-bonding interactions and their different contributions to the docking score, as hydrogen bonds between two neutral functional groups have been shown to be the most favourable, while interactions between two charged species are the least favourable. The interaction of charged ligand functional groups with receptor metal ions is described by the fifth term, with the sixth term taking the entropic cost of restricting the motion of the ligand into account. Favourable interaction energies of polar groups without hydrogen bonding capabilities in hydrophobic regions is covered by the seventh term, and terms eight and nine account for Coulombic and Van der Waals interactions respectively, with the final term accounting for solvation effects by explicitly docking water molecules into the binding site. Often neglected in docking scoring functions as they are usually computationally expensive, the solvation terms describe the solvated polar and charged groups on both the ligand and the receptor and are estimated by the explicit water molecule docking.²⁵¹

The SP portion of Glide is well suited to the initial screening of large numbers of ligands in a relatively short period of time, while the XP scoring function is better suited to the calculation of more accurate docked poses and the corresponding binding affinities. SP is “softer”, and allows for some flaws in the docked pose, whereas poses which violate known physical chemistry properties, such as loss of entropy, protein or ligand strain and desolvation effects, are heavily penalized by XP. There is a downside to the increase in accuracy of XP however – XP calculations are more expensive resource-wise, and are thus better suited to smaller numbers of compounds. The scoring function used to calculate Glide XP scores (Equation 4)²⁹⁸ is similar in structure to the scoring function used by SP. It contains energy contributions from Coulombic and Van der Waals interactions ($E_{coul} + E_{vdW}$ respectively), and also includes the favourable contributions due to binding interactions (E_{bind}) as well as the unfavourable contributions ($E_{penalty}$)²⁵¹.

$$XP\ GlideScore = E_{coul} + E_{vdW} + E_{bind} + E_{penalty} \quad (4)$$

The E_{bind} term can be further divided into individual interactions (Equation 5). E_{he} accounts for the favourable interaction energy of a lipophilic group on a ligand being surrounded by hydrophobic regions rather than the water molecules initially situated in that region, as well as for accounting for the reduction in the unfavourable interactions between said lipophilic group and the bulk water molecules upon binding. The $E_{hb,nm}$ term approximates the increased significance of hydrogen bonding between neutral groups of the ligand and receptor, something identified through both experimental and theoretical analyses of pharmaceutical drugs and their targets. $E_{hb,cc}$ accounts for the contributions of charged-charged hydrogen bond motifs, E_{pi} the favourable pi-cation and π - π stacking interactions, with the final terms dealing with the placement of halogen atoms into a hydrophobic area of the receptor and the application of a correction term in order to improve the binding affinity of smaller molecules which are unable to form the same number of interactions with the protein as a larger ligand.²⁵¹

$$E_{bind} = E_{he} + E_{hb,nm} + E_{hb,cc} + E_{PI} + E_{hb,p} + E_{phob,p} \quad (5)$$

The $E_{penalty}$ term is also separated into individual contributors (Equation 6), with E_{desolv} calculated in a similar manner as the desolvation term found in the SP scoring function, however the XP scoring function is more rigorous and weighted differently as it utilizes increased sampling techniques when docking the water molecules, and the calculation efficiency is improved as the energies are pre-

calculated when the receptor grid is generated.²⁵¹ While it does not comprise a significant portion of the overall binding energy, the E_s term penalizes those docked conformations with close internal contacts, and in doing so takes into consideration the internal strain present in these high-energy structures.²⁵¹

$$E_{penalty} = E_{desolv} + E_{Is} \quad (6)$$

While docking programs are designed to assess the ability of a ligand to bind to a specific receptor conformation, there are a number of restrictions that must be considered. Algorithms and scoring functions are intended to be relatively accurate within a timeframe which would allow for the screening of millions of compounds, and as such the results should not be the sole method for determining the binding of a ligand to a receptor. The poses generated from any of the docking algorithms are static, and do not take into account the dynamics involved in protein-ligand interactions. Other theoretical methods, such as molecular dynamics, and more sophisticated free energy calculations, such as a Molecular Mechanical/Generalized Born Surface Area (MM/GBSA) approach, should follow the initial docking calculations, as these more accurately represent the complex. A recent review by Plewczynski *et al.*³⁰⁰ highlights this point, as they found little consistency between the results of a number of docking algorithms, and more importantly, no correlation between the docking scores and *in vitro* binding affinities was observed.

1.2.4. The Final Hurdle: The Role Of Post Processing in Computational Drug Design.

“A computer lets you make more mistakes faster than any other invention in human history, with the possible exceptions of handguns and tequila.”

Mitch Ratcliffe

An important goal in drug design is the reliable estimation of the free energies of protein-ligand binding. Since the inception of computational free energy calculations, a number of approaches have been proposed, each with their own benefits and drawbacks.³⁰¹⁻³⁰³ These approaches range from fast but relatively inaccurate methods based on rough physical estimates to resource-intensive methods based on less harsh approximations of real physics.³⁰³ Ideally these free energies would be calculated directly (Figure 1.31), however, the vast majority of the energy contributions in these calculations would arise from interactions between solvent molecules, and these changes are often an order of magnitude larger than the binding energies.

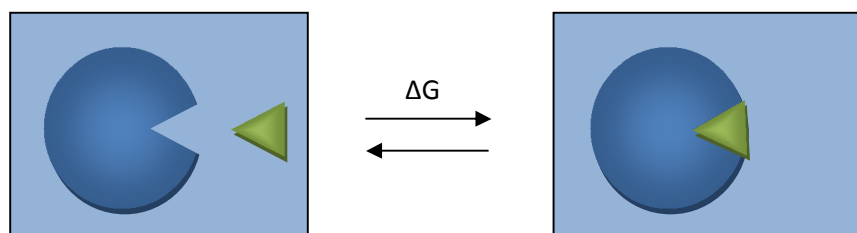


Figure 1.31. Ideal method for the calculation of free energy, using the “Lock and Key” model for simplicity.

As direct calculation of binding energies is not possible, it is necessary to divide up the calculations into smaller, more manageable pieces. One method of division is the MM/GBSA approach, where the free energy of binding is calculated from the differences between the free energies of the ligand, the protein and the complex in solution, and this method is the fastest force-field based method currently available.³⁰³⁻³⁰⁵ This process is founded on the idea that a combination of molecular mechanics (MM) energies, polar and non-polar solvation terms and an entropy term can describe the free energy of binding of a ligand to a receptor.³⁰³⁻³⁰⁵ The free energy for each component is converted into a gas phase MM energy term (ΔE_{MM}), a solvation term (ΔG_{solv}) and an entropy term ($T \cdot \Delta S$) (Equation 7).³⁰⁶

$$\begin{aligned} \Delta G &= \Delta E_{MM} + \Delta G_{solv} - T \cdot \Delta S \\ &= \Delta E_{bat} + \Delta E_{vdW} + \Delta E_{coul} + \Delta G_{solv,p} + \Delta G_{solv,np} - T \cdot \Delta S \end{aligned} \quad (7)$$

E_{MM} can be deconstructed into ΔE_{bat} (the sum of bond, angle and torsion terms in the force field), a Van der Waals term (ΔE_{vdW}) and a Coulombic term (ΔE_{coul}), while ΔG_{solv} can be broken into individual polar ($\Delta G_{solv,p}$) and non-polar ($\Delta G_{solv,np}$) components while $\Delta G_{solv,np}$ is computed as a linear function of the solvent-accessible surface area (SASA). $\Delta G_{solv,p}$ is usually calculated by solving the Generalized-Born equation (Equation 8) where ϵ_0 is the permittivity of free space, ϵ the dielectric constant, q_i the electrostatic charge on particle i , r_{ij} the distance between particles i and j and a_i the effective Born radius.³⁰³ The entropy term $T \cdot \Delta S$ is, in most cases, ignored for calculations involving congeneric series or relative free binding energies, as the calculation of this term can be a major source of errors³⁰⁶⁻³⁰⁸ however some research groups still support its use in free energy calculations.³⁰⁹

$$G_s = \frac{1}{8\pi} \left(\frac{1}{\epsilon_0} - \frac{1}{\epsilon} \right) \sum_{i,j}^N \frac{q_i q_j}{f_{GB}} \quad (8)$$

$$\text{where } f_{GB} = \sqrt{r_{ij}^2 + a_{ij}^2} e^{-D}$$

$$\text{and } D = \left(\frac{r_{ij}}{2a_{ij}} \right)^2, a_{ij} = \sqrt{a_i a_j}$$

As with most computational methods, the accuracy of the results of the MM/GBSA calculations depend on how good the underlying algorithm or model is. Schrödinger's Prime³¹⁰⁻³¹¹ makes use of an energy model known as VSGB 2.0,³¹² and in this energy model, the determination of the MM energies is based on the OPLS protein force fields, and are enhanced by a number of physics-based corrections, including terms for the more accurate treatment of hydrogen bond interactions and π -stacking.^{286,303,312-313} The implicit solvent model derives from a variable surface Generalized Born approach, wherein the variable dielectric value for each residue is fitted to a substantial set of loop and side-chain predictions, and the non-polar solvation free energy ($\Delta G_{solv,np}$) is calculated from a parametrized hydrophobic term.³⁰³ While a number of different approaches have been used to calculate binding affinities between ligands and proteins, several studies have shown that the Generalized Born method compares satisfactorily with the more computationally expensive Poisson-Boltzmann approach (MM/PBSA), which uses the significantly more complex Poisson-Boltzmann equation (Equation 9).³⁰⁶⁻³⁰⁸ Other studies have also supported the use of the Generalized Born approach, as the energies calculated after protein-ligand complex minimizations in implicit solvent gave correlations to the experimental data which were similar to those obtained using lengthy molecular dynamics simulations in explicit solvents.^{306-308,314}

$$\vec{\nabla} \cdot [\epsilon(\vec{r}) \vec{\nabla} \Psi(\vec{r})] = -4\pi \rho^f(\vec{r}) - 4\pi \sum_i c_i^\infty z_i q \lambda(\vec{r}) e^{\frac{-z_i q \Psi(\vec{r})}{kT}} \quad (9)$$

A recent study by Greenidge *et al.*³⁰³ found a significant correlation ($R^2 = 0.63$) between the experimental data (K_d or K_i values) and the calculated MM/GBSA energies for a range of structurally diverse crystal structures. The results, which made use of a variable internal dielectric constant, showed that the MM/GBSA approach yields results which are comparable, at least in principle, among different targets, and they propose that this approach is likely to be more reliable for individual series. Their study also highlighted a number of limitations of the MM-GBSA method used – they found that the inclusion of crystallographic water molecules (water molecules within 3.5 Å of the ligand) results in lowered predictive accuracy, while the inclusion of ligand strain improves the overall accuracy of the calculations.

Ultimately, all of the main scoring functions and schemes, with different degrees of complexity in their calculations, face the same problems – how to deal with complexes containing ligand-metal ion interactions or water-bridged interactions, how to take into account the energetics of water displacement, entropy and highly strained ligands. The developers and users of the scoring schemes, be they MM/GBSA-based,³⁰⁴⁻³⁰⁵ classic scoring function-based^{293,315} or based on free energy perturbations,³⁰¹ need to take responsibility for understanding the biological target, the nature of the ligands, as well as the components comprising the scoring scheme used, as knowing the limits of a scheme or function could aid in identifying the causes of problems observed.

1.2.5. Finding the Diamonds In The Rough: Linking Theory and Practice through NMR Analysis of Molecular Flexibility In Solution (NAMFIS).

"Death is forever. But so are diamonds."

Ian Fleming, *Diamonds Are Forever*.

The role of computers in drug design does not stop once a potential drug has been identified or designed and sent through the various scoring functions available. Computer analysis can be used to predict pharmacokinetic properties such as ADME-Tox (Absorption, Distribution, Metabolism Excretion and Toxicity) qualities through Quantitative Structure-Activity Relationship (QSAR) or Quantitative Structure-Property Relationship (QSPR) calculations and other chemometric applications. Computational analysis can also aid in the identification of conformers of a flexible molecule in a solution. As the vast majority of drugs are flexible molecules which modulate the activity of proteins by binding to them in a single conformation – the "bioactive" conformation- the protein is required to pay a penalty, fundamentally an entropic one, for converting the conformation of a molecule in solution into the bound conformation.³¹⁶⁻³¹⁷ In order to avoid this penalty, the scientists designing a drug molecule will often use the protein-bound conformation if it is available through techniques such as X-ray crystallography in order to modify the structure of the molecule in order to "lock" the molecule into a favourable conformation prior to binding.

Unfortunately, determining the X-ray structure of every drug bound to every important protein is not possible. In some cases, the bioactive conformation is very close to one of the several conformations present in solution, and as such it is important that a list exists of all the conformations present for a flexible molecule in solution.³¹⁶⁻³¹⁷ There does not, however, have to be a correlation between the bioactive conformation and the population of that conformation in solution - as long as the bioactive conformation is part of the conformational equilibrium, the protein will be able to select that conformation, even if the bioactive conformation is 2-5% of the conformations in solution. The challenge, then, is the determination of the population frequencies of the conformations possible for a flexible molecule in solution, or the Boltzmann population distribution. This is more difficult than appears at first glance, as the relative free energies control the populations of equilibrating conformations in solution. There is an exponential relationship between the free energy and the

equilibrium constant (Equation 10), and as such, a small change in free energy (ΔG) results in a large change in the equilibrium constant (K). For example, for a molecule with only two conformations present in solution, with a 1.8 kcal/mol difference between the conformations, the lower energy conformation is present at approximately 97%, and if the energy difference is increased to 3 kcal/mol, the higher energy conformation is all but non-existent.³¹⁶⁻³¹⁷ In “real-life” cases involving highly flexible molecules, many more conformations are present, with very small energy differences between them, and a “dominant” conformation may only be present at ~20%.

$$\Delta G = -RT \ln K \quad (10)$$

While NMR spectroscopy is useful for determining chiral center configuration, determination of the population distribution using this technique is problematic. Almost all drugs are small molecules, under 500 Da in weight, and these molecules all tend to have a number of rotatable bonds. With three possible conformations present for each bond - two gauche and one anti conformations (Figure 1.32) - a molecule with 10 rotatable bonds could have 60,000 possible conformations.³¹⁶⁻³¹⁷ While some will be excluded due to steric clashes, a large number of these conformations will be present in solution. Reduction of the temperature at which an experiment is carried out at could remove some of the conformations, however unfeasibly low temperatures would be needed in order to account for the small energy differences present. NMR spectroscopy operates on a time scale in the order of tens of milliseconds, however the interconversion between conformations is significantly faster, and as such the structures determined through NMR spectroscopy are an average, and do not exist in reality.³¹⁶⁻³¹⁷

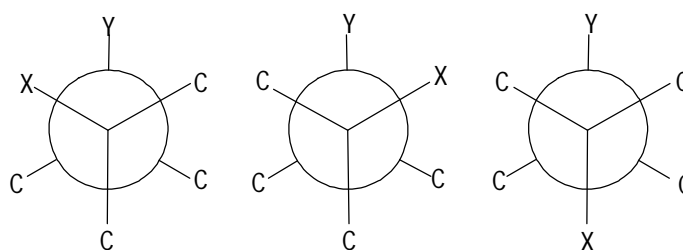


Figure 1.32. *Gauche* (left and center) and *anti-Gauche* (right) conformations.

As the structure determined through NMR spectroscopy is an average, the proton-proton coupling constant ($^3J_{H-H}$), which relates to the conformation through the Karplus Equation (Equation 11) and the resultant dihedral angles (ϕ ?),³¹⁸⁻³¹⁹ and the interproton distances determined through NOESY (Nuclear Overhauser Effect Spectroscopy) experiments are also averages.³²⁰⁻³²⁵ A single structure based on this

average data is therefore intrinsically incorrect. Another drawback is the detection limit of NMR spectroscopy - conformations present at about 2% are not detectable, even if these conformations are the bioactive conformations.

$$J(\phi) = A\cos^2\phi + B\cos\phi + C \quad (11)$$

However not all is lost. With the advancement in computational methods over the years, it is now possible to combine the average data from the NMR experiments with a set of computationally derived conformations and obtain the Boltzmann population distribution present in the solution. Named NMR Analysis of Molecular Flexibility In Solution, or NAMFIS, this method calculates the coupling constants and distances for each of the conformations generated during the conformer search, and then varies the mole fractions of these conformations until the calculated coupling constants and distances match those determined experimentally.³¹⁶⁻³¹⁷ While several combinations of conformations would satisfy the NMR data, NAMFIS decides which of the possible combinations is ideal based on a sum of square distances (SSD) metric.³²⁶

NAMFIS is able to identify individual conformations from average NMR data, and it reduces the many thousands of conformational possibilities into a relatively small number. In each of the cases studied so far, between 10 and 20 conformations were selected from the thousands generated during the conformational search.³¹⁶⁻³¹⁷ NAMFIS has also been used to elucidate the nature of bioactive conformations of a number of important drug molecules through the Boltzmann populations of the conformations present. One of the molecules studied using this approach is Taxol® (Paclitaxel) (Figure 1.33). An important cancer drug, the bioactive conformation of Taxol® in tubulin, as determined by electron crystallography, was found to be one of the smaller contributors to the NMR data, as it was present at only 2% in solution.³²⁷

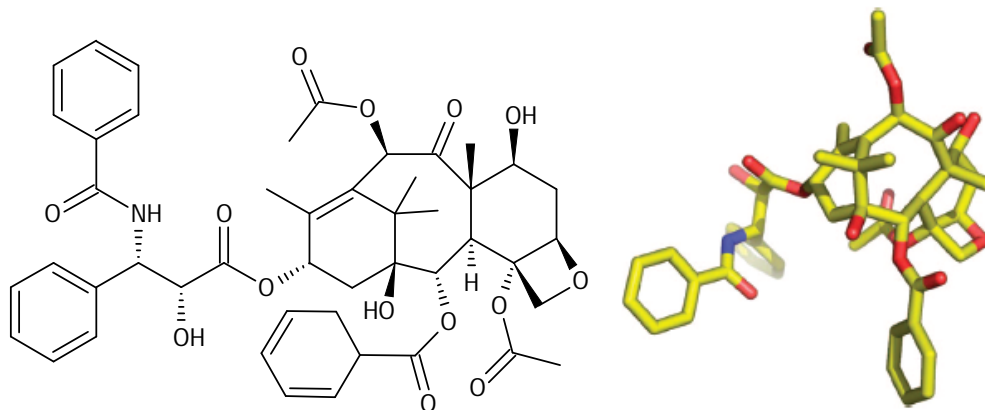


Figure 1.33. The 2D structure of Taxol® (left) and the 3D structure of Taxol® bound in tubulin (right).³²⁷

NAMFIS has also been recently used to show that dominant structure, as determined using the average NMR data, might not even occur amongst the conformations present in solution.³²⁸ In this case, the solution conformations of a 5-residue peptide, previously understood to form an α -helix in solution was shown to not include an α -helix, even as a minor conformation. This study also showed that attempting to “lock” a molecule into a specific conformation, as was done with this molecule using a metal atom, may not in fact constrain the molecule into that conformation.

NAMFIS is a powerful tool, which allows for a better representation of the NMR data as well as for correcting previous assumptions, and it also provides a starting point with which to explore the active site of a protein if the bioactive conformation is not known. NAMFIS is also able to overcome the common problem encountered in most modern docking procedures, where assigning high or low energy status to a theoretical conformation depends on the method used – as the structures satisfy NMR data, they are, by definition, low energy so as to exist in solution.³¹⁶⁻³¹⁷ One drawback to the more widespread use of NAMFIS is the amount of time and effort required to obtain accurate NOESY data from the NMR experiments and to extract the distances from this data. However, the information obtained through the use of NAMFIS vastly improved the understanding of the behavior of a molecule both in solution and bound in a protein, and it can aid in determining the bioactive conformations of important compounds, which in turn could lead to the design and implementation of drugs with better Boltzmann distributions of their bioactive conformations.

1.3. Indian Gold: The Story of Curcumin.

“Each spice has a special day to it. For turmeric it is Sunday, when light drips fat and butter-colored into the bins to be soaked up glowing, when you pray to the nine planets for love and luck.”

Chitra Banerjee Divakaruni, *The Mistress of Spices*

If a book was written about the most important plants used for medicinal purposes across the ages, a large chapter of this book would have to be devoted to *Curcuma longa* (Figure 1.34), the root of which is known as turmeric.³²⁹ Used for many centuries by practitioners of Indian Ayurvedic medicine as well as in Chinese traditional medicine, turmeric was and is still used to treat a wide range of afflictions such as jaundice, colic, chest pains and toothaches. Turmeric was also recommended to help with liver and stomach issues and menstrual difficulties, and was often used to aid in wound healing,³³⁰ to lighten scars and as an insect repellent and insecticide.^{329,331} Mentioned in Marco Polo’s descriptions of his 1280 journey to China and India, turmeric was initially introduced to European markets by Arab traders in the 13th century. And while Vasco de Gama introduced spices to the West after his visit to India in the 15th century, it was only during the British rule of India that turmeric was combined with other spices to yield “curry powder” as we now know it.³²⁹



Figure 1.34. Botanical view of the turmeric (*Curcuma longa*) plant.³³²

Or perhaps, more correctly, a large chapter of this book would be devoted to curcumin (Figure 1.35), the deceptively simple active ingredient in turmeric.³³³ Initially isolated in 1815, curcumin is merely one of a number of phytochemicals present in turmeric, the others include demethoxycurcumin, bisdemethoxycurcumin, triethylcurcumin, tetrahydrocurcumin, curcumenol, curcumol, turmerin, turmerones, turmeronols, zingiberene and eugenol.³³⁴ Turmeric is estimated to contain between two and five percent curcumin naturally, while the amount of curcumin found in commercially available preparations is approximately 75%, with the remaining 25% made up of demethoxycurcumin and bisdemethoxycurcumin, in ratios of approximately 18% and 7% respectively. These three compounds have also been isolated from other members of the *Curcuma* family, including *C. mannga*,³³⁵ *C. zedoaria*,³³⁶ *C. xanthorrhiza*,³³⁷ *C. aromatica* and *C. phaeocaulis*³³⁸ as well as in *Costus speciosus*,³³⁷ *Etingera elatior*³³⁹ and *Zingiber cassumunar*.³⁴⁰ Whether all three compounds are equally active is still a matter of debate. In most systems, curcumin is the most active compound³⁴¹⁻³⁴² but there are also systems in which bisdemethoxycurcumin is more active^{336,343} and there are thoughts that a mixture of the three compounds is more potent than any of the compounds alone.³⁴⁴⁻³⁴⁷ A number of other studies have also shown the effectiveness of curcumin-free turmeric extracts against benzo[a]pyrene-induced tumorigenesis in mice³⁴⁸ and 7,12-dimethylbenz[a]anthracene-mammary tumorigenesis in rats³⁴⁹ indicating that at least some of the activity of turmeric is independent of curcumin.

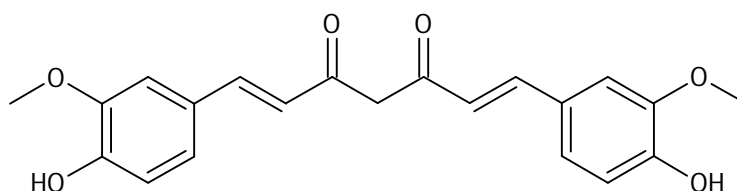


Figure 1.35. 2D structure of curcumin.

Despite the ongoing debate on whether curcumin or one of the 300 other identified compounds present in turmeric are the active agent responsible for the majority of the activity seen for turmeric,^{331,350} extensive research over the last 4 decades has shown curcumin to have therapeutic potential against a long list of diseases^{330,333,351} and the mechanism by which turmeric (or curcumin) could accelerate wound healing has been described in detail.^{345,352-359} Curcumin demonstrates remarkable activity against inflammatory disorders³⁶⁰⁻³⁶³, including pancreatitis,³⁶⁴⁻³⁶⁶ gastritis,³⁶⁷⁻³⁶⁸ colitis,³⁶⁹⁻³⁷¹ inflammatory bowel disease,³⁷² arthritis,³⁷³⁻³⁷⁶ allergy³⁷⁷⁻³⁷⁸ and fever,³⁷⁹⁻³⁸⁰ activity against various autoimmune disorders such as multiple sclerosis,³⁸¹⁻³⁸² diabetes,³⁸³⁻³⁹¹ scleroderma³⁹² and psoriasis³⁹³ and also exhibits antioxidant,^{331,394-395} anti septic, antimicrobial,³⁹⁶⁻³⁹⁹ and anticarcinogenic⁴⁰⁰ properties.

By inhibiting platelet aggregation, inflammatory responses, fibrinogen synthesis and the oxidation of low-density lipoproteins (LDLs), as well as by lowering LDL levels and elevating high-density lipoprotein (HDL) levels, curcumin is able to protect against thromboses and myocardial infarctions,^{329,331,401-410} and numerous studies have shown activity against various types of cancer,^{331,351,411} including neuroblastoma,⁴¹²⁻⁴¹³ squamous cell carcinoma,⁴¹⁴⁻⁴¹⁵ breast carcinoma,⁴¹⁶⁻⁴²¹ lung cancer,⁴²²⁻⁴²³ pancreatic carcinoma,⁴²⁴ hepatoblastoma,⁴²⁵⁻⁴²⁶ leukemia,⁴²⁷⁻⁴³³ non-Hodgkins lymphoma,⁴³⁴⁻⁴³⁵ multiple myeloma,⁴³⁶ basal cell carcinoma⁴³⁷ and melanoma.⁴³⁸⁻⁴⁴⁰ And as if the list of properties was not extensive enough, curcumin has been linked to the reduction of amyloid-induced inflammation, a characteristic of Alzheimers disease,^{119,441-446} and also shows chemosensitization, chemotherapeutic and radiosensitization activities.^{411,447-450}

Since the first reported use of curcumin to treat a human disease published in 1937,⁴⁵¹ the observations from 67 clinical trials have been published and another 33 are ongoing.^{351,452} Used either alone or in combination with other agents, such as gemcitabine, piperine, quercetin, soy isoflavones, docetaxel, sulfasalazine, prednisone, mesalamine, lactoferrin, pantoprazole and *N*-acetylcysteine, the clinical trials completed so far have shown curcumin to be beneficial as a treatment against a variety of human diseases, including cancers, skin disorders and cardiac disorders and curcumin has also shown protection against chronic arsenic exposure, alcohol intoxication and hepatic conditions.⁴⁵² The trials have also established the safety, non-toxicity and tolerability of large amounts of curcumin by patients suffering from a range of diseases, with doses of 8 g per day showing no negative side effects in these trials.⁴⁵² Current ongoing studies include evaluation of curcumin against cancer, arthritis and other inflammatory conditions, neurological conditions, diabetes and irritable bowel syndrome.⁴⁵² For some trials, curcumin is being administered alone, as nanoparticles, capsules, tablets, powders or solutions, while others involve the use of other agents and therapies, such as chemotherapy and radiation treatments.⁴⁵²

1.3.1. The Pleotropic Nature of Curcumin: A Simple Explanation.

"Happy is he who can trace effects to their causes."

Virgil

In an effort to understand the highly pleotropic activity of curcumin, a good place to start is by attempting to understand the possible ways in which curcumin could interact with a protein. Structurally, curcumin has two hydrophobic phenol rings connected by a flexible carbon chain, and the key to curcumin's ability to bind to many different targets lies within the flexibility of this molecule. Molecular docking studies have shown that curcumin can adopt a wide variety of conformations in order to maximize the interaction with the surrounding protein⁴¹¹ – the phenyl rings are able to participate in pi-pi van der Waals interactions with aromatic amino-acid side chains such as phenylalanine, tryptophan, histidine and tyrosine, while the carbonyl and phenolic functional groups are able to form hydrogen bonds to amino acids such as aspartate, asparagine, glutamate, serine, threonine and glycine. Curcumin is also able to bind to the minor groove of DNA, as it forms hydrogen bonds with AT-rich regions.⁴⁵³⁻⁴⁵⁴ Furthermore, as a β -diketone, curcumin undergoes keto-enol tautomerism (Figure 1.36), and the enol form dominates both in solution and in the solid state.⁴⁵⁵⁻⁴⁵⁶ This provides the curcumin molecule with additional modes of interaction with the protein as the enol enables the molecule to both accept and donate hydrogen bonds as well allowing the molecule to chelate the metal cations which are commonly found in the active sites of target proteins.⁴⁵⁷ An additional benefit to this keto-enol tautomerization is in the molecule's ability to undergo nucleophilic attack as a Michael acceptor, and as such curcumin is known to bind covalently to the sulfhydryls of cysteine as well as to the selenium in selenocysteine.⁴⁵⁸⁻⁴⁵⁹ In this manner, a wide range of possible protein interactions involving hydrophobic interactions, metal cation chelation, covalent bonding and hydrogen bonding are covered by one simple molecule.

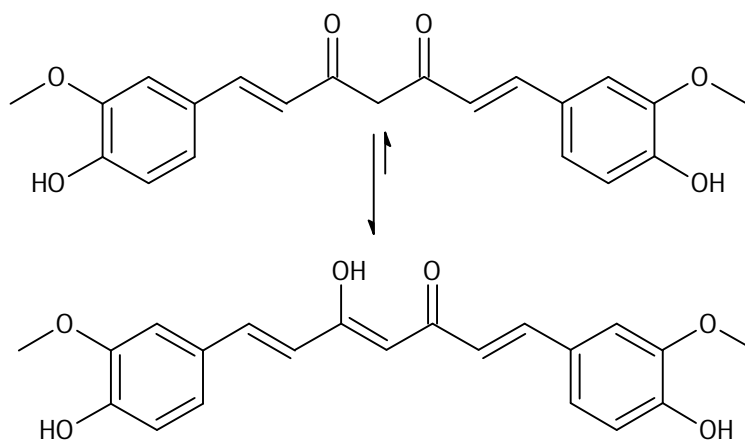


Figure 1.36. Keto-enol tautomerisation of curcumin.

While the list of diseases and disorders against which curcumin has shown activity appears lengthy, the answer could be very simple. Most chronic diseases have been shown to be the result of disregulated inflammation,⁴⁶⁰⁻⁴⁶¹ and since turmeric has traditionally been used as an anti-inflammatory agent, many diseases would appear to be treated with curcumin. In fact, curcumin could merely be resolving the inflammation rather than actually treating the source of the inflammation and therefore the root cause of the disease or disorder. Science has also provided evidence that curcumin in particular possesses potent anti-inflammatory properties,⁴⁶²⁻⁴⁷² although as a potent antioxidant, it is unclear at present whether the anti-inflammatory properties of curcumin are due to its antioxidant properties. As most well-known and well characterized antioxidant compounds do not show any anti-inflammatory properties, it is therefore unlikely that the antioxidant activity of curcumin alone is the reason for its remarkable anti-inflammatory properties.³²⁹

Another mystery in the activity of curcumin is what the metabolites of curcumin are and their respective activities, as mode of administration determines which metabolites are formed. For example, oral administration results in the formation of curcumin sulfonate and curcumin glucuronide,⁴⁷³ whereas systemic or intraperitoneal (i.p.) administration results in the metabolization of curcumin into tetrahydrocurcumin (which has been shown to be active in some systems but not in others^{351,361,474-478}), hexahydrocurcumin and hexahydrocurcuminol. It has also been suggested that it is the metabolites themselves which are responsible for the anti-inflammatory activity observed, rather than curcumin itself.⁴⁷⁹ However, when curcumin was substituted with the individual metabolites – in this case vanillin,

ferulic acid and feruloyl methane - none of the metabolites showed any significant activity, even at concentrations an order of magnitude greater than that used for curcumin.⁴⁷⁹

Regardless of the ongoing debate on whether curcumin or its metabolites are active, a large amount of research over the last 30 years has been directed towards understanding the effect of curcumin on modern molecular targets, such as transcription and growth factors, cytokines, kinases and other enzymes. Thanks to advanced molecular tools, it is now known that any given disease is controlled by over 500 different genes involved in signaling pathways, however current treatments are often based on the up or downregulation of a single target.⁴⁸⁰

The direct interactions of curcumin with some of these targets, the mode of interaction and the biological consequences of these interactions are as varied as the disorders traditionally treated with curcumin. Various inflammatory molecules such as tumor necrosis factor- α (TNF- α),⁴⁸¹ myeloid differentiation protein (MD-2),⁴⁸² cyclooxygenase-1 (COX-1) and COX-2⁴⁸³⁻⁴⁸⁴ and human α 1-acid glycoprotein⁴⁸⁵ have all been identified as direct targets of curcumin, as have a number of protein kinases, including protein kinase C (PKC),⁴⁸⁶ phosphorylase kinase,⁴⁸⁷ viral sarcoma (v-Src),⁴⁸⁸ glycogen synthase kinase (GSK-3 β)⁴⁸⁹ and ErbB2 (HER2/neu).⁴⁹⁰ Protein reductases such as thioredoxin reductase (TrxR)⁴⁵⁹ and aldose reductase (ALR2)⁴⁹¹⁻⁴⁹³ are direct targets of curcumin, as are histone acetyltransferase and deacetylase,^{458,494} glyoxalase 1,⁴⁹⁵⁻⁴⁹⁶ lipoxygenase,⁴⁹⁷⁻⁴⁹⁸ xanthine oxidase,⁴⁹⁹⁻⁵⁰⁰ lysozyme,⁵⁰¹⁻⁵⁰² matrix metalloproteinases,⁵⁰³ DNA methyltransferase 1 and polymerase- λ ,⁵⁰⁴⁻⁵⁰⁵ ribonuclease A,⁵⁰⁶ human immunodeficiency virus type 1 (HIV1) integrase and protease⁵⁰⁷⁻⁵⁰⁸ and sarco-(*endo*)-plasmic reticulum Ca²⁺ ATPase.⁵⁰⁹⁻⁵¹⁰ Furthermore, curcumin has also been found to interact directly with a number of carrier proteins such as immunoglobulin,⁵¹¹ human serum albumin,⁵¹²⁻⁵¹⁹ fibrinogen,⁵¹⁶ β -lactoglobulin⁵²⁰⁻⁵²¹ and caseins,⁵²²⁻⁵²³ as well as with cell survival proteins,⁵²⁴ prion proteins,⁵²⁵ DNA and RNA,⁴⁵⁴ metal ions such as Ca(II), Cu(II), Fe(II), Zn(III), Mn(II), and Pb(III),^{457,512,526-529} tubulin,⁵³⁰ CD13/aminopeptidase N⁵³¹ and β -amyloid aggregates,⁵³²⁻⁵³³ transthyretin⁵³⁴ and glutathione.⁵³⁵⁻⁵³⁶

1.3.2. *There's Always a Downside: The Trouble with Curcumin.*

"People are always looking for the single magic bullet that will totally change everything. There is no single magic bullet."

Temple Grandin

While curcumin appears to be a "magic bullet" for many diseases, and while a number of clinical trials are underway, it has not yet been approved as a therapeutic agent for any disease. The major reason for the lack of approval is the poor relative bioavailability of curcumin in the body. Despite an established maximum safe dose of 12 g per day,⁵³⁷⁻⁵³⁹ curcumin is poorly absorbed and rapidly metabolized, leading to low serum levels, limited tissue distribution, and a short half-life. Studies have shown that curcumin is poorly absorbed by mice and rats when delivered orally,⁵³⁹⁻⁵⁴² while the serum levels of curcumin were higher when the dose was delivered through i.p. or intravenous (i.v.) methods.⁵⁴³⁻⁵⁴⁴ Human clinical trials show similar trends, suggesting that mode of administration used is important in determining achievable serum levels.⁵⁴⁵ The pharmacokinetics of curcumin in tissues also depends on route of administration – the distribution of curcumin in body tissues when administered orally is different from the distribution observed for i.p. administration. In a study using a mouse model, i.p. administration resulted in curcumin being detected at appreciable amounts in the intestine, spleen, liver and kidneys, with only a trace amount detected in brain tissue,⁵⁴³ a finding supported by a second study using [¹⁴C]-labelled curcumin where the disappearance of radioactivity associated with the labeled curcumin molecule was monitored. Again, target organs were identified to be the liver, intestines and the kidneys, with radioactivity also detected in the lungs, muscles, heart and brain, but at much lower levels.⁵⁴⁶ In contrast, only the stomach, small intestine and cecum show traces of curcumin after oral administration.⁵⁴¹ Interestingly, in a study using tritium-labeled curcumin, the percentage of curcumin absorbed remained constant at between 60% and 66%, regardless of the dose, indicating that, in rats, there is a dose-dependent limitation to bioavailability, and that administration of additional curcumin does not result in greater absorption.⁵⁴²

As previously stated, curcumin undergoes a range of metabolism in the body, depending on the mode of administration, and as such, many studies have evaluated the pathways through which curcumin is metabolized. The first biodistribution study by Wahlstrom and Blennow reported that uptake of curcumin from the gut was poor,⁵⁴⁰ and the liver was identified later as the major site of metabolism

when ingested,⁵⁴⁷⁻⁵⁴⁸ with a further study identifying the major metabolites as glucuronides of tetrahydrocurcumin and hexahydrocurcumin, along with the minor metabolites dihydroferulic acid and ferulic acid.⁵⁴⁹ Pan *et al.* subjected plasma samples to hydrolysis with glucuronidase, and the results showed that 99% of the curcumin present in the plasma was present as the glucuronide conjugate.⁵⁴³ This study also revealed that glucuronide conjugates of dihydrocurcumin and tetrahydrocurcumin, along with curcumin-glucuronide and unconjugated tetrahydrocurcumin, are the major *in vivo* metabolites of curcumin, findings supported by Ireson *et al.*⁴⁷³ and Asai and Miyazawa.⁵⁵⁰ Curcumin was shown to undergo reduction, most likely through alcohol dehydrogenase, followed by conjugation to curcumin sulfate or curcumin glucuronide in the gastrointestinal tract by Hoehle and co-workers,⁵⁵¹ which identified this route as having important implications for the pharmacokinetic fate of curcumin *in vivo*, however, neither the glucuronide nor the sulfate derivatives show the same level of biological activity as curcumin.^{473,552}

Due to the poor bioavailability of curcumin and the related metabolism problems, several strategies have been explored and employed in attempts to improve the bioavailability of curcumin. The main focus points include metabolic pathway blocking by other agents, conjugation and structural modifications made to the curcumin molecule itself.⁵⁵³ By far the most common strategy for increasing the bioavailability of curcumin is the concomitant use of agents which are able to block the metabolic pathways of curcumin. Piperine is a known hepatic and intestinal glucuronidation inhibitor, and a study using healthy human volunteers showed that the bioavailability of 2 g of curcumin was increased 2000% simply by the administration of 20 mg of piperine.⁵³⁹ Other approaches which have shown promise include the use of nanoparticles,⁵⁵⁴ liposomes,⁵⁵⁵⁻⁵⁵⁸ phospholipid complexes⁵⁵⁹ and micelles.^{331,450} For example, curcumin nanoparticles prepared by Cheng *et al.* resulted in significantly higher plasma concentration, and the residence time in mice brain was 6-fold higher than that of regular curcumin,⁵⁶⁰ and polylactic-co-glycolic acid-encapsulated curcumin exhibited two-fold greater serum concentrations in animals.⁵⁶¹ Cyclodextrin has also been used to improve the delivery and bioavailability of curcumin, and studies show that the cellular uptake and half-life in cancer cells is increased as compared to that of free curcumin.⁵⁶²

There are a number of side effects related to the pleiotropy of the curcumin that need to be addressed as the development of more bioavailable formulations of curcumin continues. Curcumin has been shown to interact with and inhibit the activity of drug-metabolising enzymes, such as glutathione

s-transferase and cytochrome p450 both *in vitro* and in some animal models,^{343,563-564} and this raises the risk of accumulation of drugs such as acetaminophen, morphine and digoxin in the systems of people who are taking curcumin alongside these drugs. Curcumin has also been shown to induce DNA damage in cells, and increased curcumin levels in the cells could result in the induction of DNA alterations which are common in carcinogenesis.⁵⁶⁵ As a metal cation chelator, curcumin has been linked to the induction of anemia in mice⁵⁶⁶ and as both a pro-oxidant and an antioxidant in cancer cells, concern has been raised about the positive and negative implications due to the dual role of reactive oxygen species for cancer.⁵⁶⁷⁻⁵⁶⁸ Other side effects related to large doses of curcumin include headaches, nausea and diarrhea,⁵⁵³ and in a one study intractable abdominal pain was reported as a side effect affecting 5 of 17 patients with advanced pancreatic cancer.⁵⁶⁹

The third strategy employed in the fight to improve the bioavailability of curcumin is the structural modification of the curcumin molecule. Modifications have ranged from simple substituent substitution, to almost complete redesigning of the curcumin molecule.³⁵¹ For example, the phenolic hydroxyl groups can be synthesized by the demethylation of the methoxy groups³⁶⁰ and can be alkylated, acylated, glycosylated and amino acylated.⁵⁷⁰⁻⁵⁷² The linker chain can also be acylated using an arylidene group or alkylated.⁵⁷² Many of these derivatives have shown enhanced bioavailability and increased activity against a range of diseases, for instance a mono-carbonyl analogue of curcumin, B63, showed greater antiproliferative activity against colon cancer cells than curcumin did, and a dose of only 50 mg/kg of B63 was required to achieve results obtained for a 100 mg/kg dose of curcumin.⁵⁷³ Hydrazinobenzolcurcumin has been shown to induce A549 cell autophagy,⁵⁷⁴ and bis-dehydroxycurcumin shows the ability to induce autophagy in human colon cancer cells whilst leaving normal cells untouched.⁵⁷⁵ A fluoro-curcumin derivative designed and synthesized by Padhye *et al.* has demonstrated the ability to significantly decrease the level of PGE₂ by inhibiting COX-2 activity,⁴⁸³ and the curcumin analogue B06 was reported to exhibit enhanced anti-inflammatory activity through the inhibition of c-Jun N-terminal kinase/NF-κB activation as compared to curcumin.⁵⁷⁶ 5-Chlorocurcumin shows free radical scavenging properties,⁵⁷⁷ and a semicarbazole derivative of curcumin has shown efficient antiproliferative and antioxidant properties.⁵⁷⁸ Curcumin analogues have also been shown to inhibit angiogenesis^{450,579} and to bind directly to proteasomes,⁵⁸⁰ matrix metalloproteinases,⁵⁰³ DNA polymerase-λ,⁵⁰⁴ RNAse,⁵⁰⁶ protein kinase C,⁴⁸⁶ and Ca²⁺/calmodulin.⁵²⁷

1.4. A World of Pain: The Role of Cyclooxygenase in How We Feel Pain.

"Life is pain, Highness. Anyone who says differently is selling something."

The Man in Black, *The Princess Bride*

If what studies have told us are true, and that most diseases are caused by dysregulated inflammation,^{460-461,581} then perhaps a good way to treat a number of diseases would be to treat the inflammation rather than to treat the symptoms of the inflammation. In order to do this, it is vital that the mechanism and biochemical pathways of pain are well understood so that we might understand how these mechanisms and pathways can be blocked. As the great Chinese general, strategist and philosopher Sun Tzu said in *The Art of War*, "The supreme art of war is to subdue the enemy without fighting."⁵⁸²

Nociception, from the Latin "*noci*" meaning *to hurt*, is the process by which a painful stimulus is relayed from the site of stimulation to the central nervous system.⁵⁸³ There are four main steps in this process, namely stimulation, reception, transmission and pain center reception. Stimuli can be either mechanical, such as pressure, puncturing or cutting, or chemical, such as a burn. Normal perception of stimuli, such as a light touch or temperature, involves the use of somatic receptors, but when a stimulus causes pain, specific nociceptors are activated first. Nociceptors are lightly or non-myelinated and conduct signals slower than the myelinated somatic neurons, and these receptors sense pain through free nerve endings, while the somatic neurons have specialized endings. Like somatic cells, nociceptor neurons travel in peripheral sensory nerves and their cell bodies lie in the dorsal root ganglia of peripheral nerves just inside the spine. Nociceptor neurons have been identified in skin, muscle and joint tissues and in some internal organs, although the situation in the organs is more complex.⁵⁸⁴⁻⁵⁸⁷ Two classes of nociceptors have been identified, namely the thinly myelinated, faster conducting A δ fibres and the non-myelinated slower C fibers.⁵⁸⁸ A δ fibers can be further split into mechanosensitive receptors which respond to mechanical stimuli such as pressure and touch, and mechanothermal receptors which respond to heat as well as mechanical stimuli.⁵⁸⁹

The initial sharp pain felt immediately after stimulation results from a signal being conducted by the A δ receptors (Figure 1.37), and the prolonged dull ache which follows is conducted along the C fibers. Once a signal is received, it is transmitted into the spinal cord through the dorsal roots where synapses on neurons in the dorsal horn are made. These secondary neurons then transmit the signal through the spinothalamic tract to the thalamus through the medulla, where it is relayed to various areas of the somatosensory cortex.^{583,590-591} Signals are then sent to the motor nerves *via* the motor cortex and the spinal cord, causing muscle contractions which remove the body part from the source of stimulation. Signals are also transmitted to the midbrain from the somatosensory cortex and the hypothalamus which synapse on the ascending pathways to inhibit additional ascending signals.⁵⁹²

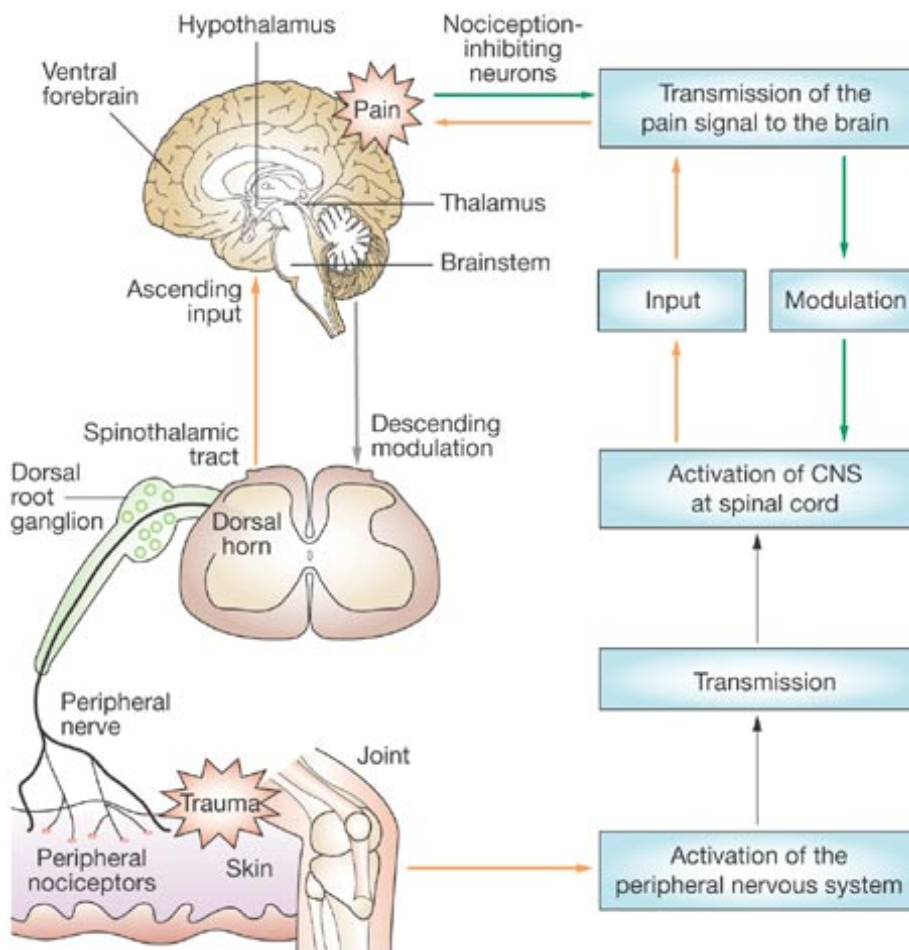


Figure 1.37. The nociceptive pain pathway.⁵⁹³

1.4.1. Pain Management: What Really Happens.

“And no, I do not have a pain-management problem, I have a pain problem.”

Dr Gregory House, *House, M.D.*

Pain management after an injury can be accomplished by interrupting the flow of impulses from the site of injury to the brain. Pain can be blocked at the injury site, along the nerve itself, and finally at the synapses in the spine and in the brain (Figure 1.38). Local anesthetics work by inhibiting the voltage-gated sodium channels in the neuron cell membrane, which effectively prevents signals from being conducted to the brain.⁵⁹⁴ With local anesthetics, a state-dependent blockade arises, as these drugs bind more rapidly to activated sodium channels in neurons that are rapidly firing. Opiate-based painkillers attach to opioid receptors found in the brain and spinal cord.⁵⁹⁵ Activation of these receptors leads to closing of the voltage sensitive calcium channels, reduction in the production of cyclic adenosine monophosphate (cAMP) and stimulation of potassium efflux. This results in a reduction of neuronal cell excitability and nerve impulse transmission, along with inhibition of neurotransmitter release.⁵⁹⁵

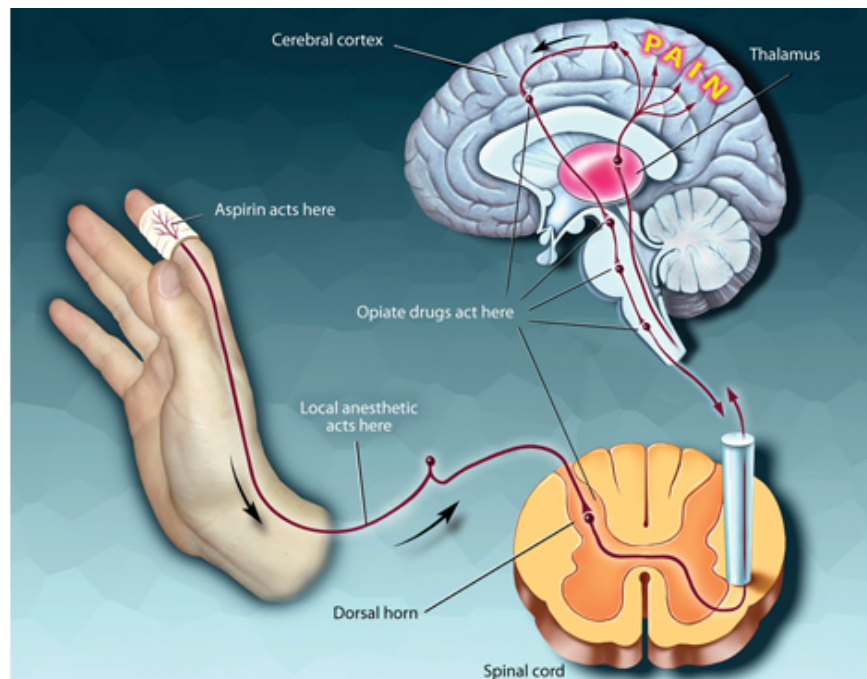


Figure 1.38. Sites of action of the various classes of painkillers.⁵⁹⁶

The action of anti-inflammatory drugs at the site of injury is slightly more complicated than that of local anesthetics and opiate-based drugs. In order to understand their action, the processes which accompany an injury need to be understood, as does the role of the various substances released. Once the stimulus is removed and tissue damage has occurred, the injured cells and the infiltrating immune cells, such as neutrophils, monocytes, lymphocytes and macrophages,⁵⁹⁷⁻⁵⁹⁸ release multiple chemical mediators into the area around the damaged tissue, creating an “inflammatory soup” which contains prostaglandins, histamines, cytokines, chemokines, nerve growth factors, bradykinins, purines, amines, ions and many others.⁵⁹⁹⁻⁶⁰⁰ Because the peripheral terminals of nociceptors contain receptors for many of these proinflammatory molecules, the activation threshold of the voltage-gated sodium channels, for example Nav1.8 or 1.9, and the transient receptor potential cation channel subtype V1 (TRPV1) is lowered. Normally responsible for detection of negative stimuli and transduction into electrical energy, reduction of the activation threshold results in increased sensitivity of the nociceptor terminals to additional pain stimulation.^{599,601-602} Termed “peripheral sensitization”, this enhanced sensitivity to stimuli contributes to inflammatory pain hypersensitivity or hyperalgesia.⁶⁰³ This pain hypersensitivity serves to protect the damaged tissues from further damage as additional mechanical stress from physical activity is discouraged. A second mechanism, termed “central sensitization” also contributes to hyperalgesia.⁶⁰⁴ Tissue injury not only results in the creation of the inflammatory soup, rather, it also stimulates the release of neurotransmitters such as glutamate and substance P from the central terminals of nociceptors,⁵⁹⁹ and increases the production of proinflammatory cytokines such as interleukin-1 β (IL-1 β) and *tumor necrosis factor- α* (TNF- α) in the spinal cord. As a result of this, the dorsal horn neurons are disinhibited and excited, causing abnormal responses to signals originating in the region of the injury.⁶⁰⁵

1.4.2. Taking Responsibility: The Family of Molecules to Blame.

“The man who passes the sentence should swing the sword. If you would take a man's life, you owe it to him to look into his eyes and hear his final words. And if you cannot bear to do that, then perhaps the man does not deserve to die.”

George R.R. Martin, *A Game of Thrones*

Despite there being a number of important substances involved in pain and inflammation, by far the most important are the family of compounds known as the prostaglandins. A group of lipid mediators produced and released in response to a number of stimuli, prostaglandins include such compounds as prostaglandin D₂ (PGD₂), PGE₂, PGF_{2α}, PGI₂ and thromboxane A₂ (TxA₂) (Figure 1.39).⁶⁰⁶ The prostaglandins and TxA₂, collectively termed prostanoids, are formed *via* three sequential enzymatic reactions, beginning with the release of arachidonic acid (AA) from membrane phospholipids by phospholipase A₂. Arachidonic acid is then converted into prostanoids, leukotrienes or epoxyeicosatrienoic acids by one of three enzymes – cyclooxygenase (COX) enzymes form the prostanoids, lipoxygenases the leukotrienes and epoxygenases form the epoxyeicosatrienoic acids.^{597,599}

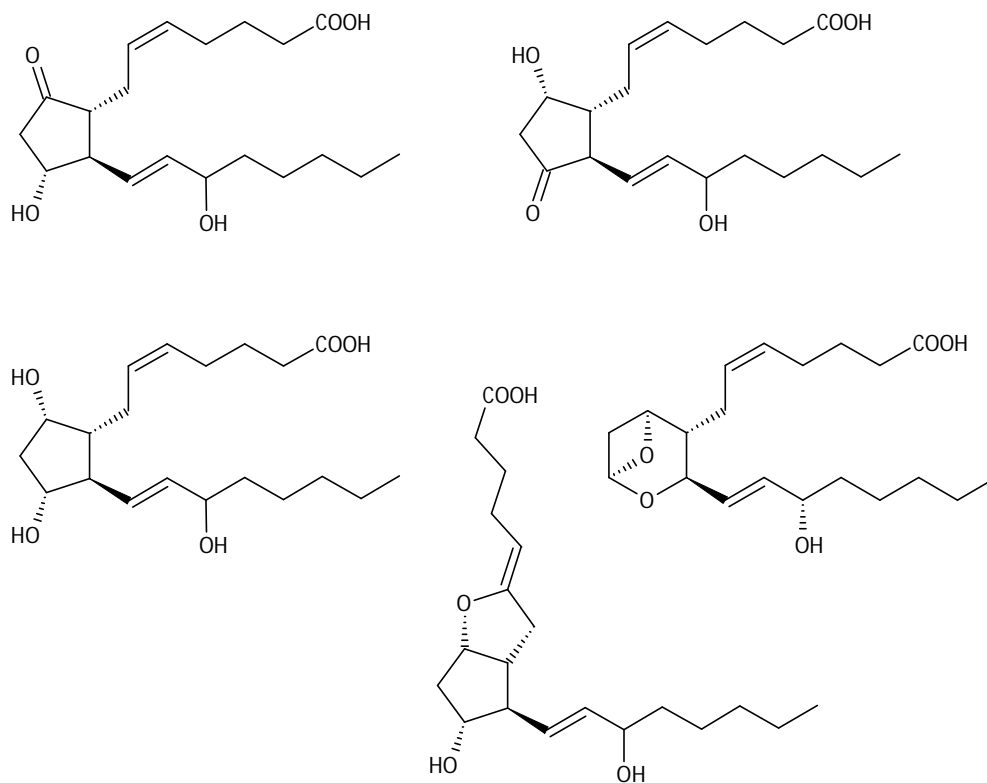


Figure 1.39. 2D structures of (clockwise from left) PGE₂, PGD₂, TxA₂, PGI₂, and PGF_{2α}.

The synthesis of all prostanoids starts in the same place– with the release of AA from the membrane. The AA is then rapidly oxidized by the cyclooxygenase function of the COX enzymes into the relatively unstable PGG₂, which is then sequentially reduced to PGH₂ by the peroxidase activity of the same COX enzyme.^{599,607-608} PGH₂ is then converted into the different prostanoids by their respective terminal isomerases and synthases – PGE synthase (PGES) for PGE₂, and PGIS, PGDS, PGFS and TxAS respectively for the remaining prostanoids (Figure 1.40).^{597,599}

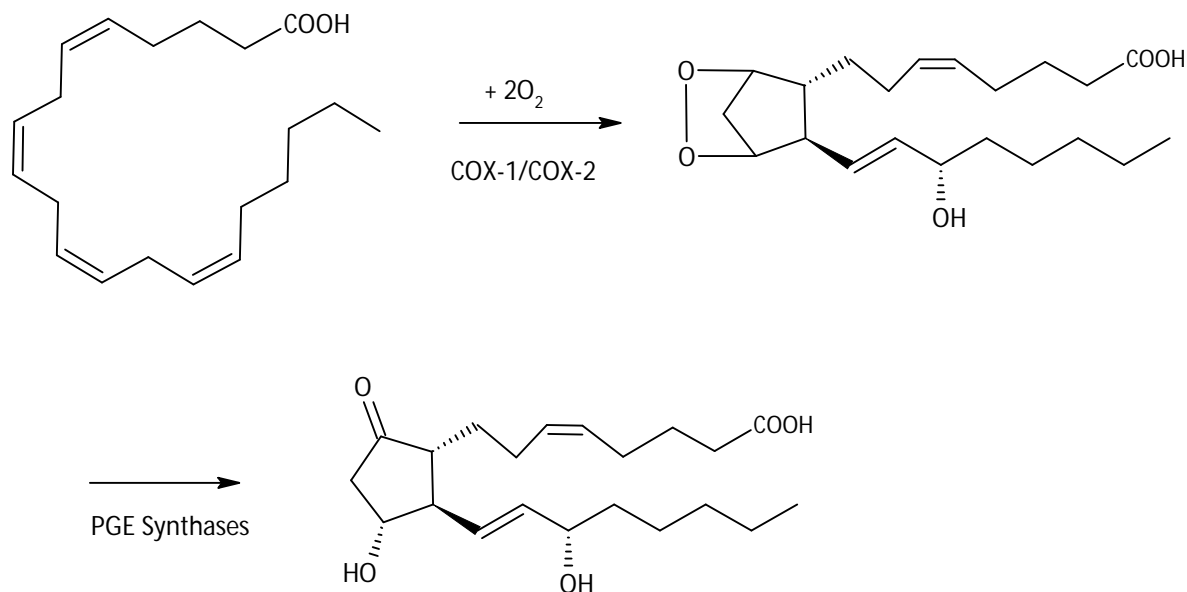


Figure 1.40. An example of prostaglandin synthesis: the formation of PGE₂ from arachidonic acid.⁶⁰⁹

Prostaglandins activate seven rhodopsin-like transmembrane G protein-coupled receptors (GPCRs), with the prostanoid receptor subfamily comprising 8 members: E prostanoid receptors 1 through 4 (EP₁₋₄), PGD receptors (DP₁), PGF receptors (FP), PGI receptors (IP) and TX receptors (TP).⁶¹⁰ These receptors couple to a range of intracellular signaling pathways which mediate the cell function effects of receptor activation. EP₂, EP₄, DP₁ and IP receptors cause an increase in intracellular cAMP by activating adenylyl cyclase, and EP₁ and FP result in the formation of inositol triphosphate and the mobilization of intracellular free calcium as they activate the phosphatidylinositol metabolism pathway.⁵⁹⁷

Of all of the PGs, of most interest in the study of inflammation is PGE₂ as all the clinical manifestations of inflammation arise due to its cellular effects.^{597-598,611} The redness and edema characteristic of inflammation result from increased blood flow to the inflamed blood tissue through PGE₂-mediated vasodilation and increased microvascular permeability and the pain associated with inflammation is due

to the interaction of PGE₂ on the peripheral sensory neurons and at central sites in the spinal cord and brain.⁶¹¹⁻⁶¹² The role of PGE₂ in promoting the activation of TH17 cells has also recently been identified.⁶¹³⁻⁶¹⁴ Members of the CD4+ helper T cell family, these cells are characterized by the production of interleukin-17 (IL-17) and represent a set of potent proinflammatory mediators which recruit neutrophils and monocytes to the site of inflammation. If the inflammatory response is thought of as a finely tuned orchestra with the interconnected processes involving multiple cell types and inflammatory mediators as musicians, then PGE₂ can be thought of as the conductor, as it plays a critical role in the directing and controlling of many facets of the inflammatory response.⁶⁰⁷

1.4.3. A Fork In the Road: Steroidal and Non-Steroidal Painkillers.

“Why are there never any good side effects? Just once I'd like to see a drug commercial that says, May cause extreme awesomeness.”

Unknown

It is here then, at the crossroads to all the prostanoids, where anti-inflammatory drugs act. Anti-inflammatory drugs fall in to one of two classes, namely steroidal anti-inflammatory drugs and non-steroidal anti-inflammatory drugs. Steroid anti-inflammatory drugs, such as prednisone, prednisolone, methylprednisolone, dexamethasone and hydrocortisone (Figure 1.41), are synthetic glucocorticosteroids or glucocorticoids, based on the naturally occurring hydrocortisol. These compounds bind to the glucocorticoid receptor, found in almost every cell, which in turn up-regulates the expression of various anti-inflammatory proteins in the nucleus of the cell, and also down-regulates the expression of pro-inflammatory proteins in the cytosol.⁶¹⁵ Regardless of the cause of the inflammation, glucocorticoids exert potent anti-inflammatory effects on a number of cell types, including macrophages, T cells, mast cells, neutrophils, eosinophils, endothelial cells and epithelial cells,⁶¹⁶ but the primary mechanism of action is the up-regulation of lipocortin-1 synthesis. Lipocortin-1 suppresses phospholipase A₂, the enzyme responsible for the release of AA into the system, and also inhibits a number of leukocyte events related to inflammation.⁶¹⁷⁻⁶¹⁸ As the release of AA is inhibited, the production of PGE₂ is essentially halted, and the major cause of inflammation is removed. Glucocorticoids have also been shown to interact with COX directly, further reducing the production of PGE₂.^{616,619} Side effects due to glucocorticoid use include immunosuppression and immunodeficiency,

hyperglycemia, gastric ulcers, osteoporosis, weight gain, adrenal insufficiency, muscle breakdown, glaucoma, cataracts, hypercortisolemia, and euphoria or psychosis associated with the excitatory effect of glucocorticoids on the central nervous system.⁶²⁰

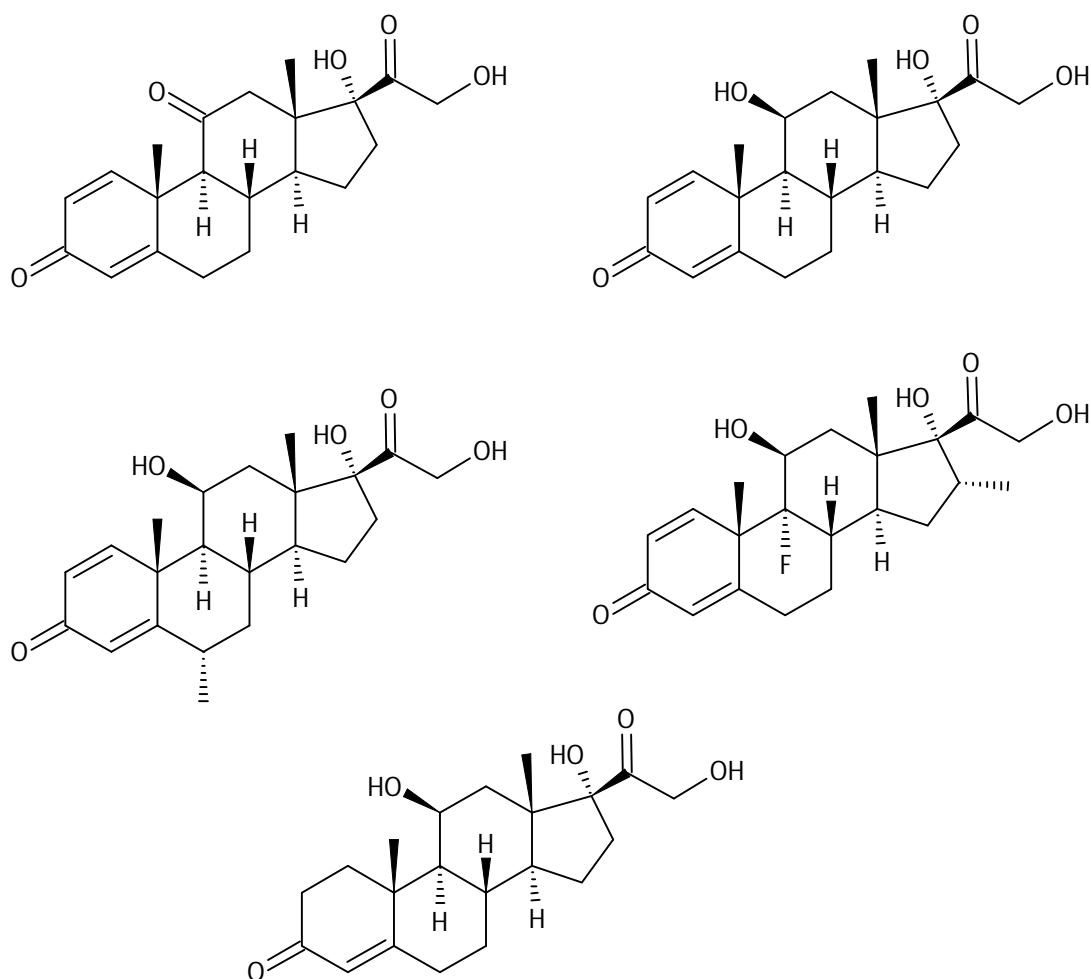


Figure 1.41. 2D structures of (clockwise from left) prednisone, prednisolone, dexamethasone, hydrocortisone and methylprednisolone

To combat the side effects of steroids, non-steroidal anti-inflammatory drugs (NSAIDs) such as ibuprofen, naproxen, sulindac, phenylbutazone, diclophenac, indomethacin and the salicylates such as acetylsalicylate (Aspirin®) (Figure 1.42) have been developed over the last century, and these compounds interrupt the synthesis of PGE₂ by interacting with COX as competitive active site inhibitors and preventing the conversion of AA into PGG₂.⁵⁹⁷ Despite existing as a homodimer, only one COX partner is used at a time for substrate binding, and the formation of prostanoids can be shut down by the binding of an NSAID to one of the monomers of the COX dimer^{597,621} - the other monomer plays what

appears to be an allosteric role, and the peroxidase activity of COX is not affected by NSAIDs.⁶²² While not as serious as the risks associated with steroid anti-inflammatory use, a wide variety of side effects related to the use of NSAIDs have been identified, including an increased risk of myocardial infarctions and strokes,⁶²³ nausea, vomiting, diarrhea and gastric ulcers,⁶²⁴ salt and fluid retention, hypertension, renal failure and analgesic nephropathy,⁶²⁵ inflammatory bowel disease and an enhanced risk of erectile dysfunction.⁶²⁶

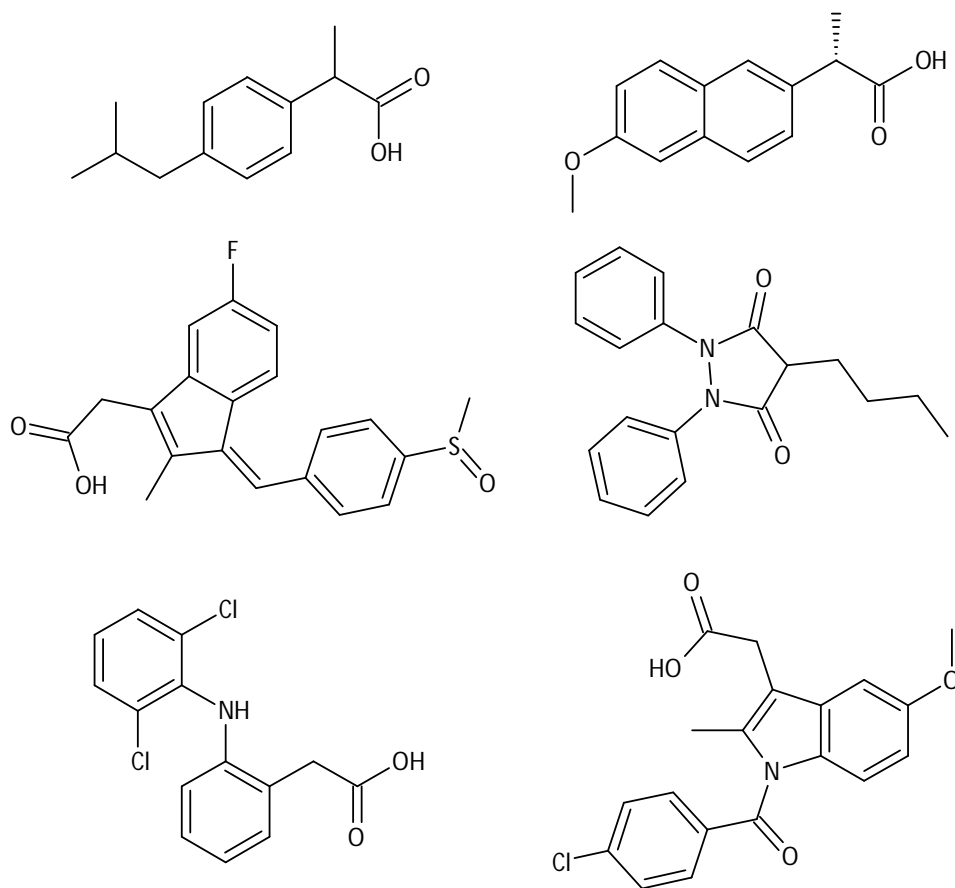


Figure 1.42. 2D structures of (clockwise from left) ibuprofen, naproxen, phenylbutazone, indomethacin, diclofenac, and sulindac.

To find a safe and effective anti-inflammatory is still a challenge for modern medicine. Existing as two distinct isoforms referred to as COX-1 and COX-2, the COX enzyme has been the focus of much research over the last 4 decades as the clinical effectiveness of structurally different NSAIDs points to the importance of prostanooids as mediators in the promotion of pain, inflammation and fever.⁶²² COX-1 is the dominant isoform and the major source of prostanooids required by the body for “housekeeping”

functions such as homeostasis, renal blood flow maintenance and gastric epithelial cytoprotection.⁶²⁷ COX-2 is the main source of prostanoids in inflammation and in proliferative diseases such as cancers,⁶²⁷ and is not expressed, or is expressed at very low levels under basal conditions. Although both isoforms contribute to prostanoid synthesis and release during inflammation,⁵⁹⁷ COX-2 is up-regulated by proinflammatory stimuli, growth factors and hormones,⁶²⁸ and it is this inducibility that has provided the rationale for the development of NSAIDs which are selective for COX-2 over COX-1, known as coxibs,⁶²⁹ along with the hypothesis that inhibition of COX-1 explains the adverse gastrointestinal side effects such as bleeding ulcers associated with NSAID use.⁶³⁰

With the discovery of the mechanism of action of NSAIDs in the 1970's came the idea that there were alternate forms of COX present,^{622,631} but the cloning and isolation of a second form of COX was only reported in 1991.⁶³² Interestingly, without confirmed knowledge of this second form of COX, a compound had been developed by the DuPont company a year earlier which showed anti-inflammatory properties without the ulcerogenic effects of the traditional NSAIDs.⁶³³ This compound, DuP-697, along with NS-398⁶³⁴, became the building block for COX-2 selective compounds (Figure 1.43), including celecoxib (Celebrex®), rofecoxib (Vioxx®) and valdecoxib (Bextra®).^{631,633}

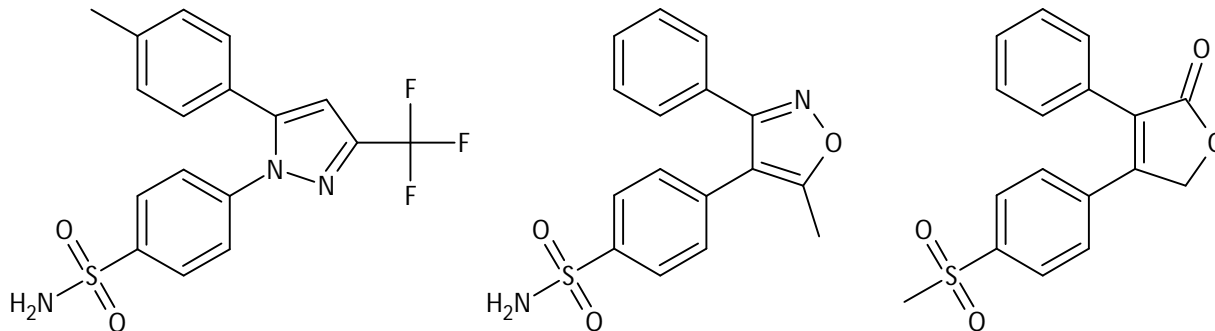


Figure 1.43. 2D structures of (left to right) the COX-2 selective compounds celecoxib, rofecoxib and valdecoxib.

Once the pieces of the puzzle had been put together, the question was then posed: "What then, in the structure of the two forms of COX, accounts for the difference in the activity of these compounds?" COX-1 and COX-2 are membrane-bound isoenzymes found in the endoplasmic reticulum (ER), and are genetically independent proteins where the genes for these enzymes show completely different properties and are located on different chromosomes – the COX-1 gene is located on chromosome 9, COX-2 is encoded by a gene on chromosome 1.⁶³⁵⁻⁶³⁶ The DNA sequences of these two genes are very similar, with a sequence identity of approximately 60%, leading to a highly conserved overall

structure.⁶³⁷⁻⁶³⁹ After post-translational modification, cleavage of the signal peptide and insertion into the ER, the molecular weight of the mature glycosylated COX enzymes differ by 5 kDa, with COX-1 having a molecular weight of 67 kDa and COX-2 a weight of 72 kDa.⁶³⁷ This weight difference is due to the presence of a truncated signal peptide, and the insertion of an 18 amino acid sequence which act as an epitope for COX-2 specific antibodies.⁶³⁸

1.4.4. Inherent Selectivity: Small Differences Equal Large Changes.

"Life's a journey and there's no predicting the outcome. The only thing you can control are your choices, and they'll define who you are."

Richard Castle, *Castle*

The key to COX-2 selectivity lies in the *ca.* 40% of the amino acid sequence which is different. Included amongst the differences are three simple amino acid substitutions which cause the active site of COX-2 to be larger than that of COX-1. The active site is a long hydrophobic channel containing areas of high electron density, with only two polar amino acid residues - arginine (Arg120 – ovine COX-1 numbering system) and glutamic acid (Glu524) - present.⁶³⁹⁻⁶⁴⁰ The larger active site found in COX-2 is due to the substitutions of valine 523 (Val523), Arg513 and Val434 for isoleucine 523 (Ile523), histidine 513 (His513) and Ile434 respectively in COX-1.⁶³¹ The valine residue at position 523 in COX-2 is less bulky than the isoleucine in COX-1, which causes a slight structural modification of the protein. This substitution allows access into an additional hydrophilic side pocket which is not accessible in COX-1, and it is this pocket which is important for COX-2 selectivity (Figure 1.44).⁶³¹ Substitution of Ile434 with Val434 results in the movement of the side chain of phenylalanine 518 (Phe518) within the protein which is able to increase the volume of the active site further. Access to this side pocket allows for interactions of inhibitors with Arg513, interactions which are thought to be crucial for the success of diaryl heterocycle inhibitors such as the coxibs. Another result of the different amino acid sequence of COX-2 is in the altered position of the side chain of leucine 384 (Leu384) at the top of the receptor channel. In COX-1, it is directed into the active site, while in COX-2 it is oriented away from the active site, again increasing the size of the active site.⁶⁴⁰⁻⁶⁴¹

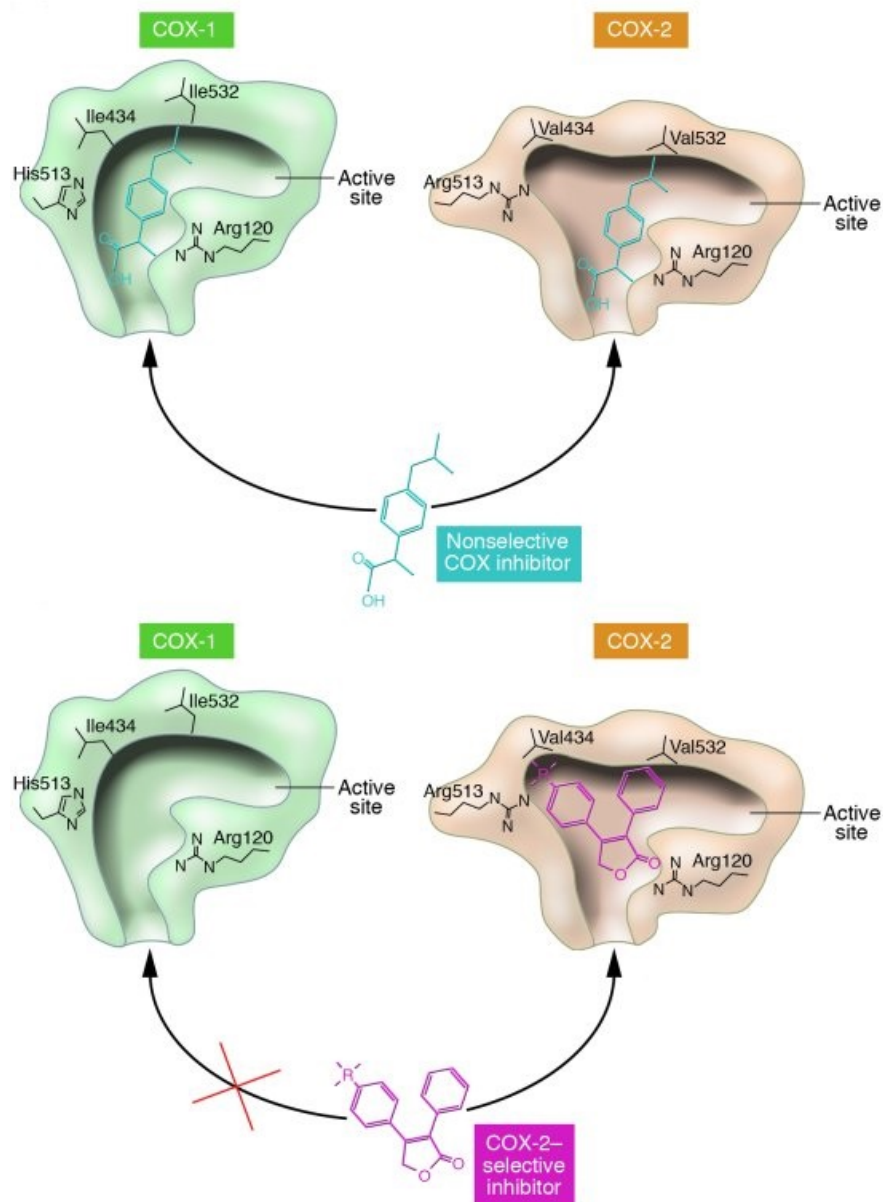


Figure 1.44. Schematic overview of how the structural differences between the COX isoforms allow for selective inhibition of COX-2.⁶⁴²

Celecoxib, marketed as Celebrex[®] (Figure 1.45), the first coxib brought to market in December 1998 by Pfizer, was built upon the scaffolds of DuP-697, a tricyclic inhibitor, and NS-398, a methanesulfonanilide-based inhibitor.⁶³³⁻⁶³⁴ Based on these and other similar compounds, the team at Searle Research and Development established that two aromatic rings situated on adjacent positions on a central ring was vital for COX-2 inhibitory activity, and that these phenyl rings could be substituted in order to fine-tune the activity of the compounds.⁶⁴³ Extensive Structure Activity Relationship (SAR) analyses concluded that

a *p*-sulfamoylphenyl or a *p*-(methylsulfonyl)phenyl group attached to position 1 of a 1,5-diaryl pyrazole ring showed a higher COX-2 selectivity than the corresponding *p*-methoxyphenyl group. SAR analysis also showed that *N*-methylation or *N,N*-dimethylation of the sulfonamide moiety significantly reduced the COX-2 activity of the compounds. A degree of flexibility with regards to substitutions at the 3-position of the pyrazole ring was noted by the research team, with trifluoromethyl and difluoromethyl substituents shown to be more active in terms of potency and selectivity.⁶⁴³ Finally, substitutions to the phenyl ring at position 5 greatly affected the potency and selectivity of compounds in vitro. Substitutions to the 2- or 4-positions provided greater potency than 3-substituted analogues, however with sensitivity noted with regard to steric hinderance at the 4-position, smaller substituents proved to be more effective than larger ones.⁶⁴³ The high lipophilicity of the active site also partially restricted the types of substitutions possible as the coxibs need to be non-polar in order to interact with the active site.⁶⁴¹ Celecoxib is approximately 20 times more selective for COX-2 over COX-1⁶⁴⁴, and is currently the only COX-2 selective NSAID still holding F.D.A. approval for osteoarthritis, rheumatoid arthritis, ankylosing spondylitis, and juvenile rheumatoid arthritis in patients 2 years and older, with sales totaling \$1.93-billion in the United States in 2013, and \$2.92-billion worldwide.⁶⁴⁵

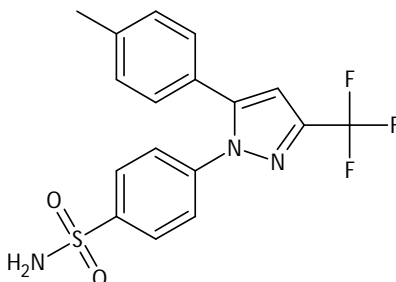


Figure 1.45. 2D structure of celecoxib, currently the only COX-2 selective compound with F.D.A. approval.

Rofecoxib (Figure 1.46), the second coxib to be released, holds the dubious honour of being the first coxib taken off the market, despite being the only one to show clinical evidence that it did not cause the same gastrointestinal side effects as did the traditional NSAIDs.⁶⁴⁶ Marketed under the name Vioxx®, rofecoxib was withdrawn from the market by Merck in September 2004 due to concerns about increased risk of heart attacks and strokes. The VIGOR⁶⁴⁶ (VIOXX GI Outcomes Research) study, which compared the efficacy and adverse effect profiles of rofecoxib and naproxen (a non-selective NSAID), showed a 4-fold increase in the risk of acute heart attacks in rofecoxib patients when compared to naproxen patients over the 12 month span of the study, with the elevated risk beginning in the second month of the study. While there was no significant difference in the mortality rates between the two groups, and no difference in the rate of heart attacks in patients without high cardiovascular risk,

patients at higher risk of heart attack prior to the commencement of the study showed a significant increase in the risk of heart attacks while taking rofecoxib.⁶⁴⁶

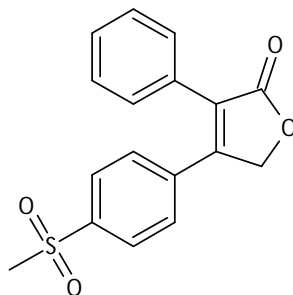


Figure 1.46. 2D structure of rofecoxib, the first COX-2 selective compound removed from the market due to safety concerns.

Valdecoxib (Figure 1.47), marketed by G.D. Searle & Company as Bextra[®] between 2001 and 2005 is another coxib removed from the market due to safety concerns. Increased cardiovascular risks were first acknowledged by Pfizer in October 2004, and soon after the American Heart Association received a report stating that patients taking Valdecoxib were more than twice as likely to suffer a heart attack or stroke as those patients taking placebos. Valdecoxib has been shown to have less adverse side effects for patients with kidney disease and heart arrhythmia than Vioxx, but the renal risks were elevated when compared to celecoxib.⁶⁴⁷ Parecoxib, the inactive amide ester pro-drug of valdecoxib, is water-soluble and therefore injectable, and is rapidly converted to valdecoxib by hepatic enzymatic hydrolysis.⁶⁴⁸ The F.D.A. issued a letter of non-approval for parecoxib in 2005, and while no official reasons were ever given, speculation suggests that political pressure from the US congress resulted in the non-approval of another COX-2 selective drug, as the effects of the Vioxx and Bextra affairs were still being felt. Parecoxib is marketed as Dynastat[®] in the European Union by Pfizer for perioperative pain control, but is not approved for cardiac surgery.

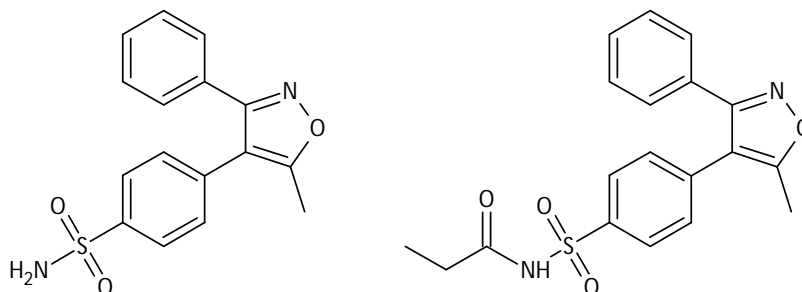


Figure 1.47. 2D structures of valdecoxib(l) and its pro-drug parecoxib (r) which is converted into valdecoxib in the liver.

Along with parecoxib, etoricoxib (Arcoxia®) is a second-generation coxib (Figure 1.48) without F.D.A. approval for use in the United States while having approval for use in other countries. Indications differ according to country, but include osteoarthritis, rheumatoid arthritis, psoriatic arthritis and gout. Studies show that a single oral dose of etoricoxib provides good quality pain control after surgery, and the adverse effects are similar to those for a placebo.⁶⁴⁹ The F.D.A. has not yet approved etoricoxib, saying that Merck must provide extensive additional evidence showing that the drug's benefits outweigh the side effects before approval can be given.⁶⁵⁰

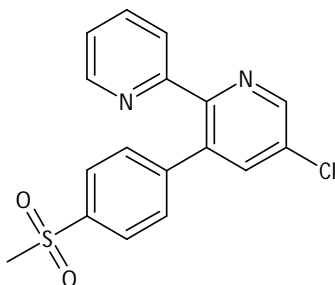


Figure 1.48. 2D structure of etoricoxib, a second-generation coxib.

While still technically a coxib, lumiracoxib (Figure 1.49) differs to the other coxibs listed here in a number of ways. Lumiracoxib, sold under the name Prexige® is a diclofenac derivative, making it an arylalkanoic acid and the only acidic coxib, whereas the other coxibs are essentially based on celecoxib. It has been shown to bind to a different site on the protein, and whilst diclofenac is non-selective, lumiracoxib shows the highest COX-2 selectivity of any NSAID.⁶⁵¹ Initially receiving approval for marketing in all European Union countries in November 2006, it was withdrawn from the Australian and New Zealand markets in August 2007, following 8 serious liver adverse events, including 2 liver transplants and 2 deaths.⁶⁵²⁻⁶⁵³ Health Canada followed suit and withdrew Prexige® in October 2007,⁶⁵⁴ and several European Union countries also withdrew approval in November and December of the same year.⁶⁵⁵

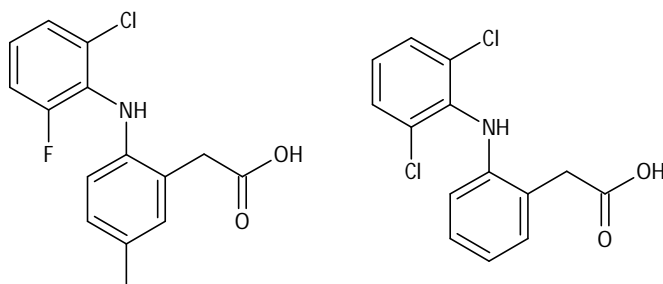


Figure 1.49. 2D structures of lumiracoxib and its parent molecule diclofenac.

To explain the selectivity of celecoxib and the other “traditional” coxibs, it is important to take into account interactions which occur between the protein and the inhibitors, and how changing amino acids within the protein affects these interactions. Within the hydrophilic pocket, the oxygen atom of the sulfonamide or sulfone group interacts with His90, glycine 192 (Gln192) and Arg513, forming hydrogen bonds between the coxib and the protein.⁶³¹ Other hydrogen bonds have been reported between the coxibs and tyrosine 355 (Tyr355), as well as with Arg120, serine 530 (Ser530) and Val523.^{640,656} While these static 3D structure studies have proven vital in understanding the mechanism of inhibition, they often do not take into account the fact that enzymes are not static, and so do not take into account enzyme flexibility and rearrangement of the hydrogen bonds surrounding the entrance to the active site. Water molecules present in the active site have also been shown to be important in understanding the selectivity of inhibitors, as they participate in dynamic hydrogen bonding with Tyr355, Arg120, Glu523 and Arg513 at the active site entrance, suggesting that active site hydration is important.^{631,657}

In the course of the search for a compound which maintained the efficacy of NSAIDs while removing the side effects, the development of the coxibs was based on the assumption that COX-1 was “good”, and that COX-2 was “bad”. However, the supposition that COX-1 and COX-2 have distinct homeostatic and pathological functions was proven to be an oversimplification.^{597,599} A number of studies have now shown that COX-2 is required for healthy renal, gastric and cardiovascular functions, and COX-1 has also been shown to have a role in inflammation,⁶⁵⁸⁻⁶⁶² with human data showing that during the initial phase of an acute inflammation, the PGE₂ formed is mostly COX-1-derived, and COX-2 –derived PGE₂ occurs within several hours.⁶²⁹ The role of COX-2 in the cardiovascular system was underscored by the increased risk of cardiovascular side effects such as heart attacks and strokes associated with rofecoxib and valdecoxib, which lead to the withdrawal of both of these drugs from the market, and for the reluctance of the F.D.A. to approve another COX-2 selective compound as a painkiller since.^{329,663-667}

1.4.5. Where To From Here: The Future Of Coxibs.

“The way I see it, every life is a pile of good things and bad things. The good things don’t always soften the bad things, but vice versa, the bad things don’t always spoil the good things and make them unimportant.”

The Doctor, *Dr Who*

While coxibs might not have a future as painkillers, there is still much hope for these compounds. With the patent on celecoxib expiring in 2015, much research has gone into the study of other uses for celecoxib, including as a cancer treatment,⁶⁶⁸ as it has been stated that prostaglandin synthesis, and therefore COX-2, is important for cancer cell growth.⁶⁶⁹⁻⁶⁷² Recent studies have also shown that over-expression of the COX-2 metabolites PGA₁ and PGA₂ interferes with the tumour apoptosis factor p53 in neuroblastomas.⁶⁷³ PGA₁ and PGA₂, when expressed in high quantities, bind to p53 and effectively sequester the protein in the cytosol and prevent it from reaching the nucleus of a cancer cell where it would cause apoptosis to occur.⁶⁷⁴ Coxibs, by inhibiting COX-2, halt tumour growth by restoring the function of p53, which allows the neuroblastoma cells to commit suicide through apoptosis. COX-2 up-regulation has also been linked to the phosphorylation and subsequent activation of the E3 ubiquitinating ligase HDM2 in neuroblastoma cells. This protein mediates p53 ligation and tagged destruction through ubiquitination, and in neuroblastoma cells, it is overexpressed. Studies have shown that the reduction in the concentration of activated HDM2 in cells by a coxib results in the restoration of p53 activity, and subsequent cellular apoptosis, although both the mechanism underpinning the hyperactivity of HDM2 in neuroblastoma cells, and the mechanism of how coxibs block the phosphorylation of HDM2 is unknown.⁶⁷⁴

The possibility that coxibs, not just celecoxib, act as anti-cancer agents solely by inhibiting COX-2 was brought into contention by a number of studies where celecoxib was shown to interact with other proteins in the cell, and could inhibit malignant cell growth without interacting with COX-2.⁶⁷⁵ Support for this hypothesis has come from other research, where analogues of celecoxib with no COX-2 selectivity displayed significant anti-cancer activity.⁶⁷⁶⁻⁶⁷⁸ These studies showed that the anti-tumour potency of a compound did not depend on whether the compound could inhibit COX-2. Further support has come from work carried out by Chuang, *et al.*, where celecoxib was shown to inhibit the growth of cancer cells, despite some of the cancer cells not containing the COX-2 enzyme at all.⁶⁷⁹

2. Aims and Objectives

"The most exciting phrase to hear in science, the one that heralds new discoveries, is not 'Eureka!' but 'That's funny...'"

Isaac Asimov

The aim of this project is to design, synthesize, analyze and test a range of novel COX-2 selective inhibitors based on a curcumin and coxib backbone, and simultaneously evaluate the modeling process of the drug design. The design phase of this project will begin with establishing an understanding of the binding present in both the curcumin and coxib parent molecules through the use of molecular modeling techniques in order to ascertain what important ligand-protein interactions are present in each of these parent compounds. The information gleaned from this study will then be incorporated into the structure of novel compounds in an effort to maximize the binding of these compounds to the protein target. The new compounds will then be subjected to computational analysis so as to determine whether the compounds interact as desired with the protein. The results obtained from the *in silico* analysis of these compounds will be used to predict which of the novel compounds will be potent inhibitors of the COX-2 protein.

The synthesis phase of the project will encompass the complete synthesis of these molecules from basic starting materials into the final products. Complete analysis of these compounds will be carried using techniques such as NMR spectroscopy, High Resolution Mass Spectrometry and X-ray crystallography, and analysis of these compounds will include NAMFIS analysis of representative molecules, to establish the solution conformations of the selected molecules. Biological testing of these compounds will be carried out using the conversion of 10-acetyl-3,7-dihydroxyphenoxazine (ADHP) into resorufin in order to determine which, if any, of these compounds are in fact selective COX-2 inhibitors. These results will aid in the determination of whether the modeling process is suitable for the design of COX-2 selective inhibitors.

3. Results and Discussion: Computational Design and Analysis of Potential COX-2 Selective Compounds

3.1. Exploring the Possibilities: Computational Analysis of Curcumin and Celecoxib

“Art matters because it is the one true great connector in a world that seems to be very unconnected, and it’s important now more than ever to shine a huge light on that connectivity that we have, that we often forget.”

Josh Groban

“Drug design is a creative act of the same magnitude as composing, sculpting, or writing. The results can touch the lives of millions, but the creator is rarely one scientist and the rewards are distributed differently in the arts than in the sciences. The mechanisms of creativity are the same, *i.e.*, incremental (plodding from darkness to dawn) or sudden (the “Eureka” effect) realization, but both are poorly understood. Creativity remains a human characteristic...There is beauty in the fusion of structure and function. As a creative enterprise, drug design is a synthesis of scientific knowledge, experience, intuition, and aesthetics. However, unlike the arts, this beauty has limited distribution; the general public is severely under-informed about the creative process whereby molecules are designed and created. Indeed, like artists, scientists are hard-pressed to enunciate their intuitive insights.” These opening paragraphs to Meyer, Swanson and Williams’ 2000 paper on molecular modeling and drug design succinctly covers the elation and frustration inherent to modern drug design.⁶⁸⁰ Inspiration (for lack of a better word) for drug design can be found in much the same way as an artist looks for ideas in the forms and functions of items, the play of light over a surface, the sounds at dawn or the church bells of a city in winter. While not as romantic as the artist’s inspirations, the muse of drug designers is often found in the more mundane – the novel compound in a rare sea sponge, or in the ingredients of traditional medicines.

With 2012 sales of over-the-counter (OTC) internal analgesics totaling over \$3.9 billion in the United States alone, and not counting the other forms of analgesics such as rubs and sprays, the painkiller

industry is the second largest contributor to the \$23 billion OTC market.⁶⁸¹ As the search for new anti-inflammatory, painkilling compounds without serious side effects is always ongoing, it is often a good idea to consult the wealth of knowledge contained in the various traditional medicines from around the world. One such compound is curcumin (Figure 3.1), one of the components of turmeric. This spice has been used for thousands of years in Indian Ayurvedic and other traditional medicines and the extensive list of treatments include numerous entries where the antiseptic, anti-oxidant, antimalarial, analgesic and anti-inflammatory properties of turmeric have been exploited.³²⁹⁻³³¹ Curcumin itself has been shown to have therapeutic potential against a number of diseases and disorders,^{330,333,351} and over 50 clinical trials utilizing curcumin are currently ongoing. However, curcumin has a number of drawbacks, including poor bioavailability and as-yet-unknown mechanisms of action, which limit its utilization in mainstream medicine, and therefore vast amounts of work have been carried out to reduce these negative aspects, including solubility enhancement and structural modifications.³²⁹⁻³³¹

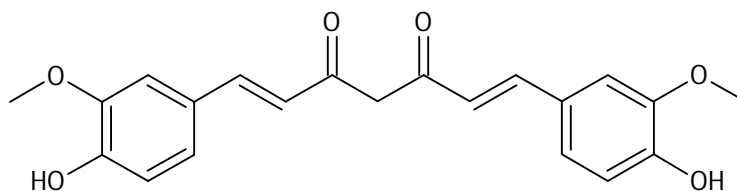


Figure 3.1. 2D structure of curcumin.

The interactions of curcumin with proteins in the solid state are notoriously difficult to study, as curcumin does not withstand X-ray irradiation.⁴⁹⁷ This protein-mediated decomposition of curcumin has prevented the acquisition of definitive answers to the question of how curcumin binds to proteins. While technically a diketone, curcumin undergoes keto-enol tautomerization (Figure 3.2), and it is the enol form (**1**) which dominates in solution and the solid state,⁴⁵⁵⁻⁴⁵⁶ although whether the enol or the diketone form (**2**) bind to the protein is unknown at present. One possible explanation for the relative proportions of the tautomers is the simultaneous extension of conjugation throughout the molecule and the formation of a stabilizing internal hydrogen bond between the enol hydrogen atom and the keto-oxygen atom. The result of this internal hydrogen bond is a thermodynamically preferred 6-membered ring.⁶⁸²

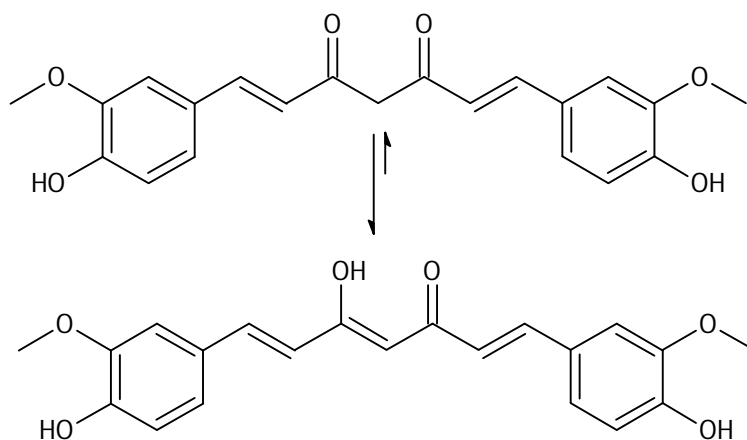


Figure 3.2. Keto-enol tautomerization of curcumin.

Despite this uncertainty, curcumin has been the subject of much study, and one of the plethora of molecular targets of curcumin are the cyclooxygenase (COX) enzymes. These enzymes are largely responsible for the formation of prostanoids from arachidonic acid, including prostacyclin and thromboxane A (Figure 3.3). Prostacyclin is known to be an effective vasodilator and also inhibits platelet aggregation, while thromboxane A₂, a vasoconstrictor, is important during injury and inflammation. At present, two main isoforms of COX are known: COX-1, which is constitutively expressed at low levels throughout the body, and the inducible COX-2, the production of which is stimulated by various inflammatory triggers.⁶⁸³

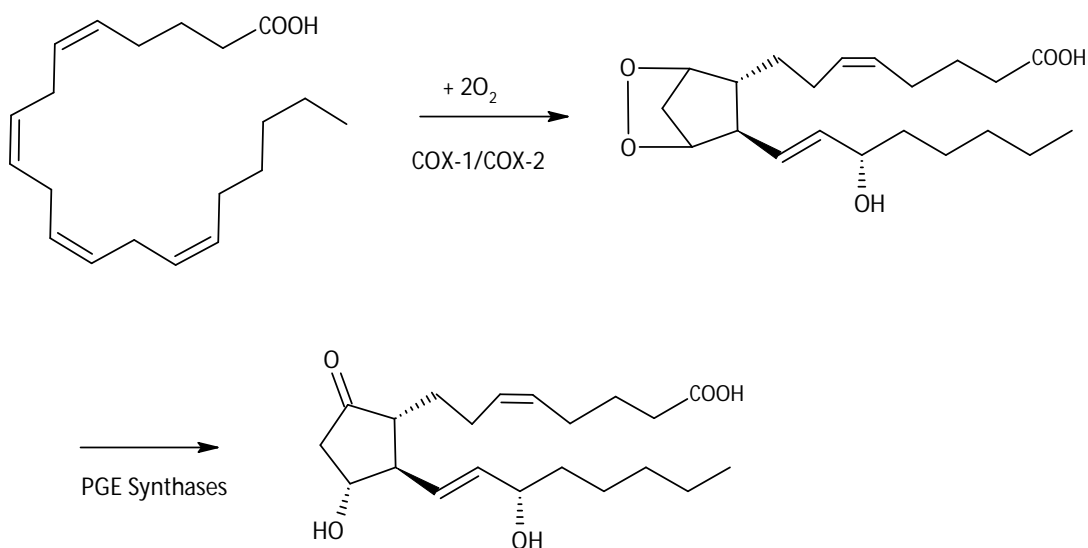


Figure 3.3. An example of prostaglandin synthesis: the formation of PGE₂ from arachidonic acid.⁶⁰⁹

Reduction of prostaglandin synthesis is the central mechanism upon which non-steroidal anti-inflammatory drugs (NSAIDs) act, and the discovery of COX-2 opened up the development of targeted NSAIDs which did not show the gastrointestinal toxicity of the non-selective NSAIDs. This led to the development of COX-2 selective anti-inflammatory compounds including celecoxib (Celebrex®), rofecoxib (Vioxx®), etoricoxib (Arcoxia®) and lumiracoxib (Prexige®) (Figure 3.4). While effective as COX-2 selective inhibitors or “coxibs”, there are a number of severe side effects associated with these compounds, including heart attacks and strokes, and these side effects have resulted in a number of these COX-2 selective compounds either being withdrawn from the market or not receiving approval for sale.

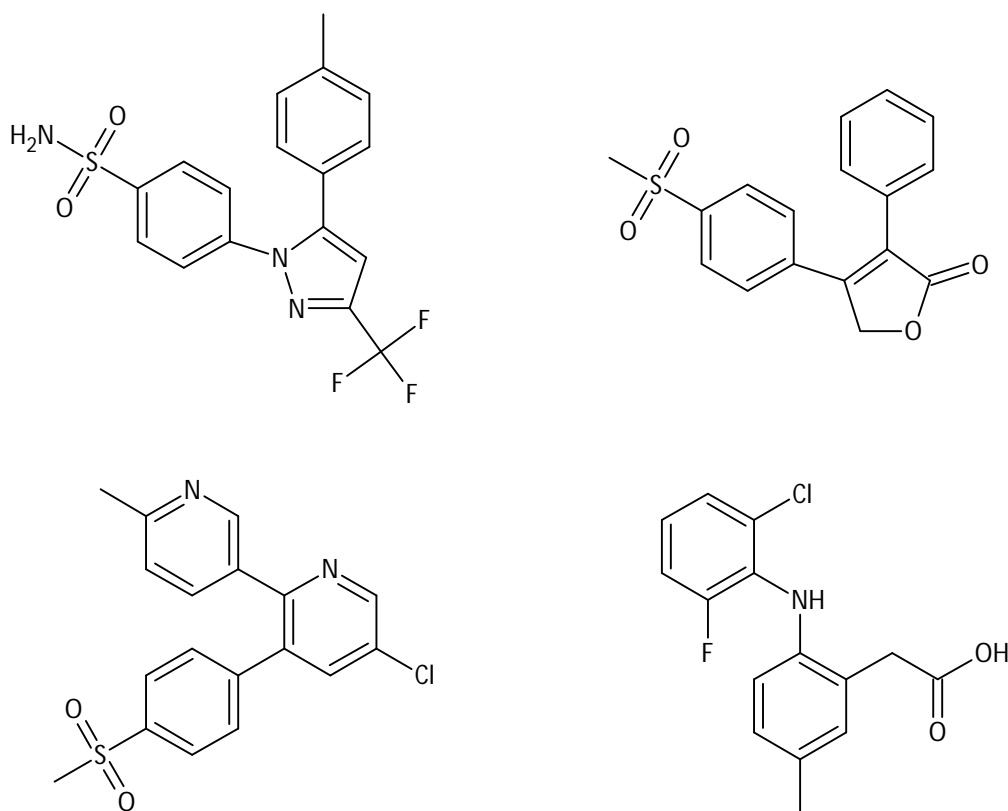


Figure 3.4. 2D structures of the coxibs (clockwise from top left) celecoxib, rofecoxib, etoricoxib and lumiracoxib.

As most of the coxibs are essentially celecoxib derivatives, these coxib compounds show remarkable structural similarity. All of these molecules contain a central ring with a 1,2-substitution pattern, and, apart from lumiracoxib - a diclofenac derivative - two additional phenyl rings. Another feature common to the coxibs is a *p*-sulfuryl group, be it a sulfonamide as seen in celecoxib and valdecoxib or a sulfone as

found in rofecoxib and etoricoxib. This *p*-sulfuryl group is vitally important to the selectivity of coxibs for COX-2 over COX-1, as it is this moiety which interacts with the secondary pocket present in COX-2 (Figure 3.5). This interaction of celecoxib with the secondary pocket is highlighted when the structures of celecoxib and arachidonic acid from the X-ray crystal structures of COX-2 (PDB files 3LN1⁶⁸⁴ and 3HS6⁶⁸⁵ respectively) are superimposed (Figure 3.6).

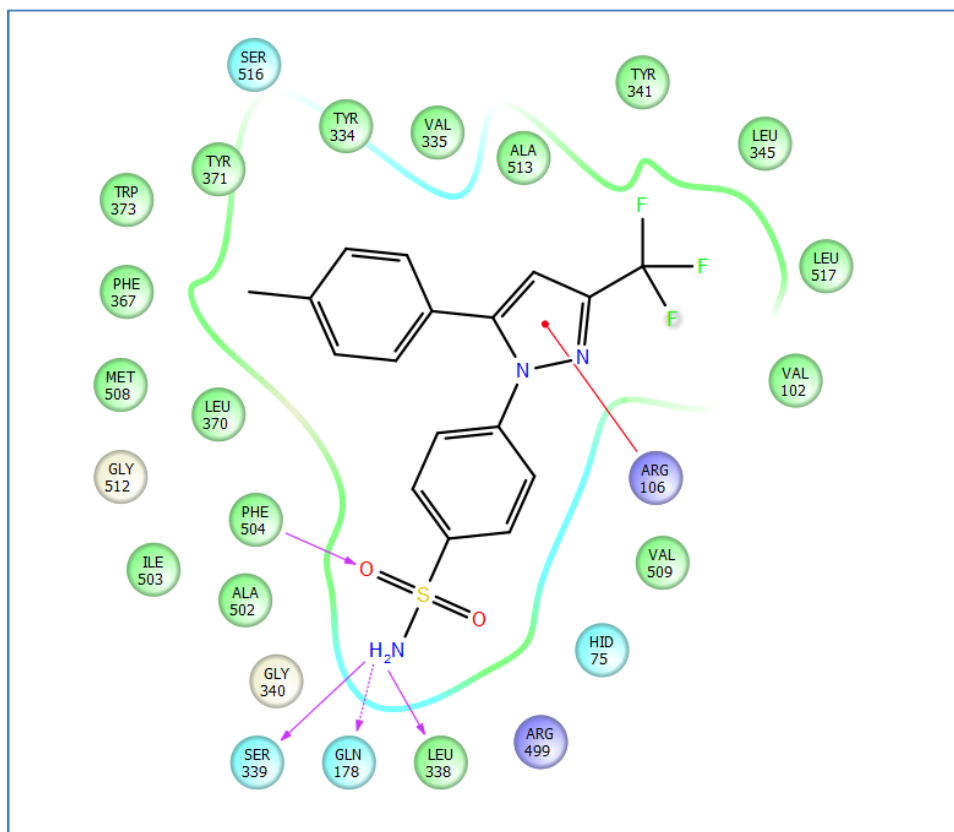


Figure 3.5. Ligand interaction diagram of celecoxib with COX-2 showing the interactions of the *p*-sulfonamide group of celecoxib with the secondary pocket present in COX-2, taken from the PDB file 3LN1.⁶⁸⁴ The red line indicates the presence of a π -cation interaction between the ligand and the protein, the solid purple lines a presence of an H-bond between the ligand and the backbone of the protein, and the dashed purple line an H-bond interaction between the ligand and a side chain.

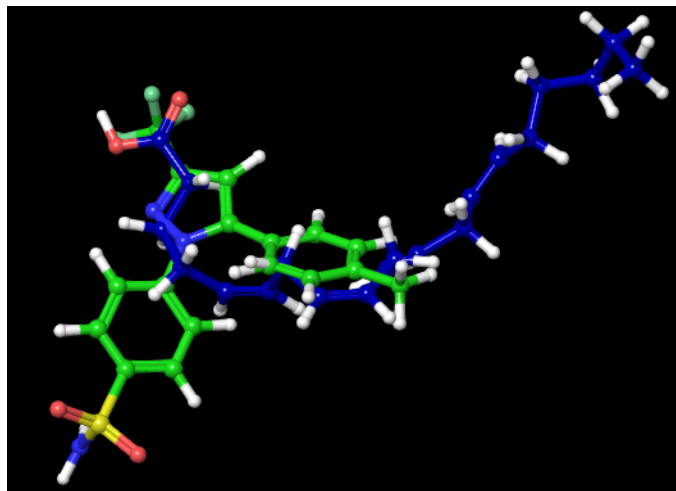


Figure 3.6. X-ray crystal structures of celecoxib (PDB file 3LN1),⁶⁸⁴ shown with green carbon atoms, and arachidonic acid (PDB file 3HS5),⁶⁸⁵ shown with blue carbon atoms.

In order to test the applicability of the docking conditions, the native celecoxib ligand was removed from the protein structure, prepared using LigPrep⁶⁸⁶ and redocked using Glide XP⁶⁸⁷ into the active site of COX-2, which had separately undergone preparation (Epik⁶⁸⁸) and the active site defined using the Receptor Grid Generation application of the Schrödinger Maestro suite.⁶⁸⁹ The poses generated were then compared to the X-ray crystal structure of celecoxib, and the root-mean-square deviation (RMSD) calculated between the generated pose and the original PDB coordinates. A final RMSD value of 0.44 Å was calculated between the best scoring docking pose generated for celecoxib and the original structure (Figure 3.7), validating the docking method used.

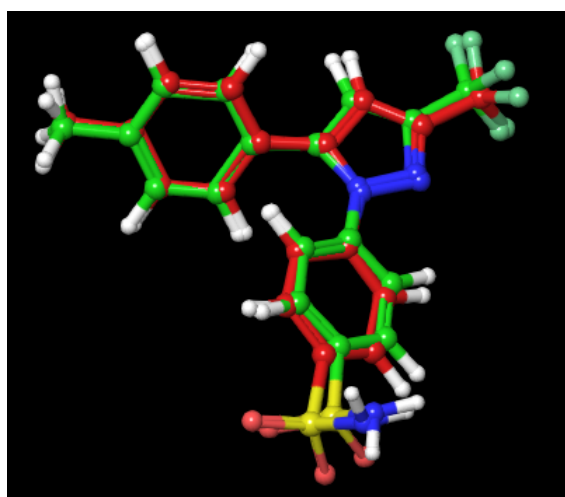


Figure 3.7. The generated pose of celecoxib with carbon atoms shown in red overlapping with the pose of celecoxib bound to COX-2, shown with green carbon atoms (PDB file 3LN1).⁶⁸⁴

Despite being a COX-2 selective compound, celecoxib is also known to bind to COX-1, and an X-ray crystal structure of celecoxib bound to COX-1 (PDB file 3KK6) was obtained in 2010 by Rimon, *et al.*⁶⁹⁰ While the docking procedure used for celecoxib and COX-2 showed good correlation, the same procedure was used in order to determine the applicability of this procedure for the docking of compounds into COX-1. An RMSD value of 0.57 Å between the docked pose and the crystal structure (Figure 3.8) again confirmed the suitability of the docking procedure towards COX-1.

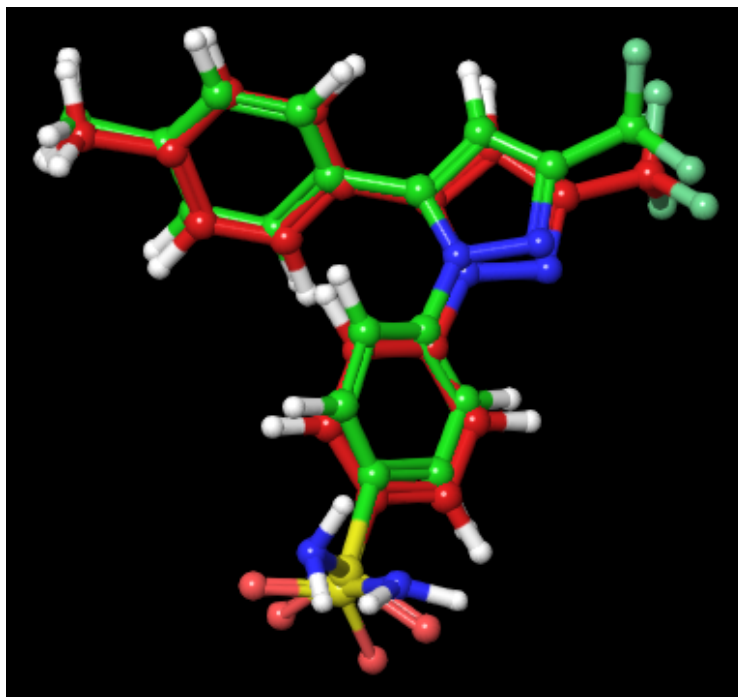


Figure 3.8. The generated pose of celecoxib, carbon atoms shown in red, overlapping with the pose of celecoxib bound to COX-1, carbon atoms shown in green (PDB file 3KK6).⁶⁹⁰

In an effort to understand the possible binding of curcumin to COX-1 and more importantly to COX-2, curcumin was subjected to the same docking process as used for celecoxib. Both **1** and **2** were docked into the protein (Table 3.1), as while **1** dominates in solution,⁴⁵⁵⁻⁴⁵⁶ it is possible for **2** to exist in solution and interact with the protein rather than the predominant enol. As MM-GBSA scores are considered better points for comparison than Glide XP scores,⁶⁹¹ the docked poses of celecoxib and the two isomers of curcumin were rescored using the Prime⁶⁸⁹ function of Schrödinger, and these results were used for comparison, along with visual inspection of the docking poses.

Table 3.1. Glide XP and Prime scores for celecoxib and the two isomers of curcumin.

Entry	Compound	COX-2		COX-1	
		Glide XP /kCal.mol ⁻¹	Prime /kCal.mol ⁻¹	Glide XP /kCal.mol ⁻¹	Prime /kCal.mol ⁻¹
1	Celecoxib	-10.650	-84.269	-11.605	-86.676
2	1	-7.888	-86.566	-10.180	-71.117
3	2	-7.371	-79.410	-11.361	-70.784

At first glance, **1** shows an improvement in binding to COX-2 and a reduction in the binding to COX-1 as compared to celecoxib, while **2** shows a reduction in binding to both proteins. However, on further inspection of the docked poses, **1** shows fewer interactions with the protein (Figure 3.9), while **2** appears to fold in such a manner as to mimic the pose and a few of the interactions found between celecoxib and COX-2 (Figure 3.10), while neither of the curcumin tautomers show the presence of π -cation interactions, as shown in Figure 3.5.

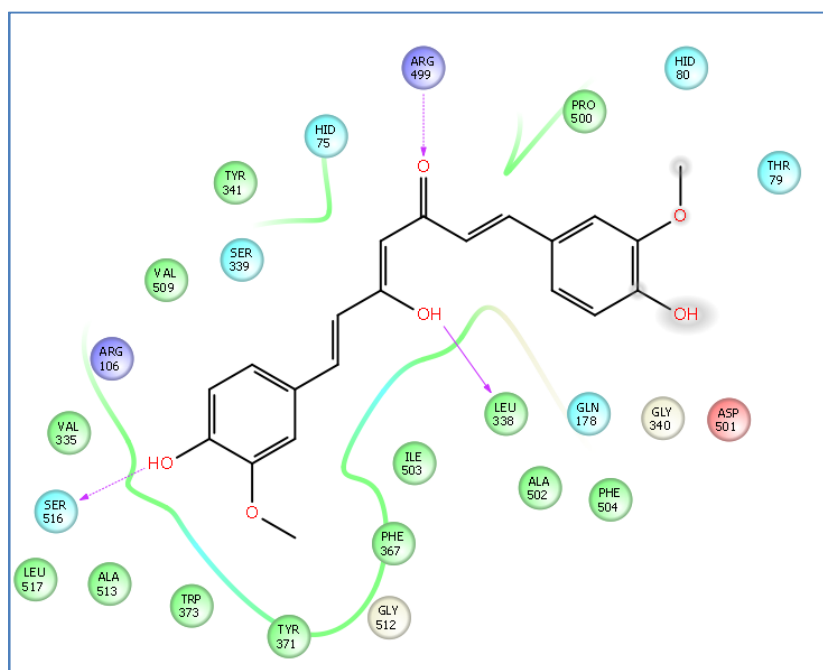


Figure 3.9. Ligand interaction diagram of **1** with COX-2 showing the interactions present between the protein and the ligand.

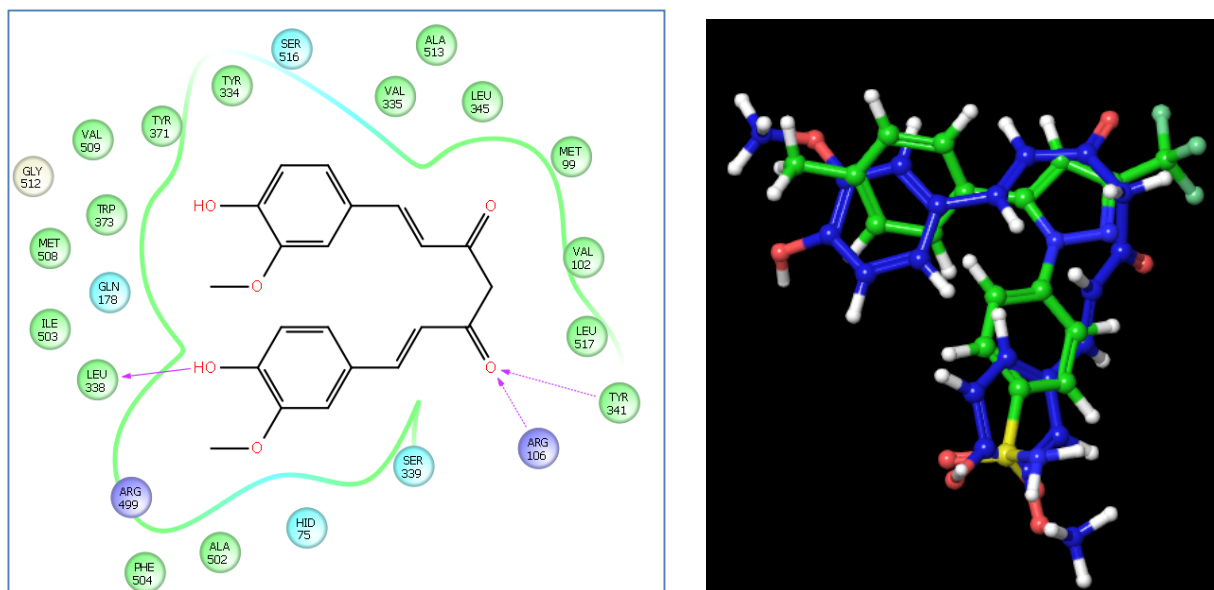


Figure 3.10. Ligand interaction diagram (left) of **2** with COX-2 and the overlap of the generated pose with the X-ray crystal structure of celecoxib in COX-2 (right).⁶⁸⁴

While the docking results show that curcumin could interact with both COX-1 and COX-2 proteins, a glaringly obvious piece of information gleaned from these docking studies is that **1** does not interact with the secondary pocket of COX-2 as desired, and based on these results, it is not expected to be selective for COX-2 over COX-1. While **2** does appear to occupy the secondary pocket, the amount of **2** present in solution is essentially zero,⁶⁹² which hinders the applicability of curcumin to wider use as a COX-2 selective compound. Consequently, a COX-2 selective compound based on curcumin would need to contain other functional groups and/or structural modifications which would enable the selective inhibition of COX-2 through contact with the secondary pocket. Another vital piece of information obtained from this study is that the pose of the compound under study is important, and that the numbers obtained from the various analyses and calculations cannot be the sole basis for judging the suitability of a ligand for a protein.

3.2. In the Beginning: Initial Design and Analysis of a Novel COX-2 Selective Compound

“Everything starts somewhere, though many physicists disagree. But people have always been dimly aware of the problem with the start of things. They wonder how the snowplough driver gets to work, or how the makers of dictionaries look up the spelling of words.”

Terry Pratchett, *Hogfather*

At this point, the important structural features of the coxibs – the 1,2-disubstituted central ring and the *p*-sulfonyl moiety – were combined with the cinnamaldehyde-type structure of curcumin to form a novel class of COX-2 selective compounds (Figure 3.11). The α - β unsaturated section of this molecule is reminiscent of curcumin, with the *p*-sulfonyl phenyl ring and its position on the central phenyl ring derived from the coxibs. With an eye on synthetic routes, and the inclusion of heteroatoms in the coxibs, an ether bond was used to link the central phenyl ring and the *p*-sulfonyl phenyl ring, and this would also allow for a degree of flexibility within the molecule. The two phenyl rings present in the chalcone portion could be easily modified with the use of substituted starting materials, which would in turn allow for the “tuning” of the molecule in order to maximize the interactions of the compound with the protein.

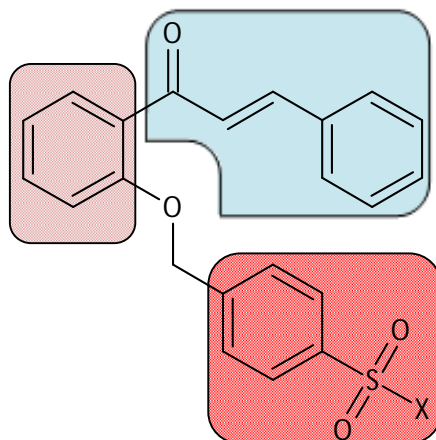


Figure 3.11. General structure of a novel class of COX-2 selective compounds identifying the important structural features derived from the parent molecules. The blue portion is derived from curcumin, the purple portion from the 1,2-disubstituted central ring of coxibs and the red portion the common *p*-sulfonyl phenyl ring also from the coxibs.

As the coxibs demonstrate a range of sulfonyl and other functional groups, a sulfonate (**3**) and a sulfonamide (**4**) (Figure 3.12) were docked in the active site of COX-2 to determine whether one group is more applicable than the other (Table 3.2). Compounds **3** and **4** were also docked into COX-1, as was the case with curcumin, and the data obtained during the docking of celecoxib are included to provide a benchmark against which to judge the scores obtained for **3** and **4**. While a protonated sulfonic acid version could also be docked, these compounds are strong acids and would dissociate almost completely in the aqueous conditions found in the body, and as such, docking of the acid would not be an accurate representation of the situation *in vivo*. Inspection of the binding energies reveals that compound **4** shows improved binding towards COX-1 but weaker binding towards COX-2 as compared to celecoxib, while compound **3** shows weaker binding towards both proteins.

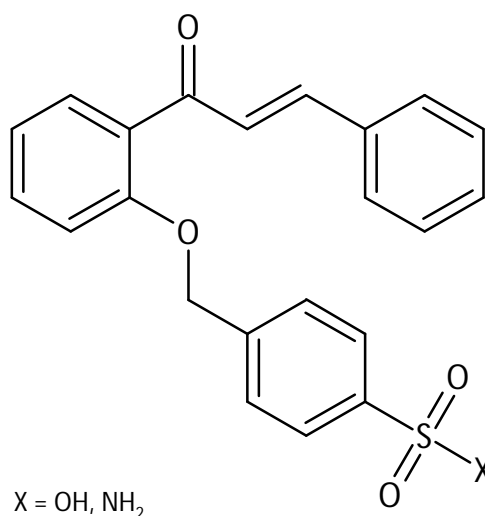


Figure 3.12. Generic structures of **3** (X = OH) and **4** (X = NH₂).

Table 3.2. Glide and Prime scores for celecoxib and compounds **3** and **4**.

Entry	Compound	COX-2		COX-1	
		Glide XP /kCal.mol ⁻¹	Prime /kCal.mol ⁻¹	Glide XP /kCal.mol ⁻¹	Prime /kCal.mol ⁻¹
1	Celecoxib	-10.650	-84.296	-11.605	-86.676
2	3	-12.619	-55.772	-10.572	-74.414
3	4	-11.378	-72.679	-12.823	-89.915

On further examination of the poses, both compounds **3** and **4** interact with the secondary pocket in COX-2 as desired and the docking poses overlap well with the X-ray crystal structure of celecoxib in COX-2 (PDB file 3LN1) (Figures 2.13 and 2.14), although the central ring of these compounds overlaps with the 5-phenyl ring of celecoxib, rather than the central pyrazole ring. Both compounds **3** and **4** are predicted to interact through hydrogen bonds with amino acid residues Arg499 and Phe504 in COX-2, sharing the Phe504 interaction with celecoxib, and **4** is predicted to further interact with Gln178, Leu338 and Ser339 as well, interactions which are shared with celecoxib. Compound **3** is also predicted to interact with Tyr341 through π - π stacking, while this interaction is not identified as likely for **4**. Interestingly, the only interactions predicted for **4** involve the sulfonamide moiety, while **3**, despite having fewer proposed interactions between the protein and the sulfonate moiety, shows COX-2 interactions between both the carbonyl oxygen atom and one of the phenyl ring.

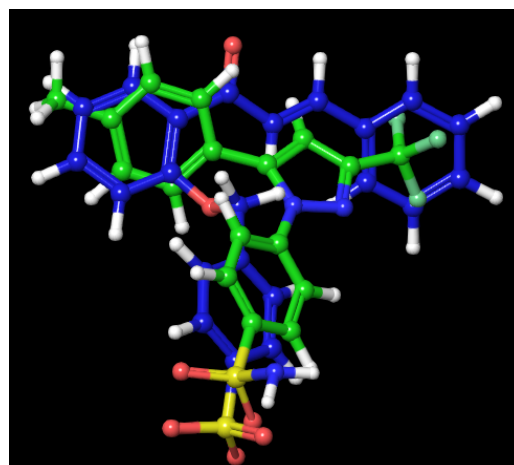
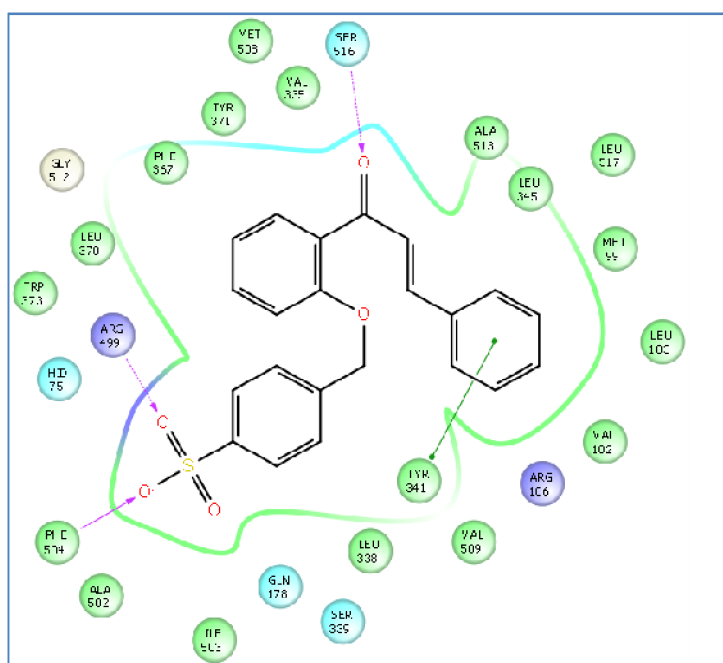


Figure 3.13. Ligand interaction diagram for **3** (left) and the docked pose of **3** (shown in blue) overlaid with the structure of celecoxib (carbon atoms shown in green) as found in the X-ray crystal structure of COX-2 (right).⁶⁸⁴

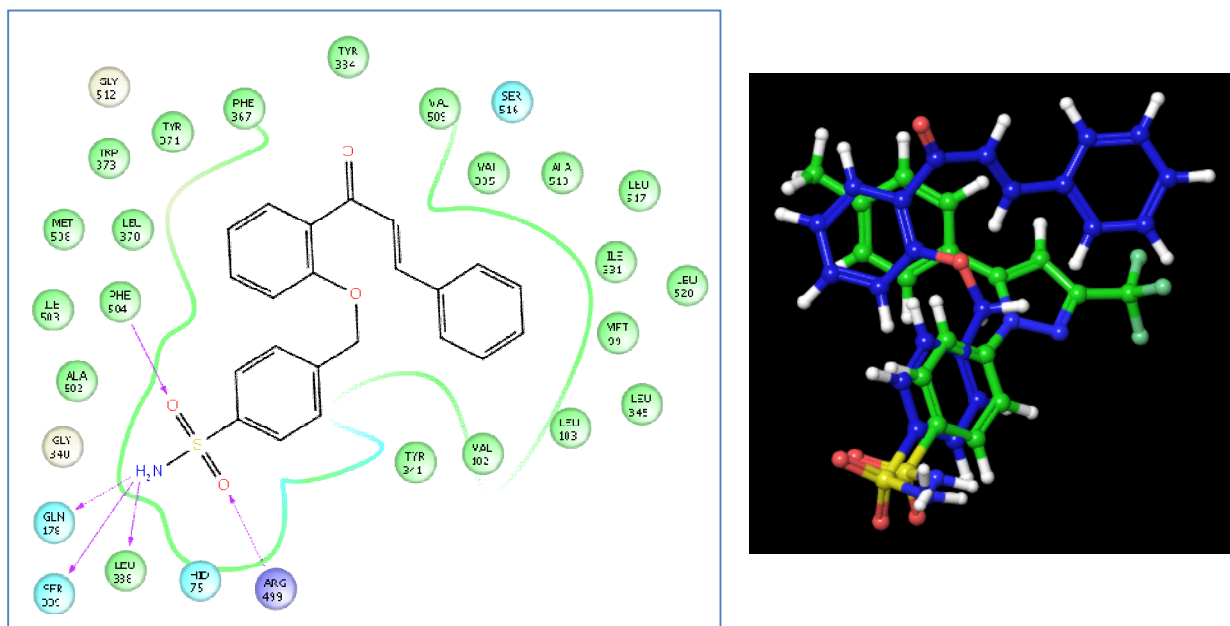


Figure 3.14. Ligand interaction diagram for **4** (left) and the docked pose of **4** (blue) overlaid with the structure of celecoxib (carbon atoms shown in green) as found in the X-ray crystal structure of COX-2 (right).⁶⁸⁴

While the ligands are predicted to interact with the same type of residues in COX-1 as COX-2, - leucines and serines - the actual residues, as expected, are not the same. Compounds **3** and **4** share a hydrogen-bond interaction to Ser516 with celecoxib, with the sulfonamide sharing two further hydrogen-bond interactions, to Leu352 and Ser353, with celecoxib. Compound **3** shares a π - π stacking interaction to tyrosine 341 (Tyr341) with celecoxib (Figure 3.15), while **4** is predicted to make two π -stacking interactions with Tyr355 and tryptophan 387 (Trp387) (Figure 3.16).

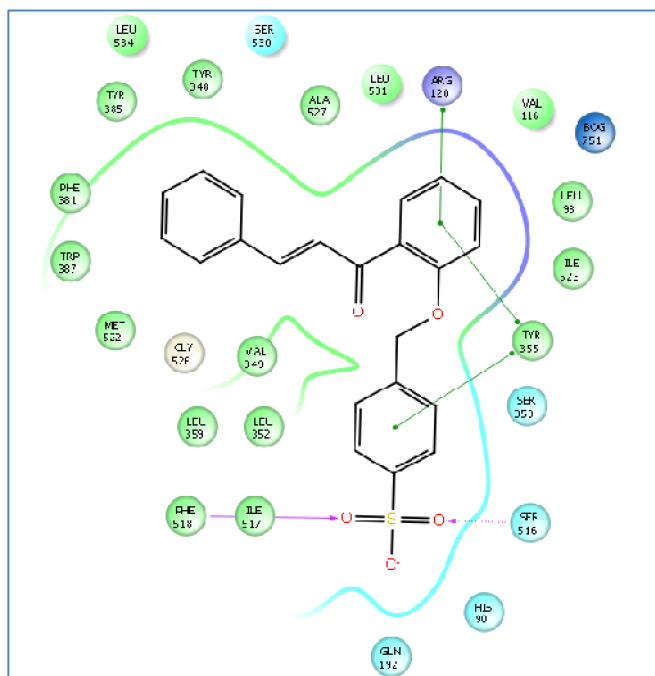


Figure 3.15. Ligand interaction diagram of **3** in COX-1 highlighting the interactions formed between ligand and protein.

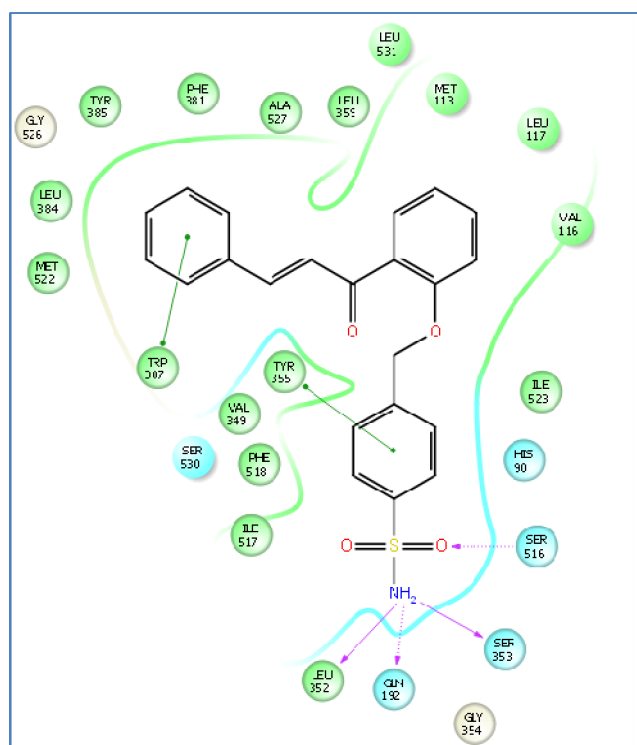


Figure 3.16. Ligand interaction diagram of **4** in COX-1 illustrating the contacts made between the protein and the docked ligand.

However there is space for improvement – compound **3** does not interact as well with the COX-2 secondary pocket as celecoxib, and compound **4** does not show interactions with COX-2 which involve the rest of the molecule. Compound **3**, while showing reduced binding towards COX-1, also shows significantly reduced binding towards COX-2. Nonetheless, these results are a positive beginning in the drug design process. The compounds interact with the protein as desired, and more importantly interact with the desired regions of the protein.

3.3. Expanding the Horizon: Design and Analysis of Sulfonate Analogs.

“Engineering, medicine, business, architecture and painting are concerned not with the necessary but with the contingent - not with how things are but with how they might be - in short, with design.”

Herbert Simon

With these promising results in hand, a range of ligands were designed in an attempt to improve on these initial compounds. These modifications include the addition of halogen atoms to both the cinnamaldehyde (A ring) and central phenyl (B) rings, as well as the introduction of the methoxy groups present in curcumin. Eleven modifications were made to the A ring, with six substitutions made on the B ring, to yield a total of 83 additional compounds. These substitutions allowed for the investigation into the influence of the nature of the substituent as well as the position of that substituent on the binding score and the pose of the compound in question. The inherent size difference between bromo-, chloro- and fluoro-substituents would permit determination of the steric restrictions at various positions within the docking site of the protein. The inclusion of methoxy substituents provides a means of studying steric effects with a different electronic effect than is present in the halogenated compounds. In addition, the presence of a fluorine atom in the molecule would also provide a means of ¹⁹F labelling, which is advantageous for both spectroscopic studies and metabolic evaluation.⁶⁹³ Fluorine, an effective isosteric replacement for oxygen, has been shown to be important in enhancing lipid solubility of the molecule, which results in enhanced biological mobility *in vivo*, as well as increasing the thermal and oxidative stability of the molecule due to the increased strength of the C-F bond.⁶⁹⁴

These compounds were prepared, docked into both COX-1 and COX-2 proteins and scored according to the established protocol. As a large number of compounds were designed and evaluated, only selected entries are presented in the tables below, with the complete tables found in the supplementary information (SI Tables 1 and 2). In order to simplify the discussion of the various substitution patterns and their effects, the substituents on the A ring will be identified using the *ortho*-/*meta*-/*para*- system of nomenclature, while substitutions made to the B-ring will be identified using the IUPAC numbering (1-, 2-, 3-), based on the parent acetophenone compounds (Figure 3.17).

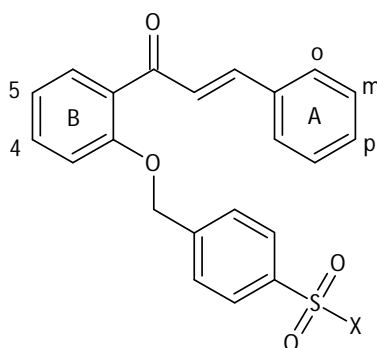


Figure 3.17. Ring identification and substituent placement for analogs of **3** and **4**.

The first series of ligands (SI Table 1) was designed using compound **3** as a foundation. All of the modifications made resulted in increases in the binding scores for COX-2, as compared to those obtained for **3**, with a number of modifications resulting in appreciable reductions in the binding scores obtained for COX-1 (Table 3.3).

Table 3.3. Glide XP and Prime scores for selected sulfonates.

Entry	B-ring ^a	A-ring ^a	Compound	COX-2		COX-1	
				Glide XP /kCal.mol ⁻¹	Prime /kCal.mol ⁻¹	Glide XP /kCal.mol ⁻¹	Prime /kCal.mol ⁻¹
1	-	-	3	-12.619	-55.772	-10.572	-74.414
2	-	<i>p</i> -Br	5	-11.436	-92.183	-11.767	-89.066
3	-	<i>p</i> -Cl	6	-11.569	-84.908	-11.223	-85.836
4	-	<i>p</i> -F	7	-12.352	-69.067	-6.414	-81.389
5	-	<i>p</i> -OMe	8	-11.898	-94.200	-9.625	-94.815
6	-	<i>m</i> -Br	9	-11.517	-103.141	-11.667	-79.280
7	-	<i>o</i> -Br	10	-12.570	-93.748	-10.102	-80.341
8	4-F	-	11	-12.664	-84.205	-10.416	-61.886
9	4-Cl	-	12	-8.049	-92.404	11.635	-83.947
10	5-F	-	13	-12.755	-87.521	-11.623	-76.281
11	5-Cl	-	14	-11.374	-100.797	-11.323	-83.647
12	4-Br	-	15	-11.013	-75.885	-10.507	-87.806
13	5-Br	-	16	-11.404	-85.328	-11.141	-87.685
14	4-F	<i>p</i> -F	17	-12.767	-86.607	-11.841	-68.525
15	4-Cl	<i>o</i> -F	18	-12.149	-88.670	-11.321	-76.413
16	4-Br	<i>p</i> -OMe	19	-11.197	-104.087	-10.097	-77.155
17	5-F	<i>p</i> -Cl	20	-12.280	-100.693	-11.121	-83.063
18	5-Cl	<i>p</i> -Br	21	-12.531	-109.956	-12.492	-95.080
19	5-Br	<i>o</i> -Br	22	-11.631	-108.849	-11.943	-95.038
20	4-F	<i>o</i> -Br	23	-11.749	-90.352	-12.126	-91.369
21	4-Cl	<i>o</i> -OMe	24	-11.534	-82.327	-10.353	-102.856
22	4-Br	<i>m</i> -Br	25	-9.959	-72.782	-10.293	-101.179
23	5-F	<i>p</i> -Br	26	-12.007	-66.972	-12.292	-94.105
24	5-Cl	<i>o</i> -Cl	27	-12.009	-95.258	-11.970	-106.313
25	5-Br	<i>p</i> -Cl	28	-12.491	-94.983	-11.607	-102.901

^a "-" indicates all hydrogen atoms present.

Addition of a *p*-substituent to the A ring resulted in enhanced binding, as compared to the unsubstituted sulfonate, to both COX-1 and COX-2 (Table 3.3, entries 2-5), while substitution of a bromine atom at either the *ortho*- or *meta*-positions (Table 3.3, entries 6 and 7) resulted in significantly enhanced binding scores ($\sim 40\text{-}50\text{ kCal.mol}^{-1}$) for COX-2, with much smaller changes ($\sim 5\text{ kCal.mol}^{-1}$) observed for the corresponding COX-1 binding scores. The poses calculated for these compounds mirror the pose determined for **3** in COX-2, with the B ring positioned in a very similar location as the 5-phenyl ring of celecoxib (Figure 3.18). This orientation within the protein results in the A-ring of each of the compounds being located towards the entrance of the active site, allowing for more flexibility, and also exposes the halogen and methoxy substituents to the solvent. These six compounds make similar contacts to the protein as is seen for **3**, namely interactions to Ser516, Arg499 and Tyr341, and also made additional contacts with residues Arg106 and Trp373, which account for the increases seen in the binding scores. When docked into COX-1, compounds **5-10** show inversion and/or rotation of the poses when compared to the pose generated for **3**. Despite this rotation and/or inversion, the docked poses for these compounds share a number of interactions with **3** – interactions with Ser516, Ile517, Phe518 and Tyr355 are common, with additional interactions to residues such as Ser530 present for more than one compound. These shared interactions partially explain the closeness observed in the COX-1 binding scores observed, as these compounds do not make a large number of additional interactions with the protein.

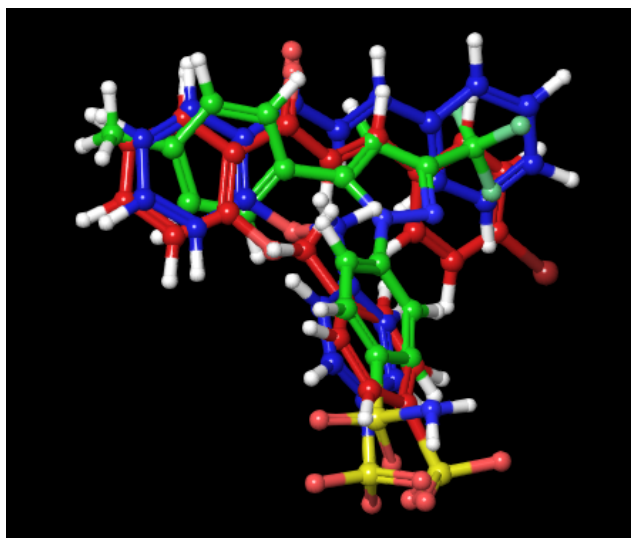
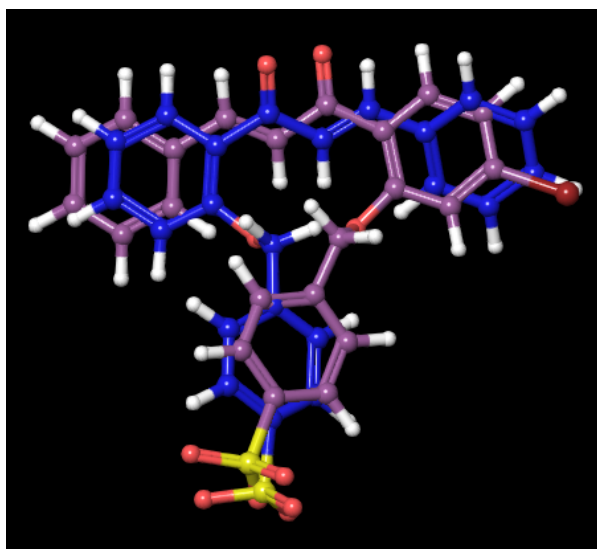


Figure 3.18. Overlap of the poses generated for compound **5** with celecoxib and **3**, when docked into COX-2, showing the close clustering obtained. Celecoxib is shown with green carbon atoms, **3** in blue and **5** in red.

Substitutions on the B ring were also shown to influence the binding scores. Addition of fluorine or chlorine atoms at either the 4- or 5-positions of the B ring (Table 3.3, entries 8-11) resulted in increasingly positive changes – defined here as a large increase in COX-2 binding and a small increase or a decrease in COX-1 binding scores – from fluorine to chlorine while substitution with bromine atoms at either of these positions resulted in ligands showing smaller changes in the COX-2 binding energies, with similar gains in COX-1 binding scores. (Table 3.3, entries 12 and 13). Rather, these two compounds yield binding scores lower than those calculated for their respective fluoro analogues. Inspection of the pose for compound **15** shows inversion of the molecule when the pose is compared to that of the parent compound **3** (Figure 3.19), and compound **16** shows rotation of the alkyl chain linking the A and B rings (Figure 3.20). This is most likely due to the steric bulk of the bromine atoms, as the poses generated for compounds **15** and **16** do not show the same degree of clustering as the fluoro- or chloro- analogues, and accordingly, slightly different interactions are formed between the ligand and the protein. This therefore results in the binding scores not “fitting the pattern” previously established. As was the case for the A-ring substitutions, compounds **11-16** also show inversion and /or rotation of the poses generated when these compounds were docked into COX-1. Compound **11**, which contains a 4-fluoro substitution, is one of the few compounds which show a reduction in the COX-1 binding scores (Table 3.3, entry 8), and evaluation of the docked pose shows both inversion and rotation of the alkyl chain as compared to **3**, leading to different ligand-protein interactions and subsequent reduction in the binding scores.



*Figure 3.19. The “inversion” of the pose generated for compound **15**, shown in purple, as compared to the pose generated for the parent sulfonate **3**, shown in blue.*

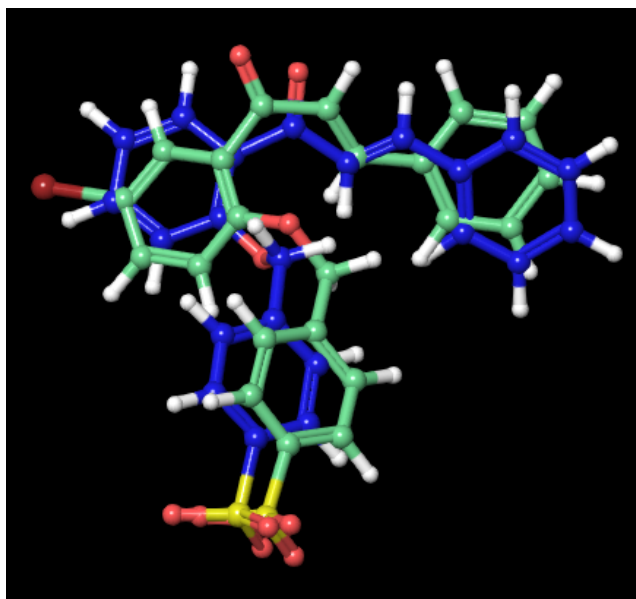


Figure 3.20. The rotation of the alkyl chain in the pose generated for **16**, shown in green, as compared to the pose generated for the parent sulfonate **3**, shown in blue.

Simultaneous substitutions of the A and B rings were also investigated, again with both positive and negative changes observed. A *p*-fluoro substituent on the A ring combined with a fluorine atom at the 4-position on the B ring -“*p*-fluoro/4-fluoro”- (compound **17**) resulted in enhancement of COX-2 binding scores, with a reduction in the COX-1 binding scores (Table 3.3, entry 14), as did an *o*-fluoro/4-chloro combination (**18**), a *p*-methoxy/4-bromo combination (**19**), a *p*-chloro/5-fluoro combination (**20**), a *p*-bromo/5-chloro combination (**21**), and surprisingly an *o*-bromo/5-bromo combination (**22**) (Table 3.3, entries 15-19). These poses again cluster well, with the only pose which did not cluster as well was that obtained for compound **22**. The inversion of this pose when judged against **3** most likely allows for some relief of the steric strain present due to the presence of two bromine atoms, while maintaining similar ligand-protein interactions (Figure 3.21). This indicates that the size as well as the location of substitutions affects the docking and binding scores. As expected, the COX-1 docked poses show inversion and/or rotation as compared to **3**, while retaining a number of the ligand-protein interactions found for **3**. These common interactions again aid in the explanation of the similar binding scores observed for compounds **17-22**.

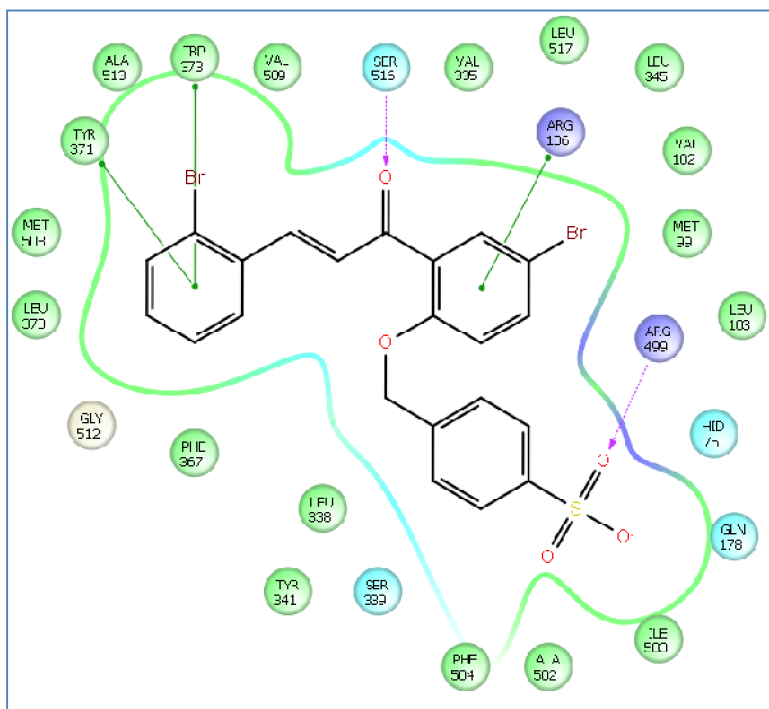


Figure 3.21. Ligand interaction diagram for **22** with COX 2, showing the predicted protein-ligand interactions.

In contrast, a combination of an *o*-bromo substituted A-ring with a 4-fluoro substituted B-ring (compound **23**) resulted in a ligand showing enhanced binding for both COX-1 and COX-2 (Table 3.3, entry 20), and significantly enhanced COX-1 binding with moderate improvement of the COX-2 binding scores was observed for *o*-methoxy/4-chloro (**24**), *m*-bromo/4-bromo (**25**), *p*-bromo/5-fluoro (**26**), *o*-chloro/5-chloro (**27**), and *p*-chloro/5-bromo ligands (**28**) (Table 3.3, entries 21-25). Interestingly, the pose generated for compound **26** shows good correlation with that generated for **3** (Figure 3.22), however it shows one of the smallest changes in the COX-2 binding scores for all the ligands (Table 3.3, entry 23). This illustrates one of the limitations of combinatorial chemistry which can be minimized, if not avoided altogether, through the use of computational methods – in this case the poses and the binding scores of **3** and **26** are very similar, and these compounds are not expected to yield significantly different results *in vitro* and *in vivo*, despite **26** containing both a fluorine and a bromine atom. As such there is almost no need to synthesize **26**, unless the substitutions are likely to enhance other physical properties. Compounds **23-28** all show the expected inversion of the docked pose in COX-1, with compound **24** also showing movement of the sulfonate group away from the position occupied by **3** and the other compounds.

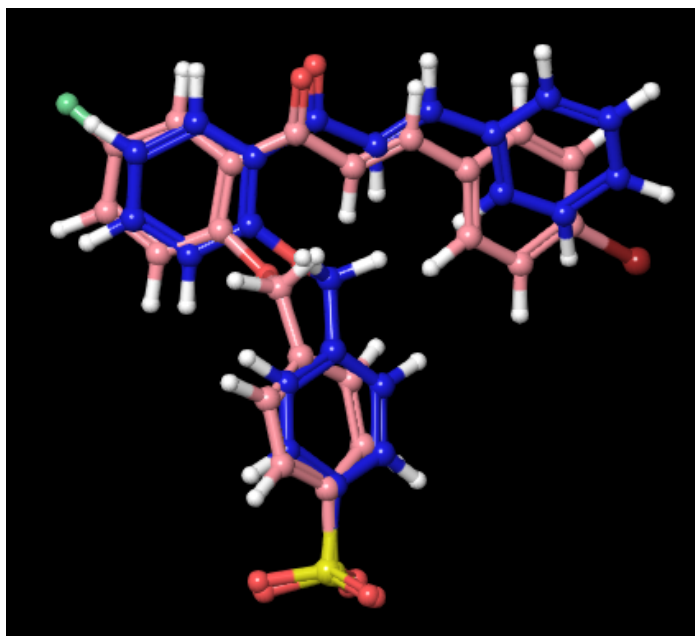


Figure 3.22. Overlap of the poses generated for **26** (shown in pink) and **3** (shown in blue).

3.4. Always Have a Backup Plan: Design and Analysis of Sulfonamide Analogs.

"Tea and cake or death?"

Eddie Izzard, *Dressed to Kill*

The second set of ligands, designed using **4** as a base, and utilizing the same modifications as for the first set of ligands, was also docked into COX-1 and COX-2 (SI Table 2). In contrast to the previous set of ligands, no modifications resulted in marked reductions in the binding scores for COX-1, and identification of trends such as those found previously was challenging.

Table 3.4. Glide XP and Prime scores for selected sulfonamides.

Entry	B-ring ^a	A-ring ^a	Compound	COX-2		COX-1	
				Glide XP /kCal.mol ⁻¹	Prime /kCal.mol ⁻¹	Glide XP /kCal.mol ⁻¹	Prime /kCal.mol ⁻¹
1	-	-	4	-11.378	-72.679	-12.823	-89.915
2	-	<i>p</i> -F	29	-11.765	-77.769	-12.821	-101.232
3	4-F	<i>p</i> -F	30	-12.537	-91.703	-13.469	-99.267
4	5-F	<i>p</i> -F	31	-12.998	-86.470	-13.337	-85.901
5	4-Br	<i>p</i> -F	32	-11.058	-101.192	-12.675	-107.264
6	4-Cl	<i>p</i> -F	33	-11.532	-93.335	-13.459	-109.749
7	5-Br	<i>p</i> -F	34	-12.852	-98.743	-13.617	-110.607
8	5-Cl	<i>p</i> -F	35	-12.032	-96.919	-13.553	-103.727
9	-	<i>o</i> -Br	36	-11.581	-97.580	-13.253	-114.414
10	4-F	<i>o</i> -Br	37	-11.438	-98.376	-13.143	-95.641
11	4-Cl	<i>o</i> -Br	38	-11.755	-124.159	-13.120	-121.787
12	4-Br	<i>o</i> -Br	39	-11.440	-120.903	-13.312	-115.491
13	5-F	<i>o</i> -Br	40	-11.708	-104.910	-12.968	-90.213
14	5-Cl	<i>o</i> -Br	41	-11.838	-112.508	-13.387	-118.002
15	5-Br	<i>o</i> -Br	42	-11.927	-112.496	-13.415	-110.871

^a "-" indicates all hydrogen atoms present.

Addition of a *p*-fluoro substituent to the A-ring of **4** results in a very small change in the COX-2 binding score (Table 3.4, entry 2), and the poses of compounds **4** and **29** are almost identical (Figure 3.23). There is a much larger difference between the COX-1 binding scores for **4** and **29**, and inspection of the poses showed that the pose for **29** is inverted and the *p*-fluorophenyl group is rotated in comparison to the pose generated for **4** (Figure 3.24). While perhaps not interesting in terms of improvement of the binding scores of **4**, the very small difference in the COX-2 binding energy between these two poses indicates that these compounds will most likely interact in very similar ways *in vivo*, and the presence of the fluorine atom in **29** functions as a label, that can be used as a tracer in metabolic studies.

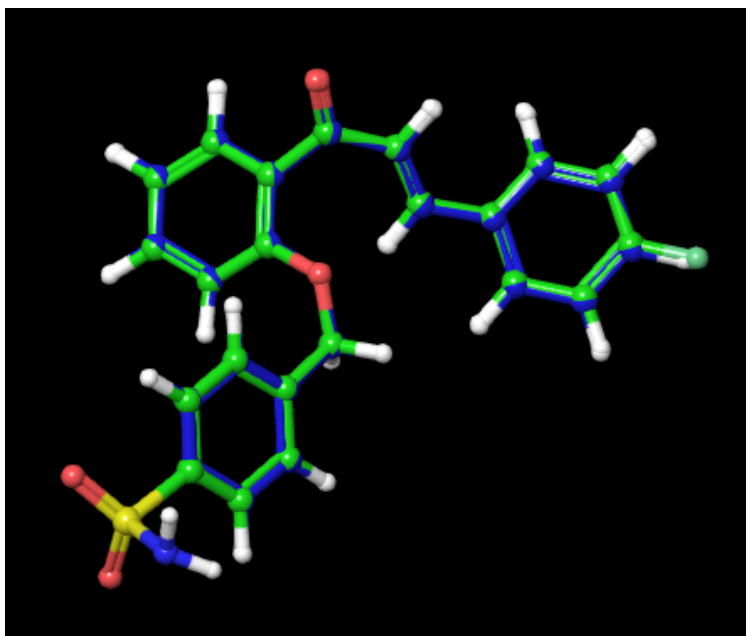


Figure 3.23. *Overlap of the poses generated for 4 (shown in blue) and 29 (shown in green) when docked into COX-2.*

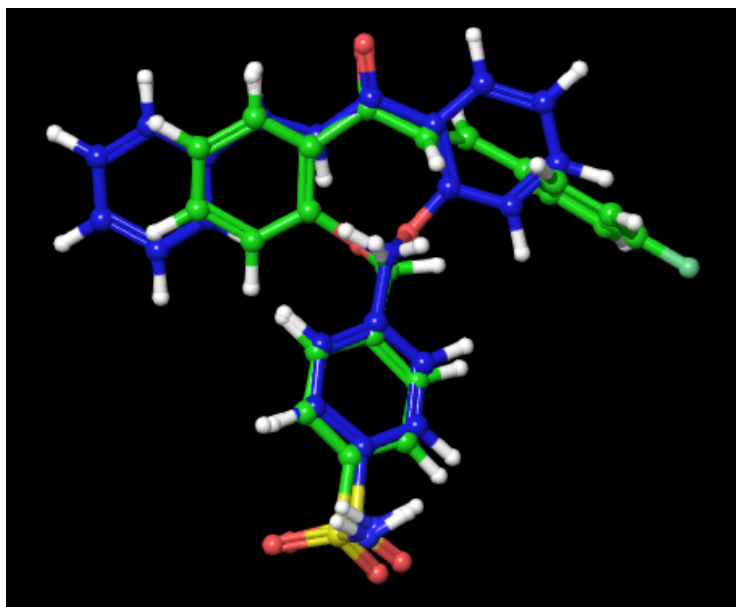


Figure 3.24. *Overlap of the poses generated for 4 (shown in blue) and 29 (shown in green) when docked into COX-1.*

Addition of a second fluorine atom to the B-ring at either the 4- or 5-positions resulted in increases to both the COX-2 and COX-1 binding scores (Table 3.4, entries 3 and 4). Examination of the poses for compounds **30** and **31** when docked into COX-2 revealed that while these two compounds show very

similar poses, the poses are different to those obtained for compounds **4** and **29** (Figure 3.25). In COX-1, compounds **29**, **30** and **31** overlap very well, with compounds **30** and **31** showing the same inversion and rotation of the *p*-fluorophenyl group as seen for compound **29**.

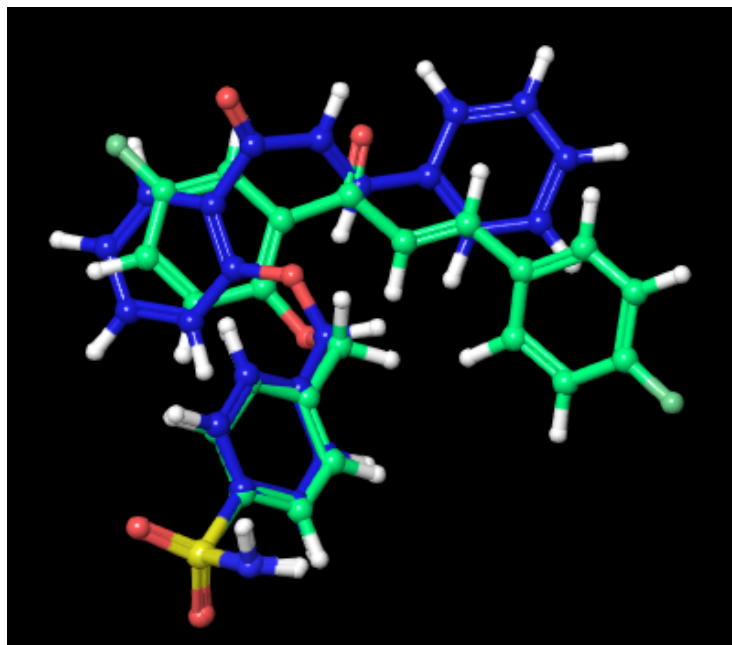


Figure 3.25. Overlap of **4** (shown in blue) and **31** (shown in green) when docked into COX-2.

Addition of bromo- or chloro- substituents at either position on the B-ring resulted in even larger changes to the binding scores for both COX-1 and COX-2 (Table 3.4, entries 5-8), and analysis of the poses shows movement of the A ring away from the position occupied by the A ring in **4** (Figure 3.26). This movement allows for the formation of a hydrogen bond between the side chain of Ser516 with the carbonyl oxygen atom in all four compounds, and, in the case of compound **32**, the formation of π - π stacking interactions between the A-ring, Arg106 and Tyr341 (Figure 3.27). The poses for compounds **32**, **33**, **34** and **35** when docked into COX-1 are all inverted as compared to **4**, and this inversion allows for interaction of the A-ring with Tyr355 (Figure 3.28), resulting in the observed increases in the COX-1 binding scores.

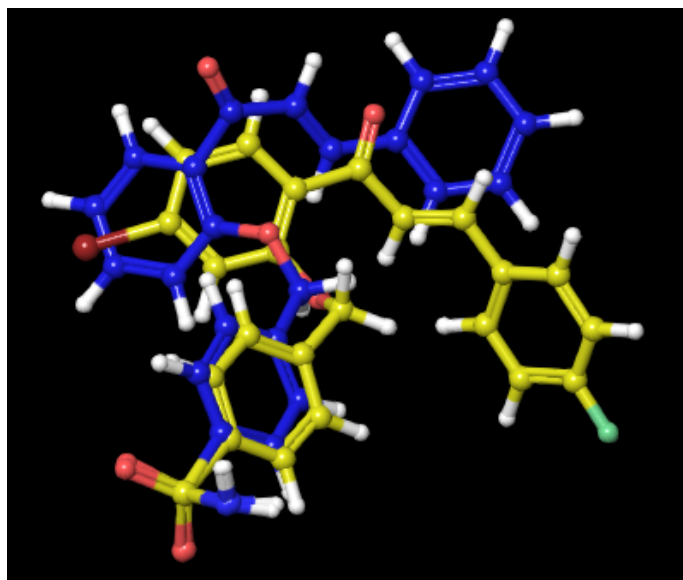


Figure 3.26. Overlap of the poses of **4** (shown in blue) and **32** (shown in yellow) when docked into COX-2.

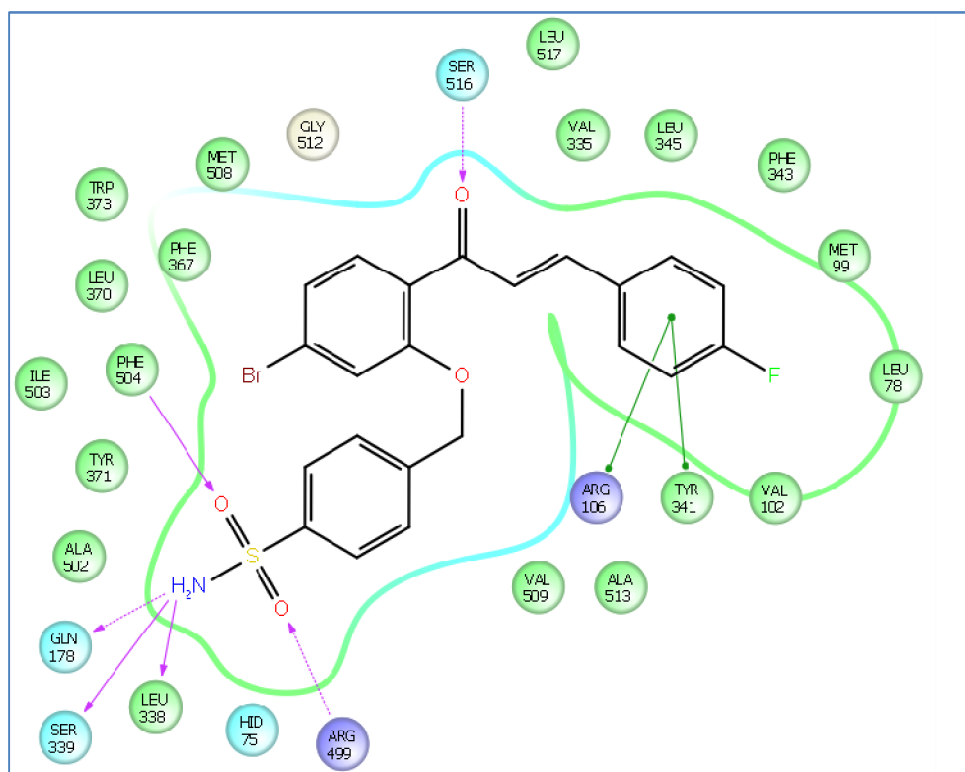


Figure 3.27. Ligand interaction diagram for **32** showing the interactions formed between the ligand and COX-2.

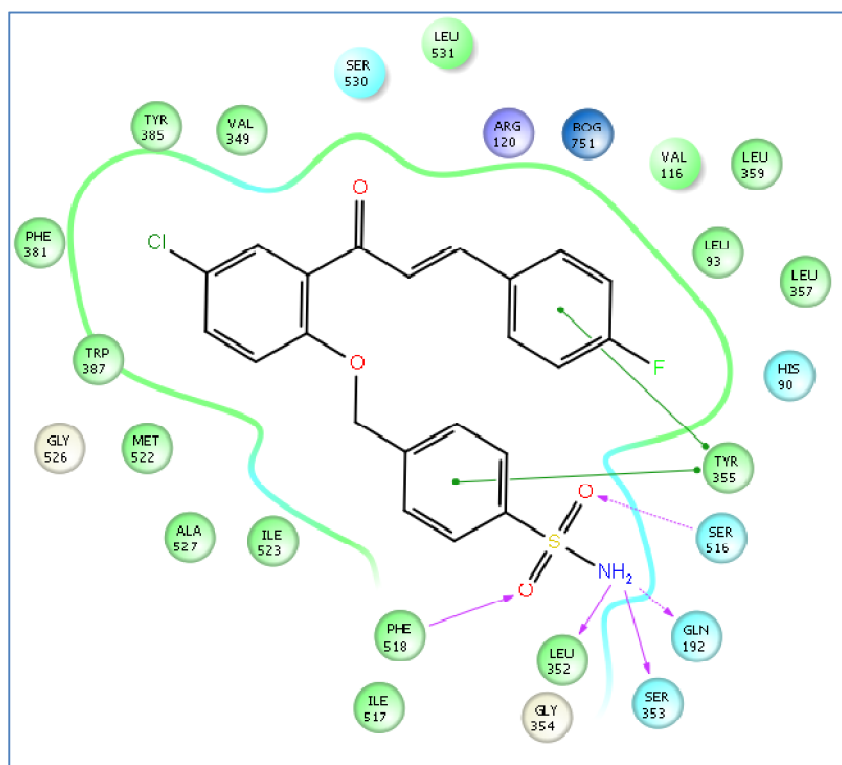


Figure 3.28. Ligand interaction diagram for **35** showing the interactions formed between the ligand and COX-1.

Inclusion of an *o*-bromo substituent on the A-ring resulted in significant increases to the binding scores for both COX-1 and COX-2 (Table 3.4, entries 9-15), with compound **38** showing the highest binding scores of -121.787 kcal/mol and -124.159 kcal/mol respectively (Table 3.4, entry 11). The phenylsulfonamide portion of the pose generated for this compound overlaps well with the parent sulfonamide (Figure 3.29), with the poses differing in the chalcone portion of the molecules. This deviation from the pose generated for **4** brings the pose generated for **38** closer into alignment with the crystal structure of celecoxib (Figure 3.30), and the additional ligand-protein interactions formed contribute to the high binding scores obtained for this compound.

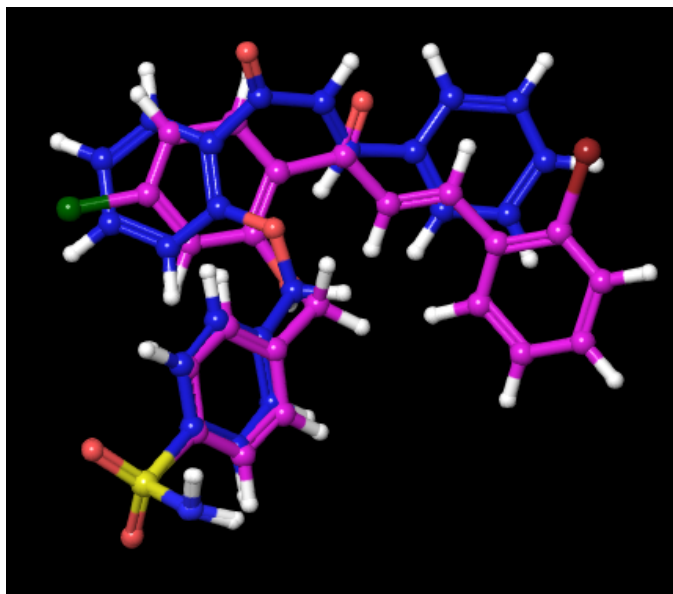


Figure 3.29. Overlap of the poses generated for **4** (shown in blue) with compound **38** (shown in purple) when docked into COX-2.

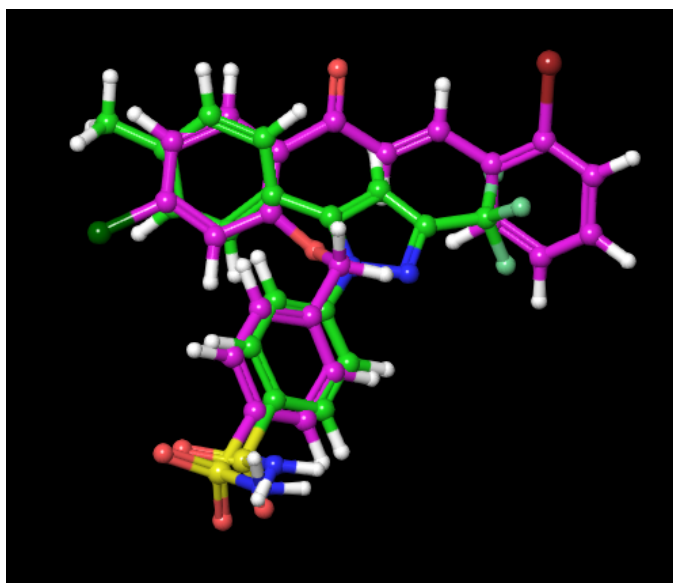


Figure 3.30. Overlap of the pose generated for **38** when docked into COX-2 (depicted in light blue) with the X-ray crystal structure of celecoxib (depicted in green).

Compound **40**, which includes an *o*-bromo/5-fluoro combination, shows a large positive change in the MM/GBSA scores (Table 3.4, entry 13), and while not having the largest binding energy, the very small change in the COX-1 binding scores make this compound interesting. Inspection of the binding pose for **40** in COX-2 showed inversion of the molecule, again allowing for the formation of additional ligand-

protein interactions (Figure 3.31). The pose generated for **40** when it is docked into COX-1 shows very similar protein-ligand interactions to that obtained for **4** (Figure 3.32), which corresponds to the small changes in the binding scores obtained.

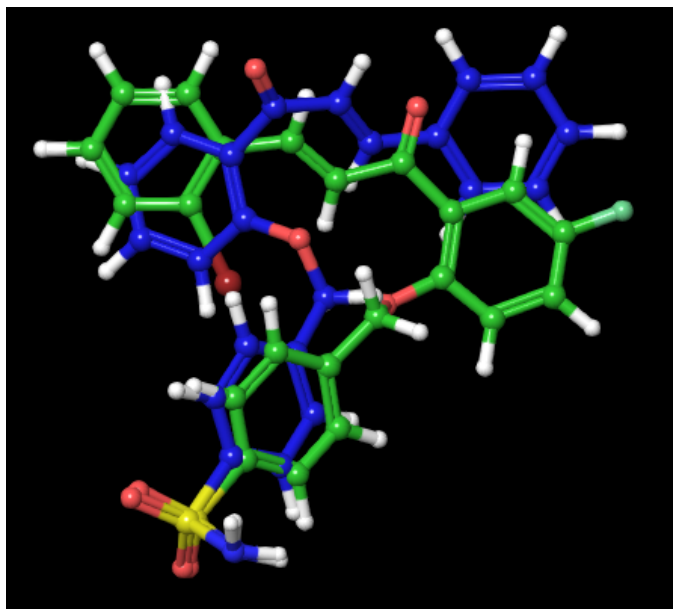


Figure 3.31. Overlap of the poses of **4** (shown in blue) with **40** (shown in green) when docked into COX-2.

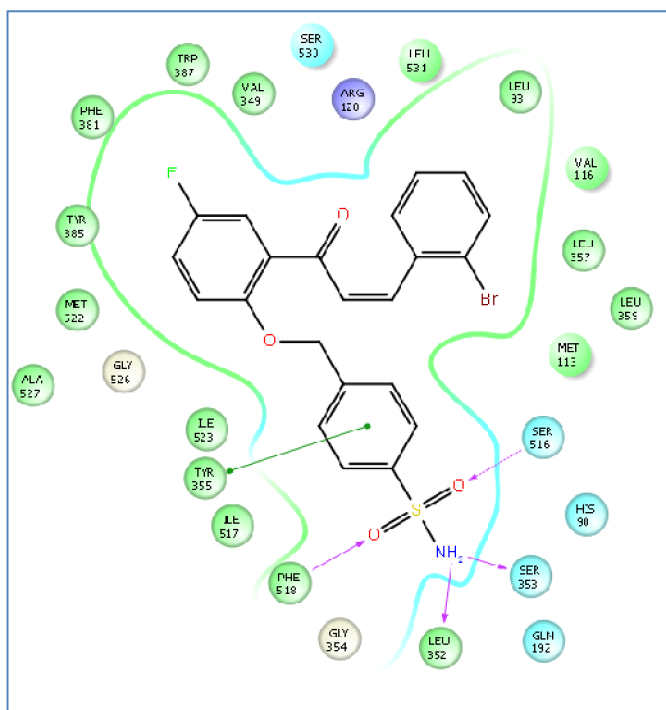


Figure 3.32. Ligand interaction diagram for **40** showing the interactions between the ligand and COX-1.

3.5. A Word to the Wise: Selection of Candidates for Synthesis.

“Knowledge is knowing that a tomato is a fruit. Wisdom is knowing that a tomato doesn't belong in a fruit salad.”

Miles Kingston

While these docking scores are good indicators of binding, these *in silico* results do not take into account *in vivo* conditions and cannot predict the actual selectivity of a compound for one protein isoform over another – for example, celecoxib shows a higher docking score for COX-1 over COX-2 (ca. $-86 \text{ kCal.mol}^{-1}$ and $-84 \text{ kCal.mol}^{-1}$ respectively), but *in vivo* it is 10-20 times more selective for COX-2 over COX-1.⁶⁴⁴ As such, docking scores such as these are only indications of binding and must not be taken as absolutes; rather they should be used in conjunction with *in vitro* binding studies in order to determine whether the docking scores are accurate representations of what occurs in the proteins.

Synthesis and testing of all 168 compounds would be ideal, as this would allow for the accurate comparison of the *in silico* docking scores with actual experimental results. However, this is intensely time-consuming and prohibitively expensive, both in terms of starting materials needed and the cost associated with the biological testing of all of these compounds. As such, a representative selection of ligands is needed which would demonstrate both *positive* and *negative* changes to the docking scores obtained. While synthesis of the twenty-five sulfonate compounds identified in Table 3.3 would allow for investigation of the changes observed in the docking scores, and various combinations thereof, synthetic challenges (described in detail in Chapter 4) severely limited the number of compounds which could be synthesized and tested. Due to these challenges, a different set of ligands was selected which showed the desired changes (Table 3.5).

Table 3.5. Glide XP and Prime scores for selected sulfonate compounds for synthesis.

Entry	B-ring ^a	A-Ring ^a	Compound	COX-2		COX-1	
				Glide XP /kCal.mol ⁻¹	Prime /kCal.mol ⁻¹	Glide XP /kCal.mol ⁻¹	Prime /kCal.mol ⁻¹
1	-	-	3	-12.619	-55.772	-10.572	-74.414
2	-	<i>p</i> -Br	5	-11.436	-92.183	-11.767	-89.066
3	-	<i>p</i> -Cl	6	-11.569	-84.908	-11.223	-85.836
4	-	<i>p</i> -F	7	-12.352	-69.067	-6.414	-81.389
5	-	<i>p</i> -OMe	8	-11.898	-94.200	-9.625	-94.815
6	-	<i>m</i> -Br	9	-11.517	-103.141	-11.667	-79.280
7	-	<i>m</i> -Cl	43	-11.001	-104.953	-11.120	-86.983
8	-	<i>m</i> -F	44	-12.687	-93.861	-5.040	-77.147
9	-	<i>o</i> -Br	10	-12.57	-93.748	-10.102	-80.341
10	-	<i>o</i> -Cl	45	-12.163	-93.155	-10.709	-89.088
11	-	<i>o</i> -F	46	-12.362	-90.999	-11.556	-78.554
12	-	<i>o</i> -OMe	47	-12.111	-70.669	-10.59	-75.929
13	4-F	-	11	-12.664	-84.205	-10.416	-61.886
14	4-F	<i>p</i> -Br	48	-12.064	-96.677	-12.223	-82.510
15	4-F	<i>p</i> -Cl	49	-11.973	-99.575	-12.093	-81.847
16	4-F	<i>p</i> -F	17	-12.767	-86.607	-11.841	-68.525
17	4-F	<i>p</i> -OMe	50	-12.059	-85.854	-10.797	-71.438
18	4-F	<i>m</i> -Br	51	-11.654	-89.884	-10.684	-92.570
19	4-F	<i>m</i> -Cl	52	-11.993	-88.717	-10.825	-86.733
20	4-F	<i>m</i> -F	53	-12.681	-90.577	-4.324	-82.781
21	4-F	<i>o</i> -Br	23	-11.749	-90.352	-12.126	-91.369
22	4-F	<i>o</i> -Cl	54	-12.646	-90.856	-11.267	-88.617
23	4-F	<i>o</i> -F	55	-12.700	-88.670	-11.441	-87.202
24	4-F	<i>o</i> -OMe	56	-12.394	-72.392	-9.992	-76.870
25	4-Cl	-	12	-8.049	-92.404	11.635	-83.947
26	4-Cl	<i>p</i> -OMe	57	-11.497	-98.497	-9.624	-86.845
27	4-Cl	<i>m</i> -Cl	58	-7.813	-88.302	-9.927	-97.391
28	4-Cl	<i>o</i> -Cl	59	-11.325	-100.695	-11.530	-92.396
29	4-Cl	<i>o</i> -F	18	-12.149	-98.884	-11.321	-76.413
30	4-Cl	<i>o</i> -OMe	24	-11.534	-82.327	-10.353	-102.856

^a "-" indicates all hydrogen atoms present.

As previously stated, the addition of a *p*-bromo-, chloro- or methoxy-substituent to **3** resulted in significantly enhanced binding scores for both COX-1 and COX-2 (Table 3.5, entries 2, 3, and 5), and the addition of a *m*-bromo or an *o*-bromo atom resulted in a large increase in the binding score obtained for COX-2, while the binding score for COX-1 is affected to a much lesser degree (Table 3.5, entries 6 and 9). Addition of an *m*-chloro atom also results in a large change in the binding score for COX-2 (Table 3.5, entry 7); however the COX-1 binding score is affected to a greater degree than was observed for the *m*-bromo compound. Addition of a *p*-fluoro or an *o*-methoxy substituent on the A-ring, while still resulting in positive changes in the COX-2 binding scores (Table 3.5, entries 4 and 12), show much smaller changes than those observed for any of the other substitutions.

The combination of an A-ring *o*-methoxy substitution with a B-ring 4-fluoro substitution (compound **56**), however, results in a molecule with a lower COX-2 binding score than those obtained for other multiple substitution patterns (Table 3.5, entry 24). This indicates that, at least in this case, the presence of the *o*-methoxy group influences the binding score more than the fluorine atom does, as the docking scores obtained for this compound are similar to those obtained for compound **47** (Table 3.5, entry 12), which does not contain a fluorine atom. In contrast to the other *o*-methoxy containing compounds, the *o*-methoxy/4-chloro combination found in compound **24** shows a large change in the COX-1 binding score (Table 3.5, entry 30), and investigation of the binding pose showed an inversion in the binding pose as compared to compound **3** (Figure 3.33). This inversion results in different interactions with the protein (Figure 3.34) and the corresponding change in the binding score.

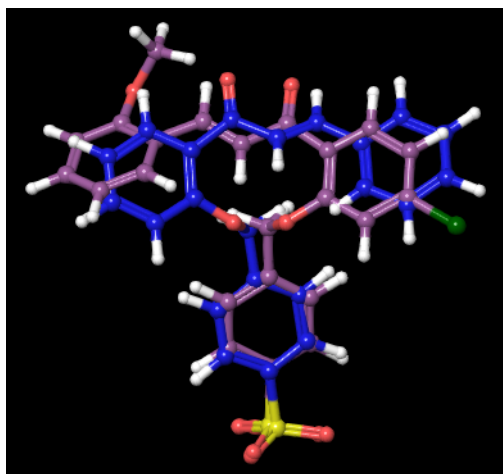


Figure 3.33. Overlap of the poses of **24** (shown in purple) and **3** (shown in blue) when docked into COX-1.

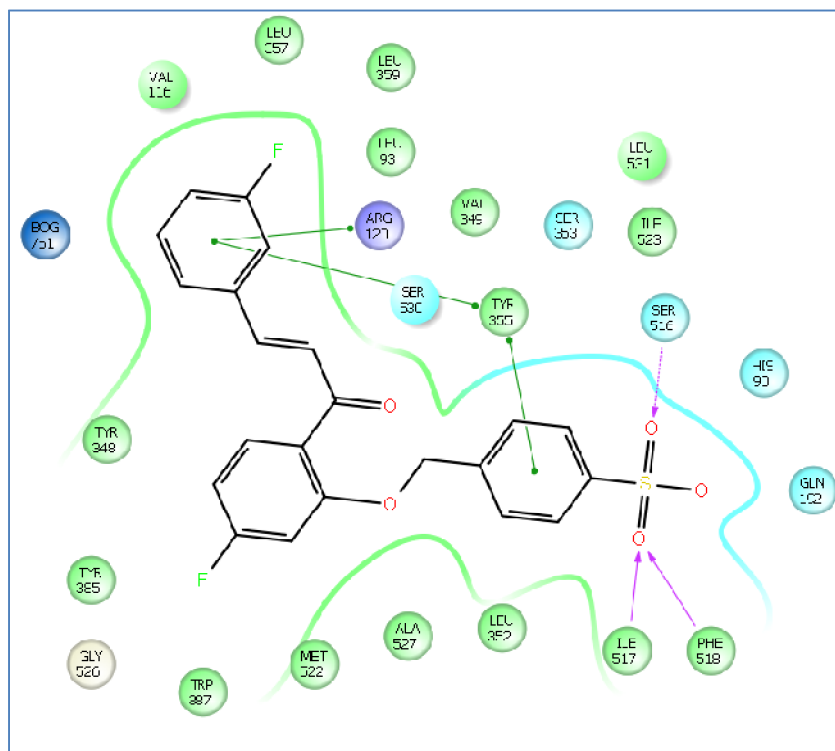


Figure 3.35. Ligand interaction diagram of 53 with COX-1.

3.6. What We Never Knew We Needed to Know: A Review.

"The only true wisdom is in knowing you know nothing."

Socrates

Docking of the known COX-2 selective compound celecoxib highlighted important interactions which are formed between the ligand molecule and amino acid residues within the active site of the protein. The binding scores calculated for celecoxib when docked into COX-1 and COX-2 are similar, indicating that the binding scores alone cannot accurately describe the *ca.* 10-fold difference in selectivity observed for celecoxib with these protein isoforms, and as such any computational information must be correlated with experimental data in order to determine the accuracy of the model used. Molecular docking shows that the dominant keto-enol tautomer of curcumin does not interact with the secondary pocket present in COX-2, and as such is not expected to be COX-2 selective. The diketone tautomer presents as a possible COX-2 selective compound, however this tautomer is almost nonexistent in solution and as such the use of this isomer as a COX-2 selective compound is unfeasible.

Based on the poses and interactions predicted for curcumin and celecoxib, two potential COX-2 selective compounds were designed using fragments common to celecoxib and other COX-2 selective compounds, as well as fragments present in curcumin. Initial docking showed that both compounds interact with the secondary pocket as desired, and make a number of connections to the protein which are present between celecoxib and COX-2. The docking results also showed that there was room for improvement, and therefore a range of modifications were made in order to explore the impact of various substitutions on the docking and binding scores, as well as to explore how the positioning of these modifications affected the docking poses and the interactions made between the protein and the ligand.

In all cases, the modifications resulted in increased MM/GBSA binding scores for COX-2, and in a few cases, a reduction in the COX-1 binding scores were noted. In total, 166 compounds were designed across the two classes and these compounds show both positive and negative changes to COX-2 and COX-1 binding scores. Due to synthetic challenges, thirty benzenesulfonate-based compounds, which characterize the changes seen in the full complement of compounds, were selected as candidates for synthesis and initial biological screening.

4. Results and Discussion: Synthesis of Target Benzenesulfonates

4.1. From the Bottom Up: Retrosynthesis and Initial Synthesis.

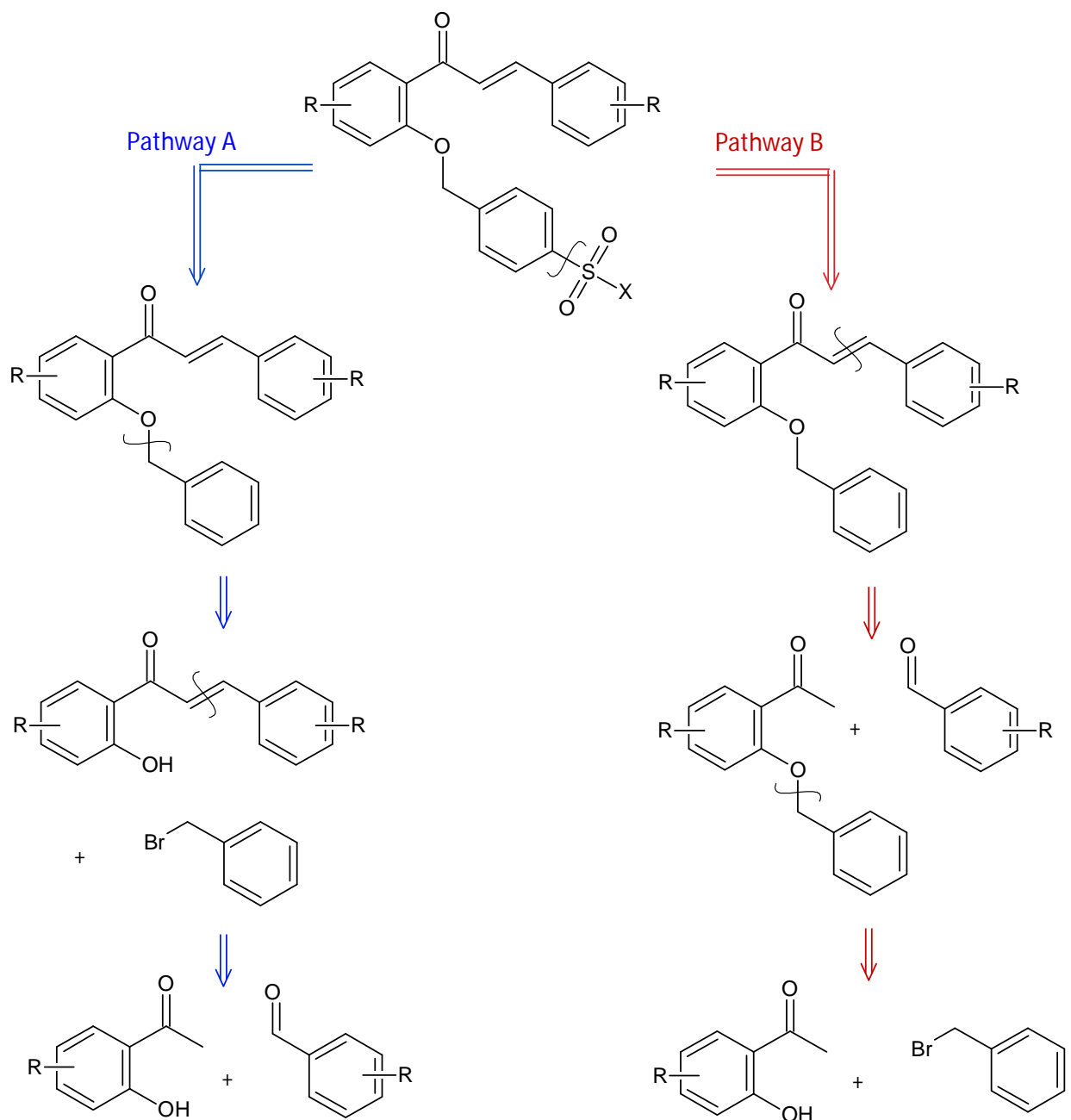
"My mind rebels at stagnation. Give me work, give me problems."

Sir Arthur Conan Doyle, *The Sign of Four*

While computational modeling is a vastly powerful tool in the process of drug design, the true test of the success of a designed drug lies in the results obtained through biological testing. Before a drug candidate can be subjected to this testing, the *in silico* molecule must be translated from the computer screen to a vial through chemical synthesis. One of the downsides to computational modeling is that a compound which shows good prospects on screen might be so synthetically challenging that the molecule might never make it to the testing phase, despite the good computational results.

After identification of suitable candidate molecules through computational modeling, retrosynthetic analysis identified two possible synthetic routes (Scheme 4.1). Pathway A involves the formation of a chalcone from a 2'-hydroxyacetophenone and a suitable benzaldehyde in a base-catalyzed condensation reaction, followed by a base-catalyzed ether formation between the phenolic oxygen atom of the acetophenone ring and an appropriate benzyl halide. Pathway B involves the same starting components; however the order of the reactions is different. In this pathway, the ether bond is created first between the phenolic oxygen atom of the 2'-hydroxyacetophenone and a benzyl halide, followed by the base-catalyzed *condensation* reaction with the benzaldehyde. The final steps in these pathways are identical – addition of a sulfonyl chloride moiety to the benzyl ring, followed by conversion to the desired sulfonic acid or sulfonamide. These pathways provide access to a wide range of compounds as a variety of substituted benzaldehydes and 2'-hydroxyacetophenones are commercially available.

Scheme 4.1. Retrosynthetic analysis of the target molecule showing two synthetic pathways.



Initial investigations into the formation of the ether bond were carried out using 2'-hydroxyacetophenone (**60**) and benzyl bromide (**61**) (Scheme 4.2), and the use of 1 equivalent of anhydrous potassium carbonate in refluxing acetonitrile⁶⁹⁵⁻⁶⁹⁷ was sufficient to effect the conversion to **62** cleanly and in almost quantitative yields in 24 hours (Table 4.1.).

Scheme 4.2. Synthesis of ether **62**.

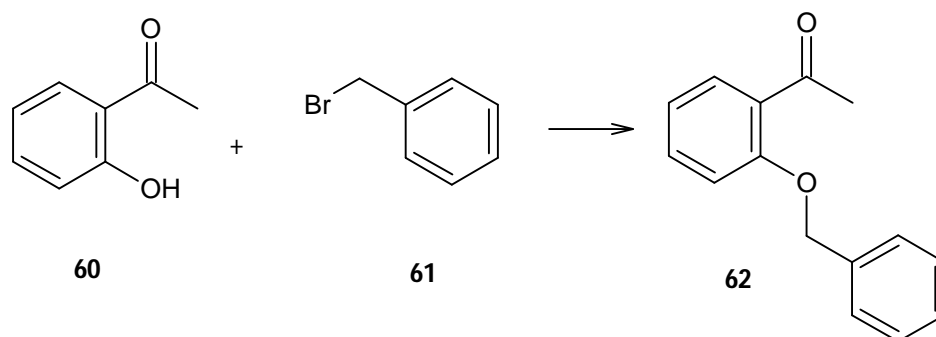


Table 4.1. Optimization of conditions for ether formation.

Reaction	Equivalents K_2CO_3	Solvent	Time at reflux /Hours	Yield /%
1	1	Me ₂ CO ⁶⁹⁶	24	66
2	1	Me ₂ CO	48	95
3	2	Me ₂ CO	24	82
4	1	MeCN	12	54
5	1	MeCN	24	89

¹H NMR spectral analysis of **62**⁶⁹⁸ showed a significant shift in the location of the methylene proton peak, from 4.60 ppm (in the spectrum of **61**) to 5.23 ppm (Figure 4.1). As this region of the spectrum is clear of other signals, the course of reactions could easily be followed by observing the relative integrals of these two signals. Slow evaporation of the solvent resulted in the formation of a crystalline solid, and X-ray spectroscopic analysis of suitable crystals of **62** (CCDC deposit number pending) revealed that the two aromatic rings are essentially perpendicular to each other, rather than existing as a planar molecule (Figure 4.2). While X-ray analysis of any of the synthesized compounds is interesting, this aspect is not of great importance to the overall project, and as such the X-ray data is presented merely for the sake of interest and will not be discussed in detail (See SI for complete structural description).

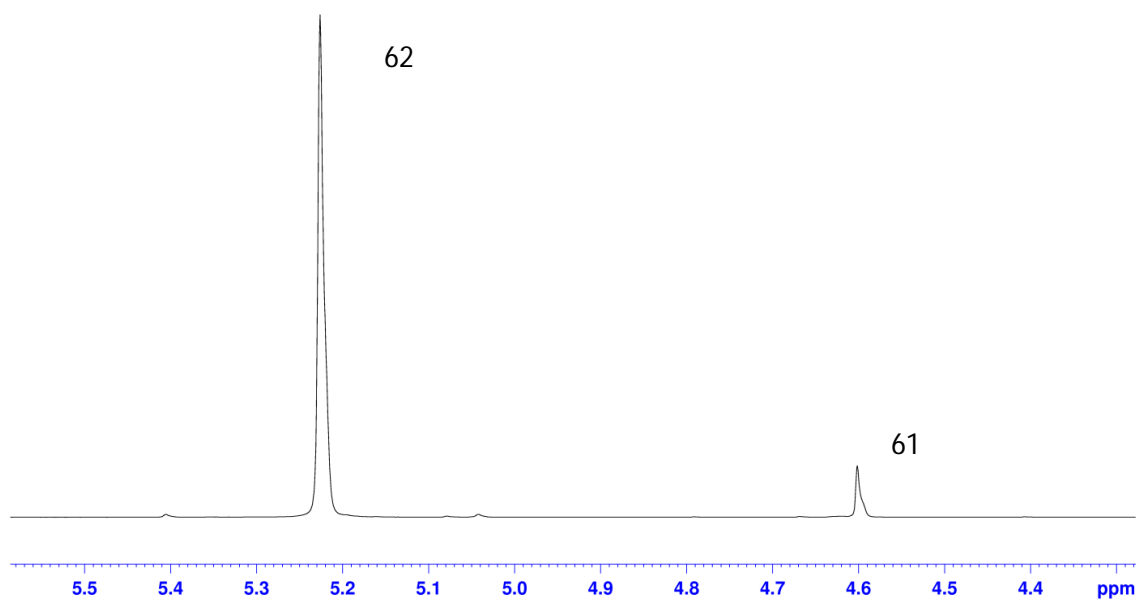


Figure 4.1. ^1H NMR spectrum of **62** showing the shift in the location of the methylene signals on formation of the ether bond.

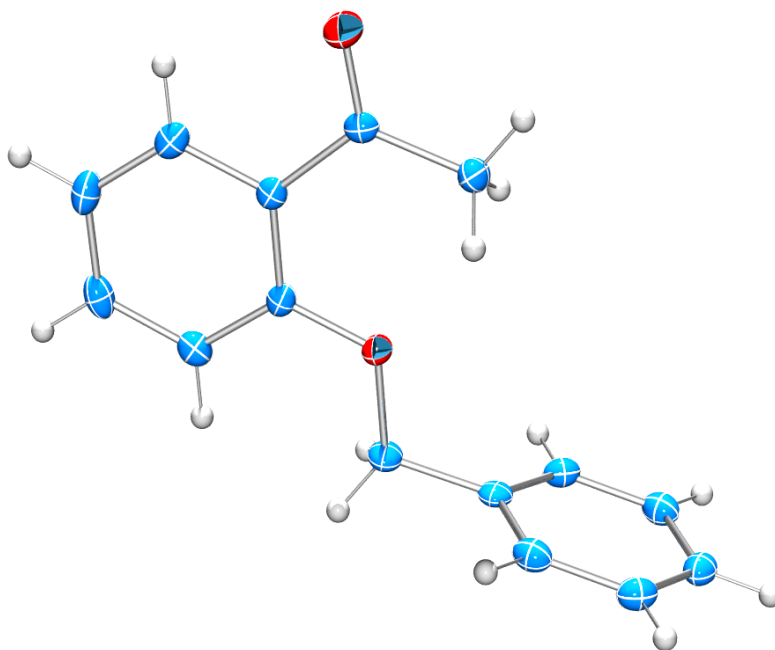


Figure 4.2. An ORTEP view of **62** showing the perpendicular arrangement of the phenyl rings. Displacement of the non-hydrogen atoms are shown at the 50% probability level.

Test reactions were also carried out to determine optimum conditions for the condensation reactions between **60** and 4-bromobenzaldehyde (**63**) (Scheme 4.3). For this reaction, the optimum conditions for the formation of chalcone **64**⁶⁹⁹ were determined to be 2 equivalents of KOH dissolved in absolute ethanol, with the reaction stirred at room temperature for 18 hours (Table 4.2), a modification of the procedure used by Zhang and Wang.⁷⁰⁰

Scheme 4.3. Synthesis of chalcone **64**.

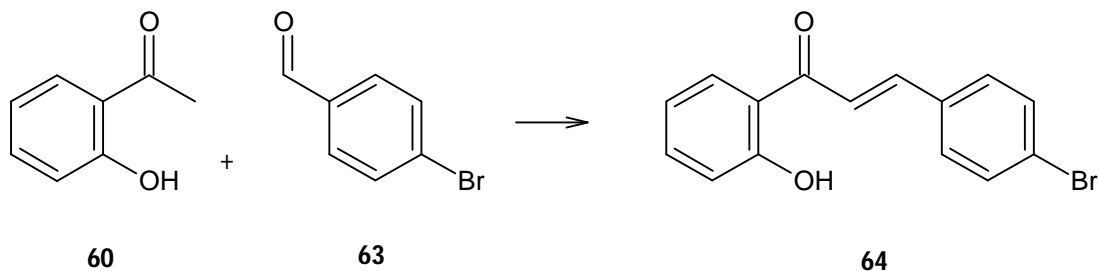


Table 4.2. Optimization of conditions for chalcone formation.

Entry	Equivalents KOH	Time /Hours	Yield /%
1	2	2	22
2	2	6	45
3	2	12	76
4	2	18	95

The appearance of two one-proton doublets with J-values greater than 15 Hz in the ¹H NMR spectrum (Figure 4.3), along with the corresponding disappearance of the aldehyde proton (~10 ppm) and the methyl protons (~2.5 ppm) confirmed the formation of a *trans* double bond⁷⁰¹ between the acetophenone and the benzaldehyde molecules as desired.

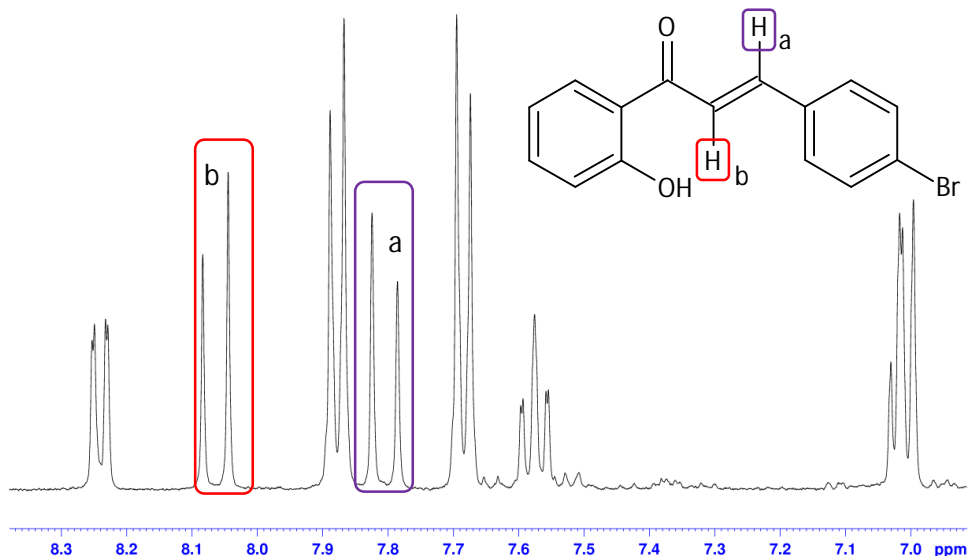
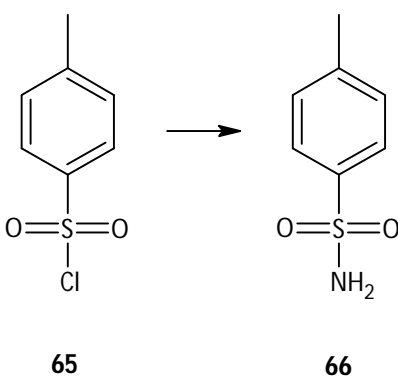


Figure 4.3. ^1H NMR spectrum of **64** highlighting the signals corresponding to the double bond protons.

Routes for the conversion of a sulfonyl chloride moiety to a sulfonamide (Scheme 4.4) were also explored using *p*-toluene sulfonyl chloride (**65**) as the analogue molecule. The sulfonyl chloride could be easily converted to the sulfonamide **66**⁷⁰² using THF/aqueous ammonia at 0°C for 1 h in high yields (over 80%) following a modification of the procedure used by Corominas and Montaña.⁷⁰³ Proton NMR spectral analysis of **66** showed the appearance of a two-proton singlet at 7.36 ppm in the ^1H NMR spectrum, corresponding to the two amide protons (Figure 4.4). The proton-observed gHSQC ^1H - $\{^{15}\text{N}\}$ spectrum of **66** shows a signal at 7.36 ppm, indicating that the protons responsible for this signal are definitely connected to a nitrogen atom, which indicates that the conversion of the sulfonyl chloride into a sulfonamide was successful.

Scheme 4.4. Synthesis of sulfonamide **66**.



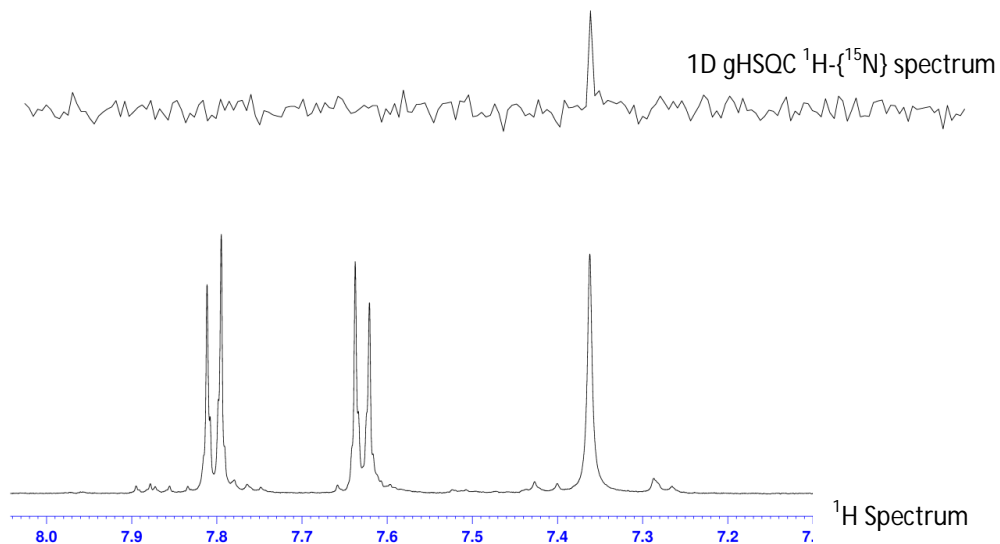


Figure 4.4. Sections of the ^1H and 1D gHSQC $^1\text{H}\{-^{15}\text{N}\}$ NMR spectra of **66** showing the presence of amine protons.

4.2. Assembling the Puzzle: Attempts towards the Synthesis of the Final Compounds.

"Murder mysteries are puzzles that are fun to resolve."

Kathy Reichs

With these procedures in hand, attention was focused on the complete synthesis of the benzenesulfonates along Pathway A. Initially five 2'-hydroxyacetophenones and five benzaldehydes were used to synthesize 24 chalcones (Scheme 4.5) in good to excellent yields (Table 4.3).

Scheme 4.5. General synthetic approach for the formation of chalcones.

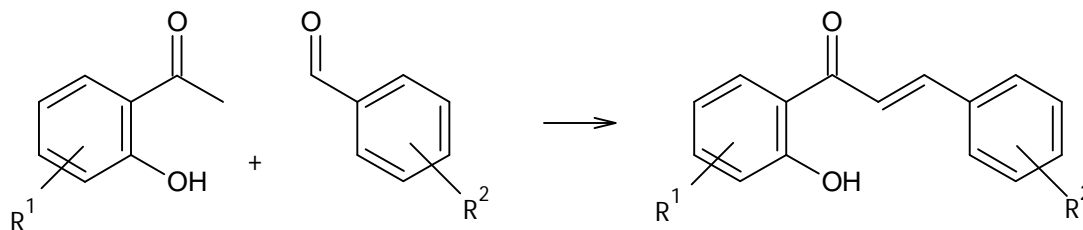


Table 4.3. Yields for formation of various chalcones.

Entry	R¹	R²	Compound	Yield /%
1	H (60)	H (67)	68 ⁷⁰⁴	86
2		4-Br (63)	69 ⁶⁹⁹	93
3		4-Cl (70)	71 ⁶⁹⁹	92
4		4-F (72)	73 ⁷⁰⁵	73
5		2-Cl (74)	75 ⁷⁰⁶	78
6	4-F (76)	67	77 ⁷⁰⁷	72
7		63	78	69
8		70	79 ⁷⁰⁸	66
9		72	80	87
10		74	81 ⁷⁰⁹	79
11	4-Cl (82)	67	83	80
12		63	84 ⁷¹⁰	67
13		70	85	84
14		72	86	82
15	5-Cl (87)	67	88 ⁶⁹⁹	67
16		63	89 ⁷¹¹	81
17		70	90 ⁶⁹⁹	74
18		72	91 ⁷¹²	79
19		74	92 ⁶⁹⁹	69
20	5-Br (93)	67	94 ⁷¹¹	68
21		63	95 ⁷¹³	68
22		70	96 ⁷¹²	61
23		72	97 ⁷¹²	81
24		74	98 ⁷¹⁴	65

Reaction conditions: acetophenone (1 mmol), benzaldehyde (1 mmol), KOH (2 mmol), EtOH, rt, 18 h.

During the course of these reactions, crystals were observed during cleanup procedures, and as such, the growth of X-ray-quality crystals was attempted. Suitable crystals were obtained for compound **73**,

and X-ray crystallographic analysis of this compound (CCDC deposit number pending) showed that, while maintaining the electron delocalization throughout, the molecule is not flat as expected, rather the benzaldehyde-derived phenyl ring is twisted away from the horizontal by 28.8° (Figure 4.5). As with compound **62**, X-ray crystallographic studies do not play a large role in the overall project and the data obtained for **73** is presented for the sake of interest (See SI for complete structural description).

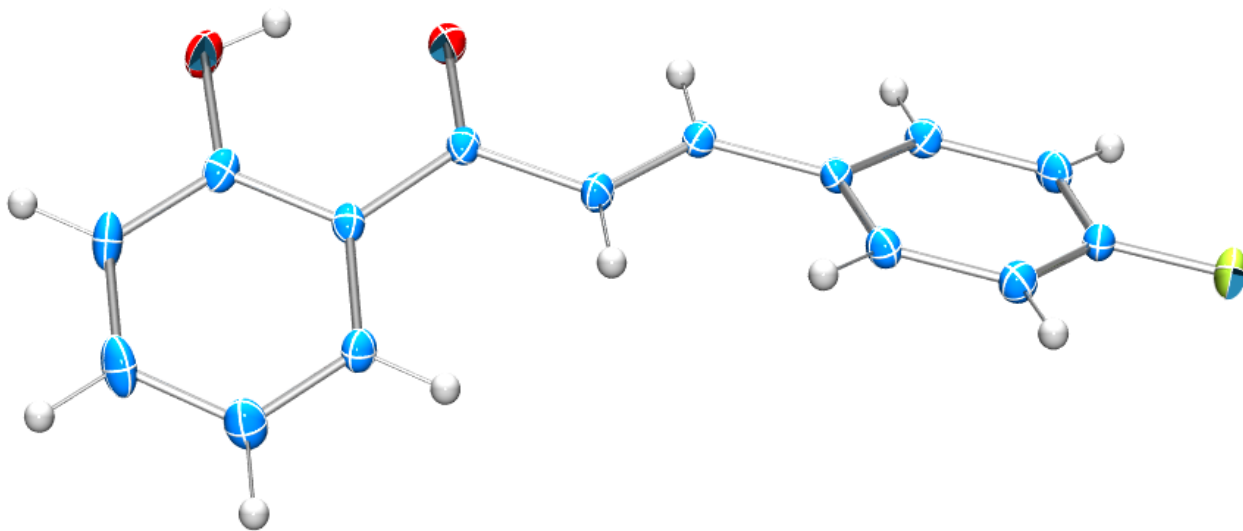


*Figure 4.5. An ORTEP view of **73** showing the out-of plane rotation of the benzaldehyde-derived phenyl ring Displacement of the non-hydrogen atoms are shown at the 50% probability level.*

While the KOH/Abs EtOH conditions were well suited to the unsubstituted **67** and the halo-substituted benzaldehydes **63**, **70**, **72** and **74**, *p*-anisaldehyde (**99**) and *o*-anisaldehyde (**100**), both methoxy-substituted benzaldehydes, coupled poorly using these conditions, with yields ranging from 27-41%. Further investigations identified NaH/THF/ $0^\circ\text{C}/4\text{ h}$ ⁷¹⁵ as conditions more suited to these benzaldehydes, and the methoxy-substituted chalcones were obtained in good to very good yields (Table 4.4). Interestingly, these conditions were not suited to the halo-benzaldehydes, as reactions using these conditions resulted in the isolation of the insoluble Na-salt of the acetophenone, with the benzaldehyde remaining in solution even when the reaction was extended to 24 hours.

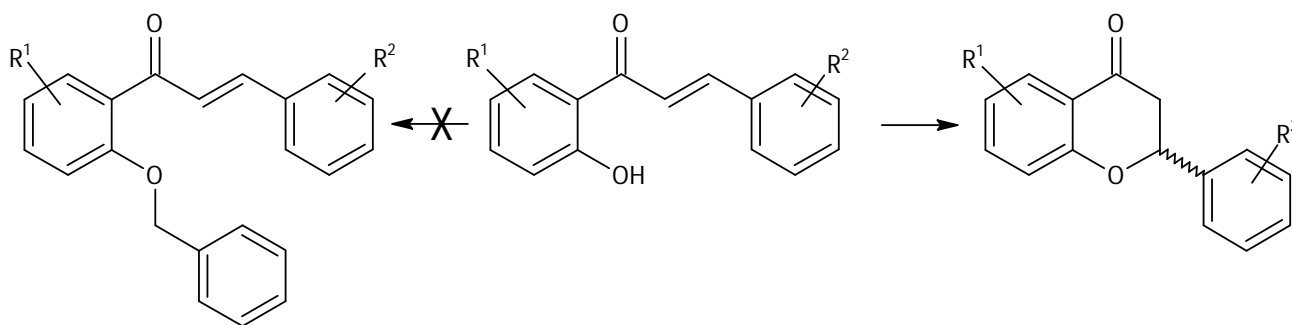
Table 4.4. Yields for the formation of methoxy-substituted chalcones.

Entry	R ¹	R ²	Chalcone	Yield /%
1	60	4-OMe (99)	101 ⁶⁹⁹	83
2		2-OMe (100)	102 ⁷¹⁶	79
3	76	99	103 ⁷¹⁷	81
4		100	104	87
5	82	99	105 ⁷¹⁰	91
6		100	106	92
7	87	99	107 ⁶⁹⁹	88
8		100	108 ⁷¹⁸	81
9	93	99	109 ⁷¹⁴	94
10		100	110	95

Reaction conditions: acetophenone (1 mmol), benzaldehyde (1 mmol), NaH (2 mmol), dry THF, 0°C, 4 h.

Addition of the benzyl group to the phenolic oxygen did not proceed as planned, despite reports of high yields in the literature.⁷¹⁹ Deprotonation of the phenolic oxygen results in preferential intramolecular condensation yielding a flavanone rather than the desired intermolecular ether formation (Scheme 4.6).⁷²⁰ This was confirmed by the appearance of three one-proton signals in the ¹H NMR spectrum, corresponding to the three aliphatic protons present in the flavanone (Figure 4.6). The two protons of the methylene group are non-equivalent, as seen in the spectrum as evidenced by the splitting pattern, which shows both vicinal and germinal coupling.

Scheme 4.6. General scheme for the base-catalyzed flavanone formation



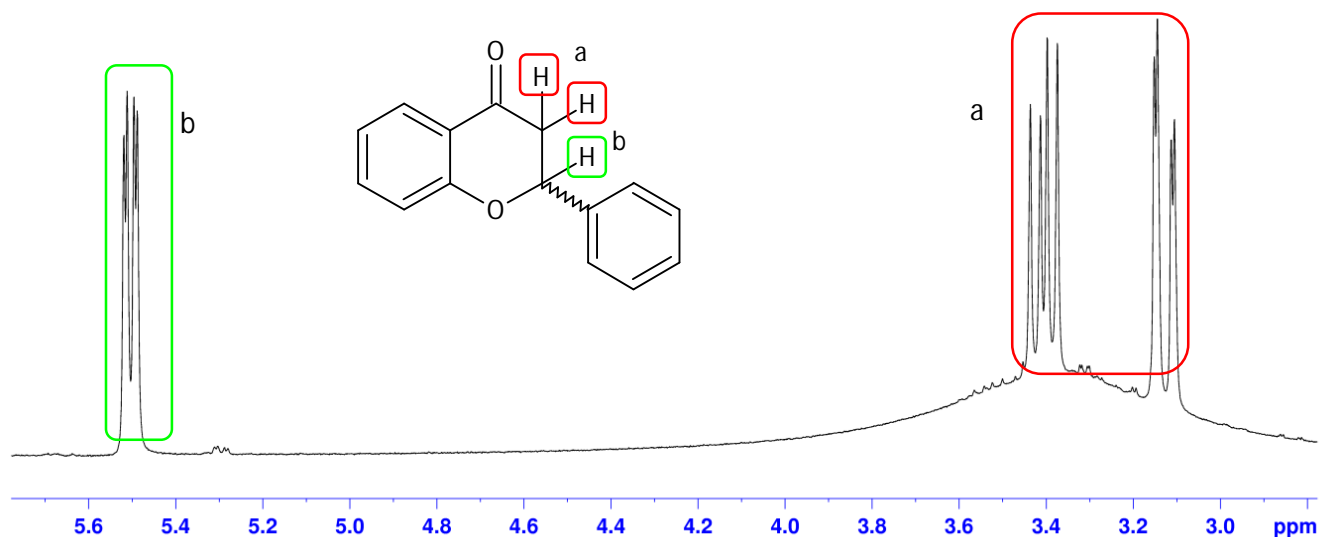


Figure 4.6. A portion of the ^1H NMR spectrum of the flavanone product showing the characteristic aliphatic proton signals with both germinal and vicinal coupling.

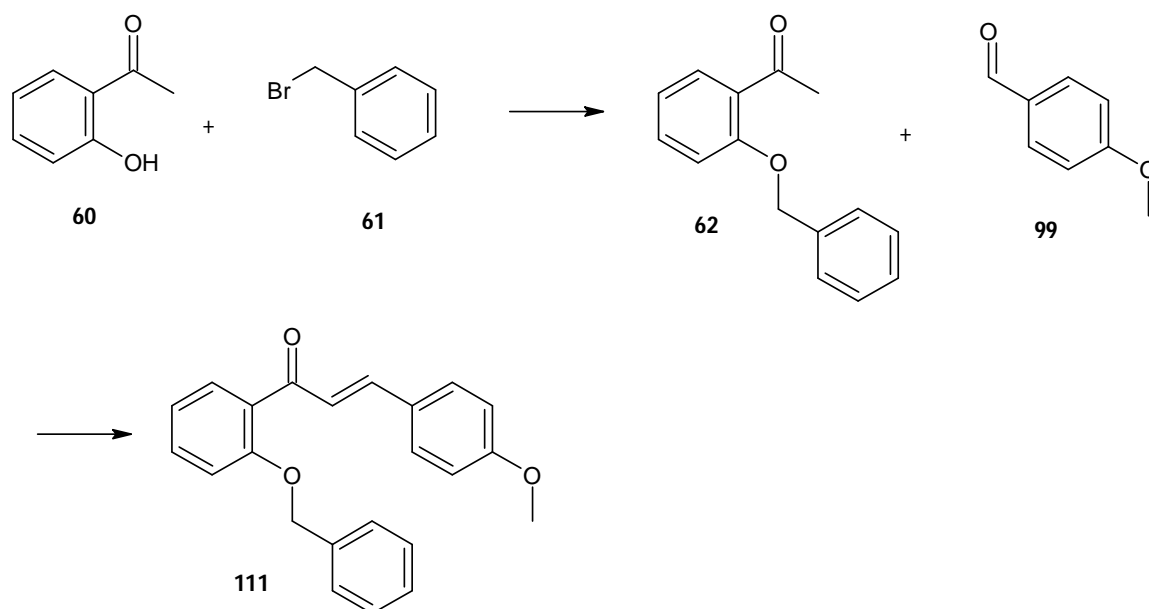
4.3. Changing Directions: Pathway B as an Alternative Route.

"I think you end up doing the stuff you were supposed to do at the time you were supposed to do it."

Robert Downey Jr.

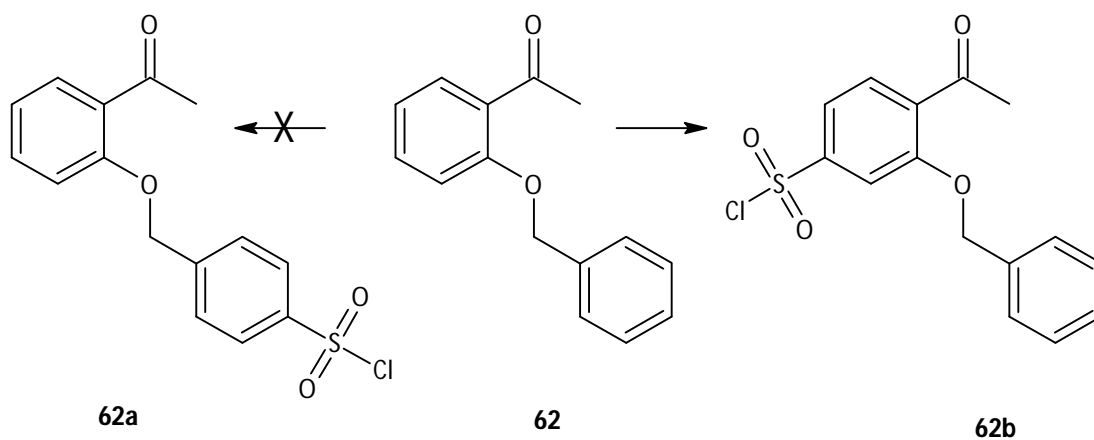
At this point, Pathway B (Scheme 4.7) was explored in order to overcome the synthetic problems encountered in Pathway A, and reactions using the established procedures for the ether reaction and the condensation reaction proceeded smoothly, yielding the desired benzylated chalcone **111**.⁷²¹

Scheme 4.7. Synthesis of **111** through Pathway B.



As these benzylated chalcones could now be synthesized easily, addition of the sulfonyl chloride moiety to form **62a** (Scheme 4.8) was attempted with chlorosulfonic acid as described by Talley, *et al.*,⁷²² in the synthesis of valdecoxib, and Silva, *et al.*⁷²³ Yields of this reaction were disappointing, with a 30% mass recovery obtained after workup, and following NMR analysis of the disappointingly complex mixture it was determined that, while the sulfonyl chloride was attached to the molecule, it was located at the 4-position of the acetophenone ring (**62b**), rather than on the benzyl ring as desired, a result which cannot be explained in terms of the relative directing effects of the substituents on the two aromatic rings.

Scheme 4.8. Addition of sulfonyl chloride to **62**.



As Pathway B appeared more appropriate for the synthesis of these compounds, alternate compounds were sought which could be manipulated to yield the final compounds with substitutions at the correct positions. Likely candidates were identified in 4-(bromomethyl)benzenesulfonyl chloride **112** and the significantly more expensive 4-(bromomethyl)benzenesulfonamide **113**¹⁶⁰ (Figure 4.7), as a replacement for benzyl bromide, as the sulfonyl moiety was already in place.

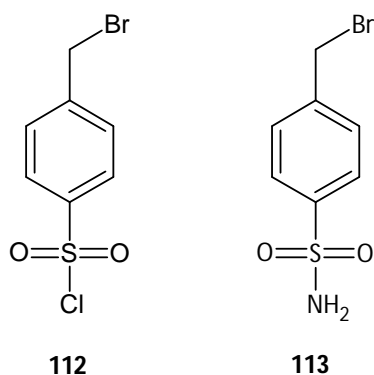
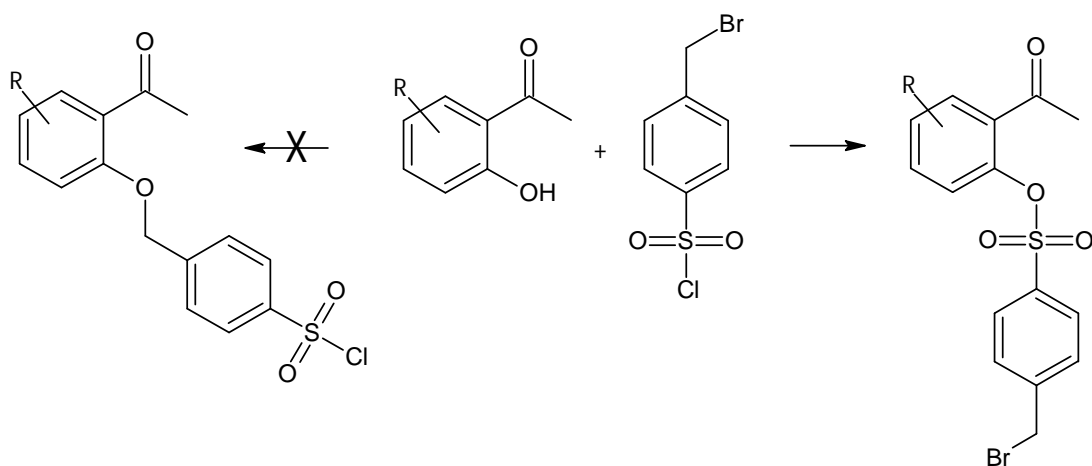


Figure 4.7. 2D structures of 4-(bromomethyl)benzenesulfonyl chloride **112** and 4-(bromomethyl)benzenesulfonamide **113**.

However, initial reactions between the 2'-hydroxyacetophenones and **112** yielded a tosylated acetophenone compound, rather than the desired ether (Scheme 4.9). As **112** is a tosyl chloride derivative, this reaction was not unexpected, and it was therefore determined that the sulfonyl chloride needed to be protected in order to form the ether bond between the bromide and the hydroxyl group. A search of the literature yielded large amounts of information on the use of sulfonyl chlorides as protecting groups, but surprisingly little information is available on the protection of the sulfonyl groups themselves.⁷²⁴

Scheme 4.9. General scheme for the formation of tosylated 2'-hydroxyacetophenones.



Rather than focus on one protecting group for both sulfonate and sulfonamide compounds, both nitrogen- and oxygen-based protecting groups were tested in order to simplify the synthetic route. A protocol for the conversion of the sulfonyl chloride to a sulfonamide using aqueous ammonia had previously been established (Scheme 4.4), and this methodology proved successful with **112**, however, while easy to synthesize, **113** proved too unstable under the subsequent reaction conditions. As attempts to protect the sulfonamide after it had been formed using amine protecting groups such as Boc and ethyl chloroformate were unsuccessful, primary and secondary amines were explored as alternatives. Initial testing of various amines and alcohols were carried out using a variety of conditions, with **65** selected as a simple test compound. This evaluation consisted of both protection^{703,725-727} and deprotection⁷²⁸⁻⁷³¹ steps in order to identify those groups which could be easily added and removed without affecting the remainder of the molecule (Table 4.5).

Scheme 4.10. Formation of protected sulfonyl chlorides and subsequent deprotection.

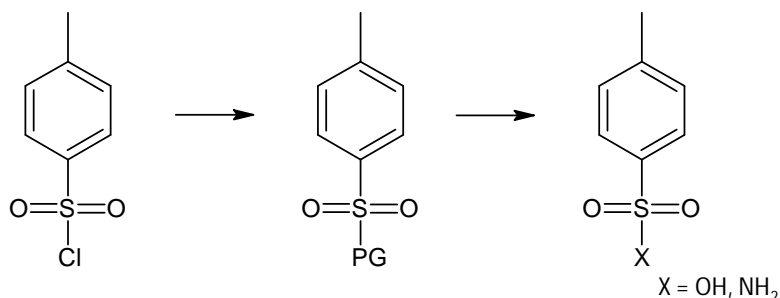


Table 4.5. Protection and Deprotection of **65**.

Entry	Amine/Alcohol	Protecting group	Compound	Protection Yield /% ^a	Deprotection Yield /% ^a
1	Diethylamine ⁷²⁵	-N(Et) ₂	114 ⁷³²	90 ^b	0 ^h
2	Diisopropylamine ⁷²⁵	-N(ⁱ Pr) ₂	115 ⁷³³	5 ^{b,c}	-
3	Dibenzylamine ⁷²⁵	-NBz ₂	116 ⁷³⁴	8 ^{b,c}	-
4	Acetamide ⁷²⁵	-NHC(=O)CH ₃	117	15 ^{b,d}	-
5	Succinamide ⁷²⁵	-NSucc	118 ⁷³⁵	25 ^{b,d}	-
6	Phthalamide ⁷²⁵	-NPhth	119 ⁷²⁵	86 ^b	81 ⁱ
7	Ethanol ⁷²⁶	-OEt	120 ⁷³⁶	90 ^e	93 ^{f,j}
8	^t Butanol ⁷²⁶	-O ^t Bu	-	0 ^{e,f}	-
9	ⁱ Propanol ⁷²⁶	-O ⁱ Pr	-	0 ^{e,f}	-
10	Phenol ⁷²⁷	-OPh	121 ⁷³⁷	75 ^g	0 ^h
11	<i>p</i> -Nitrophenol ⁷²⁷	-OPhNO ₂	122	86 ^{c,g}	0 ^h

^a ¹H NMR yield ^b **65**, amine, KOH (1.1 eq), MeCN, rt, 2 h ^c not characterized ^d uncharacterized products (NMR) ^e **65**, KOH (1.1 eq), alcohol, rt, 2 h ^f potassium salt isolated ^g **65**, KOH (1.1 eq), alcohol, THF/H₂O (20:1), 0 °C, 2 h. ^h multiple deprotection methods attempted. ⁱ hydrazine hydrate (80%), reflux, 30min ^j KOH (1 eq), EtOH/H₂O (1:2) reflux, 1h.

Based on these test reactions, phthalamide was selected as a suitable amine protecting group, and ethanol as the acid protecting group. The ethoxy group could be cleaved using a base⁷²⁶ and the phthalamide group could be easily cleaved under Gabriel-type conditions by heating with hydrazine hydrate to reflux.⁷²⁸⁻⁷²⁹ Protection of **112** proceeded smoothly, yielding the corresponding protected (bromo-methyl)tosylates **123**⁷³⁸ and **124**⁷³⁹ (Figure 4.8) in good to very good yields (Table 4.6).

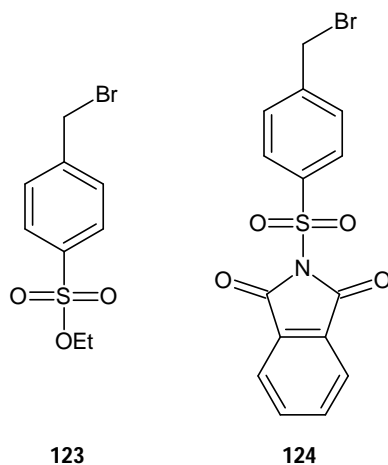


Figure 4.8. 2D structures of **123** and **124**

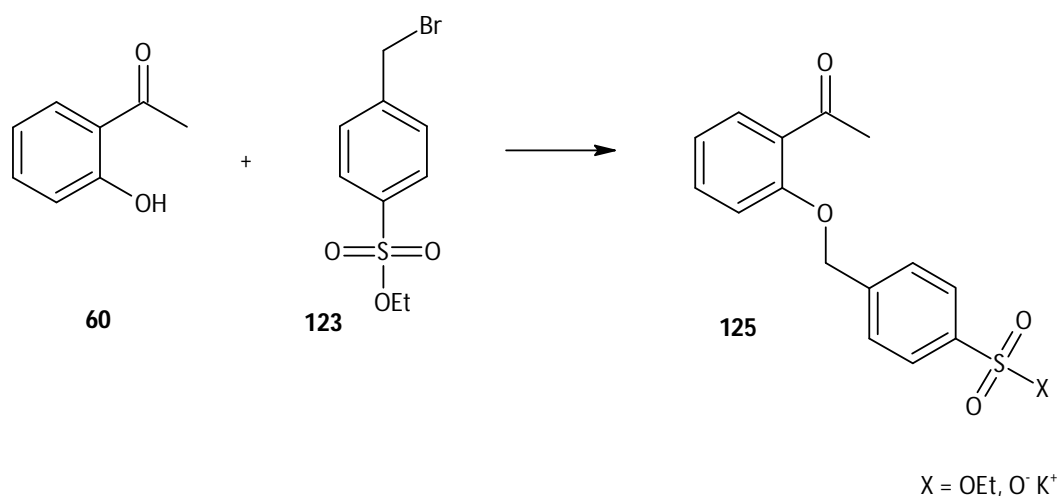
Table 4.6. Yields for the formation of protected (bromomethyl)tosylates.

Entry	Compound	Yield/%
1	123	88 ^a
2	124	84 ^b

^a**112**, KOH (1.1 eq), EtOH, rt, 2 h ^b**112**, phthalimide, KOH (1.1 eq), MeCN, 0°C, 1 h

Formation of the ether bond between **60** and **123** (Scheme 4.11) initially proved challenging as **123** is sparingly soluble in acetonitrile. However, there is sufficient **123** present in solution at any given time to allow the reaction to proceed, and to provide very good yields of the ether product after 24 hours. Interestingly, the isolated product was not the ether sulfonate with an ethoxy- protecting group as expected; rather the potassium salt of **125** was obtained as a precipitate.

Scheme 4.11. Synthesis of benzenesulfonate **125**.



As there was no evidence of sulfonate ester formation between two molecules of **123**, the hypothesis is that **123** is the reactive species, and hydrolysis to the salt follows the reaction with **60**. This hypothesis is supported by the unsuccessful reactions of the salt form of **112** with **60**. Attempts to prevent the removal of the ethoxy group were unsuccessful, as when one equivalent of potassium carbonate was used, the ether reaction proceeded to *ca.* 50% and no further, and additional attempts to convert the potassium salt back to the ether after hydrolysis were unsuccessful. Organic bases such as DBU and DABCO were also tested; however these did not yield as clean a conversion as the potassium carbonate/acetonitrile conditions. A test condensation reaction of **125** with benzaldehyde **63** showed the presence of the salt did not affect the condensation reaction, and as such, further ether reactions made use of the potassium carbonate/acetonitrile conditions as the final products could be isolated cleanly and in good yields by filtration (Table 4.7). While fluoro- and chloro-substitutions at the 4-position of the acetophenone ring were well tolerated (Table 4.7, entries 2 and 3), the 5-substituted 2'-hydroxyacetophenones **128**, **87** and **93** were remarkably unstable under these conditions (Table 4.7, entries 4-6), and even use of the mild potassium carbonate/acetone conditions⁶⁹⁶ resulted in rapid discoloration of the reaction medium and decomposition of the substituted acetophenone components.

Table 4.7. Yields for the formation of various 4-[2-(2-acetylphenyl)ethyl]benzenesulfonates.

Entry	2'-Hydroxyacetophenone	Product	Yield /%
1	H (60)	125	83
2	4-F (76)	126	79
3	4-Cl (82)	127	72
4	5-F (128)	129	15 ^a
5	5-Cl (87)	130	12 ^a
6	5-Br (93)	131	9 ^a

Conditions: **123** (1 mmol), appropriate 2'-hydroxyacetophenone (1mmol), K₂CO₃ (2 mmol, 2 eq), MeCN, reflux, 24 h. ^aNMR yield, multiple uncharacterized products.

Compound **124** on the other hand, proved to be too insoluble to be useful. It is remarkably insoluble in almost all organic solvents, apart from DMF and DMSO, and even the ether reactions carried out in DMF were low yielding. At this point, it was decided that compounds **125-127** would be carried forward into the condensation reactions, and the sulfonate converted into the sulfonamide through the sulfonyl chloride at a later stage if needed.

The condensation reactions of **125**, **126** and **127** with the various benzaldehydes (Scheme 4.12) to yield the thirty compounds identified previously made use of a modified version of the procedure used for synthesis of the chalcones (Table 4.8). Reactions using **125** and **126** (Table 4.8, entries 1-24) proceeded cleanly under the conditions employed, with yields for reactions using **126** slightly lower than those obtained for compound **125**. Reactions with **127** did not proceed as well as hoped under the conditions used for **125** and **126**, with yields ranging from 25-45% after 24 hours. Extension of the reaction time to 36 hours resulted in significantly improved yields for these compounds (Table 4.8, entries 25-30). Isolation of these compounds was uncomplicated, and only simple recrystallization techniques were required in order to obtain samples of high purity.

Scheme 4.12. General route for the synthesis of the target benzenesulfonates

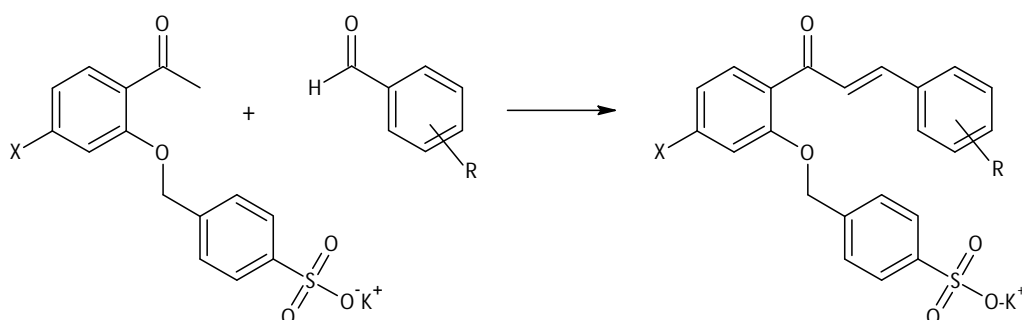


Table 4.8. Yields for the formation of target molecules.

Entry	Benzenesulfonate	Benzaldehyde	Product	Yield /%
1	H (125)	H (67)	3	73 ^a
2		4-Br (63)	5	81 ^a
3		4-Cl (70)	6	76 ^a
4		4-F (72)	7	72 ^a
5		4-OMe (99)	8	68 ^a
6		3-Br (132)	9	73 ^a
7		3-Cl (133)	43	78 ^a
8		3-F (134)	44	76 ^a
9		2-Br (135)	10	66 ^a
10		2-Cl (74)	45	68 ^a
11		2-F (136)	46	71 ^a
12		2-OMe (100)	47	64 ^a
13	4-F (126)	67	11	68 ^a
14		63	48	71 ^a
15		70	49	67 ^a
16		72	17	70 ^a
17		99	50	54 ^a
18		132	51	63 ^a
19		133	52	64 ^a
20		134	53	69 ^a
21		135	23	62 ^a
22		74	54	67 ^a
23		136	55	68 ^a
24		100	56	66 ^a
25	4-Cl (127)	67	12	69 ^b
26		99	57	65 ^b
27		134	58	61 ^b
28		74	59	60 ^b
29		136	18	62 ^b
30		100	24	59 ^b

^asulfonate (1 mmol), benzaldehyde (1 mmol), KOH (2 mmol), EtOH, rt, 24 h ^bsulfonate (1 eq), benzaldehyde (1 mmol), KOH (3 eq), EtOH, rt, 36 h.

4.4. What We Never Knew We Needed to Know: A Review.

“Review your work. You will find, if you are honest, that 90% of the trouble is traceable to loafing”.

Ford Frick

Following identification of potential COX-2 selective compounds through docking and binding studies, retrosynthetic analysis afforded two potential synthetic routes involving simple chemistry which would allow for the formation of the correct Z-isomer about the double bond. The initial route of synthesis, which involved the formation of the double bond through a base-catalysed condensation of an acetophenone with a benzaldehyde prior to the formation of the ether bond proved unsuccessful as the base-catalyzed intramolecular reaction of the chalcones yielded a flavanone rather than the desired benzyl ether. As such, this pathway was abandoned and the alternative pathway identified during the retrosynthetic analysis was explored.

Early investigations into this second synthetic pathway, which involved the formation of the ether bond prior to the base-catalyzed condensation, yielded the correct benzylated compound in high yields, however the addition of the sulfonyl chloride moiety proved unsuccessful, with low yields and addition to alternate positions about the molecule observed. At the outset, use of a benzenesulfonyl chloride compound in order to circumvent the need for chlorosulfonic acid resulted in the formation of a tosyl derivative, rather than the desired ether. Conversion of the sulfonyl chloride into a sulfonate or sulfonamide prior to the ether formation yielded “protected” species, however the protected sulfonamide proved too insoluble to be of use.

An ethyl sulfonate proved a suitable starting material for the ether formation, with high yields obtained for three 4-substituted 2'-hydroxyacetophenones, with the 5-substituted 2'-hydroxyacetophenones proving to be too inherently unstable. The ethyl group is removed during this reaction and all attempts to prevent this removal were unsuccessful; however the removal of the ethyl group did not affect the subsequent condensation reactions. The current understanding of this reaction is that the ethyl-protected sulfonate species is the reactive species, with the ethyl group removed after ether formation. This hypothesis is supported by the lack of intermolecular condensation between two benzenesulfonate molecules, as would be expected if the ethyl group is removed prior to ether formation. With suitable reactions and conditions identified, the synthesis of the thirty compounds previously identified was

carried out, using three 2'-hydroxyacetophenones and twelve benzaldehydes, in moderate to good yields. These products were isolated cleanly with only simple recrystallization techniques required to remove unwanted starting materials and side products.

5. Results and Discussion: Analysis and Identification of Compounds

5.1. The Truth of the Matter: Structure Elucidation through NMR Spectroscopy.

"The world is full of obvious things that no one ever observes."

Sherlock Holmes, *Elementary*

In the laboratory, a chemist will base the outcome of a particular reaction or isolation on historical data, either from their own findings or on information gleaned from the literature. However, things do not always go according to plan, and, because of the capricious nature of chemistry, one cannot always assume that literature is correct. In some cases, novel synthetic or isolated compounds are identified, and in other cases, incorrect identification of compounds occurs. One such example of incorrect literature which has been corrected is found in aquatolide (Figure 5.1), a humulane-derived sesquiterpenoid lactone isolated from the daisy-like *Asteriscus aquaticus*.

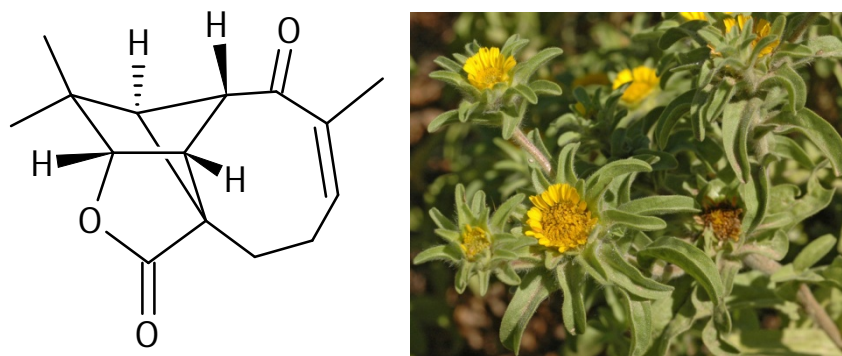


Figure 5.1. 2D structure of aquatolide and *Asteriscus aquaticus*.⁷⁴⁰

Initially characterized in 1989 by San Feliciano, *et al.*,⁷⁴¹ it was thought, based on 1D and 2D NMR analysis, to contain a very rare [2]ladderane substructure (Figure 5.2). However, extensive experimental and theoretical quantum-chemical NMR analysis by Lodewyk, *et al.* in 2012⁷⁴² showed that this novel compound did not contain the [2]ladderane core as previously reported, but rather it contained a bicyclo[2.1.1]hexane ring system, which was confirmed through X-ray crystallographic techniques. Other compounds which were initially incorrectly identified and have since been revised include asperjinone

and (+)-pestazaline B, and confusion still exists around the structure of the simpler 2,3,4,5-tetrahydro-1,5-benzoxazepine-3-ol.⁷⁴³ In most cases this misidentification is through no conscious fault of the authors, rather it is due to ambiguous spectra and, as in the case of aquatolide, a lack of sensitivity in the equipment used to carry out the analyses. With the significant improvement in the technology behind these instruments, and the resultant increase in sensitivity, it is hoped that errors in the structural elucidation of compounds become less and less common.

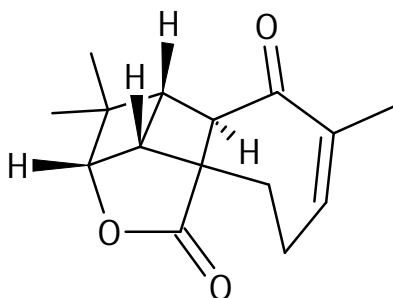
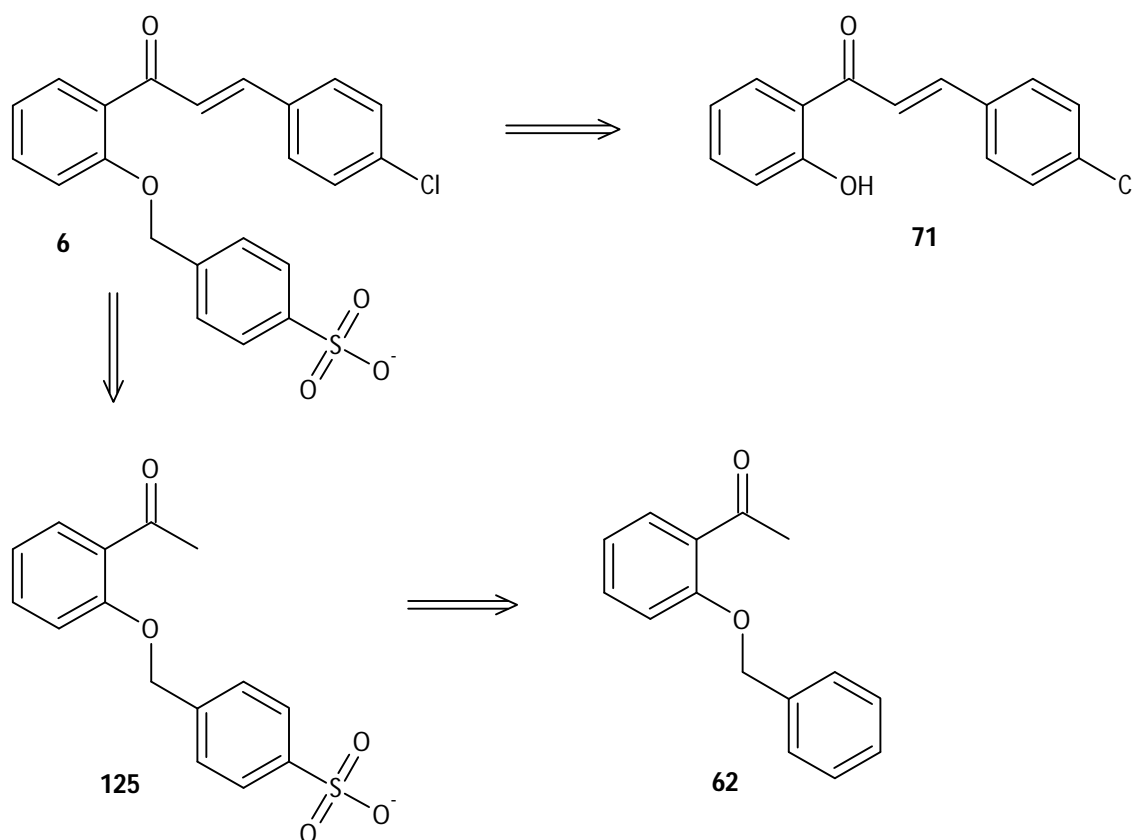


Figure 5.2. Initial incorrect structure of aquatolide.

As characterization of large, novel molecules by NMR spectroscopy can be daunting, it is therefore convenient to analyze the building blocks which make up the large molecule separately, and then compare this data to the spectra obtained for the larger molecule. The correct identification of these precursors is vital in order to avoid the incorrect structural identification of the final products. Analysis of the final compounds synthesized previously made use of the NMR characterization of the synthesized compounds **62**, **125**, **126**, **127** and the various chalcones, as well as spectra obtained for the commercially available starting materials. NMR spectral data for many of the compounds are available in the literature, however, there is a wide disparity in the field strengths at which the data have been acquired, in the solvents used, as well as the degree of completeness of the characterization. As such, each compound in this work has been completely characterized in DMSO- d_6 , with the use of D_2O where solubility and stability dictated the use of a different solvent. This approach allowed for the identification of the peaks belonging to the moieties remaining in the final compounds based on their initial structures and the spectra thereof, and allows for the comparison of chemical shifts between different compounds, which may be used for assignment of spectral data of new compounds.⁷⁰⁴ This method can be demonstrated in the NMR analysis of compound **6**, as it can be characterized based on data obtained from chalcone **71** and from **125** which in turn can be characterized based on information obtained from **62** (Scheme 5.1).

Scheme 5.1. NMR structure elucidation of **6** through analysis of precursors.



The ^1H NMR spectrum of **62** (Figure 5.3) allowed for the identification of the location of the methylene peak (Figure 5.3, peak b), as the relative integral ratios easily identify the signals corresponding to the protons of the methyl and methylene groups, both singlets with no 3J coupling. This NMR spectrum also establishes the peak pattern for the *ortho*-substituted acetophenone ring, both in fine structure and in the relative shifts. While literature spectra for compound **62** are available,⁷⁴⁴ the data is reported as acquired on a 200 MHz with the compound dissolved in CDCl_3 , and although the chemical shifts are reported, they have not been assigned to the structural fragments.

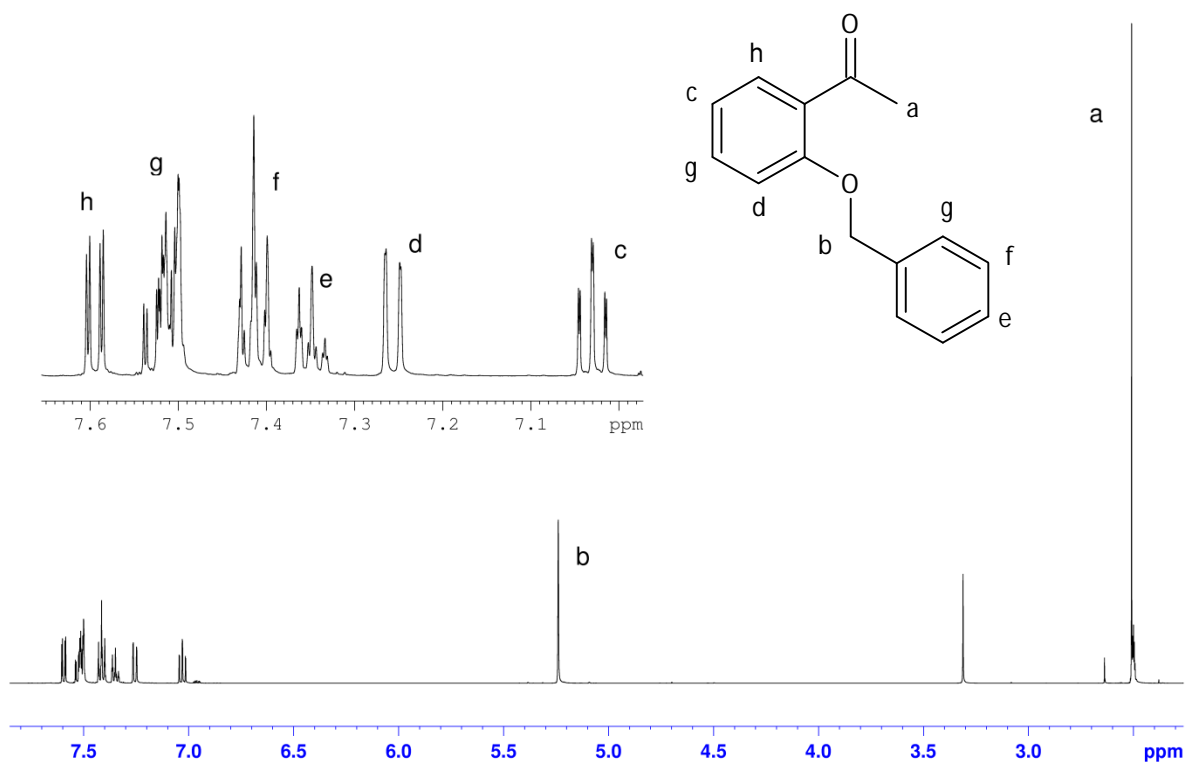


Figure 5.3 ^1H NMR spectrum and assignment of **62**.

As is often the case with this type of substitution, the fine structure arising from the ABCD spin system present in the *ortho*-substituted acetophenone ring is not resolved and the signals appear in a doublet-triplet-triplet-doublet pattern. While the order of these coupled partners is revealed by the COSY spectrum, the identity of the protons requires the use of a Nuclear Overhauser Enhancement (NOE) experiment (Figure 5.4) with selective irradiation of the methylene protons. This selective irradiation reveals through-space contacts to the acetophenone ring (Figure 5.4, peak b), from which the identity of the other protons of the acetophenone ring can be determined from the 3J COSY correlations. NOE interactions are also observed between the methylene protons and the methyl protons (Figure 5.4, peak a), as well as to the protons on the benzyl ring (Figure 5.4, peak c).

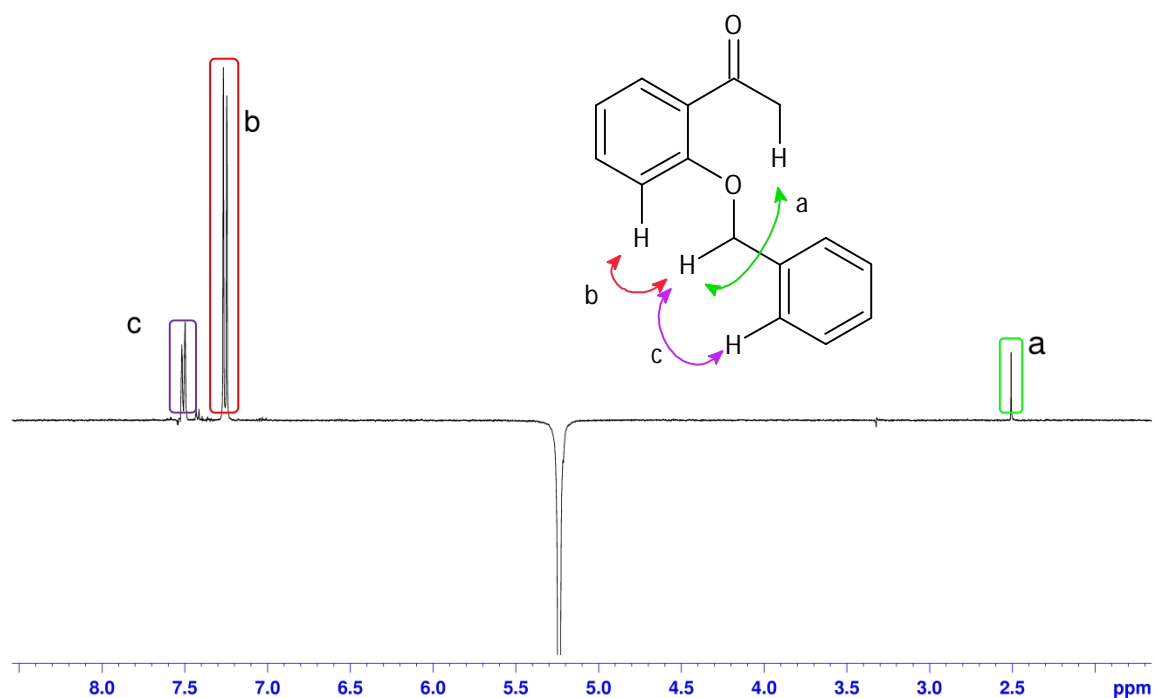


Figure 5.4. 1D NOE spectrum of **62** with selective irradiation of the methylene protons.

Comparison of the ^{13}C and the DEPT135 spectra and analysis of the HMBC spectrum allowed for the identification and assignment of the quaternary carbons as well as the methyl, methylene and methine carbon atoms. HSQC analysis of this compound revealed that the most downfield proton in the ^1H spectrum, which occupies the 6-position on the acetophenone ring, is not connected to the most downfield methine carbon atom in the ^{13}C spectrum; rather the proton occupying the 4-position is connected to this carbon.

Following the characterization of **62**, the analysis of the ^1H spectrum of **125** (Figure 5.5) was relatively straightforward. The presence of the *p*-sulfonate group on the benzyl ring resulted in the simplification of the proton spectrum into the classic *p*-substituted phenyl ring pattern of two doublets (Figure 5.5, peaks e and h), corresponding to two protons each, rather than the poorly resolved multiplets seen for **62**. Analysis of the NOESY spectrum (Figure 5.6) allowed for identification of the location of these two doublets, as a 3J COSY correlation exists between the methylene protons and the protons on the phenylsulfonate ring closer to the methylene, while no interaction is observed between the methylene protons and the protons closer to the sulfonate group.

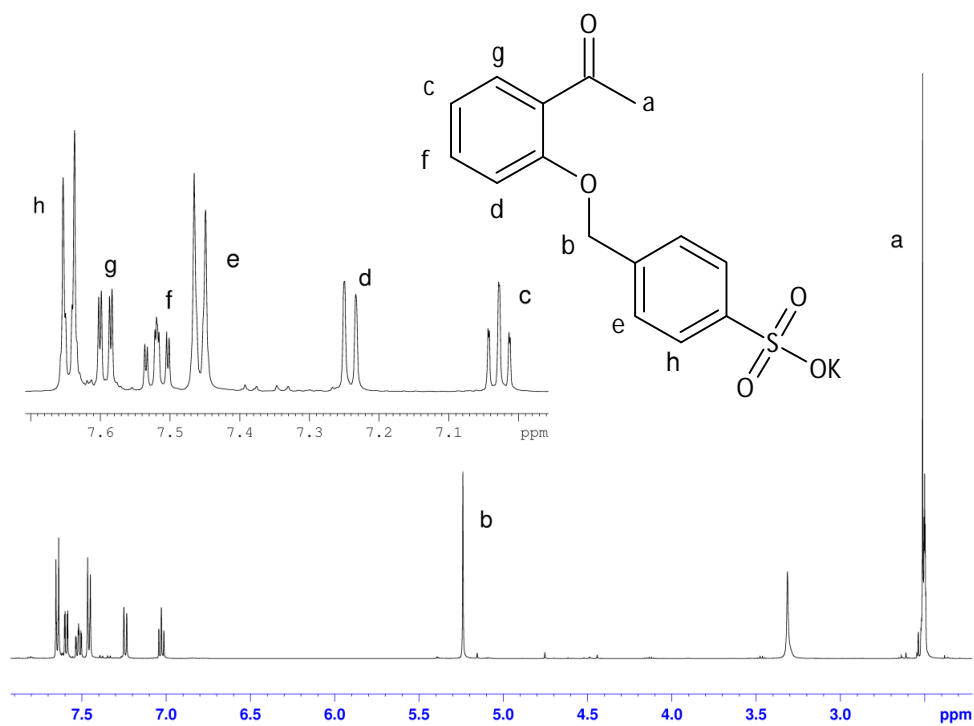


Figure 5.5. ^1H NMR spectrum and assignment of compound **125**.

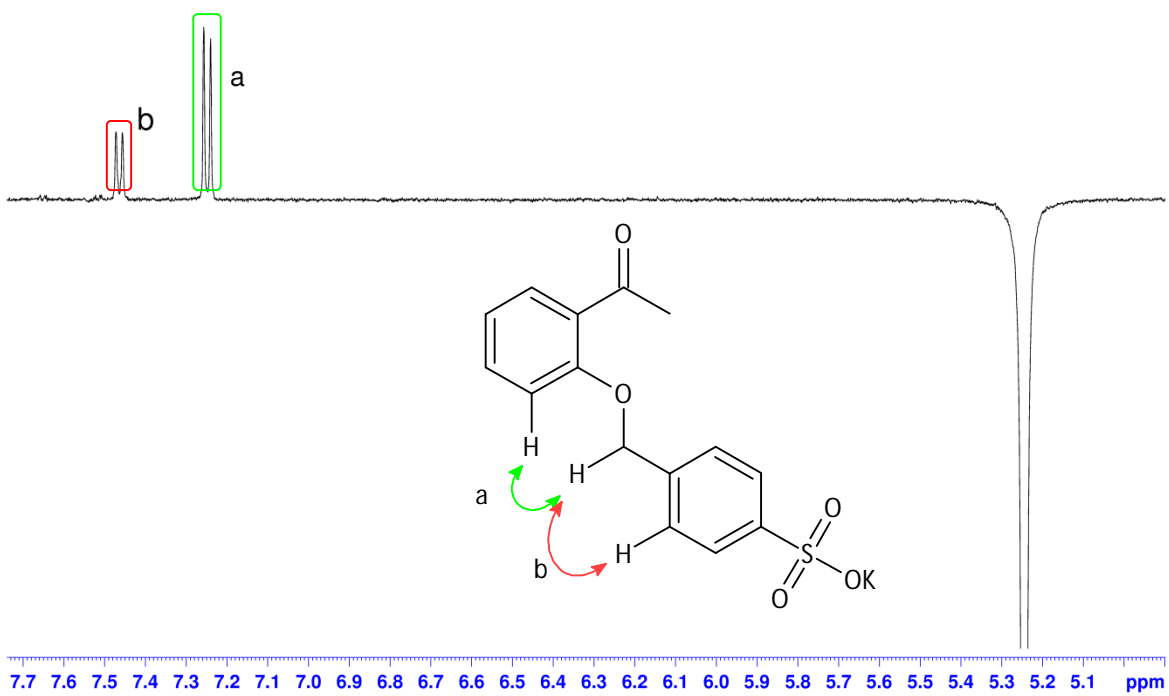


Figure 5.6. 1D NOE spectrum of **125** with selective irradiation of the methylene protons.

As with **63**, analysis and comparison of the ^{13}C , DEPT135 and HMBC spectra obtained for **125** allowed for the identification and assignment of the carbon atoms, which showed very close correlation with the data obtained for **62**, apart from the appearance of a new quaternary carbon and the subsequent loss of a methine carbon arising from the sulfonation of the benzyl ring. The data obtained from HSQC analysis of this compound corresponds with the data obtained for **62**, with the most downfield carbon signal connected to the proton at position 4 on the acetophenone ring.

Analysis of **71** also made use of the information collected from the analyses of **62** and **125**. As the protons present on the acetophenone ring had previously been identified, they could easily be distinguished in the ^1H spectrum for **71** (Figure 5.7). Evidence for the presence of a *trans* double bond in the molecule was found in the existence of two one-proton doublets in the ^1H spectrum (Figure 5.7, peaks d and f), with *trans*-bond characteristic *J* values of *ca.* 16 Hz.⁷⁰¹ The NMR spectral data are reported in literature,⁶⁹⁹ however, as was the compound **62**, no signal assignments have been made precluding a spectral comparison. As the benzaldehyde portion of the chalcone was derived from *p*-chlorobenzaldehyde, the proton signals for this ring appeared as two two-proton doublets, with the peaks differentiated through the presence (or lack) of NOESY correlations to the adjacent methine proton (Figure 5.8, peaks b and c). A COSY correlation, observed as a mixed-phase signal in the NOE spectrum (Figure 5.8, peak a), confirms the location of the signal corresponding to the two protons found on the benzaldehyde-derived phenyl ring.

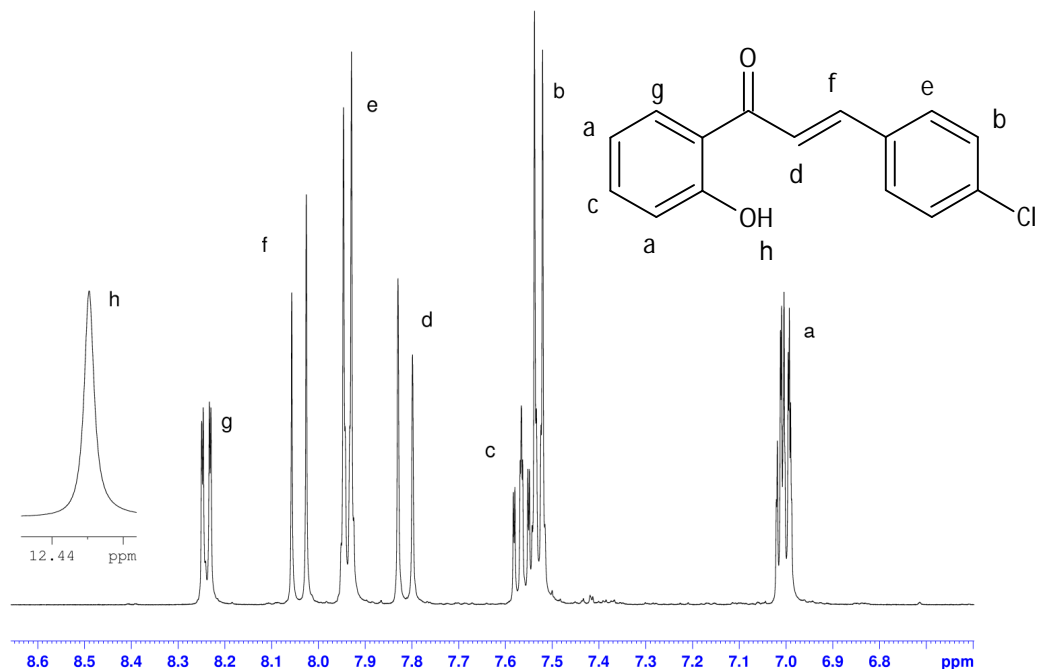


Figure 5.7. ^1H NMR spectrum and assignment for chalcone **71**.

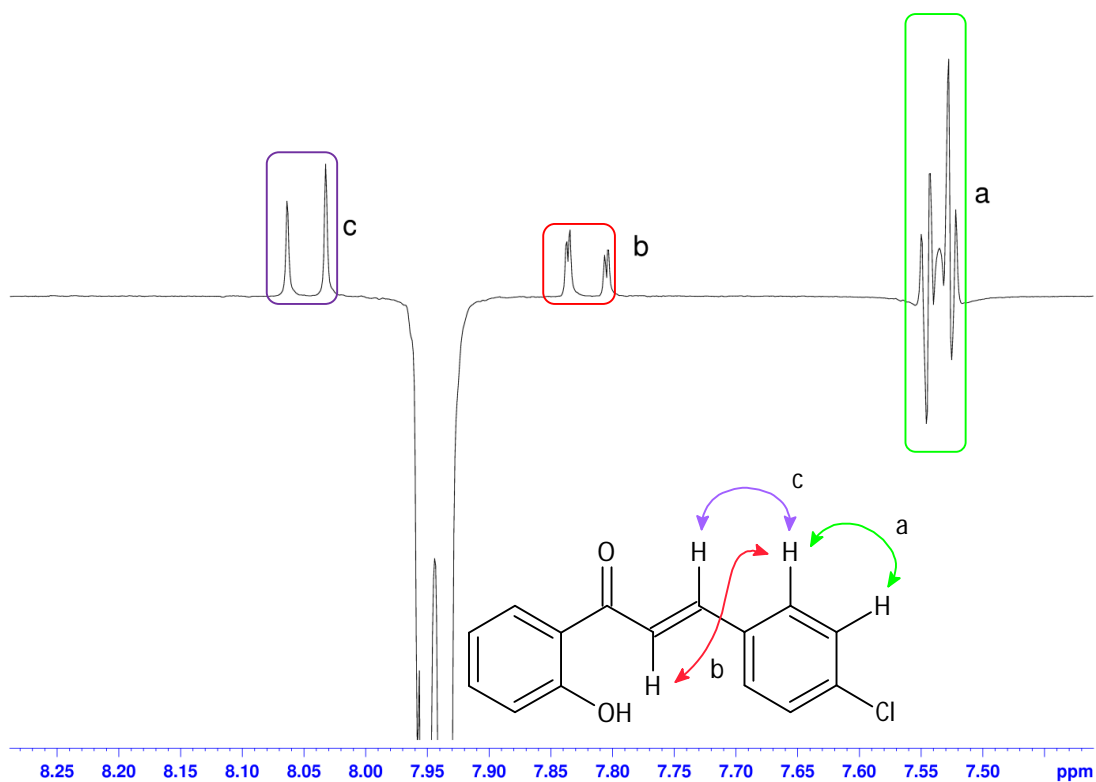


Figure 5.8. 1D NOE spectrum of **71** with selective irradiation of the methine protons.

Once the analyses of these compounds were complete, the analysis of the spectra obtained for **6** was relatively uncomplicated, as all of the peaks had previously been identified in at least one prior spectrum. The ^1H NMR spectrum of **6** (Figure 5.9) shows the presence of a methylene peak (Figure 5.9, peak a) as well as the presence of the *trans* double bond protons (Figure 5.9, peaks d and f), indicating that both of these moieties are present in the molecule. The NOESY spectrum (Figure 5.10) again showed connections between the methylene proton and the acetophenone ring (highlighted in green), between the methylene protons and the sulfonate ring (red), as seen in the spectrum of **125**, and between the methine proton of the double bond and the protons at the 2-position of the chlorophenyl ring (purple), as is seen in the spectrum of **69**.

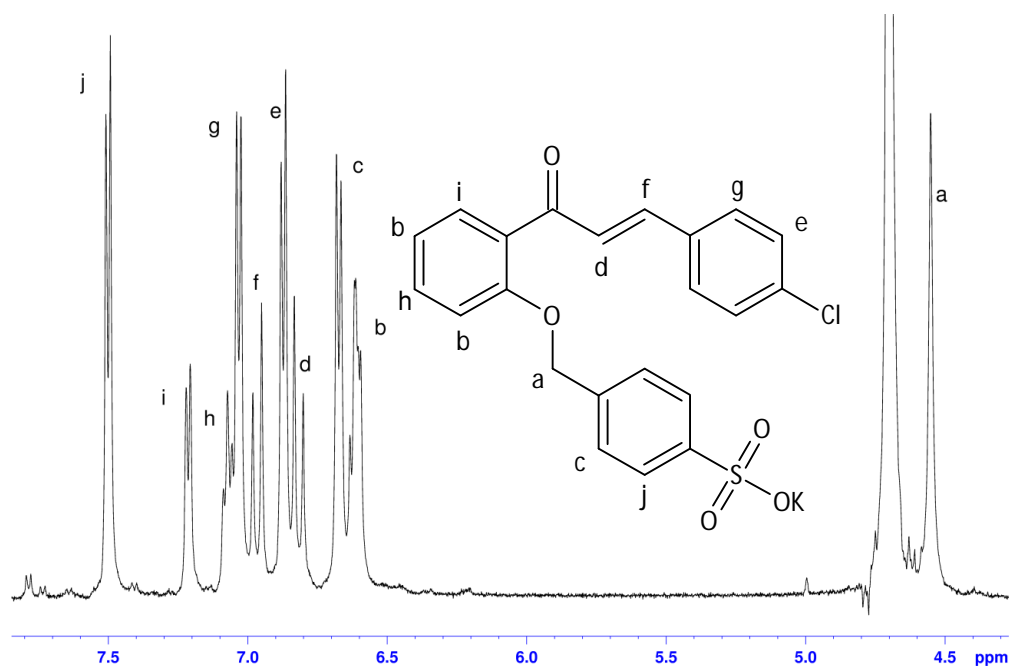


Figure 5.9. ^1H NMR spectrum and assignment of **6**.

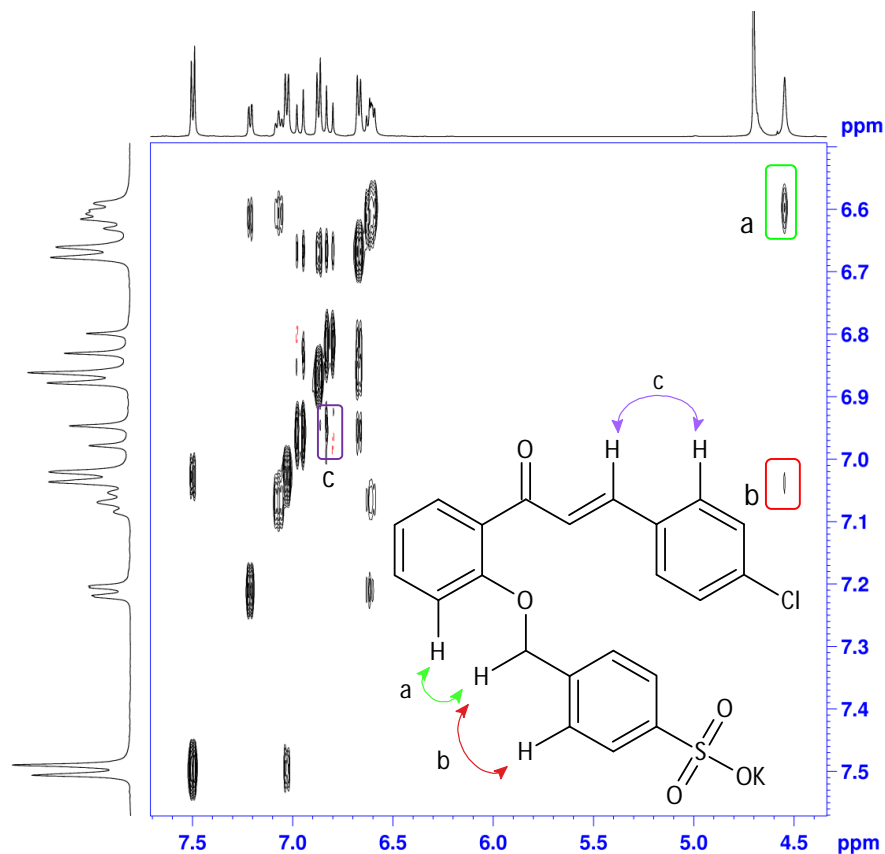


Figure 5.10. 2D NOE spectrum of **6**, showing connections between the various components.

5.2. Separate but Still Together: Diffusion-Ordered Spectroscopy as a Chromatography Technique.

“Research is formalized curiosity. It is poking and prying with a purpose.”

Zora Neale Hurston

While monitoring the course of the reactions by NMR spectroscopy, a broadening of the line width of the methylene signal was observed from starting material to product (Figure 5.11). While chemical shifts and line widths for protons connected to oxygen, nitrogen and sulfur atoms are markedly affected by changes in the solvent, as these protons are particularly sensitive to interactions with the solvent, protons connected to carbon atoms are usually less affected, often not at all, and as such the changes observed for the methylene protons are notable, if for no other than because they occur. Although largely a qualitative observation, this does point to a change in the solution mobility of the molecule

upon condensation with a benzaldehyde. This is also indicated by the solvent dependence observed for the chemical shift of the methylene protons of compound **6** (Figure 5.12).

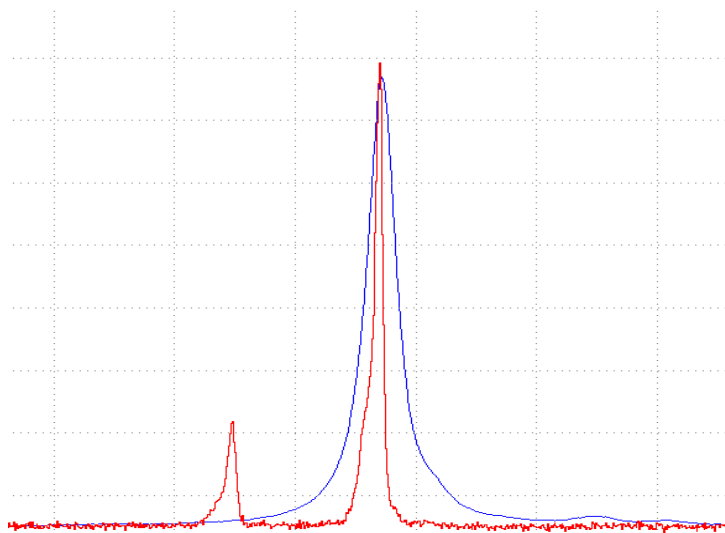


Figure 5.11. Overlap of the methylene peaks of **112** (shown in red) and **125** (shown in blue) in DMSO- d_6 . The second peak in the spectrum of **112** is a decomposition product due to the reaction of **112** with the water present in the NMR solvent.

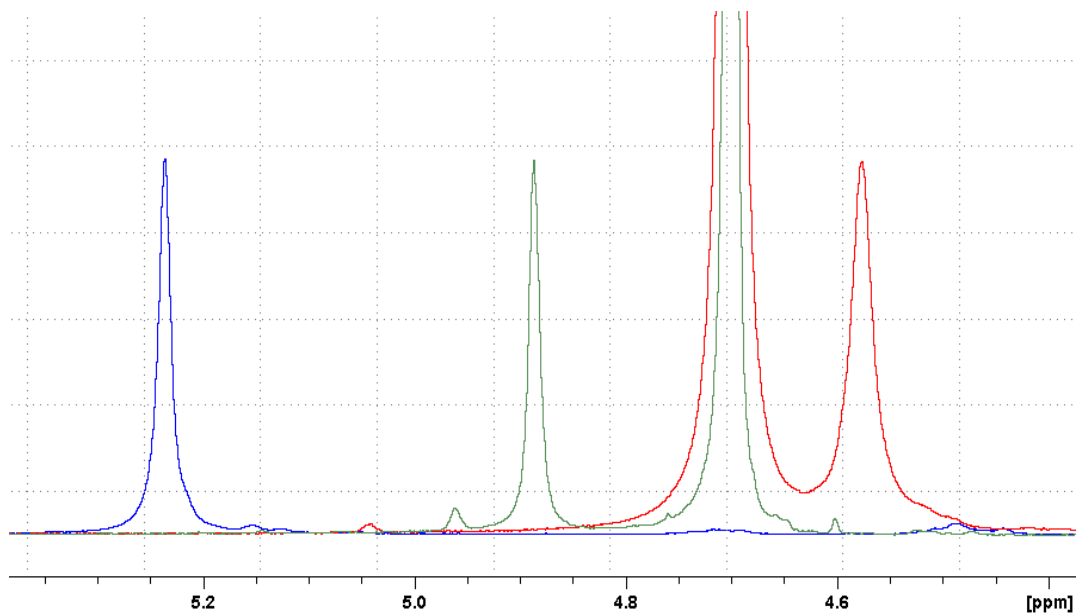


Figure 5.12. Overlays of the methylene peak region from the ^1H NMR spectra of **6**, showing the solvent-dependence of these peaks. The spectrum shown in blue was run in DMSO- d_6 , the spectrum shown in green in a mixture of D_2O and DMSO- d_6 (5:1), and the red spectrum in D_2O .

Based on this observation, a diffusion experiment was carried out on compounds **125** and **6**. These Diffusion-Ordered Spectroscopy (DOSY) experiments separate the components of a mixture on the basis of their diffusion coefficients, and simultaneously allows for measurement of the diffusion coefficient. It also provides a measure of the approximate size of the hydrodynamic radius for freely tumbling molecules in a solution,⁷⁴⁵ which in turn can provide a measure of the ability of a ligand molecule to enter into the active site of a protein. A compound with a large hydrodynamic ratio, for example, is less likely to be able to fit into the spatially-constrained active site within a protein than a compound with a small hydrodynamic ratio. As the main channel of the COX active site is relatively long and narrow, with restricted access through a small entry site, an elongated molecule with a small solvation sphere, such as arachidonic acid, will be able to enter into the active site of the COX enzymes much more easily than a large, bulky molecule with a large solvation sphere.

DOSY experiments can, in broad terms, be classified as a unique chromatographic technique, as the separation of compounds is based on physical characteristics.⁷⁴⁶ Unlike standard separation methods, however, it does not require sample preparation or method optimization, and does not affect the sample or the chemical environment during the analysis. In a DOSY experiment, a series of spin echo spectra, each with different pulsed gradient strengths, are recorded, and the decay of the signals observed. The reduction of the signals is due to the dephasing-diffusion-rephasing sequences employed.⁷⁴⁷ A 90° pulse aligns the magnetic moments of the molecules, and once this is complete, a dephasing gradient pulse disperses the magnetization. After a period of time, an 180° pulse is applied which inverts the remaining magnetization, and a second pulse then rephases these signals (Figure 5.13).

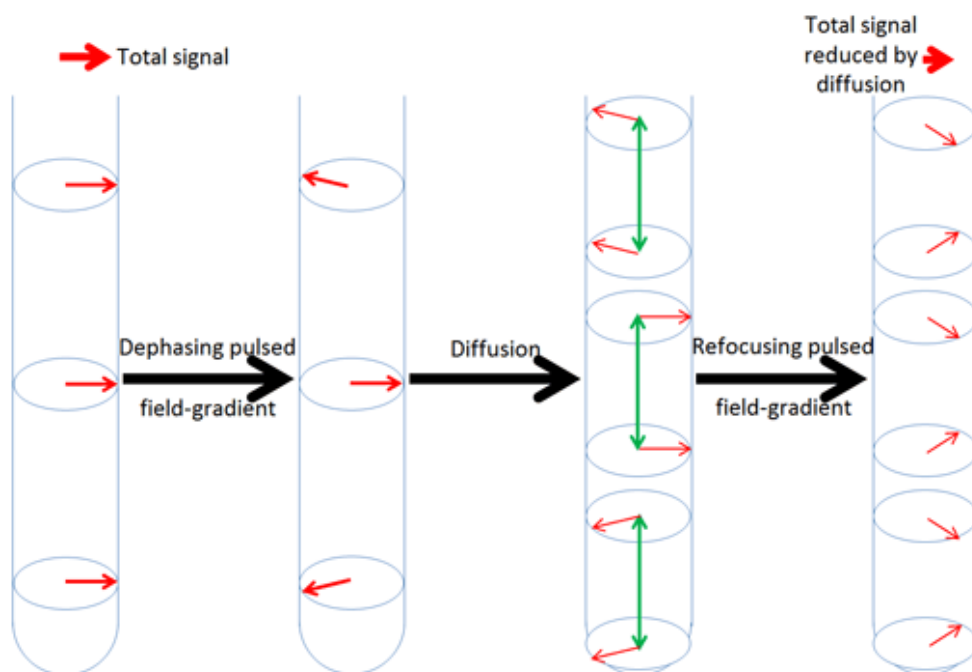


Figure 5.13. Spatial spin encoding and decoding in DOSY experiments.⁷⁴⁸

Only those signals corresponding to nuclei which have not moved significantly up or down the tube can be refocused, and as diffusion causes some of the molecules to move away, the intensities of the signals are reduced (Figure 5.14). The longer and more intense the gradient pulse, the more spatially discriminating it is, which corresponds to a weaker signal. Therefore, the duration and intensity of this magnetic pulse determines the distance a molecule can diffuse while still yielding a detectable signal.⁷⁴⁹ All signals arising from the same molecular species will decay at the same rate, with the signal loss following an exponential decay curve.

DOSY

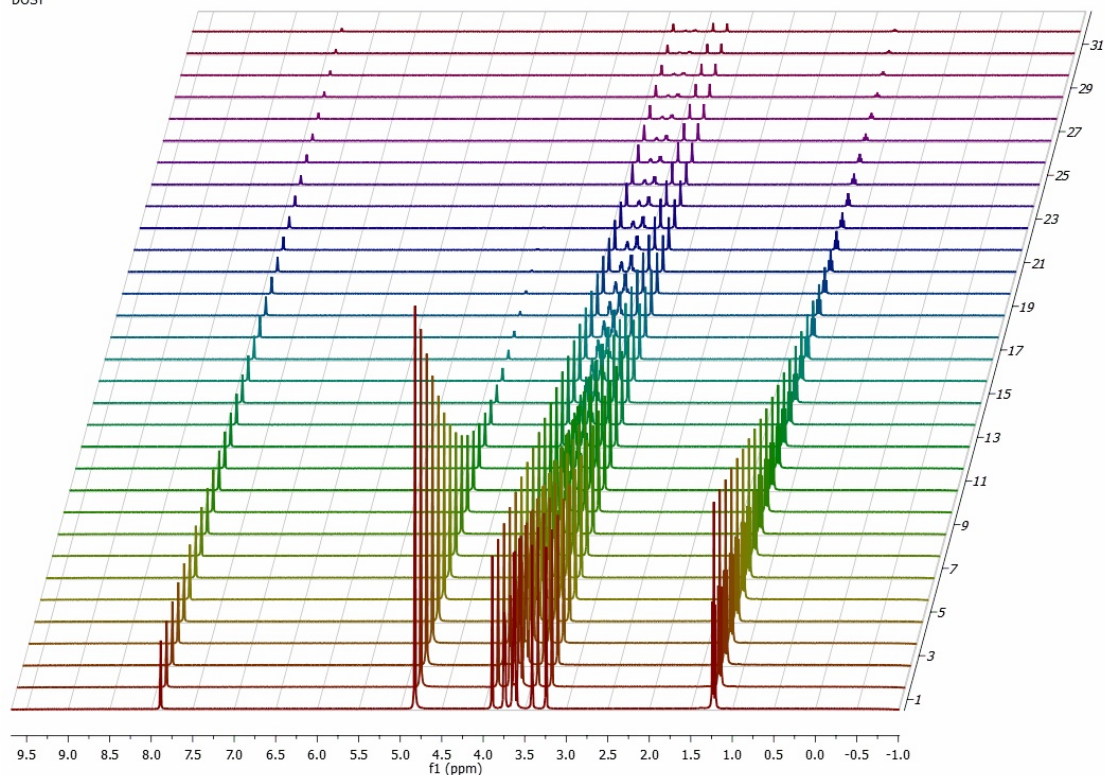


Figure 5.14. NMR diffusion spectra of a three-component mixture of water, 2-ethoxyethanol and caffeine.⁷⁵⁰

The degree of attenuation or spectral intensity (S_x) occurs at a rate proportional to the diffusion coefficient (D) of the molecule (Equation 1), where S_0 is the intensity at zero gradient (the “normal” spectrum) and Z_x encodes the different gradient amplitudes used.⁷⁴⁶

$$S_x = S_0^{-DZ_x} \quad (1)$$

There are various formulae used to determine the value of Z in terms of the gyromagnetic ratio (δ), the amplitude of the gradient applied (G), as well as one or more time parameters, such as Δ , which is the time between two pulse gradients and is related to the echo time, and δ , the width of the gradient pulse. The original Tanner-Stejskal method⁷⁵¹ (Equation 2) which uses two rectangular gradient pulses, holds for simple experiments, and this equation can undergo minor modifications for more complex pulse sequences.

$$Z = \gamma^2 G^2 \delta^2 \left(\Delta - \frac{\delta}{3} \right) \quad (2)$$

Following data processing, the 1D NMR spectra are transformed into a 2D DOSY spectrum (Figure 5.15), which allows for the identification of the number of components present in the solution, as well as identifying which signals correspond to each component.

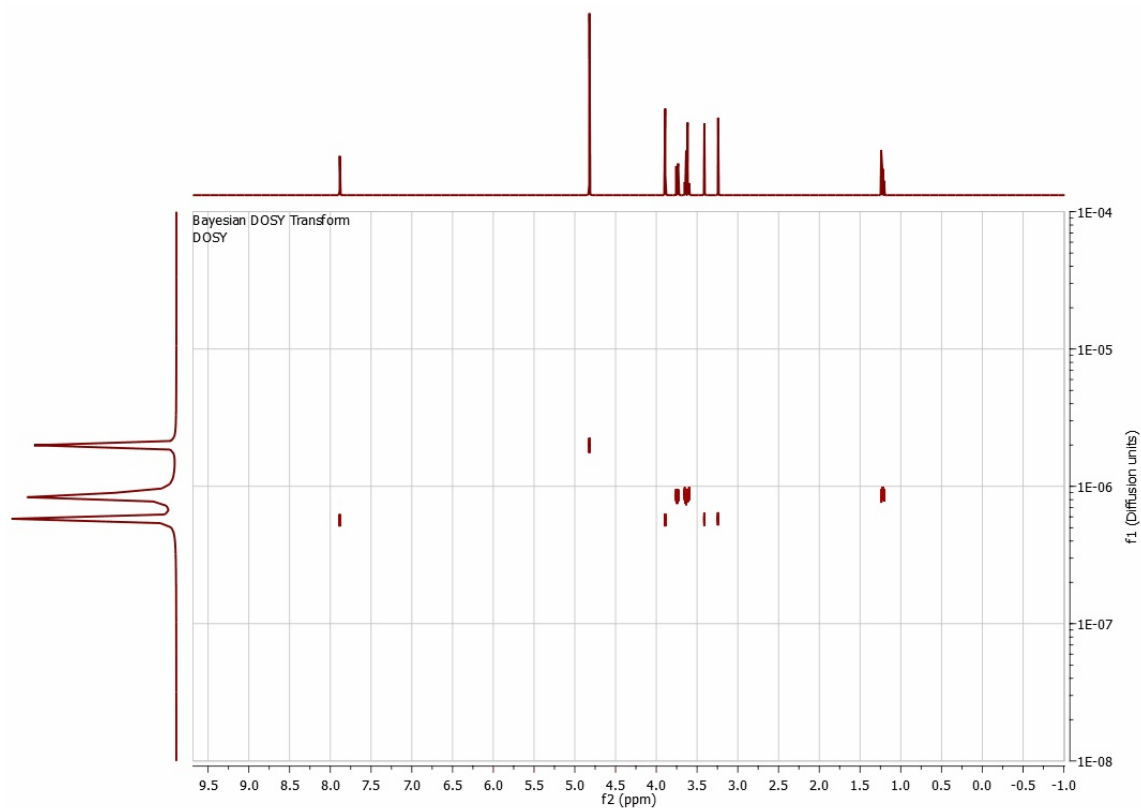


Figure 5.15. 2D DOSY spectrum of the caffeine, 2-ethoxyethanol and water mixture showing the separation of the three compounds present.⁷⁵⁰

Once this transformation is complete, the diffusion coefficient for each compound in a mixture can be determined from the y-axis of the 2D plot. This, combined with the viscosity of the solvent can be used to determine the effective molecular size in that solvent, based on the Stokes-Einstein equation (Equation 3), where r is the Van der Waals radius in meters, k is the Boltzmann constant, T the temperature in Kelvin, and η the viscosity in Pascal seconds.^{749,752} Comparison of this radius with the measured mean Van der Waals radius provides an understanding of the solvation sphere surrounding each molecule.

$$r = \frac{kT}{6\pi\eta D} \quad (3)$$

DOSY experiments were carried out on **126** in both DMSO-d₆ and D₂O, and on compound **6** in D₂O. The diffusion coefficients were then calculated for each compound using the 2D DOSY spectra (Table 5.1). As expected, the diffusion coefficients determined for **126** were different based on the solvent used, with the diffusion in DMSO-d₆ slower than that noted for D₂O.

Table 5.1. DOSY-derived diffusion coefficients for compounds **126** and **6** at 30°C.

Entry	Compound	Solvent	Diffusion coefficient, /x10 ⁻¹⁰ M ² .s ⁻¹	
			This work ^a	Literature ⁷⁵³
1	125	DMSO-d ₆	3.3	-
2	125	D ₂ O	6.4	-
3	6	D ₂ O	1.5	-

Diffusion coefficients for the non-deuterated water present in D₂O, the water present in DMSO-d₆, and the DMSO-d₅ species present in DMSO-d₆ were also calculated (Table 5.2), and these values show good correlation with those found in the literature.⁷⁵³

Table 5.2. DOSY-derived self-diffusion coefficients of solvents.

Entry	Compound	Solvent	Diffusion coefficient /x10 ⁻⁹ M ² .s ⁻¹	
			This work ^a	Literature ⁷⁵³
1	H ₂ O	D ₂ O	2.5	2.6 ^a
2	H ₂ O	DMSO-d ₆	1.1	-
3	DMSO-d ₅	DMSO-d ₆	0.76	0.73, 0.89 ^b

^aT = 30°C, ^bExperiments carried out at 25°C and 35°C.

With the diffusion coefficients for compounds **126** and **6** in hand, the Stokes radius for each molecule was calculated using the Stokes-Einstein equation (Equation 3, above) and compared to the Van der Waals radii, as calculated using the volume_calc.py script available in the Schrödinger package¹⁷² (Table 5.3).

Table 5.3. Stokes Radii for compounds **126** and **6**.

Entry	Compound	Solvent	Stokes Radius /Å	VDW radius /Å
1	125	DMSO-d ₆	3.72	3.34
2	125	D ₂ O	4.45	3.34
3	6	D ₂ O	18.9	3.68

Based on these results, it is immediately apparent that the size of the solvation sphere which forms around the molecules is dependent on the solvent used, with a larger solvation sphere forming with the use of D₂O (Table 5.3, entries 1 and 2). This increase is most likely due to the increased interactions between the anionic compound **125** and the more polar water molecules than the interactions possible in DMSO. Comparison of the Stokes radii to the calculated Van der Waals radii also shows an increase in the “effective” size of the molecule in solution due to the presence of the solvation sphere. This is not unexpected, as Van der Waals volumes and radii are calculated as isolated gas-phase molecules without the solvent interactions inherent in solutions. The number of solvent molecules present in the solvation shell could theoretically be determined from these radii, however these estimates depend on the sixth root of the gradient strength calibration, and slight theoretical and experimental errors lead to large changes in the number of solvent molecules present.⁷⁴⁹ As the solvation sphere is constantly fluctuating, the number of molecules calculated depends on the timescale of the method used to calculate it – the smaller the timescale, the larger the solvent shell. The diffusion timescale is several collisions in the order of 100 picoseconds, whereas NMR timescales are milliseconds to seconds-long, and as a result signals arising from bound solvent molecules do not arise.⁷⁴⁹

The large difference between the Stokes radius and the Van der Waals radius for compound **6** (Table 5.3, entry 3) appears to show a huge five-fold increase in the size of the molecule on solvation. However, as the Stokes-Einstein equation makes use of literature values for η , it does not take into account the changes in the viscosity of the solution, and as such an inflated value is obtained for the Stokes radius for this compound. A more accurate measurement of the Stokes radii for this and other compounds requires the determination of the viscosity of the solution used for these DOSY experiments and the subsequent use of that value for η , rather than making use of literature values. This is a complex undertaking, requiring extensive study into areas such as the concentration-dependence of the viscosity, and as such is beyond the scope of this project.

5.3. Linking the Abstract with the Concrete: Putting NMR Analysis of Molecular Flexibility in Solution (NAMFIS) to Work.

“When you're curious, you find lots of interesting things to do.”

Walt Disney

As previously stated, NMR Analysis of Molecular Flexibility In Solution, or NAMFIS, combines the theoretical with the practical in order to determine the populations of conformations in solution. Conformations are randomly generated *in silico* using software such as Schrödinger's MacroModel, with an applicable force field (MMFF, OPLS-2005, etc) and in either a specific solvent or in the gas phase. Once the structures have been energy-minimized and the duplicates eliminated, these conformers are then screened using constraints determined from NOE/ROE (Rotating Frame Overhauser Enhancement) experiments (Figure 5.16). The internuclear distances are determined by calculating the crosspeak volume^{326,754-761} based on the isolated spin pair approximation (ISPA),⁷⁶² using an internal calibration distance (Equation 4). The result is a set of conformers which provide a best fit for the experimental parameters, and represent the most likely solution distribution.



Figure 5.16. Processes in NMR Analysis of Molecular Flexibility In Solution (NAMFIS) analysis.

$$\frac{NOE_1}{NOE_2} = \left(\frac{Distance_1}{Distance_2} \right)^{-6} \quad (4)$$

The power of this, and other similar techniques,⁷⁶³⁻⁷⁶⁴ lies in the ability of these techniques to identify what conformations are present in solution, rather than an averaged structure derived from NMR data. Comparison of the conformations identified as present in solution with poses derived from docking methodologies reveals the likelihood that a compound could bind into a protein, as compounds with similar solution and bound conformations would be more likely to interact with a protein than a compound with vastly different solution and bound conformations. Due to the well-resolved, clearly assignable ¹H NMR spectrum obtained, **6** was selected as a candidate for NAMFIS analysis and the conformational search yielded 3630 unique conformations from a total of 86915 conformations, produced using two force fields (MMFF and OPLS-2005) and two solvent matrices (CHCl₃ and H₂O).

These conformations were generated using the GBSA constant dielectric model within an energy window of 21.0 kJ/mol (5.02 kcal/mol), and minimization was carried out using full-matrix-Newton-Raphson (FMNR) minimization (OPLS-2005, H₂O) within the same energy window (21 kJ/mol) on a comparison of "heavy atoms plus OH and SH".

NOE spectra were obtained for **6** (Figure 5.17), and analysis of this data allowed for the determination of the interproton contacts and distances necessary for NAMFIS analysis of the 3630 conformations generated (See SI Table for full input and output files). Application of the experimentally determined constraints to the conformer pool identified six conformations which together satisfied the conditions of the NAMFIS analysis (Table 5.4).

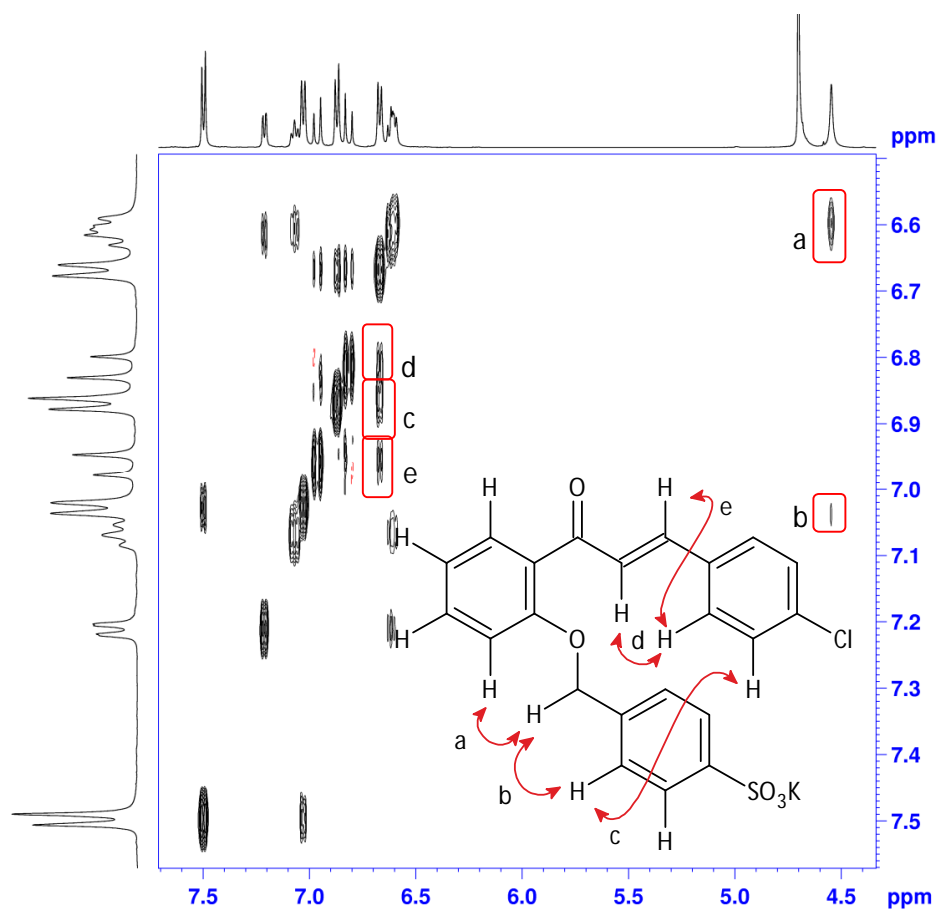


Figure 5.17. 2D NOE spectrum and assignment of compound **6** for NAMFIS analysis.

Table 5.4. Experimental and calculated NOE distances for **6**.

Entry	Proton Interactions	NOE distances /Å		Difference /Å
		Experimental	Calculated	
1	H31-H38	2.70	2.69	0.01
2	H38-H40	3.68	3.67	0.01
3	H37-H40	3.79	3.82	0.03
4	H28-H38	4.42	4.42	0.00
5	H28-H35	2.66	2.64	0.02
6	H28-H30	3.65	3.65	0.00
7	H29-H30	3.98	4.03	0.05
8	H29-H35	2.71	2.73	0.02

Mixing time 180 ms, calibration distance 2.48 Å.

Of the six conformations identified, four poses are responsible for >95% of the solution population, and one of these conformations accounts for almost 50% of the distribution (Table 5.5). When the top two conformers are compared, it is interesting to note that the major differences between these conformers are the rotation of the benzyl group and the rotation of the α,β -portion, both of which contribute to the RMSD value of 0.64 Å (Figure 5.18).

Table 5.5. Population distribution and RMSD values of NAMFIS conformers.

Entry	Conformer number	Population distribution	RMSD /Å	
		/%	COX-2	COX-1
1	6-602	47.21	1.79	1.76
2	6-1360	21.59	1.61	1.51
3	6-2492	15.37	1.39	1.34
4	6-111	11.42	1.56	1.54
5	6-2456	2.54	2.17	2.36
6	6-3448	1.54	1.36	1.27

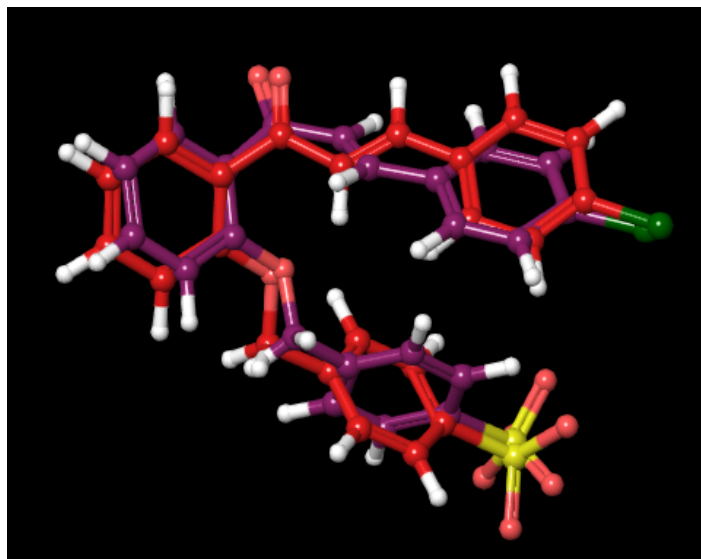


Figure 5.18. Overlay of the top NAMFIS-derived conformers **6-602** (shown in purple) and **6-1360** (shown in red).

While comparison of the top conformers is interesting, superposition of these conformations with the docked pose of **6** allows for comparison of the predicted solution conformations with the predicted docked conformation. An RMSD value of 1.58 Å is obtained when **6-602** is superimposed onto the docked pose of **6** in COX-2 (Figure 5.19), and the overlap of **6-602** onto the predicted COX-1 binding position, while not as good with an RMSD of 1.76 Å, is still acceptable (Figure 5.20).

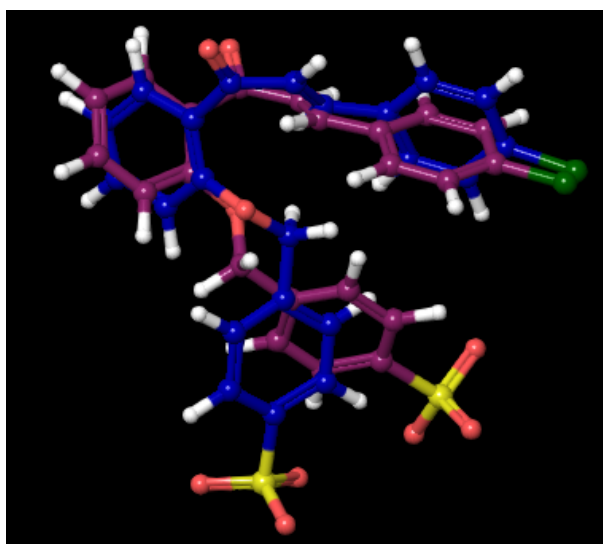


Figure 5.19. Overlay of the pose generated for **6** when docked into COX-2 (shown in blue) with the NAMFIS-derived conformer **6-602** (shown in purple).

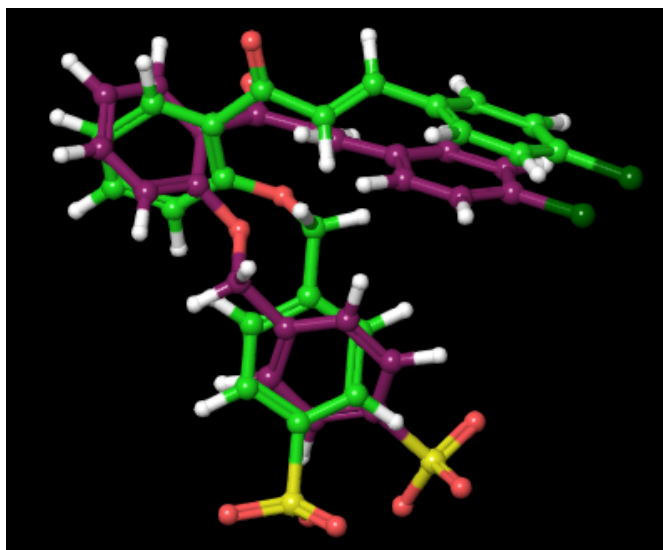


Figure 5.20. Overlay of the pose generated for **6** when docked into COX-1 (shown in green) with the NAMFIS-derived conformer **6-602** (shown in purple).

Superposition of **6-1360** with the docked pose of **6** in COX-2 reveals a moderate RMSD of 1.61 Å (Figure 5.21), while overlaying the poses of **6-1360** and **6** in COX-1 yields an RMSD value of 1.51 Å (Figure 5.22). Despite not overlapping perfectly, the NAMFIS poses are essentially separated by the rotation of a single bond, something which could be easily accomplished in binding to a protein.

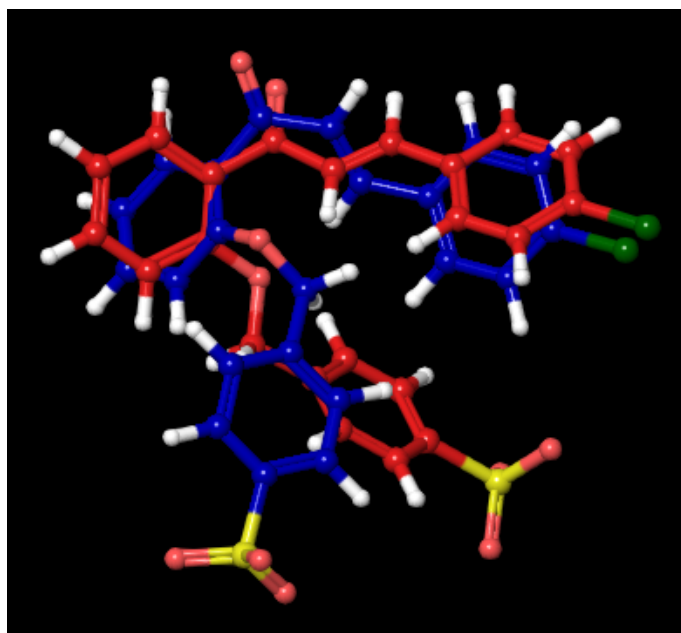


Figure 5.21. Overlay of the pose generated for **6** when docked into COX-2 (shown in blue) with the NAMFIS-derived conformer **6-1360** (shown in red).

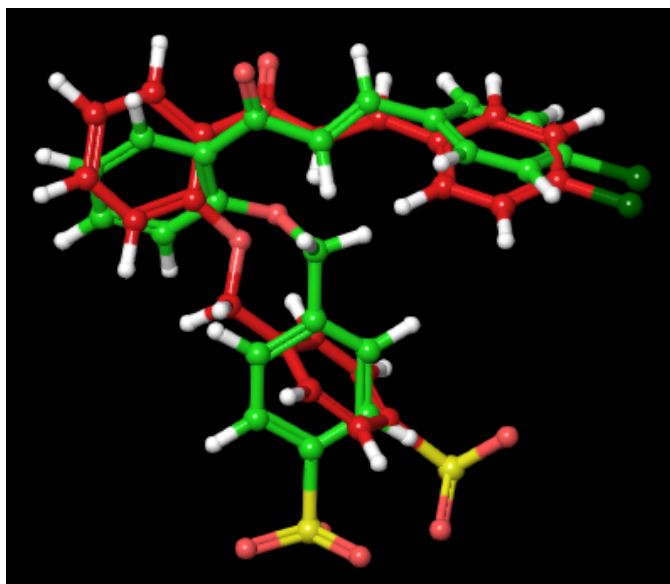


Figure 5.22. Overlay of the pose generated for **6** when docked into COX-1 (shown in green) with the NAMFIS-derived conformer **6-1360** (shown in red).

The third most prominent conformer **6-2492** (Table 5.5, entry 3) shows the best RMSD values of 1.39 Å and 1.34 Å when compared to the poses for **6** when docked into COX-2 and COX-1 respectively. As this conformer accounts for 15% of the population, it is possible for this conformer to successfully bind to both COX-2 (Figure 5.23) and COX-1 (Figure 5.24). With all of the top four conformations showing RMSD values of less than 2 Å for both COX-1- and COX-2-docked **6**, it is likely that any one (or all) of these conformations could bind into the proteins *in vitro*. The definitive binding pose, however, can only be determined through co-crystallization of the ligand and the protein and subsequent X-ray crystallographic analysis, and even then that pose might not be present at observable levels in the solution conformer distribution.³²⁶

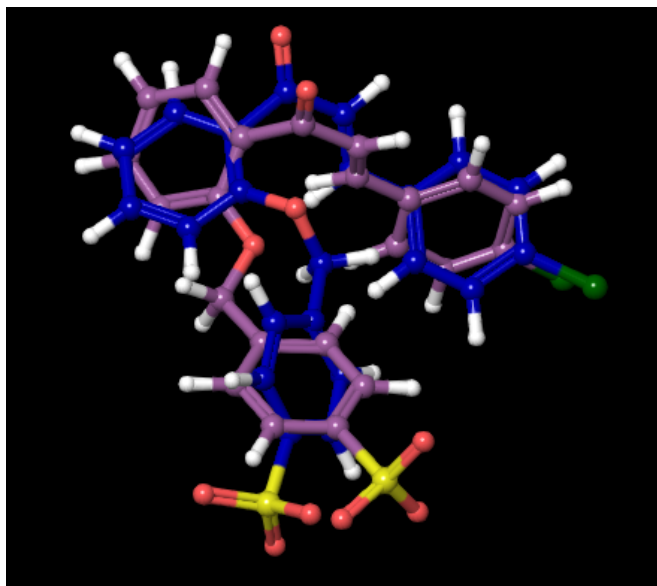


Figure 5.23. Overlay of the pose generated for **6** when docked into COX-2 (shown in blue) with the NAMFIS-derived conformer **6-2492** (shown in purple).

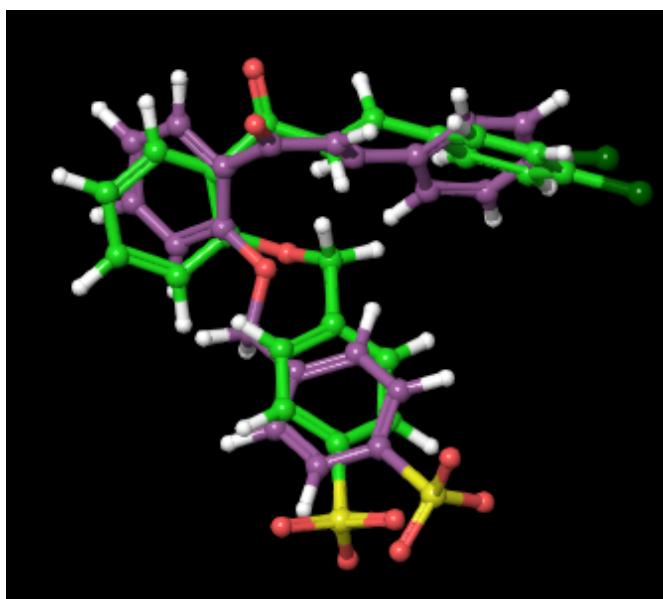


Figure 5.24. Overlay of the pose generated for **6** when docked into COX-1 (shown in green) with the NAMFIS-derived conformer **6-2492** (shown in purple).

5.4. What We Never Knew We Needed to Know: A Review.

“Education is learning what you didn’t even know you didn’t know.”

Daniel J. Boorstin

As one cannot assume that the product obtained from a reaction is the expected product, complete spectroscopic analysis of all synthesized compounds must be carried out in order to definitively determine the identity of a compound, no matter how sure one is of the outcome of a reaction. As such, complete NMR spectroscopic analysis of the synthesized compounds were carried out as a matter of course. While appearing daunting, the NMR spectroscopic analysis of the final benzenesulfonate compounds can be simplified through the identification and analysis of simpler compounds which are components of the final compound. For example, analysis of the unsubstituted **62** allowed for identification of the methylene proton and carbon signals, while analysis of **71** and other chalcones made the identification of the α,β -unsaturated portion of the final molecule straightforward.

During the course of analysis, broadening of the line widths of methylene peak in the ^1H NMR spectrum was observed on formation of the ether bond. This broadening indicates that the solution mobility of the molecule has changed upon condensation. Based on this observation, DOSY experiments were carried out on **125** and **6** in order to determine the diffusion coefficients and hydrodynamic radii for these compounds. The experiments carried out on **125** showed that the size of the hydration sphere is dependent on the solvent used, while similar experiments carried out on **6** identified a need to take the viscosity of the sample into account when calculating the effective radii of compounds rather than using literature values for the solvents used.

NAMFIS analysis of **6** identified six conformers from a pool of 3630 potential conformers as existing in solution, with four poses comprising >95% of the solution population. While none of the poses identified are exact matches when compared to the pose generated for **6** in either COX-1 or COX-2, all but one pose show RMSD values of less than 2 Å, which indicates that any of these five conformers could bind into the proteins.

6. Results and Discussion: Inhibition Screening and Selectivity Determination

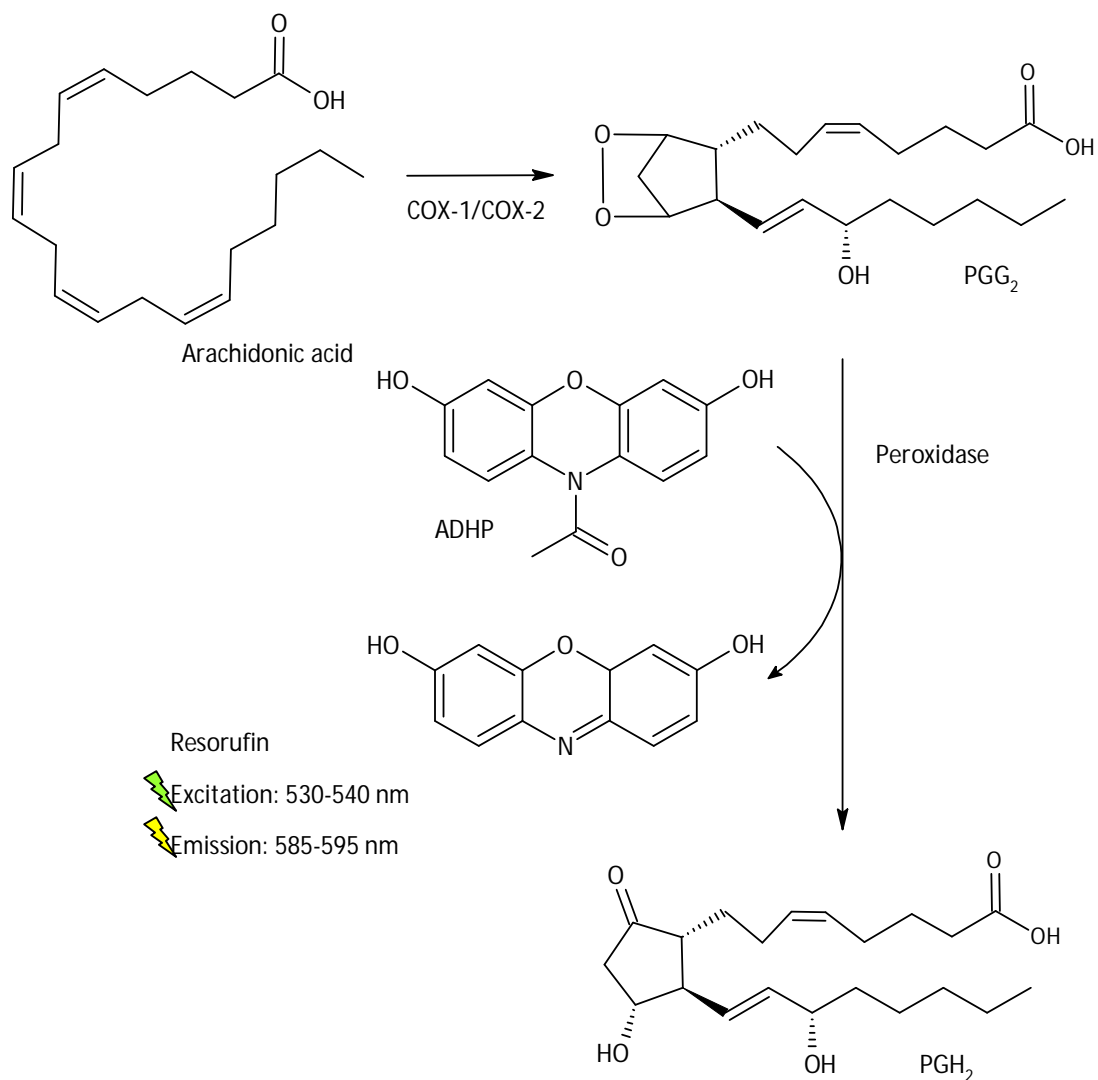
6.1. When Worlds Collide: Theory Vs. Experiment.

"It doesn't matter how beautiful your theory is, it doesn't matter how smart you are. If it doesn't agree with experiment, it's wrong."

Richard P. Feynman

With the hurdles of synthesis and identification successfully navigated, the final challenge in the design of these COX-2 selective compounds to be cleared is the *in vitro* testing to determine whether these compounds are in fact selective for COX-2 as desired. One of the easiest methods of COX screening lies in the bifunctionality of the COX enzyme, with the COX component first converting arachidonic acid into a hydroperoxy endoperoxide (PGG₂), which is then reduced to the alcohol (PGH₂) by the peroxidase element of the enzyme.⁷⁶⁵⁻⁷⁶⁶ Screening of COX activity can be accomplished due to a side reaction of PGG₂ with 10-acetyl-3,7-dihydroxyphenoxazine (ADHP) which produces resorufin, a highly-fluorescent compound (Scheme 6.1). The fluorescence of resorufin can easily be analyzed using an excitation wavelength of 530-540 nm and an emission wavelength of 585-595 nm, both ranges which are easily accessible using modern plate readers. The presence of fluorescence in a sample indicates that the enzyme is active, whereas the reduction or lack of fluorescence indicates that the enzyme has been deactivated by an inhibitor. The amount of fluorescence present also allows for determination of the percent inhibition of a particular compound.

Scheme 6.1. COX screening using the conversion of ADHP into resorufin.



Screening of the 30 synthesized compounds was carried out using a COX Fluorescent Inhibitor Screening Assay Kit (Item 700100) from Cayman Chemicals. As the concentration needed was not known, several concentrations of **3** were made and tested against both COX-1 and COX-2 proteins (Table 6.1) so as to determine an appropriate concentration for further testing. The reference standards DuP-697 and SC-560 (Figure 6.1) were included in the testing so as to provide a benchmark for the relative level of inhibition.

Table 6.1. Concentration-dependent inhibition of COX-2 and COX-1.

Entry	Compound	Concentration /nM	Percentage Inhibition /%	
			COX-2	COX-1
1	3	100	35 ± 4	12 ± 3
2	3	50	22 ± 8	0
3	3	25	20 ± 6	0
4	3	10	18 ± 5	0
5	3	5	14 ± 7	0
6	3	100,000	36 ± 2	19 ± 3
7	DuP-697	3,000 ^a	>90 ^b	- ^c
8	SC-560	3,300 ^a	- ^c	>90 ^b

^aManufacturer recommended concentration ^bResults obtained indistinguishable from background values ^cNot tested

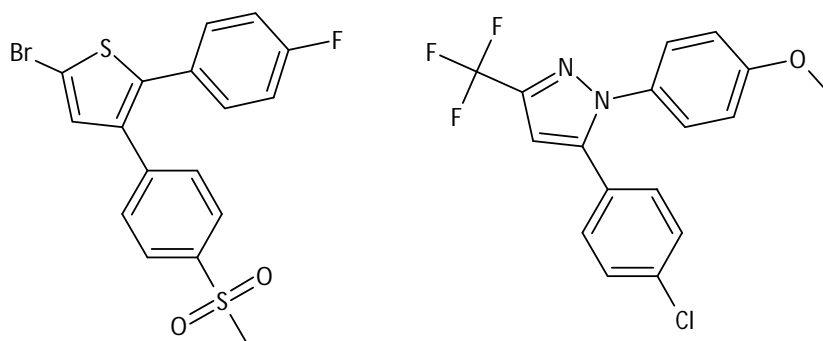


Figure 6.1. 2D structures of DuP-697 (left) and SC-560 (right).

At 100 nM, **3** inhibits both COX-2 and COX-1 (Table 6.1, entry 1) at a promising ratio of *ca.* 3:1, however when the concentration is increased 1000-fold to 100 μ M (Table 6.1, entry 6), the value for the inhibition of COX-2 essentially remains unchanged while the percentage inhibition for COX-1 increases significantly from 12% to 19%. This points to the presence of a slightly different kinetic pathway for COX-1 than is seen for COX-2, however complete elucidation of these details is beyond the scope of the project. While **3** does show COX-2 inhibition at lower concentrations, the standard deviation values which accompany the inhibition scores are greater than that observed at 100 nM, and as such are not as

reliable. These *in vitro* results, however, might not necessarily correspond with the inhibition which would be seen *in vivo*. Lumiracoxib, for example, shows a 500-fold greater selectivity for COX-2 over COX-1 *in vivo*, but *in vitro* it appears as a relatively weak COX-2 inhibitor (ca. 50%).⁷⁶⁷

As an initial result, the selectivity observed for **3** is satisfying, as it shows that this drug design methodology does work. While one cannot directly compare the *in silico* results obtained for one protein with the results obtained for another, no matter how closely related, it is heartening to see some form of selectivity. With the FDA and other agencies being reluctant to grant approval for COX-2 selective compounds as painkillers due to the associated risk, other avenues, including as potential cancer therapeutics, can be explored,⁶⁶⁸ as a number of cancers have been linked to COX-2 up-regulation.⁶⁶⁹⁻⁶⁷² PGA₁ and PGA₂, both COX-2 metabolites, have been shown to bind to the tumour growth factor p53 in neuroblastomas, effectively inactivating the apoptotic process governed by this factor.⁶⁷³⁻⁶⁷⁴ By inhibiting COX-2, p53 function is restored, and the cancerous cells undergo apoptosis. COX-2 inhibition has also been shown to prevent the development of colorectal cancers in mice with genetic predisposition towards these cancers due to an APC (Adenomatous polyposis coli) gene mutation.⁷⁶⁸ Therefore, should this and other compounds not prove suitable for the roles for which they were originally designed there exist a number of alternative uses which can be explored.

6.2. An Unexpected Turn of Events: When Experiment and Theory Clash.

"Testing leads to failure, and failure leads to understanding".

Burt Rutan

With these satisfying results in hand, the remaining 29 compounds were tested against COX-2 at 100 nM (Table 6.2) following the procedures used previously. Despite the optimistic results obtained for **3**, only two compounds, **56** and **57** (Table 6.2, entries 24 and 26), show comparable inhibition scores, with four others showing slight reduction in the degree of inhibition recorded (Table 6.2, entries 16, 25, 28 and 29). The remaining 23 compounds show significant reduction in the inhibition scores obtained, with a number of the substitutions resulting in the complete elimination of inhibition.

Table 6.2. COX-2 inhibition values, Glide XP and Prime scores.

Entry	Compound	Percentage Inhibition /%	Glide XP /kCal.mol⁻¹	Prime /kCal.mol⁻¹
1	3	35 ± 4	-12.619	-55.772
2	5	0	-11.436	-92.183
3	6	0	-11.569	-84.908
4	7	0	-12.352	-69.067
5	8	0	-11.898	-94.200
6	9	0	-11.517	-103.141
7	43	0	-11.001	-104.953
8	44	14 ± 3	-12.687	-93.861
9	10	8 ± 3	-12.570	-93.748
10	45	4 ± 2	-12.163	-93.155
11	46	0	-12.362	-90.999
12	47	6 ± 2	-12.111	-70.669
13	11	14 ± 2	-12.664	-84.205
14	48	0	-12.064	-96.677
15	49	0	-11.973	-99.575
16	17	28 ± 6	-12.767	-86.607
17	50	3 ± 1	-12.059	-85.854
18	51	5 ± 1	-11.654	-89.884
19	52	2 ± 1	-11.993	-88.717
20	53	0	-12.681	-90.577
21	23	0	-11.749	-90.352
22	54	0	-12.646	-90.856
23	55	5 ± 2	-12.700	-88.670
24	56	42 ± 3	-12.394	-72.392
25	12	20 ± 2	-8.049	-92.404
26	57	35 ± 4	-11.497	-98.497
27	58	16 ± 1	-7.813	-88.302
28	59	28 ± 5	-11.325	-88.670
29	18	15 ± 3	-12.149	-82.327
30	24	23 ± 4	-11.534	-98.884

Comparison of the degree of inhibition to the Prime binding scores obtained showed no obvious correlations, with a number of compounds with very good binding scores yielding very poor inhibition values, and conversely, a number of low-scoring compounds showing good inhibition. For example, compound **43** received the highest binding score (Table 6.2, entry 7), however it shows no inhibition *in vitro*, while compound **56**, which has a comparatively poor score, shows an inhibition value of over 40% (Table 6.2, entry 24). This discrepancy highlights one of the major shortcomings of using computationally-derived data as the sole basis for lead compound identification – *in silico* binding and docking scores are calculated based on poses generated from a user-restricted portion of the protein and does not take into account *in vitro* conditions present. Comparison of the poses generated for these compounds with that generated for **3** does not illuminate a reason for the incongruity either – apart from the poses for compounds **12**, **58** and **59**, which show inversion, the poses overlap very well with the pose calculated for **3**. In this case, the computational model does not appear to accurately describe the mode of inhibition observed, and further studies are required in order to ascertain a link between the theoretical and experimental data.

It is possible that interactions between the ligand and the protein occur at sites other than the active site, and these compounds are therefore allosteric inhibitors rather than competitive inhibitors,⁷⁶⁹ as is the case of Pfizer's maraviroc (Selzentry®), an antiretroviral compound which acts as a negative allosteric CCR5 modulator.⁷⁷⁰ Allosteric compounds act by binding to allosteric sites, often resulting in conformational changes to the protein, which can either enhance or reduce the activity of the protein (Figure 6.2). While COX-2 is a homodimer of two tightly-associated monomers with apparently identical primary structures, each monomer has a unique function, with one monomer responsible for the conversion of arachidonic acid into PGH₂, while the other functions as an allosteric monomer.^{621,771-774} Irrefutable proof as to the location of the inhibitor within the protein however would only be gained through the X-ray spectroscopic study of a co-crystallized protein-ligand complex, a delicate and painstaking process in and of itself.

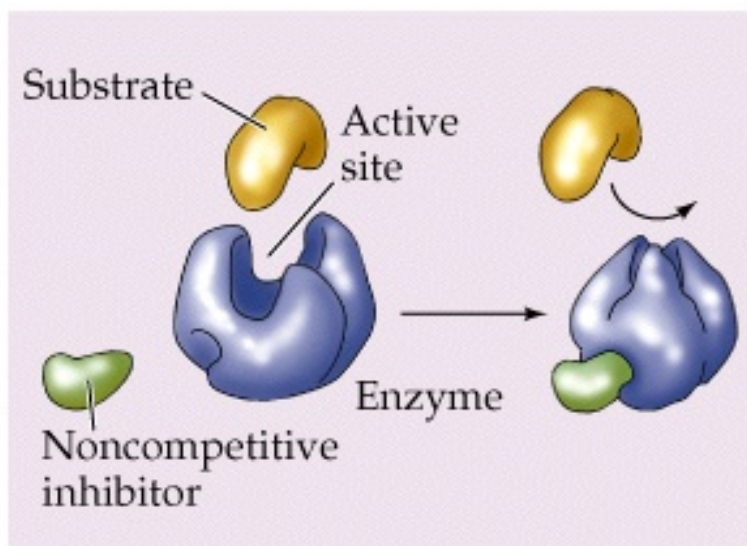


Figure 6.2. Allosteric inhibition of proteins.⁷⁷⁵

As a number of the compounds tested show COX-2 inhibition as intended, these compounds were also screened against COX-1 in order to determine the potential selectivity. Even with the promising results obtained for **3**, all of the additional compounds show significant COX-1 inhibition (Table 6.3). As was the case with the inhibition scores for COX-2, there does not appear to be a link between either the Glide XP docking or the Prime binding scores and the degree of inhibition observed, with low-scoring compounds showing good inhibition, and high-scoring compounds yielding inhibition scores much lower than expected. This lack of congruency between the computationally-derived docking and binding scores and the experimental data again illustrates the need for additional testing and study in order to identify a method of prediction which could be applied to additional work on these and other compounds. Again, it is possible that these compounds are allosteric rather than competitive inhibitors, as a similar heterodimer situation as is seen for COX-2 has been identified for COX-1.^{621,771,774,776-778}

Table 6.3. COX-1 inhibition values, Glide XP and Prime scores.

Entry	Compound	Percentage Inhibition /%	Glide XP /kCal.mol⁻¹	Prime /kCal.mol⁻¹
1	3	12 ± 3	-10.572	-74.414
2	5	47 ± 2	-11.767	-89.066
3	6	35 ± 2	-11.223	-85.836
4	7	32 ± 1	-6.414	-81.389
5	8	32 ± 2	-9.625	-94.815
6	9	23 ± 1	-11.667	-79.280
7	43	22 ± 2	-11.120	-86.983
8	44	62 ± 2	-5.040	-77.147
9	10	62 ± 1	-10.102	-80.341
10	45	56 ± 1	-10.709	-89.088
11	46	43 ± 2	-11.556	-78.554
12	47	32 ± 4	-10.590	-75.929
13	11	27 ± 5	-10.416	-61.886
14	48	32 ± 2	-12.223	-82.510
15	49	24 ± 2	-12.093	-81.847
16	17	65 ± 7	-11.841	-68.525
17	50	64 ± 8	-10.797	-71.438
18	51	58 ± 1	-10.684	-92.570
19	52	60 ± 1	-10.825	-86.733
20	53	60 ± 2	-4.324	-82.781
21	23	45 ± 2	-12.126	-91.369
22	54	40 ± 3	-11.267	-88.617
23	55	34 ± 5	-11.441	-87.202
24	56	80 ± 2	-9.992	-76.870
25	12	87 ± 2	-11.635	-83.947
26	57	71 ± 4	-9.624	-86.845
27	58	71 ± 3	-9.927	-97.391
28	59	61 ± 4	-11.530	-92.396
29	18	50 ± 5	-11.321	-76.413
30	24	58 ± 4	-10.353	-102.856

6.3. Gazing into the Crystal Ball: The Future of Isoform-Selective Coxibs.

“Only you can control your future”.

Dr Seuss

While these results do not show the desired results, they do open avenues into the development of a non-selective, non-steroidal COX inhibitor, similar in action to the “general” painkillers such as aspirin and ibuprofen. With the sales of painkillers totaling almost \$4 billion in 2012,⁶⁸¹ there is a large market for over-the-counter analgesics, and a number of compounds tested show promise as both COX-1 (Table 6.2, entries 24-30) and COX-2 inhibitors (Table 6.1, entries 24-30). The hypothesis that COX-2 is solely responsible for inflammation has been questioned by a number of investigations, and current belief is that both isoforms are responsible for pain.⁷⁷⁹⁻⁷⁸² COX-1 is thought to be to blame for the initial prostanoid response to tissue injury, whereas COX-2 is responsible for the long-term synthesis of prostaglandins,⁷⁸³⁻⁷⁸⁶ and as such a dual inhibitor would allow for the reduction of both the immediate and sustained pain felt after injury. Non-selective COX inhibitors could also be used as anti-cancer agents, as a number of studies have shown that non-selective celecoxib analogues have significant anti-cancer activities, with the potency of a compound not having any correlation with selectivity.⁶⁷⁵⁻⁶⁷⁸ The use of non-selective compounds as cancer therapeutics is not without precedence - ketorolac (Figure 6.3), a heterocyclic acetic acid derivative, is a non-selective NSAID which has shown the ability to reduce the recurrence of breast cancers when administered perioperatively,⁷⁸⁷ and the more common NSAID compounds aspirin and ibuprofen have been shown to have cancer-preventative properties.⁷⁸⁸

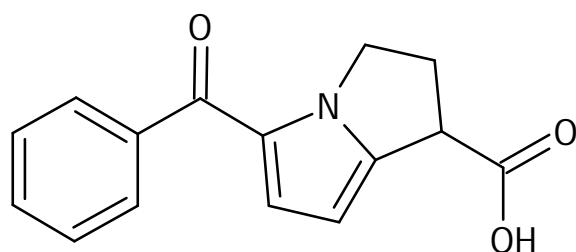


Figure 6.3. 2D structure of ketorolac.

Another interesting opportunity arises in the potential development of a COX-1 selective compound. Despite not being a major focus in the fight against pain in recent years, increased or over-expression of COX-1 is involved in a number of other conditions and diseases, and a targeted COX-1 inhibitor might aid in combating these diseases as well as acting as a painkiller. COX-1 is involved in post-surgery pain

processing,⁷⁸⁹ and COX-1 inhibitors, administered spinally either before or after surgery, have allowed for the treatment of post-operative pain.⁷⁹⁰⁻⁷⁹¹ Interestingly, similar administration of COX-2 selective compounds showed no effect on prostaglandin synthesis.⁷⁹¹ Compounds such as **23** and **50-54** show very little, if any, COX-2 inhibition (Table 6.1, entries 17-22) while showing good inhibition of COX-1 (Table 6.2, entries 17-22), and would be suitable candidates for further exploration and additional testing. The use of a COX-1 selective pain-relieving compound is not unprecedented, as Mofezolac[®], an isoxazoleacetic acid (Figure 6.4), is available in a number of countries for just such an application.⁷⁹²

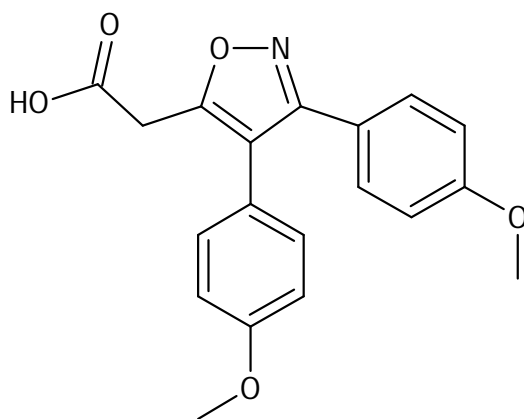


Figure 6.4. 2D structure of Mofezolac[®], a COX-1 selective analgesic.

As previously stated, the COX enzymes are responsible for more than just pain. Inhibition of COX-1 has also been shown to have a cardio-protective effect in low doses, much the same as is observed for low doses of aspirin. COX-1-derived prostanoids play a vital part in the hardening of arteries associated with atherosclerosis and atherothrombosis. Thromboxanes, responsible for the aggregation of platelets and for platelet-vessel interactions, are dependent on platelet COX-1 expression,⁷⁹³⁻⁷⁹⁴ and inhibition of COX-1 would reduce the ability of platelets to aggregate into atherosclerotic plaques. Non-aspirin-based COX-1 inhibitors, such as the compounds presented above, would also allow for the treatment of aspirin-sensitive patients or patients which show "aspirin resistance".⁷⁹³

Another potential role for a COX-1 selective inhibitor is as an anti-cancer drug. COX-1 is overexpressed in ovarian cancer, where it promotes the production of angiogenic growth factor,⁷⁹⁵ and is up-regulated in a number of cancers, including human breast⁷⁹⁶ and prostate cancers,⁷⁹⁷ and in murine lung tumorigenesis models,⁷⁹⁸ as well as in squamous cell carcinoma and human cervix adenocarcinoma.⁷⁹⁹ Finally, microglia-localized COX-1 plays a vital role in neuroinflammation, a key stage in the development of a number of neurodegenerative diseases, such as Alzheimer's disease, Parkinson's disease, HIV-associated dementia, and is a contributor to the effects of brain injury due to trauma, ischemic stroke or epilepsy. Both pharmacological inhibition and genetic negation of COX-1 activity reduces the inflammatory response, and also reduces neuronal loss.⁸⁰⁰ This indicates that a NSAID which shows greater selectivity for COX-1 over COX-2 is more likely to reduce the neuroinflammation observed in these disorders,⁸⁰⁰ and a COX-1 selective compound, such as those examined here, could provide a new therapeutic approach to neurodegenerative disorders where neuroinflammation is a large component.

One aspect which has not been addressed during the analysis of these compounds is the time-dependent nature of COX inhibitors. These analyses were carried out using the incubation times recommended by the manufacturer, however as altering these times can significantly alter the values obtained, determination of the optimal incubation times for each compound tested would be ideal. It is possible that a compound which shows poor inhibition under these conditions might prove to be a good inhibitor with an adjusted incubation period. Prescreening optimization is economically unviable with the number of compounds tested, but the importance of determining the correct timing for these analyses cannot be overlooked and would need to be investigated should these compounds be taken further.

6.4. What We Never Knew We Needed to Know: A Review.

“Get your facts first. Then you can distort them as you please.”

Mark Twain

While the search for a novel COX-2 selective inhibitor is perhaps not as clear-cut as hoped, these results demonstrate the ability of these compounds to inhibit the COX enzymes, and in the case of **3**, to selectively inhibit COX-2 three times more effectively than COX-1 (*ca.* 3:1) at 100 nM. This unsubstituted **3** shows potential as a COX-2 selective compound, while a number of the compounds show promise as COX-1 selective compounds, including **23** and **50-54**, with inhibition scores of over 40%. In addition to these isoform-selective compounds, several compounds show potential as non-selective NSAIDs, such as **12** and **56-58**. As there does not appear to be a correlation with either the Glide XP binding scores or the Prime docking scores obtained for these compounds, further analysis, both *in silico* and *in vitro*, is required to determine whether the inhibition observed arises due to interaction of the compounds with the COX active site, or whether allosteric inhibition is responsible for the activity observed.

Should these compounds not prove suitable as either COX-1 or COX-2 selective analgesic compounds, there are a number of external opportunities where these compounds might prove useful. Overexpression of COX-2 has been linked to increased cell growth and a number of cancers,⁶⁶⁸⁻⁶⁷² such as neuroblastomas,⁶⁷³ and inhibition of COX-2 allows for the restoration of tumour apoptosis factor p53 activity and subsequent cell death through apoptosis.⁶⁷⁴ Coxibs have also been shown to act as anti-cancer agents even when the malignant cells do not contain COX-2,^{675,679} and this is also true for non-selective compounds as well.⁶⁷⁶⁻⁶⁷⁸ COX-1 selective compounds are not limited to analgesic uses – a number of cancers show up-regulation of this protein,⁷⁹⁶⁻⁷⁹⁹ and COX-1-derived prostaglandins have been identified in several neuroinflammatory diseases and disorders.⁸⁰⁰ Whether these compounds will prove to be suitable drug candidates will depend on the results of additional extensive testing and investigation, including ADME, toxicity and other biological evaluations.

7. Conclusion

"Enjoy the journey of life and not just the endgame."

Benedict Cumberbatch

The search for effective non-steroidal anti-inflammatory compounds without serious side effects is an ongoing one, and with the failure of High-Throughput Screening (HTS) in providing new drug-like compounds, many researchers are returning to the world of natural products and their derivatives in order to identify new lead compounds. One compound which has been the focus of much investigation is curcumin, the diferuloyl methane compound found in turmeric. This compound was chosen as a model for compounds which would selectively target the inducible form of cyclooxygenase (COX), the enzyme responsible for the first step in the conversion of arachidonic acid into the various prostaglandins and thromboxanes in the inflammatory process. An *in silico* investigation into the binding of curcumin and celecoxib, a known COX-2 selective analgesic compound, was conducted and important ligand-protein interactions were identified which would need to be mimicked by a novel COX-2 selective compound. However, as the docking and binding scores for celecoxib when docked into COX-2 are similar to the results obtained on docking into COX-1, computational results cannot be the sole criterion used when identifying a potential lead compound, as literature reports celecoxib showing 10-20-fold selectivity for COX-2 over COX-1 *in vivo*.

Based on these results, two potential COX-2 selective compounds were designed using moieties found in curcumin as well as moieties common to celecoxib and other known COX-2 selective compounds. Initial docking results showed that both compounds interact with the secondary pocket present in COX-2 as desired, and a number of ligand-protein interactions are made that mimic those seen between celecoxib and COX-2, while also identifying the potential for improvement, both in docking and binding scores as well as with interactions between the protein and the ligands. Therefore, a range of modifications were made to these two parent compounds in order to explore the impact of the various substitutions on the docking and binding scores and on the protein-ligand interactions. In all cases, the modifications resulted in an increase in the COX-2 binding scores when the scores were compared to that calculated for the parent compound, and in a few cases, reductions in the COX-1 binding scores were observed.

Thirty of the 166 compounds designed were selected for synthesis and biological screening as these compounds exemplified the range of changes observed in the full complement of compounds.

Retrosynthetic analysis identified two potential routes involving simple chemistry, which would allow for the formation of the correct Z-isomer about the double bond. The initial synthetic route, which involved the formation of the double bond through a base-catalysed condensation of an acetophenone with a benzaldehyde prior to the formation of the ether bond proved unsuccessful as the base-catalyzed intramolecular reaction of the chalcones yielded a flavanone rather than the desired benzyl ether, and as such this pathway was abandoned in favour of the alternate pathway. Early investigations into this second synthetic pathway, which involved the formation of the ether bond prior to the base-catalyzed condensation, yielded the correct benzylated compound in high yields, however the addition of the sulfonyl chloride moiety proved unsuccessful, with low yields and addition to other positions within the molecule observed. At the outset, use of a benzenesulfonyl chloride compound in order to circumvent the need for chlorosulfonic acid resulted in the formation of a tosyl derivative, rather than the desired ether. Conversion of the sulfonyl chloride into a sulfonate or sulfonamide prior to the ether formation yielded "protected" species, however the protected sulfonamide proved too insoluble to be of use.

High yields were obtained when an ethyl-protected benzenesulfonate was combined with three 4-substituted 2'-hydroxyacetophenone, however, the corresponding 5-substituted 2'-hydroxyacetophenone proved too unstable and rapid decomposition was observed even with the use of milder reaction conditions. Removal of the ethyl protecting group occurs during the ether formation reaction; nevertheless this does not affect the subsequent condensation. The current understanding of this reaction is that the ethyl-protected sulfonate species is the reactive species, with the ethyl group removed after ether formation. This hypothesis is supported by the lack of intermolecular addition between two benzenesulfonate molecules, as would be expected if the ethyl group is removed prior to ether formation. With suitable reactions and conditions identified, the synthesis of the thirty compounds previously identified was performed, using three 2'-hydroxyacetophenones and twelve benzaldehydes, in moderate to good yields. These products were isolated cleanly with only simple recrystallization techniques required to remove unwanted starting materials and side products.

Complete spectroscopic analysis of all synthesized compounds was carried out in order to definitively determine the identity of all the compounds. While appearing daunting, the NMR spectroscopic analysis of the final benzenesulfonate compounds was simplified through the identification and analysis of simpler compounds which are components of the final compound. During the course of analysis, broadening of the line widths of methylene peak in the ^1H NMR spectrum was observed on formation of the ether bond, indicating a change in the solution mobility of the compound. DOSY experiments were carried out on two compounds, and the diffusion coefficients and hydrodynamic radii were determined for both compounds. The size of the hydration sphere was shown to be solvent-dependent, and a need for the determination of the viscosity of the solution used for the DOSY experiments was identified, as effective radius calculations make use of literature viscosity values, rather than taking into account the viscosity of the solution under investigation.

In order to identify the conformations present in solution, NMR Analysis of Molecular Flexibility In Solution (NAMFIS) made use of NOE correlations to identify six conformers as existing in solution, from a pool of 3630 potential conformations. Of these six conformers, four poses comprise >95% of the solution population, with one pose comprising almost 50%. While none of the poses are exact matches when compared to the pose generated for 6 in either COX-1 or COX-2, all but one pose show RMSD values of less than 2 Å, which indicates that any of these five conformers could bind into the proteins.

Initial inhibition screening results of the unsubstituted parent benzenesulfonate compound appeared to show three-fold selectivity of COX-2 over COX-1 at 100 nM. Testing of the substituted compounds revealed that these compounds are not COX-2 selective as desired, rather a number show promise as COX-1 selective compounds, with inhibition scores of over 40%, and several other compounds show potential as non-selective COX inhibitors. There appears to be no correlation between the inhibition results and either the Glide XP docking scores or the Prime binding scores, and as such, additional computational analysis as well as experimental testing is required to identify a correlation between the theoretical results and the experimental data. It is possible that these compounds could behave differently *in vivo* than is observed *in vitro*, as is the case for lumiracoxib, and it is also possible that the mode of inhibition is allosteric in nature, rather than the competitive inhibition model used here. Should these compounds not prove suitable as analgesic compounds, a number of alternative uses exist for

COX-isoform selective and non-selective compounds, ranging from cancer treatments to the reduction of neuroinflammation seen in diseases such as Alzheimer's disease and Parkinson's disease.

8.Future Work

“End? No, the journey doesn't end here. Death is just another path, one that we all must take. The grey rain-curtain of this world rolls back, and all turns to silver glass, and then you see it.”

Gandalf, *Lord of the Rings*.

Research of any kind, especially in science, often yields more questions than answers, and the research presented here is no exception. As such, there is significant scope for future work based on the results obtained during this project. Questions which have arisen include the suitability of the current computational model in describing the binding observed *in vitro*, as the results obtained during the *in silico* calculations do not appear to correlate with those obtained during the inhibition study. Additional work, with regards to both computational and experimental aspects, is therefore required to gain more understanding into the binding of these compounds to the proteins. Once a suitable model has been identified, work on an additional series of compounds, which make use of an imine rather than a carbonyl moiety (Figure 8.1) can be carried out, as the presence of a primary imine would allow for the formation of an additional hydrogen bond to the protein. Imine-containing compounds have also shown promise as antiplasmodial drugs during the liver stage of malaria,⁸⁰¹ and as vasorelaxants and platelet-aggregation inhibitors,⁸⁰²⁻⁸⁰⁴ and a number of potent hallucinogenic compounds⁸⁰⁵⁻⁸⁰⁷ contain imines.

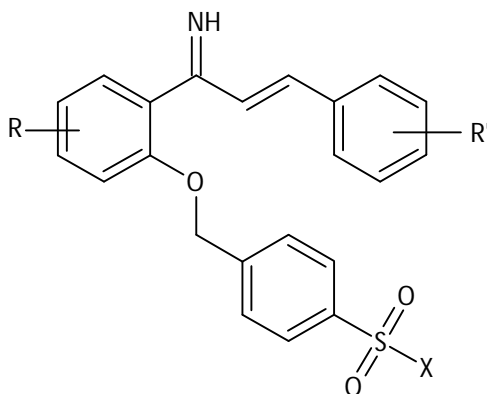
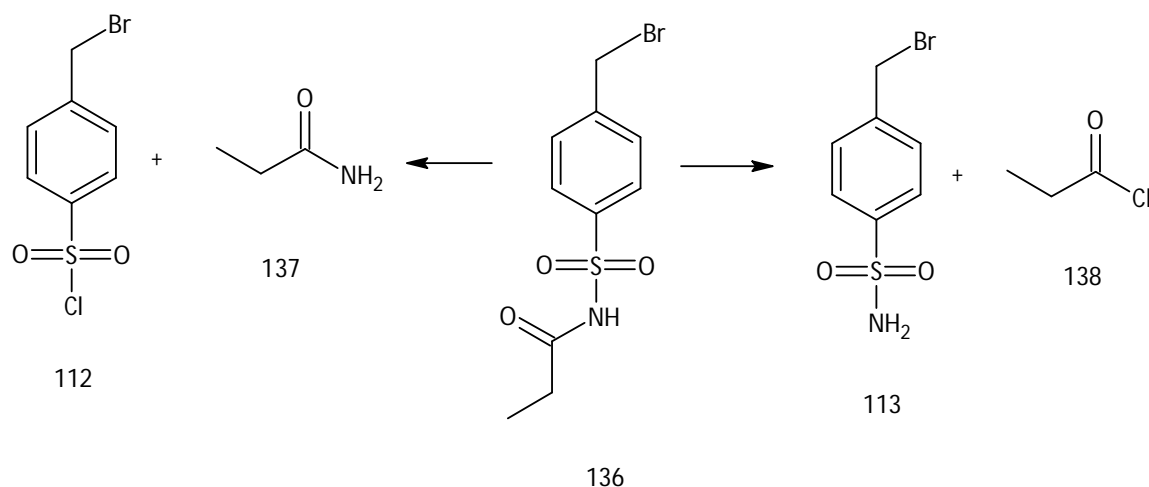


Figure 8.1. Imine-based analogs.

With reference to the challenges met during the synthesis of the benzenesulfonamide compounds, protection of the amine could be accomplished using a propanamide group (Figure 8.2), as is seen in the commercially-available pro-drug parecoxib. This propanamide group of parecoxib is cleaved *in vivo* by hepatic enzyme hydrolysis,⁶⁴⁸ yielding the active sulfonamide drug valdecoxib. Synthesis of the

propanamide-protected compound **136** could be achieved through the reaction of propanamide **137** and tosyl chloride **113** under similar conditions as those used for the formation of the phthalamide-protected **125**, or through the protection of the sulfonamide **113** with propanoyl chloride **138** (Scheme 8.1).

Scheme 8.1. Potential synthetic routes to the propanamide-protected benzenesulfonamide.



One of the advantages to using programs such as NAMFIS is that the conformation and population results can be verified through comparison of the experimental NMR spectra with spectra based on the individual conformations. Programs such as Gaussian are able to compute theoretical ^1H and ^{13}C NMR peaks based on the conformations identified by NAMFIS, and, if the NAMFIS calculations are correct, the experimental and theoretical spectra should correlate well. Calculation of the predicted NMR spectra for **6** using the conformations identified through NAMFIS analysis, and comparison of these predicted spectra with the experimentally-derived spectra would allow for the confirmation of the NAMFIS results.

As previously stated, COX inhibitors often show time-dependent inhibition, and as such, an investigation into the time-dependent nature of the compounds is needed. This, along with additional concentration-dependent testing, could identify potential COX-isoform selective compounds which do not appear as valid leads under the current testing conditions. As *in vitro* testing results do not always correlate with the results seen in *in vivo* testing, cell-based assaying of the compounds would allow for a more complete picture of the selectivity and potency of these compounds, while ADME and toxicity

calculations would aid in the identification of leads, and screening of these compounds against other targets would identify other potential uses for these compounds.

9. Methods and Materials

9.1. General Information.

^1H , ^{13}C , ^{15}N and ^{19}F NMR spectra were recorded on either a Bruker Avance III 500 or Bruker Avance III 400 spectrometer at frequencies of 500 MHz/400 MHz (^1H), 125 MHz/100 MHz (^{13}C), 51 MHz (^{15}N) and 376 MHz (^{19}F) using one of a 5 mm BBOZ probe 19F-31P-109Ag- $\{^1\text{H}\}$, 5 mm BBIZ probe 1H- $\{^31\text{P}-109\text{Ag}\}$, or a 5 mm TBIZ probe 1H- $\{^31\text{P}\}$ - $\{^31\text{P}-103\text{Rh}\}$. All proton and carbon chemical shifts are quoted in ppm and are relative to the relevant solvent signal (e.g. DMSO- d_6 : ^1H , 2.50 ppm, ^{13}C , 39.50 ppm; D_2O : ^1H , 4.72 ppm; CDCl_3 : ^1H , 7.26 ppm, ^{13}C , 77.00 ppm). Proton-proton coupling constants are reported in Hertz. All experiments were conducted at 30 °C unless specified otherwise. High-resolution Mass Spectrometry was carried out on a Waters Acquity UPLC + LCT Premier TOF-MS, with either electrospray (ES) or atmospheric pressure chemical ionization (AP) acquisition modes in either + or - mode. Single crystal X-ray diffraction data was collected on either a Bruker Apex II Duo diffractometer fitted with μS microsources (Cu and Mo) and Quasar mirror optics, or on a Bruker Smart Apex II diffractometer with a Mo fine focus sealed tube source. Crystals were mounted in Paratone[®] oil on either a 100 micron or 200 micron MiTeGEN cryoloop. Multiscan absorption corrections were used, and all unit cell data and full sets of intensities were collected at 100(1) K using a Mo radiation source. Melting points were recorded on a Stuart SMP3 melting point apparatus, and are uncorrected.

^1H diffusion (DOSY) experiments were performed using a high-resolution 5 mm BBOZ probe 19F-31P-109Ag- $\{^1\text{H}\}$, with a gradient calibration of 5.35 G/mm. Diffusion time and gradient pulse length calibrations were adjusted for 90-95 % signal attenuation between gradient strengths 5 % and 95 % (2.7 G/cm and 50.8 G/cm) using the ledbpgp2s1d pulse program, with diffusion times in the range of 150 - 250 ms and gradient pulse lengths between 1200 and 1500 μs . Diffusion measurements were conducted at a regulated sample temperature of 30 °C using the ledbpgp2s (longitudinal-eddy-current-delay-bipolar-gradient-pulse-2-spoil-gradients) pulse program⁸⁰⁸ with 16 linearly spaced steps between the starting and final gradient levels. NOE spectra were acquired using a

standard gradient NOE pulse program (noesygpqh). Data were processed with the diffusion software of Topspin 2.1pl6.

Molecular docking and binding studies were carried out using Schrödinger Small-Molecule Drug Discovery Suite, Version 2014-2, on a desktop computer with an Intel™ Core™2 Quad 2.5 GHz processor with 8GB RAM on a Windows®7 (64-bit) platform. Protein crystal structures (3LN1 and 3KK6) were downloaded from the RSC Protein Database website (<http://www.rcsb.org/pdb/home/home.do>) and prepared using the "Protein Preparation Wizard" within the Schrödinger Maestro suite, prior to the creation of the receptor grid from the coordinates of the bound ligand. All compounds were prepared using the "LigPrep" application prior to docking with Glide XP using default settings. The poses were then rescored using Prime to generate MM/GBSA scores, with protein flexibility set at 4.0 Å. The conformational search for NAMFIS analysis was carried out using Macromodel, with either MMFF or OPLS-2005 used as the forcefield, and in either chloroform or water. The GBSA constant dielectric model was applied within an energy window of 21.0 kJ/mol (5.02 kcal/mol). Minimization of the four sets of conformations into final conformer pool of 3630 structures was performed with full-matrix-Newton-Raphson (FMNR) minimization (OPLS-2005, H2O) within the same energy window (21 kJ/mol) on a comparison of "heavy atoms plus OH and SH". NAMFIS comparisons were carried out using NAMFIS 2.5.0 on a 64-bit CentOS (5.8) Linux platform via a series of Python 2 scripts.

All chemicals were purchased from Sigma-Aldrich or Merck and used without further purification. The COX Fluorescent Inhibitor Screening Assay (Cayman Chemical, item 700100) was purchased from BIOCOM Biotech and used as directed, with compounds dissolved in distilled water. Fluorescence was recorded using a Perkin Elmer EnSpire 2300 Multimode Reader with irradiation at 535 nm and emission measured at 590 nm.

9.2. Synthesis and Analysis.

1-[2-(benzyloxy)phenyl]ethanone (62)⁶⁹⁸

To a suspension of K₂CO₃ (0.691 g, 5 mmol) in MeCN (30 ml) was added 2'-hydroxyacetophenone **60** (0.681 g, 5 mmol) and benzyl bromide **61** (0.885 g, 5 mmol), and the solution was heated to reflux for 24 h.⁶⁹⁵⁻⁶⁹⁷ The solution was cooled, filtered and the solvent removed *in vacuo* to yield a clear, pale yellow solid (1.011 g, 89%). ¹H NMR (DMSO-*d*₆): δ 2.51 (s; 3 H; CH₃), 5.24 (s; 2 H; CH₂), 7.03 (td; *J* = 7.48, 0.92; 1 H; CH-CH-C_q-C_q=O), 7.26 (dd; *J* = 8.40, 0.64; 1 H; CH-C_q-O), 7.33-7.37 (m; 1 H; CH-CH-CH-C_q-CH₂), 7.40-7.43 (m; 2 H; CH-CH-C_q-CH₂), 7.50-7.54 (m; 3 H; CH-C_q-CH₂ and CH-CH-C_q-O), 7.60 (dd; *J* = 7.68, 1.84; 1 H; CH-C_q-C_q=O). ¹³C NMR (DMSO-*d*₆): δ 31.64 (s; 3 H; CH₃), 69.99 (s; 2 H; CH₂), 120.55 (d; 1 C; CH-CH-C_q-C_q=O), 113.59 (d; 1 C; CH-C_q-O), 127.95 (d; 1 C; CH-CH-CH-C_q-CH₂), 128.45 (d; 2 C; CH-CH-C_q-CH₂), 127.78 (d; 2 C; CH-C_q-CH₂), 128.25 (s; 1 C; C_q-C_q=O), 129.47 (d; 1 C; CH-C_q-C_q=O), 133.59 (d; 1 C; CH-CH-C_q-O), 136.45 (s; 1 C; C_q-CH₂), 157.39 (s; 1 C; C_q-O), 198.80 (s; 1 C; C_q=O). HRMS: Calculated mass for C₁₅H₁₄O₂Na 249.0891; mass found 249.0895. M.P 40-41 °C (Lit⁸⁰⁹ 41-42 °C).

4-methylbenzenesulfonamide (66)⁷⁰²

To a solution of THF (10 ml) and aqueous ammonia (5 ml) on ice was added sulfonyl chloride **65** (0.192 g 1 mmol), and the reaction was stirred on ice for 2 h. EtOAc (10 ml) and H₂O (5 ml) were added, and the resultant layers were separated.⁷⁰³ The organic layer was dried with Na₂SO₄ and the solvent removed *in vacuo* without heat to yield a white solid (0.144 g, 84%). ¹H NMR (DMSO-*d*₆): δ 2.38 (s, 3 H, CH₃); 7.25 (br.s, 2 H, NH₂); 7.36 (d, *J* = 8.2, 2 H, 2x CH-C_q-S); 7.71 (d, *J* = 8.2, 2x CH-C_q-CH₂). ¹³C NMR (DMSO-*d*₆): δ 21.36 (q, 1 C, CH₃); 126.08 (d, 2 C, 2x CH-C_q-CH₂); 129.74 (d, 2 C, 2x CH-C_q-S); 141.92 (s, 1 C, C_q-CH₂); 142.29 (d, 1 C, C_q-S). ¹⁵N NMR (DMSO-*d*₆): δ 95.4. HRMS: Calculated mass for C₇H₉O₂NS 171.0354 mass found 170.0273 for C₇H₈O₂NS (M-1). M.P 134-136 °C (Lit⁸¹⁰ 135-137 °C).

General Procedure for Chalcone Synthesis: Method A.⁷⁰⁰

The appropriate 2'-hydroxyacetophenone (1 mmol) and the appropriate benzaldehyde (1 mmol) were added to a stirred solution of KOH (0.112 g, 2 mmol) in abs EtOH (10 ml), and stirred at room

temperature for 18 h. Acidification of the yellow solution with HCl (conc) yielded a yellow precipitate which was removed by filtration and allowed to air dry.

Method B.⁷¹⁵

To a stirred suspension of NaH (0.048 g, 2 mmol) in dry THF (16 ml) under N₂ at 0°C was added a solution of the appropriate 2'-hydroxyacetophenone (1 mmol) in dry THF (2ml), followed by a solution of the appropriate benzaldehyde (1 mmol) in dry THF (2 ml). The resulting pale yellow suspension was stirred at 0°C for 4 h. H₂O (10ml) was added to quench the reaction, and the resultant yellow solution was extracted with 3x 20 ml portions of CHCl₃. The organic layers were combined and dried with Na₂SO₄, and the solvent was removed *in vacuo*, yielding a yellow solid.

(2E)-1-(2-hydroxyphenyl)-3-phenylprop-2-en-1-one (68)⁷⁰⁴

Method A, 2'-hydroxyacetophenone **60** (0.136 g, 1 mmol) and benzaldehyde **67** (0.106 g, 1 mmol) afforded **68** as a yellow solid (0.193 g, 86%). ¹H NMR (DMSO-*d*₆): δ 7.01 (d, *J* = 8.3, 1 H, CH-C_q-O); 7.02 (t, *J* = 7.1, CH-CH-C_q-C_q); 7.48-7.49 (m, 3 H, 2x CH-CH-C_q-CH and CH-CH-CH-C_q-CH=CH); 7.57 (td, *J* = 7.7, 1.4, CH-CH-C_q-O); 7.84 (d, *J* = 15.5, 1 H, CH-CH-C_q=O); 7.83-7.92 (m, 2 H, 2x CH-C_q-CH=CH); 8.03 (d, *J* = 15.5, CH-C_q=O); 8.26 (d, *J* = 8.3, CH-C_q-C_q); 12.45 (br.s, 1 H, OH). ¹³C NMR (DMSO-*d*₆): δ 117.66 (d, 1 C, CH-C_q-O); 119.12 (d, 1 C, CH-CH-C_q-C_q); 120.76 s, 1 C, C_q-C_q=O); 121.81 (d, 1 C, CH-C_q=O); 128.90 (d, 2 C, 2x CH-C_q-CH=CH or 2x CH-CH-C_q-CH=CH); 129.08 (d, 2 C, 2x CH-C_q-CH=CH or 2x CH-CH-C_q-CH=CH); 130.81 (d, 1 C, CH-C_q-C_q or CH-CH-CH-CH-CH); 130.89 (d, 1 C, CH-C_q-C_q or CH-CH-CH-CH-CH); 134.39 (s, 1 C, C_q-CH=CH); 136.24 (d, 1 C, CH-CH-C_q-O); 144.69 (CH=CH-C_q=O); 161.73 (s, 1 C, C_q-O); 193.56 (s, 1 C, C_q=O). HRMS: Calculated mass for C₁₅H₁₂O₂ 224.0837; mass found 225.0914 for C₁₅H₁₃O₂ (M+1). M.P 89-90 °C (Lit⁸¹¹ 90-91 °C).

(2E)-3-(4-bromophenyl)-1-(2-hydroxyphenyl)prop-2-en-1-one (69)⁶⁹⁹

Method A; 2'-hydroxyacetophenone **60** (0.138 g, 1 mmol) and benzaldehyde **63** (0.185 g, 1 mmol) afforded **69** as a yellow solid (0.282 g, 93%). ¹H NMR (DMSO-*d*₆): δ 7.00 (d, *J* = 8.4, 1 H, CH-C_q-O); 7.01 (t, *J* = 7.1, 1 H, CH-CH-C_q-C_q); 7.57 (td, *J* = 7.8, 1.5, 1 H, CH-CH-C_q-O); 7.68 (d, *J* = 8.4, 2 H, 2x CH-C_q-Br); 7.80 (d, *J* = 15.5, 1 H, CH=CH-C_q=O); 7.88 (d, *J* = 8.5, 2 H, 2x CH-CH-C_q-Br); 8.24 (d, *J* = 8.2, 1 H, CH-C_q-C_q); 12.39 (br.s, 1 H, OH). ¹³C NMR (DMSO-*d*₆): δ 117.67 (d, 1 C, CH-C_q-O); 119.14 (d, 1 C, CH-CH-C_q-C_q); 120.75 (s,

1 C, C_q-C_q=O); 122.67 (d, 1 C, CH-C_q=O); 124.30 (s, 1 C, C_q-Br); 130.86 (d, 1 C, CH-C_q-C_q); 130.95 (d, 2 C, 2x CH-CH-C_q-Br); 131.89 (d, 2 C, 2x CH-C_q-Br); 133.71 (C_q-CH=CH-C_q=O); 136.34 (d, 1 C, CH-CH-C_q-O); 143.34 (d, 1 C, CH=CH-C_q=O); 161.72 (s, 1 C, C_q-O); 193.45 (s, 1 C, C_q=O). HRMS: Calculated mass for C₁₅H₁₁O₂Br 301.9942; mass found 300.9866 for C₁₅H₁₀O₂Br (M-1). M.P 137-139 °C (Lit⁶⁹⁹ 138-139 °C).

(2E)-3-(4-chlorophenyl)-1-(2-hydroxyphenyl)prop-2-en-1-one (71)⁶⁹⁹

Method A; 2'-hydroxyacetophenone **60** (0.133 g, 1 mmol) and benzaldehyde **70** (0.146 g, 1 mmol) afforded **71** as a yellow solid (0.238 g, 92%). ¹H NMR (DMSO-*d*₆): δ 6.99 – 7.02 (m, 2 H, CH-C_q-OH and CH-CH-C_q-C_q=O); 7.53 (d, *J* = 8.5, 2 H, 2 x CH-C_q-Cl); 7.55 – 7.58 (m, *J* = 7.7, 1 H, CH-CH-C_q-OH); 7.81 (d, *J* = 15.6, 1 H, CH=CH-C_q); 7.94 (d, *J* = 8.5, 2 H, 2 x CH-C_q-CH=CH); 8.04 (d, *J* = 15.6, 1 H, O=C_q-CH=CH); 8.24 (dd, *J* = 8.3, 1.6, 1 H, CH-C_q-C_q=O); 12.43 (br.s, 1 H, OH). ¹³C NMR (DMSO-*d*₆): δ 117.67 (d, 1 C, CH-C_q-OH); 119.11 (d, 1 C, CH-CH-C_q-C_q=O); 120.70 (s, 1 C, C_q-C=O); 122.54 (d, 1 C, CH=CH-C_q=O); 128.93 (d, 2 C, 2 x CH-C_q-Cl); 130.74 (d, 2 C, 2 x CH-C_q-CH=CH); 130.85 (d, 1 C, CH-C_q-C_q=O); 133.37 (s, 1 C, C_q-CH=CH-C_q=O); 135.40 (s, 1 C, C_q-Cl); 136.32 (d, 1 C, CH-CH-C_q-OH); 143.15 (d, 1 C, CH=CH-C_q=O); 161.78 (s, 1 C, C_q-OH); 193.43 (s, 1 C, C_q=O). HRMS: Calculated mass for C₁₅H₁₁O₂Cl 258.0447; mass found 257.0361 for C₁₅H₁₀O₂Cl (M-1). M.P 147-148 °C (Lit⁶⁹⁹ 148-150 °C).

(2E)-3-(4-fluorophenyl)-1-(2-hydroxyphenyl)prop-2-en-1-one (73)⁷⁰⁵

Method A; 2'-hydroxyacetophenone **60** (0.132 g, 1 mmol) and benzaldehyde **72** (0.124 g, 1 mmol) afforded **73** as a yellow solid (0.179 g, 73%). ¹H NMR (DMSO-*d*₆): δ 6.99 (d, *J* = 7.8, 1 H, CH-C_q-O); 7.08-7.13 (m, 1 H, CH-CH-C_q-C_q=O); 7.29 (t, *J* = 8.9, 1 H, 1 of 2 CH-C_q-F); 7.31 (t, *J* = 8.8, 1 H, 1 of 2 CH-C_q-F); 7.53-7.58 (m, 1 H, CH-C_q-C_q=O); 7.59-7.63 (m, 2 H, 1 of 2 CH-CH-C_q-F and CH-CH-C_q-O); 7.83 (d, *J* = 14.9, 1 H, CH=CH-C_q=O); 7.96-8.04 (m, 2 H, CH-C_q=O and 1 of 2 CH-CH-C_q-F); 12.49 (br.s, 1 H, OH). ¹³C NMR (DMSO-*d*₆): δ 115.30 (dd, ²*J*_{19F-13C} = 21.6, 1 C, 1 of 2 CH-C_q-F); 115.93 (dd, ²*J*_{19F-13C} = 20.8, 1 C, 1 of 2 CH-C_q-F); 117.95 (d, 1 C, CH-CH-C_q-C_q=O); 118.83 (d, 1 C, CH-C_q-O); 120.57 (s, 1 C, C_q-C_q=O); 120.88 (s, 1 C, C_q-CH=CH-C_q=O); 121.46 (d, 1 C, CH-C_q=O); 128.84 (dd, ³*J*_{19F-13C} = 8.4, 1 C, 1 of 2 CH-CH-C_q-F); 131.44 (dd, ³*J*_{19F-13C} = 6.9, 1 C, 1 of 2 CH-CH-C_q-F); 136.16 (d, 1 C, CH-CH-C_q-O); 143.21 (d, 1 C, CH=CH-C_q=O);

160.94 (s, 1 C, C_q-O); 163.38 (d, ¹J_{19F-13C} = 248.7, 1 C, C_q-F); 193.40 (s, 1 C, C_q=O). HRMS: Calculated mass for C₁₅H₁₁O₂F 242.0743; mass found 241.0667 for C₁₅H₁₀O₂F (M-1). M.P 114-115 °C (Lit⁷⁰⁵ 115-117 °C).

(2E)-3-(2-chlorophenyl)-1-(2-hydroxyphenyl)prop-2-en-1-one (75)⁷⁰⁶

Method A; 2'-hydroxyacetophenone **60** (0.135 g, 1 mmol) and benzaldehyde **74** (0.147 g, 1 mmol) afforded **75** as a yellow solid (0.201 g, 78%). ¹H NMR (DMSO-*d*₆): δ 7.01 (t, *J* = 7.2, 1 H, CH-CH-C_q-C_q); 7.02 (d, *J* = 8.1, 1 H, CH-C_q-O); 7.44-7.52 (m, 2 H, CH-C_q-Cl and CH-CH-C_q-C_q-Cl); 7.57 (t, *J* = 7.6, 1 H, CH-CH-C_q-O); 7.58 (d, *J* = 7.6, 1 H, CH-CH-C_q-Cl); 8.05 (d, *J* = 15.5, 1 H, CH=CH-C_q-O); 8.12 (d, *J* = 15.6, 1 H, CH-C_q=O); 8.21 (m, 2 H, CH-C_q-C_q-Cl and CH-C_q-C_q=O); 12.20 (br.s, 1 H, OH). ¹³C NMR (DMSO-*d*₆): δ 117.71 (d, 1 C, CH-C_q-O); 119.10 (d, 1 C, CH-CH-C_q-C_q); 121.04 (s, 1 C, C_q-C_q=O); 124.99 (d, 1 C, CH-C_q=O); 127.67 (d, 1 C, CH-C_q-Cl or CH-CH-C_q-C_q-Cl); 128.88 (d, 1 C, CH-C_q-C_q-Cl); 130.02 (d, 1 C, CH-CH-C_q-Cl); 130.88 (d, 1 C, CH-C_q-C_q=O); 132.04 (s, 1 C, C_q-C_q-Cl); 132.16 (d, 1 C, CH-C_q-Cl or CH-CH-C_q-C_q-Cl); 136.29 (d, 1 C, CH-CH-C_q-O); 161.50 (s, 1 C, C_q-O), 193.02 (s, 1 C, C_q=O). HRMS: Calculated mass for C₁₅H₁₁O₂Cl 258.0447; mass found 257.0367 for C₁₅H₁₀O₂Cl (M-1). M.P 101-103 °C (Lit⁸¹² 102 °C).

(2E)-1-(4-fluoro-2-hydroxyphenyl)-3-phenylprop-2-en-1-one (77)⁷⁰⁷

Method A; 2'-hydroxyacetophenone **76** (0.155 g, 1 mmol) and benzaldehyde **67** (0.105 g, 1 mmol) afforded **77** as a yellow solid (0.174 g, 72%). ¹H NMR (DMSO-*d*₆): δ 6.86 (d, *J* = 9.5, 1 H, CH-C_q-O) 6.88 (td, *J* = 7.4, 4.8, 1 H, CH-CH-C_q-F); 7.46-7.50 (m, 3 H, 2x CH-CH-C_q-CH=CH and CH-CH-CH-CH-CH); 7.85 (d, *J* = 15.5, 1 H, CH=CH-C_q=O); 7.90-7.93 (m, 2 H, 2x CH-C_q-CH=CH); 8.03 (d, *J* = 15.5, 1 H, CH-C_q=O); 8.38 (dd, *J* = 9.6, 7.0, 1 H, CH-C_q-C_q); 12.98 (s, 1 H, OH). ¹³C NMR (DMSO-*d*₆): δ 107.04 (dd, ²J_{19F-13C} = 21.7, 1 C, CH-C_q-O); 109.61 (dd, ²J_{19F-13C} = 26.5, 1 C, CH-CH-C_q-F); 117.97 (s, 1 C, C_q-C_q=O); 121.76 (s, 1 C, C_q-CH=CH-C_q=O); 126.60 (d, 2 C, 2x CH-C_q-CH=CH or CH-CH-C_q-CH=CH); 128.51 (d, 1 C, CH-C_q=O); 128.91 (d, 2 C, 2x CH-C_q-CH=CH or CH-CH-C_q-CH=CH); 130.99 (d, 1 C, CH-CH-CH-CH-CH); 133.74 (dd, ³J_{19F-13C} = 11.6, 1 C, CH-C_q-C_q=O); 164.29 (d, ³J_{19F-13C} = 13.8, 1 C, C_q-O); 167.89 (d, ¹J_{19F-13C} = 253.6, 1 C, C_q-F); 192.50 (s, 1 C, C_q=O). HRMS: Calculated mass for C₁₅H₁₁O₂F 242.0743; mass found 241.0654 for C₁₅H₁₀O₂F (M-1). M.P 109-111 °C (Lit⁷⁰⁷ 110-111 °C).

(2E)-3-(4-bromophenyl)-1-(4-fluoro-2-hydroxyphenyl)prop-2-en-1-one (78)

Method A; 2'-hydroxyacetophenone **76** (0.154 g, 1 mmol) and benzaldehyde **63** (0.187 g, 1 mmol) afforded **78** as a yellow solid (0.215 g, 69%). ¹H NMR (DMSO-*d*₆): δ 6.88 (m, 2 H, 2x CH-C_q-F); 7.68 (d, *J* = 8.4, 2 H, 2x CH-C_q-Br); 7.80 (d, *J* = 15.6, 1 H, CH=CH-C_q=O); 7.87 (d, *J* = 8.5, 2 H, 2x CH-CH-C_q-Br); 8.03 (d, *J* = 15.5, CH-C_q=O); 8.36 (d, *J* = 8.1, 1 H, CH-C_q-C_q); 12.85 (br.s, 1 H, OH). ¹³C NMR (DMSO-*d*₆): δ 104.25 (dd, ²*J*_{19F-13C} = 23.4, 1 C, CH-C_q-O); 106.87 (dd, ²*J*_{19F-13C} = 24.6, 1 C, CH-CH-C_q-F); 118.09 (s, 1 C, C_q-C_q=O); 122.67 (d, 1 C, CH-C_q=O); 124.35 (s, 1 C, C_q-CH=CH-C_q=O); 130.95 (d, 2 C, 2x CH-CH-C_q-Br); 131.88 (d, 2 C, 2x CH-C_q-Br); 133.67 (s, 1 C, C_q-CH=CH-C_q=O); 133.77 (dd, ³*J*_{19F-13C} = 12.3, 1 C, CH-C_q-C_q); 143.31 (d, 1 C, CH=CH-C_q=O); 164.38 (s, 1 C, C_q-O); 167.78 (d, ¹*J*_{19F-13C} = 253.6, 1 C, C_q-F); 192.22 (s, 1 C, C_q=O). HRMS: Calculated mass for C₁₅H₁₀O₂BrF 319.9848; mass found 318.9770 for C₁₅H₉O₂BrF (M-1). M.P 108-110 °C.

(2E)-3-(4-chlorophenyl)-1-(4-fluoro-2-hydroxyphenyl)prop-2-en-1-one (79)⁷⁰⁸

Method A; 2'-hydroxyacetophenone **76** (0.155 g, 1 mmol) and benzaldehyde **70** (0.144 g, 1 mmol) afforded **79** as a yellow solid (0.177 g, 66%). ¹H NMR (DMSO-*d*₆): δ 6.85 (m, 2 H, 2x CH-C_q-F); 7.59 (d, *J* = 8.5, 2 H, 2x CH-C_q-Cl); 7.83 (d, *J* = 15.6, 1 H, CH=CH-C_q=O); 7.96 (d, *J* = 8.5, 2 H, 2x CH-CH-C_q-Cl); 8.04 (d, *J* = 15.5, 1 H, CH-C_q=O); 8.39 (d, *J* = 7.8, 1 H, CH-C_q-C_q); 12.95 (br.s, 1 H, OH). ¹³C NMR (DMSO-*d*₆): δ 104.47 (dd, ²*J*_{19F-13C} = 26.1, 1 C, CH-C_q-O); 107.07 (dd, ²*J*_{19F-13C} = 22.7, 1 C, CH-CH-C_q-F); 128.55 (s, 1 C, C_q-C_q=O); 128.99 (d, 2 C, 2x CH-C_q-Cl); 130.82 (d, 2 C, 2x CH-CH-C_q-Cl); 133.33 (s, 1 C, C_q-CH=CH-C_q=O); 133.79 (dd, ³*J*_{19F-13C} = 11.6, 1 C, CH-C_q-C_q); 135.50 (s, 1 C, C_q-Cl); 143.42 (d, 1 C, CH=CH-C_q=O); 164.40 (s, 1 C, C_q-O); 192.35 (s, 1 C, C_q=O); C_q-F not observed. HRMS: Calculated mass for C₁₅H₁₀O₂ClF 276.0353; mass found 275.0265 for C₁₅H₉O₂ClF (M-1). M.P 182-184 °C (Lit⁷⁰⁸ 184-186 °C).

(2E)-1-(4-fluoro-2-hydroxyphenyl)-3-(4-fluorophenyl)prop-2-en-1-one (80)

Method A; 2'-hydroxyacetophenone **76** (0.156 g, 1 mmol) and benzaldehyde **72** (0.122 g, 1mmol) afforded **80** as a yellow solid (0.227 g, 87%). ¹H NMR (DMSO-*d*₆): δ 6.95 (td, *J* = 4.3, 2.5, 1 H, C_q-C_q-CH-CH-C_q-F); 7.02 (dd, *J* = 10.3, 2.4, 1 H, CH-C_q-O); 7.25-7.34 (m, 2 H, 2x CH-CH-C_q-CH=CH); 7.59-7.63 (m, 1 H, 1 of 2 CH-C_q-CH=CH); 7.81 (d, *J* = 15.5, 1 H, CH=CH-C_q=O); 7.87 (dd, *J* = 6.8, 8.7, 1 H, CH-C_q-C_q=O); 7.97 (dd, *J* = 5.9, 8.9, 1 H, 1 of 2 CH-C_q-CH=CH); 8.01 (d, *J* = 15.9, 1 H, CH-C_q=O); 12.99 (br.s, 1 H, OH). ¹³C NMR (DMSO-*d*₆): δ 104.72 (dd, ²*J*_{19F-13C} = 23.6, 1 C, CH-C_q-O); 109.66 (dd, ²*J*_{19F-13C} = 25.4, 1 C, C_q-C_q-CH-CH-C_q-F); 115.36 (dd, ²*J*_{19F-13C} = 21.7, 1 C, 1 of 2 CH-CH-C_q-CH=CH); 115.93 (dd, ²*J*_{19F-13C} = 21.7, 1 of 2 CH-CH-C_q-CH=CH); 117.86 (s, 1 C, C_q-C_q=O); 122.30 (d, 1 C, CH-C_q=O); 128.94 (dd, ³*J*_{19F-13C} = 7.9, 1 C, 1 of 2 CH-C_q-CH=CH); 129.13 (dd, ³*J*_{19F-13C} = 11.6, 1 C, CH-C_q-C_q=O); 131.38 (dd, ³*J*_{19F-13C} = 8.9, 1 C, 1 of 2

CH-C_q-CH=CH); 134.73 (s, 1 C, C_q-CH=CH-C_q=O); 142.99 (d, 1 C, CH=CH-C_q=O); 162.05 (d, ¹J_{19F-13C} = 244.8, 1 C, C_q-CH-C_q-F or CH-C_q-CH-CH-C_q-F); 162.66 (s, 1 C, C_q-O); 164.02 (d, ¹J_{19F-13C} = 257.6, C_q-CH-C_q-F or CH-C_q-CH-CH-C_q-F); 190.13 (s, 1 C, C_q=O). HRMS: Calculated mass for C₁₅H₁₀O₂F₂ 260.0649; mass found 259.0570 for C₁₅H₉O₂F₂ (M-1). M.P 110-112 °C.

(2E)-1-(4-chloro-2-hydroxyphenyl)-3-(4-fluorophenyl)prop-2-en-1-one (81)⁷⁰⁹

Method A; 2'-hydroxyacetophenone **76** (0.154 g, 1 mmol) and benzaldehyde **74** (0.146 g, 1 mmol) afforded **81** as a yellow solid (0.224 g, 79%). ¹H NMR (DMSO-*d*₆): δ 7.01 (d, *J* = 8.3, 1 H, CH-CH-C_q-Cl); 7.08 (s, 1 C, CH-C_q-O); 7.40-7.50 (m, 3 H, CH-CH-CH-CH-CH and 2x CH-C_q-CH=CH); 7.80 (d, *J* = 15.8, 1 H, CH=CH-C_q=O); 7.84-7.90 (m, 2 H, 2x CH-CH-C_q-CH=CH); 7.98 (d, *J* = 15.5, 1 H, CH-C_q=O); 8.19 (d, *J* = 8.5, 1 H, CH-C_q-C_q=O); 12.43 (br.s, 1 H, OH). ¹³C NMR (DMSO-*d*₆): δ 117.90 (d, 1 C, CH-C_q-O); 119.59 (d, 1 C, CH-CH-C_q-Cl); 121.90 (d, 1 C, CH-C_q=O); 122.75 (s, 1 C, C_q-C_q=O); 128.52 (d, 2 C, 2x CH-C_q-CH=CH); 128.91 (d, 2 C, 2x CH-CH-C_q-CH=CH); 130.86 (d, 1 C, CH-CH-CH-CH-CH); 132.44 (CH-C_q-C_q=O); 134.46 (s, 1 C, C_q-CH=CH-C_q=O); 138.41 (s, 1 C, C_q-Cl); 140.33 (d, 1 C, CH=CH-C_q=O); 161.50 (s, 1 C, C_q-O); 190.59 (s, 1 C, C_q=O). HRMS: Calculated mass for C₁₅H₁₁O₂Cl 258.0447; mass found 257.0365 for C₁₅H₁₀O₂Cl (M-1). M.P 113-114 °C.

(2E)-3-(4-bromophenyl)-1-(4-chloro-2-hydroxyphenyl)prop-2-en-1-one (83)

Method A; 2'-hydroxyacetophenone **82** (0.171 g, 1 mmol) and benzaldehyde **67** (0.103 g, 1 mmol) afforded **83** as a yellow solid (0.207 g, 80%). ¹H NMR (DMSO-*d*₆): δ 7.03 (dd, *J* = 8.6, 2.0, 1 H, CH-CH-C_q-Cl); 7.10 (d, *J* = 2.0, 1 H, CH-C_q-O); 7.66 (d, *J* = 8.5, 2 H, 2x CH-C_q-Br); 7.77 (d, *J* = 15.6, 1 H, CH=CH-C_q=O); 7.83 (d, *J* = 8.5, 2 H, 2x CH-CH-C_q-Br); 7.99 (d, *J* = 15.5, 1 H, CH-C_q=O); 8.19 (d, *J* = 8.6, 1 H, CH-C_q-C_q=O); 12.52 (br.s, 1 H, OH). ¹³C NMR (DMSO-*d*₆): δ 117.36 (d, 1 C, CH-C_q-O); 119.25 (d, 1 C, CH-CH-C_q-Cl); 120.39 (s, 1 C, C_q-C_q=O); 123.10 (d, 1 C, CH-C_q=O); 124.34 (s, 1 C, C_q-Br); 130.84 (d, 2 C, 2x CH-CH-C_q-Br); 131.08 (d, 2 C, 2x CH-C_q-Br); 132.39 (d, 1 C, CH-C_q-C_q=O); 133.66 (s, 1 C, C_q-CH=CH-C_q=O); 139.98 (s, 1 C, C_q-Cl); 143.28 (d, 1 C, CH=CH-C_q=O); 162.13 (s, 1 C, C_q-O); 192.95 (s, 1 C, C_q=O). HRMS: Calculated mass for C₁₅H₁₀O₂BrCl 335.9552; mass found 334.9478 for C₁₅H₉O₂BrCl (M-1). M.P 109-111 °C.

(2E)-1-(4-chloro-2-hydroxyphenyl)-3-(4-chlorophenyl)prop-2-en-1-one (84)⁷¹⁰

Method A; 2'-hydroxyacetophenone **82** (0.170 g, 1 mmol) and benzaldehyde **63** (0.188 g, 1 mmol) afforded **84** as a yellow solid (0.226 g, 67%). ¹H NMR (DMSO-*d*₆): δ 7.06 (dd, *J* = 8.5, 2.1, 1 H, CH-CH-C_q-C_q=O); 7.10 (d, *J* = 2.0, 1 H, C_q-CH-C_q-Cl); 7.53 (d, *J* = 8.5, 2 H, 2x CH-C_q-Cl); 7.80 (d, *J* = 15.8, 1 H,

CH=CH-C_q=O); 7.93 (d, *J* = 8.5, 2 H, 2x CH-CH-C_q-Cl); 8.21 (d, *J* = 8.7, 1 H, CH-C_q-C_q=O); 12.48 (br.s, 1 H, OH). ¹³C NMR (DMSO-*d*₆): δ 117.32 (d, 1 C, CH-C_q-O); 119.37 (d, 1 C, CH-CH-C_q-C_q=O); 120.23 (s, 1 C, C_q-C_q=O); 122.88 (d, 1 C, CH-C_q=O); 128.95 (d, 2 C, 2x CH-C_q-Cl); 130.41 (d, 2 C, 2x CH-CH-C_q-Cl); 132.41 (d, 1 C, CH-C_q-C_q=O); 133.31 (s, 1 C, C_q-CH=CH-C_q=O); 135.49 (s, 1 C, CH-C_q-CH-CH-C_q-Cl); 140.05 (s, 1 C, C_q-CH-C_q-Cl); 143.36 (d, 1 C, CH=CH-C_q=O); 162.08 (s, 1 C, C_q-O); 192.46 (s, 1 C, C_q=O). HRMS: Calculated mass for C₁₅H₁₀O₂Cl₂ 292.0057; mass found 290.9986 for C₁₅H₉O₂Cl₂ (M-1). M.P 149-150 °C (Lit⁷¹⁰ 150-151 °C).

(2E)-1-(4-chloro-2-hydroxyphenyl)-3-(4-fluorophenyl)prop-2-en-1-one (85)

Method A; 2'-hydroxyacetophenone **82** (0.172 g, 1 mmol) and benzaldehyde **70** (0.144 g, 1 mmol) afforded **85** as a yellow solid (0.252 g, 84%). ¹H NMR (DMSO-*d*₆): δ 7.04 (dd, *J* = 8.6, 2.0, 1 H, CH-CH-C_q-Cl); 7.10 (d, *J* = 2.0, 1 H, CH-C_q-O); 7.30 (t, *J* = 8.8, 2 H, 2x CH-C_q-F); 7.80 (d, *J* = 15.5, 1 H, CH=CH-C_q=O); 7.96 (d, *J* = 15.6, 1 H, CH-C_q=O); 7.96 (dd, *J* = 5.7, 8.6, 2 H, 2x CH-CH-C_q-F); 8.20 (d, *J* = 8.6, 1 H, CH-C_q=C_q=O); 12.57 (br.s, 1 H, OH). ¹³C NMR (DMSO-*d*₆): δ 115.93 (dd, ²*J*_{19F-13C} = 22.0, 2 C, 2x CH-C_q-F); 117.29 (d, 1 C, CH-C_q-O); 119.32 (d, 1 C, CH-CH-C_q-Cl); 120.20 (s, 1 C, C_q-C_q=O); 121.95 (d, 1 C, CH-C_q=O); 131.01 (s, C_q-CH=CH-C_q=O); 131.48 (dd, ³*J*_{19F-13C} = 8.7, 2 C, 2x CH-CH-C_q-F); 132.34 (d, 1 C, CH-C_q-C_q=O); 139.96 (s, 1 C, C_q-Cl); 143.63 (d, 1 C, CH=CH-C_q=O); 162.06 (s, 1 C, C_q-O); 163.58 (d, ¹*J*_{19F-13C} = 249.6, 1 C, C_q-F); 192.47 (s, 1 C, C_q=O). HRMS: Calculated mass for C₁₅H₁₀O₂ClF 276.0353; mass found 275.0266 for C₁₅H₉O₂ClF (M-1). M.P 119-121 °C.

(2E)-1-(4-chloro-2-hydroxyphenyl)-3-(2-chlorophenyl)prop-2-en-1-one (86)

Method A; 2'-hydroxyacetophenone **82** (0.170 g, 1 mmol) and benzaldehyde **72** (0.125 g, 1 mmol) afforded **86** as a yellow solid (0.229 g, 82%). ¹H NMR (DMSO-*d*₆): δ 7.06 (dd, *J* = 8.5, 1.9, 1 H, C_q-CH-CH-C_q-Cl); 7.12 (d, *J* = 1.8, 1 H, CH-C_q-O); 7.43-7.53 (m, 2 H, CH-CH-CH-C_q-Cl and CH-CH-C_q-C_q-Cl); 7.58 (d, *J* = 7.6, 1 H, CH-CH-CH-C_q-Cl); 7.98 (d, *J* = 15.5, 1 H, CH-C_q=O); 8.09 (d, *J* = 15.6, 1 H, CH=CH-C_q=O); 8.15-8.19 (m, 2 H, CH-C_q-C_q=O and CH-C_q-C_q-Cl); 12.28 (br.s, 1 H, OH). ¹³C NMR (DMSO-*d*₆): δ 117.30 (d, 1 C, CH-C_q-O); 119.44 (d, 1 C, CH-CH-C_q-Cl); 120.55 (s, 1 C, C_q-C_q=O); 125.22 (d, 1 C, CH-C_q=O); 127.26 (d, 1 C, CH-CH-CH-C_q-Cl or CH-CH-CH-C_q-Cl); 128.64 (d, 1 C, CH-C_q-C_q=O or CH-C_q-C_q-Cl); 130.04 (d, 1 C, CH-CH-CH-C_q-Cl); 131.96 (s, 1 C, C_q-C_q-Cl); 132.24 (d, 1 C, CH-CH-CH-C_q-Cl or CH-CH-CH-C_q-Cl); 132.45 (d, 1 C, CH-C_q-C_q=O or CH-C_q-C_q-Cl); 134.46 (s, 1 C, C_q-C_q-Cl); 138.90 (d, 1 C,

CH=CH-C_q=O); 140.04 (s, 1 C, C_q-CH-C_q-Cl); 161.75 (s, 1 C, C_q-O); 192.01 (s, 1 C, C_q=O). HRMS: Calculated mass for C₁₅H₁₀O₂Cl₂ 292.0057; mass found 290.9979 for C₁₅H₉O₂Cl₂ (M-1). M.P 114-115 °C.

(2E)-1-(5-chloro-2-hydroxyphenyl)-3-phenylprop-2-en-1-one (88)⁶⁹⁹

Method A; 2'-hydroxyacetophenone **87** (0.171 g, 1 mmol) and benzaldehyde **67** (0.106 g, 1 mmol) afforded **88** as a yellow solid (0.175 g, 67%). ¹H NMR (DMSO-*d*₆): δ 7.04 (d, *J* = 8.8, 1 H, CH-C_q-OH); 7.47-7.49 (m, 3 H, 2x CH-C_q-CH=CH and CH-CH-CH-CH-CH); 7.58 (dd, *J* = 8.9, 2.6, 1 H, CH-CH-C_q-Cl); 7.82 (d, *J* = 15.6, 1 H, CH-CH-C_q=O); 7.90-7.93 (m, 2 H, 2x CH-CH-C_q-CH=CH); 7.99 (d, *J* = 15.5, 1 H, CH-C_q=O); 8.18 (d, *J* = 2.6, 1 H, CH-C_q-Cl); 12.23 (s, 1 H, OH). ¹³C NMR (DMSO-*d*₆): δ 119.71 (d, 1 C, CH-C_q-OH); 122.21 (s, 1 C, C_q-C_q=O); 122.31 (d, 1 C, CH-C_q=O); 128.95 (d, 2 C, 2x CH-C_q-CH=CH); 129.32 (d, 2 C, 2x CH-CH-C_q-CH=CH); 129.73 (s, 1 C, C_q-CH-C_q); 131.13 (d, 1 C, CH-CH-CH-CH-CH); 134.28 (s, 1 C, C_q-CH=CH-C_q=O); 135.47 (d, 1 C, CH-CH-C_q-Cl); 145.32 (d, 1 C, CH=CH-C_q=O); 159.38 (s, 1 C, C_q-O); 192.39 (s, 1 C, C_q=O). HRMS: Calculated mass for C₁₅H₁₁O₂Cl 258.0447; mass found 257.0368 for C₁₅H₁₀O₂Cl (M-1). M.P 98-100 °C (Lit⁶⁹⁹ 99-101 °C).

(2E)-3-(4-bromophenyl)-1-(5-chloro-2-hydroxyphenyl)prop-2-en-1-one (89)⁷¹¹

Method A; 2'-hydroxyacetophenone **87** (0.170 g, 1 mmol) and benzaldehyde **63** (0.189 g, 1 mmol) afforded **89** as a yellow solid (0.228 g, 81%). ¹H NMR (DMSO-*d*₆): δ 7.04 (d, *J* = 8.8, 1 H, CH-C_q-O); 7.58 (dd, *J* = 8.9, 2.6, 1 H, CH-CH-C_q-Cl); 7.68 (d, *J* = 8.4, 2 H, 2x CH-C_q-Br); 7.79 (d, *J* = 15.5, 1 H, CH=CH-C_q=O); 7.88 (d, *J* = 8.5, 2 H, 2x CH-CH-C_q-Br); 8.02 (d, *J* = 15.6, 1 H, CH-C_q=O); 8.23 (d, *J* = 2.6, 1 H, CH-C_q-C_q); 12.20 (s, 1 H, OH). ¹³C NMR (DMSO-*d*₆): δ 119.55 (d, 1 C, CH-C_q-O); 122.20 (s, 1 C, C_q-Cl or C_q-C_q=O); 122.31 (s, 1 C, C_q-Cl or C_q-C_q=O); 122.94 (d, 1 C, CH-C_q=O); 124.20 (s, 1 C, C_q-Br); 129.62 (d, 1 C, C_q-CH-C_q-C_q); 131.06 (d, 2 C, 2x CH-CH-C_q-Br); 131.89 (d, 2 C, 2x CH-C_q-Br); 133.16 (s, 1 C, C_q-CH-CH-C_q-Br); 135.47 (d, 1 C, CH-CH-C_q-Cl); 143.75 (d, 1 C, CH=CH-C_q=O); 159.80 (s, 1 C, C_q-O); 195.60 (s, 1 C, C_q=O). HRMS: Calculated mass for C₁₅H₁₀O₂BrCl 335.9552; mass found 334.9474 for C₁₅H₉O₂BrCl (M-1). M.P 177-178 °C (Lit⁷¹¹ 178-179 °C).

(2E)-1-(5-chloro-2-hydroxyphenyl)-3-(4-chlorophenyl)prop-2-en-1-one (90)⁶⁹⁹

Method A; 2'-hydroxyacetophenone **87** (0.172 g, 1 mmol) and benzaldehyde **70** (0.149 g, 1 mmol) afforded **90** as a yellow solid (0.119 g, 74%). ¹H NMR (DMSO-*d*₆): δ 7.04 (d, *J* = 8.9, 1 H, CH-C_q-OH); 7.54 (d, *J* = 8.3, 2 H, 2x CH-C_q-Cl); 7.58 (dd, *J* = 8.9, 2.5, 1 H, CH-CH-C_q-Cl); 7.81 (d, *J* = 15.6, 1 H, CH-CH-C_q=O);

7.96 (d, $J = 8.5$, 2 H, 2x C_q-CH-CH-C_q-Cl); 8.01 (d, $J = 15.6$, 1 H, CH-C_q=O); 8.24 (d, $J = 2.3$, 1 H, C_q-CH-C_q-Cl); 12.21 (s, 1 H, OH). ¹³C NMR (DMSO-*d*₆): δ 119.67 (d, 1 C, CH-C_q-O); 121.22 (s, 1 C, C_q-CH-C_q-Cl); 122.92 (d, 1 C, CH-C_q=O); 128.97 (d, 2 C, 2x CH-CH-C_q-Cl); 129.66 (d, 1 C, C_q-CH-C_q-Cl); 130.14 s, 1 C, C_q-C_q=O); 130.93 (d, 2 C, 2x CH-CH-C_q-Cl); 133.35 (s, 1 C, C_q-CH=CH-C_q=O); 135.48 (d, 1 C, CH-CH-C_q-OH); 135.55 (C_q-CH-CH-C_q-Cl); 143.69 (d, 1 C, CH=CH-C_q=O); 159.81 (s, 1 C, C_q-O); 192.31 (s, 1 C, C_q=O). HRMS: Calculated mass for C₁₅H₁₀O₂Cl₂ 292.0057; mass found 290.9980 for C₁₅H₉O₂Cl₂ (M-1). M.P 185-178 °C (Lit⁶⁹⁹ 186-189 °C).

(2E)-1-(5-chloro-2-hydroxyphenyl)-3-(4-fluorophenyl)prop-2-en-1-one (91)⁷¹²

Method A; 2'-hydroxyacetophenone **87** (0.171 g, 1 mmol) and benzaldehyde **72** (0.122 g, 1 mmol) afforded **91** as a yellow solid (0.219 g, 79%). NMR (DMSO-*d*₆): δ 7.05 (d, $J = 8.9$, 1 H, CH-C_q-O); 7.30 (t, $J = 8.8$, 2 H, 2x CH-C_q-F); 7.55 (dd, $J = 8.9$, 7.6, 1 H, CH-CH-C_q-Cl); 7.81 (d, $J = 15.5$, 1 H, CH=CH-C_q=O); 7.94 (d, $J = 15.6$, 1 H, CH-C_q=O); 7.99 (dd, $J = 5.7$, 8.6, 2 H, 2x CH-CH-C_q-F); 8.21 (d, $J = 2.6$, 1 H, CH-C_q-C_q=O); 12.24 (br.s, 1 H, OH). ¹³C NMR (DMSO-*d*₆): δ 115.92 (dd, ² $J_{19F-13C} = 21.7$, 2 C, 2x CH-C_q-F); 119.62 (d, 1 C, CH-C_q-O); 122.06 (d, 1 C, CH-C_q=O); 122.49 (s, 1 C, C_q-Cl or C_q-C_q=O); 122.82 (s, 1 C, C_q-Cl or C_q-C_q=O); 129.59 (d, 1 C, CH-C_q-C_q=O); 131.05 (s, 1 C, C_q-CH=CH-C_q=O); 131.62 (dd, ³ $J_{19F-13C} = 8.7$, 2 C, 2x CH-CH-C_q-F); 135.31 (d, 1 C, CH-CH-C_q-Cl); 143.89 (d, 1 C, CH=CH-C_q=O); 159.83 (s, 1 C, C_q-O); 163.62 (d, ¹ $J_{19F-13C} = 249.4$, 1 C, C_q-F); 192.25 (s, 1 C, C_q=O). Calculated mass for C₁₅H₁₀O₂ClF 276.0353; mass found 275.0264 for C₁₅H₉O₂ClF (M-1). M.P 179-180 °C (Lit⁷¹¹ 181-182 °C).

(2E)-1-(5-chloro-2-hydroxyphenyl)-3-(2-chlorophenyl)prop-2-en-1-one (92)⁶⁹⁹

Method A; 2'-hydroxyacetophenone **87** (0.170 g, 1 mmol) and benzaldehyde **74** (0.148 g, 1 mmol) afforded **92** as a yellow solid (0.208 g, 69%). ¹H NMR (DMSO-*d*₆): δ 7.05 (d, $J = 8.9$, 1 H, CH-C_q-O); 7.43-7.53 (m, 2 H, CH-C_q-C_q-Cl and CH-CH-C_q-C_q-Cl); 7.56 (m, 2 H, CH-CH-CH-C_q-Cl and CH-CH-C_q-O); 8.01 (d, $J = 15.5$, 1 H, CH-C_q=O); 8.09 (d, $J = 15.2$, 1 CH=CH-C_q=O); 8.19 (d, $J = 2.6$, 1 H, C_q-CH-C_q-Cl); 8.21 (dd, $J = 7.5$, 1.8, 1 H, CH-CH-CH-C_q-Cl); 12.01 (s, 1 H, OH). ¹³C NMR (DMSO-*d*₆): δ 119.62 (d, 1 C, CH-C_q-O); 122.77 (s, 1 C, C_q-CH-C_q-Cl or C_q-C_q=O); 122.95 (s, 1 C, C_q-CH-C_q-Cl or C_q-C_q=O); 125.20 (d, 1 C, CH-C_q=O); 127.66 (d, 1 C, CH-C_q-C_q-Cl or CH-CH-CH-C_q-Cl); 128.77 (d, 1 C, CH-CH-CH-C_q-Cl); 130.04 (d, 1 C, CH-CH-CH-C_q-Cl); 131.93 (s, 1 C, C_q-C_q-Cl); 132.32 (d, 1 C, CH-C_q-C_q-Cl or CH-CH-CH-C_q-Cl); 134.52 (s, 1 C, C_q-C_q-Cl); 135.44 (d, 1 C, CH-CH-C_q-O); 139.18 (d, 1 C, CH=CH-C_q=O); 159.51 (s, 1 C, C_q-O); 191.87 (s, 1 C,

C_q=O). HRMS: Calculated mass for C₁₅H₁₀O₂Cl₂ 292.0057; mass found 290.9981 for C₁₅H₉O₂Cl₂ (M-1). M.P 100-102 °C (Lit⁶⁹⁹ 101-103 °C).

(2E)-1-(5-bromo-2-hydroxyphenyl)-3-phenylprop-2-en-1-one (94)⁷¹¹

Method A; 2'-hydroxyacetophenone **93** (0.216 g, 1 mmol) and benzaldehyde **67** (0.104 g, 1 mmol) afforded **94** as a yellow solid (0.207 g, 68%). ¹H NMR (DMSO-*d*₆): δ 6.99 (d, *J* = 8.8, 1 H, CH-C_q-O); 7.42-7.51 (m, 3 H, 2x CH-C_q-CH=CH and CH-CH-CH-CH-CH); 7.69 (dd, *J* = 8.7, 2.5, 1 H, CH-CH-C_q-Br); 7.82 (d, *J* = 15.6, 1 H, CH=CH-C_q=O); 7.90-7.93 (m, 2 H, 2x CH-CH-C_q-CH=CH); .99 (d, *J* = 15.5, 1 H, CH-C_q=O); 8.33 (d, *J* = 2.5, 1 H, C_q-CH-C_q-Br); 12.25 (s, 1 H, OH). ¹³C NMR (DMSO-*d*₆): δ 110.36 (s, 1 C, C_q-Br); 120.00 (d, 1 C, CH-C_q-O); 122.26 (d, 1 C, CH-C_q=O); 123.19 (s, 1 C, C_q-C_q=O); 128.87 (d, 2 C, 2x CH-C_q-CH=CH); 129.23 (d, 2 C, 2x CH-CH-C_q-CH=CH); 131.04 (d, 1 C, CH-CH-CH-CH-CH); 132.47 (d, 1 C, C_q-CH-C_q-Br); 134.35 (s, 1 C, C_q-CH=CH-C_q=O); 138.13 (d, 1 C, CH-CH-C_q-O); 145.21 (d, 1 C, CH=CH-C_q=O); 160.12 (s, 1 C, C_q-O); 192.32 (s, 1 C, C_q=O). HRMS: Calculated mass for C₁₅H₁₁O₂Br 301.9942; mass found 300.9865 for C₁₅H₁₀O₂Br (M-1). M.P 95-97 °C (Lit⁷¹¹ 94-96 °C).

(2E)-1-(5-bromo-2-hydroxyphenyl)-3-(4-bromophenyl)prop-2-en-1-one (95)⁷¹³

Method A; 2'-hydroxyacetophenone **93** (0.217 g, 1 mmol) and benzaldehyde **63** (0.189 g, 1 mmol) afforded **95** as a yellow solid (0.265 g, 68%). ¹H NMR (DMSO-*d*₆): δ 6.98 (d, *J* = 8.8, 1 H, CH-C_q-OH); 7.68 (d, *J* = 8.5, 2 H, 2x CH-C_q-Br); 7.68 (dd, *J* = 8.8, 2.5, 1 H, CH-CH-C_q-O); 7.79 (d, *J* = 14.8, 1 H, CH=CH-C_q=O); 7.89 (d, *J* = 8.4, 2 H, 2x CH-CH-C_q-Br); 8.01 (d, *J* = 15.7, 1 H, CH-C_q=O); 12.23 (s, 1 H, OH). ¹³C NMR (DMSO-*d*₆): δ 110.32 (s, 1 C, C_q-CH-C_q-Br); 120.02 (s, 1 C, CH-C_q-O); 122.94 (s, 1 C, CH-C_q=O); 123.08 (s, 1 C, C_q-C_q=O); 124.56 (s, 1 C, C_q-CH-CH-C_q-Br); 131.08 (d, 2 C, 2x CH-CH-C_q-Br); 131.87 (d, 2 C, 2x CH-C_q-Br); 132.50 (d, 1 C, C_q-CH-C_q-Br); 133.64 (s, 1 C, C_q-CH=CH-C_q=O); 138.24 (d, 1 C, CH-CH-C_q-Br); 143.75 (d, 1 C, CH=CH-C_q=O); 160.17 (s, 1 C, C_q-O); 192.20 (s, 1 C, C_q=O). HRMS: Calculated mass for C₁₅H₁₀O₂Br₂ 379.9047; mass found 378.8981 for C₁₅H₉O₂Br₂ (M-1). M.P 179-181 °C (Lit⁷¹¹ 180-182 °C).

(2E)-1-(5-bromo-2-hydroxyphenyl)-3-(4-chlorophenyl)prop-2-en-1-one (96)⁷¹²

Method A; 2'-hydroxyacetophenone **93** (0.214 g, 1 mmol) and benzaldehyde **70** (0.145 g, 1 mmol) afforded **96** as a yellow solid (0.209 g, 61%). ¹H NMR (DMSO-*d*₆): δ 6.99 (d, *J* = 8.8, 1 H, CH-C_q-O); 7.54 (d, *J* = 8.5, 2 H, 2x CH-C_q-Cl); 7.69 (dd, *J* = 8.7, 2.3, 1 H, CH-CH-C_q-Br); 7.80 (d, *J* = 15.6, 1 H, CH=CH-C_q=O); 7.96 (d, *J* = 8.5, 2 H, 2x CH-CH-C_q-Cl); 8.00 (d, *J* = 15.5, 1 H, CH-C_q=O); 8.33 (d, *J* = 2.3, 1 H, C_q-CH-C_q-Cl); 12.22 (s, 1 H, OH). ¹³C NMR (DMSO-*d*₆): δ 110.33 (s, 1 C, C_q-Br); 120.02 (d, 1 C, CH-C_q-O); 122.96 (d, 1 C,

CH-C_q=O); 123.12 (s, 1 C, C_q-C_q=O); 128.94 (d, 2 C, 2x CH-C_q-Cl); 130.89 (d, 2 C, 2x CH-CH-C_q-Cl); 132.50 (d, 1 C, C_q-CH-C_q-Br); 133.37 (s, 1 C, C_q-CH=CH-C_q=O); 143.66 (d, 1 C, CH=CH-C_q=O); 160.16 (s, 1 C, C_q-O); 192.27 (s, 1 C, C_q=O). HRMS: Calculated mass for C₁₅H₁₀O₂BrCl 335.9552; mass found 334.9475 for C₁₅H₉O₂BrCl (M-1). M.P 178-179 °C (Lit⁷¹¹ 179-180 °C).

(2E)-1-(5-bromo-2-hydroxyphenyl)-3-(4-fluorophenyl)prop-2-en-1-one (97)⁷¹²

Method A; 2'-hydroxyacetophenone **93** (0.216 g, 1 mmol) and benzaldehyde **72** (0.125 g, 1 mmol) afforded **97** as a yellow solid (0.263 g, 81%). ¹H NMR (DMSO-*d*₆): δ 6.99 (d, *J* = 8.8, 1 H, CH-C_q-O); 7.30 (t, *J* = 8.9, 2 H, 2x CH-C_q-F); 7.66 (dd, *J* = 8.8, 2.4, 1 H, CH-CH-C_q-Br); 7.80 (d, *J* = 15.5, 1 H, CH=CH-C_q=O); 7.93 (d, *J* = 15.5, 1 H, CH-C_q=O); 7.99 (dd, *J* = 6.5, 8.6, 2 H, 2x CH-CH-C_q-F); 8.31 (d, *J* = 2.3, 1 H, CH-C_q-C_q=O); 12.28 (br.s, 1 H, OH). ¹³C NMR (DMSO-*d*₆): δ 110.26 (s, 1 C, C_q-Br); 115.90 (dd, ²*J*_{19F-13C} = 21.7, 2 C, 2x CH-C_q-F); 120.00 (d, 1 C, CH-C_q-O); 122.04 (d, 1 C, CH-C_q=O); 123.08 (s, 1 C, C_q-C_q=O); 131.03 (s, 1 C, C_q-CH=CH-C_q=O); 131.63 (dd, ³*J*_{19F-13C} = 8.1, 2 C, 2x CH-CH-C_q-F); 132.44 (d, 1 C, CH-C_q-C_q=O); 138.10 (d, 1 C, CH-CH-C_q-Br); 143.10 (d, 1 C, CH=CH-C_q=O); 160.19 (s, 1 C, C_q-O); 163.61 (d, ¹*J*_{19F-13C} = 249.4, 1 C, C_q-F); 192.19 (s, 1 C, C_q=O). HRMS: Calculated mass for C₁₅H₁₀O₂BrF 319.9848; mass found 318.9774 for C₁₅H₉O₂BrF (M-1). M.P 160-162 °C (Lit⁷¹¹ 162-164 °C).

(2E)-1-(5-bromo-2-hydroxyphenyl)-3-(2-chlorophenyl)prop-2-en-1-one (98)⁷¹⁴

Method A; 2'-hydroxyacetophenone **93** (0.215 g, 1 mmol) and benzaldehyde **74** (0.146 g, 1 mmol) afforded **98** as a yellow solid (0.224 g, 65%). ¹H NMR (DMSO-*d*₆): δ 6.99 (d, *J* = 7.9, 1 H, CH-C_q-O); 7.45-7.49 (m, 2 H, CH-C_q-Cl and CH-CH-CH-C_q-Cl); 7.58 (dd, *J* = 7.7, 1.4, 1 H, CH-CH-C_q-Cl); 7.66 (d, *J* = 8.7, 1 H, CH-CH-C_q-Br); 8.00 (d, *J* = 15.8, 1 H, CH-C_q=O); 8.08 (d, *J* = 15.6, 1 H, CH=CH-C_q=O); 8.19 (d, *J* = 7.4, 1 H, CH-C_q-C_q-Cl); 8.25 (s, 1 H, C_q-CH-C_q-Br); 11.92 (br.s, 1 H, OH). ¹³C NMR (DMSO-*d*₆): δ 113.38 (s, 1 C, C_q-Br); 120.66 (d, 1 C, CH-C_q-O); 122.08 (s, 1 C, C_q-C_q=O); 125.65 (d, 1 C, CH-C_q=O); 127.64 (d, 1 C, CH-C_q-Cl or CH-CH-CH-C_q-Cl); 128.72 (d, 1 C, CH-C_q-C_q-Cl); 130.38 (d, 1 C, CH-C_q-Cl or CH-CH-CH-C_q-Cl); 132.02 (d, 1 C, CH-CH-C_q-Cl); 132.52 (d, 1 C, C_q-CH-C_q-Br); 134.46 (s, 1 C, C_q-C_q-Cl); 135.59 (s, 1 C, C_q-Cl); 137.98 (CH-CH-C_q-Br); 138.53 (d, 1 C, CH=CH-C_q=O); 159.97 (s, 1 C, C_q-O); 189.95 (s, 1 C, C_q=O). HRMS: Calculated mass for C₁₅H₁₀O₂BrCl 335.9552; mass found 334.9480 for C₁₅H₉O₂BrCl (M-1). M.P 97-99 °C

(2E)-1-(2-hydroxyphenyl)-3-(4-methoxyphenyl)prop-2-en-1-one (101)⁶⁹⁹

Method B; 2'-hydroxyacetophenone **60** (0.133 g, 1 mmol) and benzaldehyde **99** (0.136 g, 1 mmol) afforded **101** as a yellow solid (0.210 g, 83%). ¹H NMR (DMSO-*d*₆): δ 3.84 (s, 3 H, CH₃); 6.99 (d, *J* = 8.5, 1

H, CH-C_q-OH); 7.00 (td, *J* = 8.5, 0.9, 1 H, CH-CH-C_q-C_q); 7.04 (d, *J* = 8.8, 2 H, 2x CH-C_q-O-CH₃); 7.56 (td, *J* = 7.7, 1.4, 1 H, CH-CH-C_q-OH) 7.84 (d, *J* = 15.4, 1 H, CH=CH-C_q=O); 7.87 (d, *J* = 7.9, 2 H, 2x CH-CH-C_q-O-CH₃); 7.91 (d, *J* = 15.2, 1 H, CH-C_q=O); 8.26 (dd, *J* = 8.1, 1.1, 1 H, CH-C_q-C_q); 12.69 (s, 1 H, OH). ¹³C NMR (DMSO-*d*₆): δ 55.41 (q, 1 C, CH₃); 114.46 (d, 2 C, 2x CH-C_q-O-CH₃); 117.66 (d, 1 C, CH-C_q-OH); 118.86 (d, 1 C, CH-C_q=O); 119.01 (CH-CH-C_q-C_q); 120.56 (s, 1 C, C_q-C_q=O); 127.06 (s, 1 C, C_q-CH=CH-C_q=O); 130.68 (d 1 C, CH-C_q-C_q); 131.18 (d, 2 C, 2x CH-CH-C_q-O-CH₃); 136.12 (d, 1 C, CH-CH-C_q-OH); 145.01 (d, 1 C, CH=CH-C_q=O); 161.69 (s, 1 C, C_q-OH or C_q-O-CH₃); 161.96 (s, 1 C, C_q-OH or C_q-O-CH₃); 193.54 (s, 1 S, C_q=O). HRMS: Calculated mass for C₁₆H₁₄O₃ 254.0942; mass found 255.1017 for C₁₆H₁₅O₃ (M+1). M.P 94-95 °C (Lit⁸¹³ 95-96 °C).

(2E)-1-(2-hydroxyphenyl)-3-(2-methoxyphenyl)prop-2-en-1-one (102)⁷¹⁶

Method B; 2'-hydroxyacetophenone **60** (0.131 g, 1 mmol) and benzaldehyde **100** (0.135 g, 1 mmol) afforded **102** as a yellow solid (0.198 g, 79%). ¹H NMR (DMSO-*d*₆): δ 3.91 (s, 1 H, CH₃); 6.99 (d, *J* = 8.3, 1 H, CH-C_q-OH); 7.00 (t, *J* = 7.1, 1 H, CH-CH-C_q-C_q=O); 7.05 (d, *J* = 7.6, 1 H, CH-CH-C_q-CH=CH); 7.13 (t, *J* = 8.3, 1 H, CH-C_q-O-CH₃); 7.48 (td, *J* = 7.8, 1.4, 1 H, CH-CH-C_q-O-CH₃); 7.56 (td, *J* = 7.7, 1.3, 1 H, CH-CH-C_q-OH); 7.98 (d, *J* = 15.5, 1 H, CH-C_q=O); 7.99 (dd, *J* = 8.8, 1.2, 1 H, CH-C_q-C_q-O-CH₃); 8.16 (d, *J* = 15.8, 1 H, CH=CH-C_q=O); 12.51 (s, 1 C, OH). ¹³C NMR (DMSO-*d*₆): δ 55.78 (q, 1 C, CH₃); 111.86 (d, 1 C, CH-C_q-O-CH₃); 117.66 (d, 1 C, CH-C_q-OH); 119.11 (d, 1 C, CH-CH-C_q-C_q=O); 120.78 (s, 1 C, C_q-C_q-O-CH₃); 121.42 (d, 1 C, CH-C_q=O); 122.67 (s, 1 C, C_q-C_q=O); 128.74 (d, 1 C, CH-C_q-C_q-O-CH₃); 130.64 (d, 1 C, CH-C_q-C_q=O); 132.72 (d, 1 C, CH-CH-C_q-O-CH₃); 136.15 (d, 1 C, CH-CH-C_q-OH); 139.23 (d, 1 C, CH=CH-C_q=O); 158.41 (s, 1 C, C_q-O-CH₃); 161.77 (s, 1 C, C_q-OH); 193.67 (s, 1 C, C_q=O). Method B, 79%. HRMS: Calculated mass for C₁₆H₁₄O₃ 254.0942; mass found 255.1012 for C₁₆H₁₅O₃ (M+1). M.P 109-111 °C (Lit⁸¹⁴ 111-112 °C).

(2E)-1-(4-fluoro-2-hydroxyphenyl)-3-(4-methoxyphenyl)prop-2-en-1-one (103)⁷¹⁷

Method B; 2'-hydroxyacetophenone **76** (0.155 g, 1 mmol) and benzaldehyde **99** (0.134 g, 1 mmol) afforded **103** as a yellow solid (0.221 g, 81%). ¹H NMR (DMSO-*d*₆): δ 3.84 (s, 3 H, CH₃); 6.84 (d, *J* = 9.8, 1 H, C_q-CH-C_q-F); 6.85 (td, *J* = 9.5, 2.5, 1 H, CH-CH-C_q-F); 7.04 (d, *J* = 8.7, 2 H, 2x CH-C_q-O-CH₃); 7.84 (d, *J* = 15.4, 1 H, CH-C_q=O); 7.88 (d, *J* = 15.2, 1 H, CH=CH-C_q=O); 7.89 (d, *J* = 8.8, 2 H, 2x CH-CH-C_q-O-CH₃); 8.39 (dd, *J* = 8.3, 6.8, 1 H, CH-CH-C_q-F); 13.16 (s, 1 H, OH). ¹³C NMR (DMSO-*d*₆): δ 55.54 (q, 1 C, CH₃); 104.26 (dd, ²*J*_{19F-13C} = 24.0, 1 C, C_q-CH-C_q-F); 106.96 (dd, ²*J*_{19F-13C} = 23.2, 1 C, CH-CH-C_q-F); 114.51 (d, 2 C, 2x CH-C_q-O-CH₃); 117.82 (s, 1 C, C_q-C_q=O); 118.75 (d, 1 C, CH-C_q=O); 127.04 (s, 1 C, C_q-CH=CH-C_q=O);

131.34 (d, 2 C, 2x CH-CH-C_q-O-CH₃); 145.33 (d, 1 C, CH=CH-C_q=O); 133.63 (dd, ³J_{19F-13C} = 10.7, 1 C, CH-C_q-C_q=O); 161.81 (s, 1 C, C_q-O-CH₃); 164.72 (s, 1 C, C_q-OH); 166.73 (d, ¹J_{19F-13C} = 253.3, 1 C, C_q-F); 192.52 (s, 1 C, C_q=O). HRMS: Calculated mass for C₁₆H₁₃O₃F 272.0848; mass found 271.0767 for C₁₆H₁₂O₃F (M-1). M.P 109-111 °C (Lit⁷⁰⁷ 111-112 °C).

(2E)-1-(4-fluoro-2-hydroxyphenyl)-3-(2-methoxyphenyl)prop-2-en-1-one (104)

Method B; 2'-hydroxyacetophenone **76** (0.156 g, 1 mmol) and benzaldehyde **100** (0.135, 1 mmol) afforded **104** as a yellow solid (0.239 g, 87%). ¹H NMR (DMSO-*d*₆): δ 3.91 (s, 3 H, CH₃); 6.85 (d, *J* = 9.6, 1 H, C_q-CH-C_q-F); 6.88 (td, *J* = 6.9, 2.5, 1 H, CH-CH-C_q-F); 7.05 (t, *J* = 7.5, 1 H, CH-CH-CH-C_q-O-CH₃); 7.14 (t, *J* = 8.4, 1 H, CH-C_q-O-CH₃); 7.48 (td, *J* = 7.8, 1.4, CH-CH-C_q-O-CH₃); 7.96 (d, *J* = 15.6, 1 H, CH-C_q=O); 7.99 (dd, *J* = 7.7, 1.3, 1 H, CH-C_q-C_q-O-CH₃); 8.16 (d, *J* = 15.6, 1 H, CH=CH-C_q=O); 8.33 (dd, *J* = 6.7, 9.4, 1 H, CH-C_q-C_q=O); 12.99 (s, 1 H, OH). ¹³C NMR (DMSO-*d*₆): δ 55.75 (q, 1 C, CH₃); 104.20 (dd, ²J_{19F-13C} = 22.5, 1 C, CH-C_q-OH); 106.88 (dd, ²J_{19F-13C} = 22.4, 1 C, CH-CH-C_q-F); 111.88 (d, 1 C, CH-C_q-O-CH₃); 118.04 (s, 1 C, C_q-C_q=O); 120.72 (d, 1 C, CH-CH-C_q-C_q-O-CH₃); 121.25 (d, 1 C, CH-C_q=O); 122.63 (s, 1 C, C_q-C_q-O-CH₃); 128.71 (d, 1 C, CH-C_q-C_q-O-CH₃); 132.83 (d, 1 C, CH-CH-C_q-O-CH₃); 133.56 (dd, ³J_{19F-13C} = 12.2, 1 C, CH-C_q-C_q=O); 139.38 (d, 1 C, CH=CH-C_q=O); 158.49 (s, 1 C, C_q-O-CH₃); 164.13 (d, ¹J_{19F-13C} = 235.8, 1 C, C_q-F); 164.38 (s, 1 C, C_q-OH); 192.53 (s, 1 C, C_q=O). HRMS: Calculated mass for C₁₆H₁₃O₃F 272.0848; mass found 271.0765 mass for C₁₆H₁₂O₃F (M-1). M.P. 99-101 °C.

(2E)-1-(4-chloro-2-hydroxyphenyl)-3-(4-methoxyphenyl)prop-2-en-1-one (105)⁷¹⁰

Method B; 2'-hydroxyacetophenone **82** (0.170 g, 1 mmol) and benzaldehyde **99** (0.136 g, 1 mmol) afforded **105** as a yellow solid (0.264 g, 91%). ¹H NMR (DMSO-*d*₆): δ 3.83 (s, 3 H, CH₃); 7.00-7.06 (m, 3 H, 2x CH-C_q-O-CH₃ and CH-CH-C_q-Cl); 7.08 (d, 1 H, CH-C_q-OH); 7.81-7.83 (m, CH=CH-C_q=O and CH-C_q=O); 7.86 (d, *J* = 8.82 H, CH-C_q-CH=CH); 8.24 (d, *J* = 8.8, 1 H, CH-C_q-C_q=O); 12.81 (br.s, 1 H, OH). ¹³C NMR (DMSO-*d*₆): δ 55.39 (q, 1 C, CH₃); 114.46 (d, 2 C, 2x CH-C_q-O-CH₃); 117.35 (d, 1 C, CH-C_q-OH); 119.13 (d, 1 C, CH-CH-C_q-CH or CH-C_q=O); 119.20 (d, 1 C, CH-CH-C_q-CH or CH-C_q=O); 120.00 (s, 1 C, C_q-C_q=O); 126.99 (s, 1 C, C_q-CH=CH-C_q=O); 131.21 (d, 2 C, 2x CH-C_q-CH=CH); 132.26 (d, 1 C, CH-C_q-C_q=O); 139.87 (s, 1 C, C_q-Cl); 145.26 (d, 1 C, CH=CH-C_q=O); 161.77 (s, 1 C, C_q-O-CH₃); 162.49 (s, 1 C, C_q-OH); 192.50 (s, 1 C, C_q=O). HRMS: Calculated mass for C₁₆H₁₃O₃Cl 288.0553; mass found 287.0468 for C₁₆H₁₂O₃Cl (M-1). M.P. 127-128 °C (Lit⁷¹⁰ 128-129 °C).

(2E)-1-(4-chloro-2-hydroxyphenyl)-3-(2-methoxyphenyl)prop-2-en-1-one (106)

Method B; 2'-hydroxyacetophenone **82** (0.171 g, 1 mmol) and benzaldehyde **100** (0.134g, 1 mmol) afforded **106** as a yellow solid (0.266 g, 92%). ¹H NMR (DMSO-*d*₆): δ 3.90 (s, 3 H, CH₃); 7.02-7.06 (m, 2 H, CH-CH-C_q-C_q=O and CH-CH-C_q-CH=CH); 7.09 (d, *J* = 2.0, 1 H, CH-C_q-OH); 7.13 (d, *J* = 8.3, 1 H, CH-C_q-O-CH₃); 7.47 (t, *J* = 8.5, 1 H, CH-CH-C_q-O-CH₃); 7.92 (d, 15.7, CH-C_q=O); 7.96 (dd, *J* = 7.7, 1.2, 1 H, CH-C_q-CH=CH); 8.13 (d, *J* = 15.8, 1 H, CH=CH-C_q=O); 8.17 (d, *J* = 8.7, 1 H, CH-C_q-C_q=O); 12.52 (br.s, 1 H, OH). ¹³C NMR (DMSO-*d*₆): δ 55.79 (q, 1 C, CH₃); 111.91 (d, 1 C, CH-C_q-O-CH₃); 117.37 (d, 1 C, CH-C_q-OH); 119.37 (d, 1 C, CH-CH-C_q-Cl or CH-CH-C_q-C_q-O-CH₃); 120.33 (s, 1 C, C_q-C_q=O); 120.73 (d, 1 C, CH-CH-C_q-Cl or CH-CH-C_q-C_q-O-CH₃); 121.77 (d, 1 C, CH-C_q=O); 122.73 (s, 1 C, C_q-C_q-O-CH₃); 128.72 (d, 1 C, CH-C_q-CH=CH); 132.28 (CH-C_q-C_q=O); 132.84 (d, 1 C, CH-C_q-CH=CH); 139.45 (s, 1 C, C_q-Cl); 139.90 (d, 1 C, CH=CH-C_q=O); 158.47 (s, 1 C, C_q-O-CH₃); 162.18 (s, 1 C, C_q-OH); 192.37 (s, 1 C, C_q=O). HRMS: Calculated mass for C₁₆H₁₃O₃Cl 288.0553; mass found 287.0474 for C₁₆H₁₂O₃Cl (M-1). M.P. 121-123 °C.

(2E)-1-(5-chloro-2-hydroxyphenyl)-3-(4-methoxyphenyl)prop-2-en-1-one (107)⁶⁹⁹

Method B; 2'-hydroxyacetophenone **87** (0.172 g, 1 mmol) and benzaldehyde **99** (0.135 g, 1 mmol) afforded **107** as a yellow solid (0.256 g, 88%). ¹H NMR (DMSO-*d*₆): δ 3.84 (s, 3 H, CH₃); 7.02 (d, *J* = 8.7, 1 H, CH-C_q-OH); 7.03 (d, *J* = 8.7, 2 H, 2x CH-C_q-O-CH₃); 7.56 (dd, *J* = 8.7, 2.5, 1 H, CH-CH-C_q-Cl); 7.82 (d, *J* = 15.7, 1 H, CH-C_q=O); 7.90 (d, *J* = 15.0, 1 H, CH=CH-C_q=O); 7.91 (d, *J* = 8.7, 2 H, 2x CH-CH-C_q-O-CH₃); 8.27 (d, *J* = 2.6, 1 H, C_q-CH-C_q-Cl); 12.50 (s, 1 H, OH). ¹³C NMR (DMSO-*d*₆): δ 55.41 (q, 1 C, CH₃); 114.44 (d, 2 C, 2x CH-C_q-O-CH₃); 119.16 (d, 1 C, CH-C_q-OH); 119.62 (d, 1 C, CH-C_q=O); 122.22 (s, 1 C, C_q-Cl or C_q-C_q=O); 122.81 (s, 1 C, C_q-Cl or C_q-C_q=O); 127.02 (s, 1 C, C_q-CH=CH-C_q=O); 129.53 (d, 1 C, C_q-CH-C_q-Cl); 131.42 (d, 2 C, 2x CH-CH-C_q-O-CH₃); 135.33 (s, 1 C, CH-CH-C_q-Cl); 145.68 (d, 1 C, CH=CH-C_q=O); 160.09 (s, 1 C, C_q-OH); 161.84 (s, 1 C, C_q-O-CH₃); 192.44 (s, 1 C, C_q=O). HRMS: Calculated mass for C₁₆H₁₃O₃Cl 288.0553; mass found 287.0473 for C₁₆H₁₂O₃Cl (M-1) M.P. 87-88 °C (Lit⁶⁹⁹ 88-90 °C).

(2E)-1-(5-chloro-2-hydroxyphenyl)-3-(2-methoxyphenyl)prop-2-en-1-one (108)⁷¹⁸

Method B; 2'-hydroxyacetophenone **87** (0.173 g, 1 mmol) and benzaldehyde **100** (0.134 g, 1 mmol) afforded **108** as a yellow solid (0.236 g, 81%). ¹H NMR (DMSO-*d*₆): δ 3.90 (s, 3 H, CH₃); 7.03 (d, *J* = 9.0, 1 H, CH-C_q-OH); 7.05 (t, *J* = 8.5, 1 H, CH-CH-CH-C_q-O-CH₃); 7.13 (d, *J* = 8.4, 1 H, CH-C_q-O-CH₃); 7.48 (td, *J* = 7.8, 1.5, 1 H, CH-CH-C_q-O-CH₃); 7.56 (dd, *J* = 8.8, 2.6, 1 H, CH-CH-C_q-Cl); 7.93 (d, *J* = 15.5, 1 H, CH-C_q=O); 8.03 (dd, *J* = 7.7, 1.2, 1 H, CH-C_q-C_q-O-CH₃); 8.15 (d, *J* = 15.7, 1 H, CH=CH-C_q=O); 8.18 (d, *J* = 2.6, 1 H,

C_q-CH-C_q-Cl); 12.25 (s, 1 H, OH). ¹³C NMR (DMSO-*d*₆): δ 55.76 (q, 1 C, CH₃); 111.86 (CH-C_q-O-CH₃); 119.59 (d, 1 C, CH-C_q-OH); 120.66 (d, 1 C, CH-CH-CH-C_q-O); 121.77 (d, 1 C, CH-C_q=O); 122.61 (s, 1 C, C_q-Cl or C_q-C_q=O); 122.66 (C_q-C_q-O-CH₃); 122.83 (s, 1 C, C_q-Cl or C_q-C_q=O); 128.52 (d, 1 C, CH-C_q-C_q-O-CH₃); 129.50 (d, 1 C, C_q-CH-C_q-Cl); 132.88 (d, 1 C, CH-CH-C_q-O-CH₃); 135.22 (d, 1 C, CH-CH-C_q-Cl); 139.46 (CH=CH-C_q=O); 158.39 (C_q-O-CH₃); 159.70 (C_q-OH); 192.37 (s, 1 C, C_q=O). HRMS: Calculated mass for C₁₆H₁₃O₃Cl 288.0553; mass found 287.0472 for C₁₆H₁₂O₃Cl (M-1). M.P. 115-117 °C.

(2E)-1-(5-bromo-2-hydroxyphenyl)-3-(4-methoxyphenyl)prop-2-en-1-one (109)⁷¹⁴

Method B; 2'-hydroxyacetophenone **93** (0.215 g, 1 mmol) and benzaldehyde **99** (0.135 g, 1 mmol) afforded **109** as a yellow solid (0.314 g, 94%). ¹H NMR (DMSO-*d*₆): δ 3.84 (s, 3 H, CH₃); 6.97 (d, *J* = 8.8, 1 H, CH-C_q-OH); 7.04 (d, *J* = 8.7, 2 H, 2x CH-C_q-O-CH₃); 7.68 (dd, *J* = 8.8, 2.3, 1 H, CH-CH-C_q-Br); 7.81 (d, *J* = 15.4, 1 H, CH-C_q=O); 7.88 (d, *J* = 14.9, 1 H, CH=CH-C_q=O); 7.91 (d, *J* = 8.6, 2 H, 2x CH-CH-C_q-O-CH₃); 8.37 (d, *J* = 2.4, 1 H, C_q-CH-C_q-Br); 12.51 (s, 1 H, OH). ¹³C NMR (DMSO-*d*₆): δ 55.40 (q, 1 C, CH₃); 110.22 (s, 1 C, C_q-Br); 114.42 (d, 2 C, 2x CH-C_q-O-CH₃); 119.19 (d, 1 C, CH-C_q=O); 120.01 (d, 1 H, CH-C_q-OH); 122.85 (s, 1 C, C_q-C_q=O); 127.01 (s, 1 C, C_q-CH=CH-C_q=O); 131.38 (d, 2 C, 2x CH-CH-C_q-O-CH₃); 132.35 (d, 1 C, C_q-CH-C_q-Br); 138.08 (d, 1 C, CH-CH-C_q-Br); 145.67 (d, 1 C, CH=CH-C_q=O); 160.44 (s, 1 C, C_q-O-CH₃); 161.82 (s, 1 C, C_q-OH); 192.34 (s, 1 C, C_q=O). HRMS: Calculated mass for C₁₆H₁₃O₃Br 332.0048; mass found 330.9966 for C₁₆H₁₂O₃Br (M-1). M.P. 100-103 °C (Lit⁸¹⁵ 102-104 °C).

(2E)-1-(5-bromo-2-hydroxyphenyl)-3-(2-methoxyphenyl)prop-2-en-1-one (110)

Method B; 2'-hydroxyacetophenone **93** (0.216 g, 1 mmol) and benzaldehyde **99** (0.134 g, 1 mmol) afforded **110** as a yellow solid (0.317 g, 95%). ¹H NMR (DMSO-*d*₆): δ 3.90 (s, 3 H, CH₃); 6.97 (d, *J* = 8.8, 1 H, CH-C_q-OH); 7.05 (t, *J* = 7.5, CH-CH-CH-C_q-O-CH₃); 7.13 (d, *J* = 8.3, CH-C_q-O-CH₃); 7.48 (td, *J* = 7.8, 1.3; CH-CH-C_q-O-CH₃); 7.67 (dd, *J* = 8.8, 2.4, 1 H, CH-CH-C_q-Br); 7.92 (d, *J* = 15.7, 1 H, CH-C_q=O); 8.03 (dd, *J* = 7.7, 1.2, 1 H, CH-C_q-C_q-O-CH₃); 8.14 (d, *J* = 15.6, 1 H, CH=CH-C_q=O); 8.28 (dd, *J* = 2.2, 1 H, C_q-CH-C_q-Br); 12.25 (s, 1 H, OH). ¹³C NMR (DMSO-*d*₆): δ 55.78 (q, 1 C, CH₃); 110.29 (s, 1 C, C_q-Br); 111.87 (d, 1 C, CH-C_q-O-CH₃); 119.99 (d, 1 C, CH-C_q-OH); 120.65 (d, 1 C, CH-CH-CH-C_q-O); 121.83 (d, 1 C, CH-C_q=O); 122.63 (s, 1 C, C_q-C_q-O-CH₃); 123.34 (s, 1 C, C_q-C_q=O); 128.52 (d, 1 C, CH-C_q-C_q-O-CH₃); 132.37 (d, 1 C, C_q-CH-C_q-Br); 132.88 (d, 1 C, CH-CH-C_q-O-CH₃); 137.99 (CH-CH-C_q-Br); 139.44 (d, 1 C, CH=CH-C_q=O); 158.39 (s, 1 C, C_q-O-CH₃); 160.06 (s, 1 C, C_q-OH); 192.32 (s, 1 C, C_q=O). HRMS: Calculated mass for C₁₆H₁₃O₃Br 332.0048; mass found 330.9973 for C₁₆H₁₂O₃Br (M-1). M.P. 106-108 °C.

4-(bromomethyl)benzenesulfonamide (113)¹⁶⁰

To a solution of THF (10 ml) and aqueous ammonia (5 ml) on ice was added sulfonyl chloride **112** (0.269 g, 1 mmol), and the reaction stirred on ice for 1 hour.⁷⁰³ EtOAc (10 ml) and H₂O (5 ml) were added, and the resultant layers were separated. The organic layer was dried with Na₂SO₄ and the solvent removed *in vacuo* without heat to yield a white solid (0.202 g, 81 %). ¹H NMR (DMSO-*d*₆): δ 4.76 (s, 2 H, CH₂); 7.36 (br.s, 2 H, NH₂); 7.62 (d, *J* = 8.4, 2 H, 2x CH-C_q-S); 7.80 (d, *J* = 8.3, 2x CH-C_q-CH₂). ¹³C NMR (DMSO-*d*₆): δ 33.42 (t, 1 C, CH₂); 126.52 (d, 2 C, 2x CH-C_q-CH₂); 130.22 (d, 2 C, 2x CH-C_q-S); 142.36 (s, 1 C, C_q-CH₂); 144.27 (d, 1 C, C_q-S). ¹⁵N NMR (DMSO-*d*₆): δ 95.5. HRMS: Calculated mass for C₇H₉O₂NSBr 248.9459; mass found 249.9468 for C₇H₁₀O₂NSBr (M+1). M.P 189-191 °C (Lit⁸¹⁶ 191-192 °C).

General procedure for Protection of Sulfonyl Chloride: Method C: (Amine protecting groups)

KOH (0.610 g, 1.1 mmol) was dissolved in MeCN (25 ml), and then the appropriate amine (1 mmol) was added. The solution was stirred at room temperature for 30 mins, before the appropriate sulfonyl chloride (1 mmol) was added and the reaction stirred at room temperature for 2 hours.⁷²⁵ The precipitate was filtered off and allowed to air dry. An additional portion of material (5-15%) could be recovered from the filtrate; however this required labor-intensive separation from unreacted starting materials.

Deprotection: The sulfonamide was dissolved in hydrazine hydrate (80%, 25 ml) and the solution was heated to reflux for 20 mins.⁷²⁹ The reaction was then removed from heat and allowed to cool to room temperature, after which H₂O (10 ml) and EtOAc (50 ml) were added. The organic layer was removed, dried over MgSO₄ and the solvent removed *in vacuo* without heat.

Method D (Alkyl alcohol protecting groups)

KOH (0.608 g, 1.1 mmol) was added to the appropriate alcohol (20 ml) and stirred to dissolve. Na₂SO₄ was added to remove the water, followed by the appropriate sulfonyl chloride (1 mmol) and the reaction was stirred at room temperature for 2 hours.⁷²⁶ The solution was filtered and the solvent removed *in vacuo*.

Deprotection: The sulfonate was added to a solution of KOH (1.122 g, 2 mmol), EtOH (20 ml) and H₂O (10 ml) and heated to reflux for 1 hr.⁷³⁰ The solution was allowed to cool and the resulting ppt filtered off and allowed to air dry.

Method E (Phenol protecting groups)

KOH (0.609 g, 1.1 mmol) was added to THF/H₂O (10 ml, 20:1) and allowed to dissolve. Na₂SO₄ was added to remove the water, followed by the appropriate phenol (1 mmol) and sulfonyl chloride **65** (0.191 g, 1 mmol). The reaction was stirred at 0 °C for 2 hours,⁷²⁷ before warming to room temperature. The solution was filtered and the solvent removed *in vacuo*.

Deprotection: KOH (1.122 g, 2 mmol) was added to abs EtOH (5 ml) and stirred to dissolve, before addition to a solution of the appropriate sulfonate in CHCl₃ (20 ml). The reaction was heated to reflux for 2 hours, and allowed to cool.⁷³¹ H₂O (30 ml) and EtOAc (30 ml) was added, and the organic layer removed, dried over MgSO₄ and removed *in vacuo*.

***N,N*-diethyl-4-methylbenzenesulfonamide (114)**⁷³²

Method C; Diethylamine (0.073 g, 1 mmol) and sulfonyl chloride **65** (0.192 g, 1 mmol) afforded **114** as a white solid (0.205 g, 90%). ¹H NMR (CDCl₃): δ 1.12 (t, *J* = 7.1, 6 H, 2x CH₂-CH₃); 2.41 (s, 3 H, C_q-CH₃); 3.23 (q, *J* = 7.1, 4 H, 2x CH₂); 7.28 (d, *J* = 8.0, 2 H, 2x CH-C_q-CH₃); 7.69 (d, *J* = 8.1, 2 H, CH-C_q-S). M.P. 57-59 °C (Lit⁸¹⁷ 58-59 °C).

***2*-[(4-Methylphenyl)sulfonyl]-1*H*-isoindole-1,3(2*H*)-dione (119)**⁷²⁵

Method C; Phthalamide (0.147 g, 1 mmol) and sulfonyl chloride **65** (0.191 g, 1 mmol) afforded **119** as a white solid (0.259 g, 86%, deprotection 81%). ¹H NMR (DMSO-*d*₆): δ 2.40 (s, 3 H, CH₃); 7.48 (d, *J* = 8.2, 2 H, 2x CH-C_q-CH₃); 7.92 (d, *J* = 1.5, 4 H, 2x CH-C_q-C_q=O and 2 x CH-CH-C_q-C_q); 7.98 (d, *J* = 8.5, 2 H, 2x CH-C_q-S). M.P. 229-230 °C (Lit⁸¹⁸ 230 °C).

Ethyl 4-methylbenzenesulfonate (120)

⁷³⁶

Method D; Ethanol (20 ml) and sulfonyl chloride **65** (0.192 g, 1 mmol) afforded **120** as an off-white solid (0.180 g, 90%, deprotection 93%). ¹H NMR (CDCl₃): δ 1.29 (t, *J* = 7.1, 3 H, CH₂-CH₃); 2.44 (s, 3 H, C_q-CH₃);

4.10 (q, $J = 7.2$, 2 H, CH₂); 7.34 (d, $J = 8.2$, 2 H, 2x CH-C_q-CH₃); 7.478 (d, $J = 8.5$, 2 H, 2x CH-C_q-S). M.P. 31-33 °C (Lit⁸¹⁹ 33-34 °C).

Phenyl 4-methylbenzenesulfonate (121)⁷³⁷

Method E; Phenol (0.094 g, 1 mmol) and sulfonyl chloride **65** (0.193 g, 1 mmol) afforded **121** as a white solid (0.186 g, 75%). ¹H NMR (DMSO-*d*₆): δ 2.42 (s, 3 H, CH₃); 7.02 (d, $J = 7.7$, 2 H, 2x CH-CH-C_q-O); 7.31 (t, $J = 7.0$, 1 H, CH-CH-CH-C_q-O); 7.38 (t, $J = 7.5$, 2 H, 2x CH-C_q-O); 7.46 (d, $J = 7.7$, 2 H, 2x CH-C_q-CH₃); 7.73 (d, $J = 7.9$, 2 H, 2x CH-C_q-S). M.P. 93-94 °C (Lit⁸²⁰ 94-95 °C).

4-Nitrophenyl 4-methylbenzenesulfonate (122)

Method E; 4-nitrophenol (0.139 g, 1 mmol) and sulfonyl chloride **65** (0.194 g, 1 mmol) afforded **122** as a white solid (0.251 g, 86%). ¹H NMR (CDCl₃): δ 2.26 (s, 3 H, CH₃); 6.98 (d, $J = 9.1$, 2 H, 2x CH-C_q-O); 7.15 (d, $J = 8.1$, 2 H, 2x CH-C_q-CH₃); 7.52 (d, $J = 8.3$, 2 H, 2x CH-C_q-S); 7.98 (d, $J = 9.1$, 2 H, 2x CH-C_q-N=O). M.P. 99-101 °C.

Ethyl 4(bromomethyl)benzenesulfonate (123)⁷³⁸

Method D; Ethanol (20 ml) and sulfonyl chloride **112** (0.269 g, 1 mmol) afforded **123** as a pale beige solid (0.272 g, 88%). ¹H NMR (DMSO-*d*₆): δ 1.21 (t, $J = 7.1$, 3 H, CH₃); 4.12 (q, $J = 7.1$, 2 H, CH₂-CH₃); 4.79 (s, 2 H, CH₂-Br); 7.76 (d, $J = 8.4$, 2 H, 2x CH-C_q-CH₂); 7.89 (d, $J = 8.3$, 2 H, 2x CH-C_q-S). ¹³C NMR (DMSO-*d*₆): δ 14.79 (q, 1 C, CH₃); 32.32 (t, 1 C, CH₂-Br); 67.79 (t, 1 C, CH₂-CH₃); 127.89 (d, 2 C, 2x CH-C_q-S); 130.42 (d, 2 C, 2x CH-C_q-CH₂); 135.18 (s, 1 C, C_q-S); 144.39 (s, 1 C, C_q-CH₂). HRMS: Calculated mass for C₇H₆O₃S 248.9221; mass found 248.9230. M.P. 39-41 °C

2-[[4-(bromomethyl)phenyl]sulfonyl]-1H-isoindole-1,3(2H)-dione (124)⁷³⁹

Method C; phthalamide (0.146 g, 1 mmol) and sulfonyl chloride **112** (0.268 g, 1 mmol) afforded **124** as a white solid (0.3319 g, 84%). ¹H NMR (DMSO-*d*₆): δ 4.48 (s, 2 H, CH₂); 7.58 (d, $J = 8.4$, 2 H, 2x CH-C_q-CH₂); 7.81 (dd, $J = 5.6, 3.0$, 2 H, 2x CH-C_q-C_q or 2x CH-CH-C_q-C_q); 7.92 (dd, $J = 5.6, 3.0$, 2 H, 2x CH-C_q-C_q or 2x CH-CH-C_q-C_q); 8.19 (d, $J = 8.5$, 2 H, 2x CH-C_q-S). ¹³C NMR (DMSO-*d*₆): δ 31.02 (t, 1 C, CH₂); 124.67 (d, 2 C, 2x CH-C_q-C_q or 2x CH-CH-C_q-C_q); 128.96 (d, 2 C, CH-C_q-S); 129.89 (d, 2 C, 2x CH-C_q-CH₂); 130.91 (s, 2 C, 2x C_q-C_q=O); 135.59 (d, 2 C, 2x CH-C_q-C_q or 2x CH-CH-C_q-C_q); 138.17 (s, 1 C, C_q-S); 144.78 (s, 1 C, C_q-CH₂); 162.83 (s, 2 C, 2x C_q=O). HRMS: Calculated mass for C₁₅H₁₀O₄BrNS 378.9514; mass found 378.9509. M.P. 221-223 °C

General procedure for the Synthesis of Target Compounds– Method F

Compound **123** (0.309 g, 1 mmol), the appropriate 2'-hydroxyacetophenone (1 mmol) and K_2CO_3 (0.275 g, 2 mmol) were added to THF (30 ml) and heated to reflux for 24 hours. The resulting cream precipitate was filtered from solution and allowed to air dry.

Method G

Compound **123** (0.309 g, 1 mmol), appropriate 2'-hydroxyacetophenone (1 mmol) and K_2CO_3 (0.415 g, 3 mmol) were added to THF (30 ml) and heated to reflux for 36 hours. The resulting cream precipitate was filtered from solution and allowed to air dry.

Potassium 4-[2-(2-acetylphenyl)ethyl]benzenesulfonate (125)

Method F; sulfonate **123** (0.310 g, 1 mmol) and 2'-hydroxyacetophenone **60** (0.136 g, 1 mmol) afforded **125** as a pale beige solid (0.285 g, 83%). 1H NMR (DMSO- d_6): δ 2.51 (s, 3 H, CH_3); 5.24 (s, 2 H, CH_2); 7.03 (ddd, 1 H, $J = 7.7, 7.3, 1.0$, $CH-CH-C_q-Cq=O$); 7.24 (d, 1 H, $J = 8.2$, $CH-C_q-O$); 7.46 (d, 2 H, $J = 8.3$, 2 x $CH-C_q-CH_2$); 7.52 (ddd, 1 H, $J = 8.4, 7.3, 1.9$, $CH-CH-C_q-O$); 7.59 (dd, 1 H, $J = 7.7, 1.8$, $CH-C_q-Cq=O$); 7.64 (s, 2 H, $J = 8.2$, 2 x $CH-C_q-S$). ^{13}C NMR (DMSO- d_6): δ 31.72 (q, 1 C, CH_3); 69.73 (t, 1 C, CH_2); 113.63 (d, 1 C, $CH-C_q-O$); 120.57 (d, 1 C, $CH-CH-C_q-Cq=O$); 125.71 (d, 2 C, 2 x $CH-C_q-S$); 127.15 (d, 2 C, 2 x $CH-C_q-CH_2$); 128.17 (s, 1 C, $C_q-Cq=O$); 129.50 (d, 1 C, $CH-C_q-Cq=O$); 133.65 (d, 1 C, $CH-CH-C_q-O$); 136.57 (s, 1 C, C_q-CH_2 or C_q-S); 148.04 (s, 1 C, C_q-CH_2 or C_q-S); 157.40 (s, 1 C, C_q-O); 198.79 (s, 1 C, $C_q=O$). HRMS: Calculated mass for $C_{15}H_{13}O_5S$ 305.0477; mass found 305.0484. Decomposes above 180 °C.

Potassium 4-[2-(2-acetyl-5-fluorophenyl)ethyl]benzenesulfonate (126)

Method F; sulfonate **123** (0.309 g, 1 mmol) and 2'-hydroxyacetophenone **76** (0.154 g, 1 mmol) afforded **126** as a pale beige solid (0.286 g, 79%). 1H NMR (DMSO- d_6): δ 2.48 (s, 3 H, CH_3); 5.25 (s, 2 H, CH_2); 6.87 (td, $J = 8.4, 2.4$, 1 H, $CH-CH-C_q-F$); 7.17 (dd, $J = 11.5, 2.4$, 1 H, $Cq-CH-Cq$); 7.47 (d, $J = 8.3$, 2 H, 2 x $CH-C_q-CH_2$); 7.65 (d, $J = 8.2$, 2 H, 2 x $CH-C_q-S$); 7.71 (dd, $J = 8.7, 7.2$, 1 H, $CH-C_q-Cq=O$). ^{13}C NMR (DMSO- d_6): δ 31.67 (q, 1 C, CH_3); 70.35 (t, 1 C, CH_2); 101.56 (dd, $^2J_{19F-13C} = 25.9$, 1 C, $C_q-CH-Cq$); 107.53 (dd, $^2J_{19F-13C} = 21.9$, 1 C, $CH-CH-C_q-F$); 124.53 (s, 1 C, $C_q-Cq=O$); 125.75 (d, 1 C, 2 x $CH-C_q-S$); 127.37 (d, 1 C, 2 x $CH-C_q-CH_2$); 132.01 (dd, $^3J_{19F-13C} = 11.2$, 1 C, $CH-C_q-Cq=O$); 135.96 (s, 1 C, C_q-CH_2); 148.24 (s, 1 C, C_q-S);

159.44 (d, $^3J_{19F-13C} = 11.1$, 1 C, C_q-O-CH_2); 165.34 (d, $^1J_{19F-13C} = 250.3$, 1 C, C_q-F); 197.00 (s, 1 C, $C_q=O$). ^{19}F NMR (DMSO- d_6): δ -104.5 (m, 1 F, C_q-F). HRMS: Calculated mass for $C_{15}H_{12}O_5FS$ 323.0389; mass found 323.0385. Decomposes above 195 °C.

Potassium 4-[2-(2-acetyl-5-chlorophenyl)ethyl]benzenesulfonate (127)

Method G; sulfonate **123** (0.311 g, 1 mmol) and 2'-hydroxyacetophenone **82** (0.170 g, 1 mmol) afforded **127** as a pale beige solid (0.272 g, 72%). 1H NMR (D_2O , 40°C): δ 2.48 (s, 3 H, CH_3); 5.27 (s, 2 H, CH_2); 7.10 (dd, $J = 8.3, 1.6$, 1 H, $CH-CH-C_q-Cl$); 7.36 (d, $J = 1.6$, 1 H, C_q-CH-C_q-Cl); 7.46 (d, $J = 8.1$, 2 H, 2 x $CH-C_q-CH_2$); 7.57 (d, $J = 8.3$, 1H, $CH-C_q-C_q=O$); 7.66 (d, $J = 7.9$, 2 H, 2 x $CH-C_q-S$). ^{13}C NMR (DMSO- d_6): δ 32.09 (q, 1 C, CH_3); 65.22 (t, 1 C, CH_2); 114.07 (d, 1 C, $CH-C_q-O$); 120.89 (d, 1 C, $CH-CH-C_q-Cl$); 126.26 (d, 2 C, 2 x $CH-C_q-S$); 127.08 (s, 1 C, $C_q-C_q=O$); 127.82 (d, 2 C, 2 x $CH-C_q-CH_2$); 131.52 (d, 1 C, $CH-C_q-C_q=O$); 136.45 (s, 1 C, C_q-Cl); 138.67 (s, 1 C, C_q-CH_2); 146.03 (s, 1 C, C_q-S); 159.08 (s, 1 C, C_q-O); 198.16 (s, 1 C, $C_q=O$). HRMS: Calculated mass for $C_{15}H_{12}O_5ClS$ 339.0094; mass found 339.009. Decomposes above 195 °C.

General procedure for the Synthesis of the Target Compounds: Method H:

The appropriate sulfonate (1 mmol) and the appropriate benzaldehyde (1 mmol) were added to a stirred solution of KOH (0.275 g, 2 mmol) in abs EtOH (10 ml), and stirred at room temperature for 24 hours. The precipitate was filtered from solution and allowed to air dry. The precipitate was recrystallized from water, filtered and allowed to air dry.

Method I:

The appropriate sulfonate (1 mmol) and the appropriate benzaldehyde (1 mmol) were added to a stirred solution of KOH (0.414 g, 3 mmol) in abs EtOH (10 ml), and stirred at room temperature for 36 hours. The precipitate was filtered from solution and allowed to air dry. The precipitate was then recrystallized from water, filtered and allowed to air dry.

Potassium 4-(2-{2-[(2E)-3-phenylprop-2-enoyl]phenoxy)methyl}benzenesulfonate (3)

Method H; sulfonate **125** (0.344 g, 1 mmol) and benzaldehyde **67** (0.104 g, 1 mmol) afforded **3** as an off-white solid (0.315 g, 73%). 1H NMR (D_2O , 40°C): δ 5.07 (br.s, 2 H, CH_2); 7.09 (t, $J = 7.5$, 1 H, $CH-CH-C_q-C_q$); 7.16 (d $J = 8.8$, $CH-C_q-O$); 7.25 (d, $J = 16.3$, 1 H, $CH-C_q=O$); 7.31 (d, $J = 7.3$, 2 H, 2x $CH-C_q-CH=CH$); 7.35 (t, J

= 7.6, 2 H, 2x CH-CH-C_q-CH=CH); 7.39 (d, *J* = 7.5, 2 H, 2x CH-C_q-CH₂); 7.38-7.43 (m, 3 H); 7.41 (d, *J* = 16.2, 1 H, CH=CH-C_q=O); 7.50 (d, *J* = 7.5, 1 H, CH-C_q-C_q=O); 7.55 (t, *J* = 8.7, 1 H, CH-CH-C_q-O); 7.58 (d, *J* = 8.2, 2 H, 2x CH-C_q-S). ¹³C NMR (DMSO-*d*₆): δ 71.34 (t, 1 C, CH₂); 115.14 (d, 1 C, CH-C_q-O); 123.12 (d, 1 C, CH-CH-C_q-C_q=O); 127.31 (d, 2 C, 2x CH-C_q-S); 128.28 (d, 1 C, CH-C_q=O); 129.45 (s, 1 C, C_q-C_q=O); 129.66 (d, 2 C, 2x CH-C_q-CH₂); 130.09 (d, 2 C, 2x CH-C_q-CH=CH); 130.74 (d, 2 C, 2x CH-CH-C_q-CH=CH); 131.81 (d, 1 C, CH-C_q-C_q=O); 132.83 (d, 1 C, CH-CH-CH-CH-CH); 135.59 (s, 1 C, C_q-CH=CH-C_q=O); 136.01 (d, 1 C, CH-CH-C_q-O); 140.69 (s, 1 C, C_q-CH₂); 143.43 (s, 1 C, C_q-S); 146.69 (d, 1 C, CH=CH-C_q=O); 158.60 (s, 1 C, C_q-O); 197.10 (s, 1 C, C_q=O). HRMS: Calculated mass for C₂₂H₁₇O₅S 393.0797; mass found 393.0797. Decomposes above 230 °C.

Potassium 4-(2-(2-[(2E)-3-(4-bromophenyl)prop-2-enoyl]phenoxy)methyl)benzenesulfonate (5)

Method H; sulfonate **125** (0.343 g, 1 mmol) and benzaldehyde **63** (0.188 g, 1 mmol) afforded **5** as an off-white solid (0.414 g, 81%). ¹H NMR (D₂O, 40 °C): δ 4.86 (br.s, 2 H, CH₂); 6.78 (d, *J* = 7.4, 2 H, 2x CH-CH-C_q-Br); 6.90-6.95 (m, 2 H, CH-C_q-O and CH-CH-C_q-C_q); 6.95 (d, *J* = 16.7, 1 H, CH-C_q=O); 7.09 (d, *J* = 15.8, 1 H, CH=CH-C_q=O); 7.21 (d, *J* = 7.1, 2 H, 2x CH-C_q-Br); 7.26 (d, *J* = 7.9, 2 H, CH-C_q-CH₂); 7.35 (d, *J* = 7.6, 1 H, CH-C_q-C_q=O); 7.39 (t, *J* = 7.7, CH-CH-C_q-O); 7.57 (d, *J* = 8.2, 2x CH-C_q-S). ¹³C NMR (DMSO-*d*₆): δ 69.85 (t, 1 C, CH₂); 113.55 (CH-C_q-O); 121.44 (d, 1 C, CH-CH-C_q-C_q); 124.67 (s, 1 C, C_q-CH=CH-C_q=O or C_q-C_q=O); 125.79 (d, 2 C, 2x CH-C_q-S); 126.89 (d, 1 C, CH-C_q=O); 127.36 (s, 1 C, C_q-CH=CH-C_q=O or C_q-C_q=O); 128.09 (d, 2 C, 2x CH-C_q-CH₂); 129.72 (d, 2 C, 2x CH-CH-C_q-Br); 130.41 (d, 1 C, CH-C_q-C_q=O); 131.96 (d, 2 C, 2x CH-C_q-Br); 132.99 (s, 1 C, C_q-Br); 134.61 (d, 1 C, CH-CH-C_q-O); 139.10 (s, 1 C, C_q-CH₂); 142.63 (s, 1 C, C_q-S); 143.10 (d, 1 C, CH=CH-C_q=O); 157.21 (s, 1 C, C_q-O); 194.26 (s, 1 C, C_q=O). HRMS: Calculated mass for C₂₂H₁₆O₅BrS 470.9902; mass found 470.9913. Decomposes above 220 °C.

Potassium 4-(2-(2-[(2E)-3-(4-chlorophenyl)prop-2-enoyl]phenoxy)methyl)benzenesulfonate (6)

Method H; sulfonate **125** (0.346 g, 1 mmol) and benzaldehyde **70** (0.145 g, 1 mmol) afforded **6** as an off-white solid (0.351 g, 76%). ¹H NMR (D₂O, 40 °C): δ 4.57 (br.s, 2 H, CH₂); 6.62 (d, *J* = 8.4, 1 H, CH-C_q-O); 6.63 (t, *J* = 7.3, 1 H, CH-CH-C_q-C_q=O); 6.69 (d, *J* = 8.3, 2 H, 2 x CH-C_q-CH=CH); 6.83 (d, *J* = 15.6, 1 H, CH-C_q=O); 6.89 (d, *J* = 8.3, 2 H, 2 x CH-C_q-Cl); 6.98 (d, *J* = 15.8, 1 H, CH=CH-C_q=O); 7.05 (d, *J* = 8.0, 2 H, 2 x CH-CH-C_q-S); 7.08 (t, *J* = 7.7, 1 H, CH-CH-C_q-O); 7.23 (dd, *J* = 7.5, *J* = 1.3, 1 H, CH-C_q-C_q); 7.52 (d, *J* = 8.2, 2 H, 2 x CH-C_q-S). ¹³C NMR (D₂O, 40 °C): δ 69.56 (t, 1 C, CH₂); 113.26 (d, 1 C, CH-C_q-O); 121.00 (d, 1 C,

CH-CH-C_q-C_q=O); 125.79 (d, 2 C, 2 x CH-C_q-S); 126.81 (d, 1 C, CH=CH-C_q=O); 127.62 (s, 1 C, C_q-C_q=O); 127.70 (d, 2 C, 2x CH-CH-C_q-S); 128.92 (d, 2 C, 2 x CH-C_q-Cl); 129.42 (d, 2 C, 2x CH-C_q-CH=CH); 130.41 (d, 1 C, CH-C_q-C_q=O); 132.65 (s, 1 C, C_q-CH=CH); 133.98 (d, 1 C, CH-CH-C_q-O); 135.82 (s, 1 C, C_q-Cl); 138.86 (s, 1 C, C_q-S or C_q-CH₂); 142.13 (d, 1 C, CH=CH-C_q=O); 142.83 (s, 1 C, C_q-S or C_q-CH₂); 157.11 (s, 1 C, C_q-O); 192.35 (s, 1 C, C_q=O). HRMS: Calculated mass for C₂₂H₁₆O₅ClS 427.0407; mass found 427.0412. Decomposes above 220 °C.

Potassium 4-(2-{2-[(2E)-3-(4-fluorophenyl)prop-2-enoyl]phenoxy)methyl}benzenesulfonate (7)

Method H; sulfonate **125** (0.345 g, 1 mmol) and benzaldehyde **72** (0.123 g, 1 mmol) afforded **7** as an off-white solid (0.324 g, 72%). ¹H NMR (D₂O, 40 °C): δ 5.09 (s, 2 H, CH₂); 7.05-7.12 (m, 3 H, 2x CH-C_q-F and CH-CH-C_q-C_q=O); 7.17 (d, J = 15.8, 1 H, CH-C_q=O); 7.18 (d, J = 8.5, 1 H, CH-C_q-O); 7.26-7.30 (m, 2 H, 2x CH-CH-C_q-F); 7.38 (d, J=15.9, 1 H, CH=CH-C_q=O); 7.42 (d, J = 8.2, 2 H, 2x CH-C_q-CH₂); 7.53 (dd, J = 7.7, 1.6, 1 H, CH-C_q-C_q=O); 7.57 (td, J = 7.1, 1.6, 1 H, CH-CH-C_q-O); 7.62 (d, J = 8.1, 2 H, 2x CH-C_q-S). ¹³C NMR (D₂O, 40 °C): δ 71.36 (t, 1 C, CH₂); 115.12 (d, 1 C, CH-C_q-O); 117.66 (dd, ²J_{19F-13C} = 21.7, 2 C, 2x CH-C_q-F); 123.07 (d, 1 C, CH-CH-C_q-C_q=O); 127.30 (d, 2 C, 2x CH-C_q-S); 127.95 (d, 1 C, CH-C_q=O); 129.67 (s, 1 C, C_q-C_q=O or C_q-CH=CH-C_q=O); 129.72 (d, 2 C, 2x CH-C_q-CH₂); 131.82 (d, 1 C, CH-C_q-C_q=O); 131.98 (s, 1 C, C_q-C_q=O or C_q-CH=CH-C_q=O); 132.13 (dd, ³J_{19F-13C} = 9.3, 2 C, 2x CH-CH-C_q-F); 136.03 (d, 1 C, CH-CH-C_q-O); 140.61 (s, 1 C, C_q-CH₂); 144.54 (s, 1 C, C_q-S); 145.24 (d, 1 C, CH=CH-C_q=O); 158.65 (s, 1 C, C_q-O) 166.78 (d, ¹J_{19F-13C} = 250.9, 1 C, C_q-F); 196.59 (s, 1 C, C_q=O). HRMS: Calculated mass for C₂₂H₁₆O₅FS 411.0702; mass found 411.0707. Decomposes above 230 °C.

Potassium 4-(2-{2-[(2E)-3-(4-methoxyphenyl)prop-2-enoyl]phenoxy)methyl}benzenesulfonate (8)

Method H; sulfonate **125** (0.344 g, 1 mmol) and benzaldehyde **99** (0.137 g, 1 mmol) afforded **8** as an off-white solid (0.314 g, 68%). ¹H NMR (D₂O, 40 °C): δ 3.76 (s, 3 H, CH₃); 4.98 (s, 2 H, CH₂); 6.79 (d, J = 8.4, 2 H, 2x CH-CH-C_q-O-CH₃); 6.98-7.13 (m, 5 H, 2x CH-C_q-O-CH₃, CH-C_q=O, CH-C_q-O-CH₂ and CH-CH-C_q-C_q=O); 7.32 (d, J = 15.9, 1 H, CH=CH-C_q=O); 7.36 (d, J = 8.0, 2 H, 2x CH-C_q-CH₂); 7.44-7.55 (m, 2 H, CH-CH-C_q-O-CH₂ and CH-C_q-C_q=O); 7.62 (d, J = 8.2, 2 H, 2x CH-C_q-S). ¹³C NMR (D₂O, 40 °C): δ 57.01 (q, 1 C, CH₃); 71.21 (t, 1 C, CH₂); 114.90 (d, 1 C, CH-C_q-O-CH₂); 116.07 (d, 2 C, 2x CH-CH-C_q-O-CH₃); 122.95 (d, 1 C, CH-CH-C_q-C_q=O); 125.87 (d, 1 C, CH-C_q=O); 127.29 (d, 2 C, 2x CH-C_q-S); 128.45 (s, 1 C, C_q-C_q=O or C_q-CH=CH-C_q=O); 129.31 (s, 1 C, C_q-C_q=O or C_q-CH=CH-C_q=O); 129.68 (d, 2 C, 2x CH-C_q-CH₂); 131.82 (d, 1 C, CH-C_q-C_q=O); 131.99 (d, 2 C, 2x CH-C_q-O-CH₃); 135.80 (d, 1 C, CH-CH-C_q-O-CH₂); 140.54 (s, 1 C, C_q-CH₂); 144.61 (s, 1 C, C_q-S); 146.27 (d, 1 C, CH=CH-C_q=O); 158.57 (s, 1 C, C_q-O-CH₂); 162.87 (s, 1 C,

C_q-O-CH₃); 195.98 (s, 1 C, C_q=O). HRMS: Calculated mass for C₂₃H₁₉O₆S 423.0902; mass found 423.0916. Decomposes above 240 °C.

Potassium 4-(2-(2-[(2E)-3-(3-bromophenyl)prop-2-enoyl]phenoxy)methyl)benzenesulfonate (9)

Method H; sulfonate **125** (0.342 g, 1 mmol) and benzaldehyde **132** (0.186 g, 1 mmol) afforded **9** as an off-white solid (0.373 g, 73%). ¹H NMR (D₂O, 40°C): δ 4.77 (br.s, 2 H, CH₂); 6.77 (t, J = 7.4, 1H, CH-CH-C_q-C_q=O); 6.81 (d, J = 8.5, 1 H, CH-C_q-O) 6.95-6.98 (m, 3 H, CH-C_q=O, CH-C_q-CH=CH and CH-C_q-Br); 7.07 (d, J = 15.7, 1 H, CH=CH-C_q=O) 7.16 (br.s, 1 H, C_q-CH-C_q-Br) 7.19-7.22 (m, 4 H, CH-CH-C_q-O, 2x CH-C_q-CH₂ and CH-CH-C_q-Br); 7.29 (dd, J = 7.6, 1.5, 1 H, CH-C_q-C_q=O) 7.61 (d, J = 8.3, 2 H, 2 x CH-C_q-S). ¹³C NMR (D₂O, 40°C): δ 70.99 (t, 1 C, CH₂); 114.81 (d, 1 C, CH-C_q-O); 122.63 (d, 1C, CH-CH-C_q-C_q); 123.96 (s, 1 C, C_q-Br); 127.31 (d, 2 C, 2x CH-C_q-S); 128.34 (d, 1 C, CH-C_q=O); 129.01 (d, 2 C, 2x CH-C_q-CH₂); 129.16 (d, 1 C, CH-CH-C_q-Br); 129.41 (s, 1 C, C_q-C_q=O); 131.73 (d, 1 C, CH-C_q-C_q); 132.13 (d, 1 C, CH=CH-C_q-CH-CH or CH-CH-C_q-Br) 132.18 (d, 1 C, C_q-CH-C_q-Br); 134.71 (d, 1 C, d, 1 C, CH=CH-C_q-CH-CH or CH-CH-C_q-Br); 135.47 (d, 1 C, CH-CH-C_q-O); 137.76 (s, 1 C, C_q-CH=CH); 140.36 (s, 1 C, C_q-CH₂); 143.39 (s, 1 C, CH=CH-C_q=O); 144.64 (s, 1 C, C_q-S); 158.36 (s, 1 C, C_q-O); 194.48 (s, 1 C, C_q=O). HRMS: Calculated mass for C₂₂H₁₆O₅BrS 470.9902; mass found 470.9902. Decomposes above 210 °C.

Potassium 4-(2-(2-[(2E)-3-(3-chlorophenyl)prop-2-enoyl]phenoxy)methyl)benzenesulfonate (43)

Method H; sulfonate **125** (0.346 g, 1 mmol) and benzaldehyde **133** (0.145 g, 1 mmol) afforded **43** as an off-white solid (0.364 g, 78%). ¹H NMR (D₂O, 40°C): δ 4.80 (s, 2 H, CH₂); 6.79 (t, J = 7.3, 1 H, CH-CH-C_q-C_q=O); 6.85 (d, J = 8.3, 1 H, CH-C_q-O); 6.91 (d, J = 7.1, 1 H, CH-C_q-CH-C_q-Cl); 6.99-7.15 (m, 5 H, C_q-CH-C_q-Cl, CH-CH-C_q-Cl, CH-CH-C_q-Cl, CH-C_q=O and CH=CH-C_q=O); 7.23 (d, J = 8.1, 2 H, 2x CH-C_q-CH₂); 7.26 (t, J = 7.7, 1 H, CH-CH-C_q-O); 7.33 (d, J = 7.4, 1 H, CH-C_q-C_q=O); 7.61 (d, J = 8.1, 2 H, 2x CH-C_q-S). ¹³C NMR (D₂O, 40°C): δ 70.97 (t, 1 C, CH₂); 114.68 (d, 1 C, CH-C_q-O); 122.61 (d, 1 C, CH-CH-C_q-C_q=O); 127.17 (d, 1 C, C_q-CH-C_q-Cl); 127.27 (d, 2 C, 2x CH-C_q-S); 127.81 (d, 1 C, CH-C_q=O or CH-CH-C_q-CH=CH); 127.83 (d, 1 C, CH-C_q=O or CH-CH-C_q-CH=CH); 129.05 (d, 2 C, 2x CH-C_q-CH₂); 129.33 (s, 1 C, C_q-C_q=O); 131.72 (d, 1 C, CH-CH-C_q-Cl); 131.76 (d, 1 C, CH-C_q-C_q=O); 135.49 (d, 1 C, CH-CH-C_q-Cl); 135.55 (s, 1 C, C_q-CH-C_q-Cl or C_q-Cl); 137.48 (s, 1 C, C_q-CH-C_q-Cl or C_q-Cl); 140.21 (s, 1 C, C_q-CH₂); 143.22 (d, 1 C, CH=CH-C_q=O); 144.83 (s, 1 C, C_q-S); 158.42 (s, 1 C, C_q-O); 194.30 (s, 1 C, C_q=O). HRMS: Calculated mass for C₂₂H₁₆O₅ClS 427.0407; mass found 427.0414. Decomposes above 215 °C.

Potassium 4-(2-(2-[(2E)-3-(3-fluorophenyl)prop-2-enoyl]phenoxy)methyl)benzenesulfonate (44)

Method H; sulfonate **125** (0.344 g, 1 mmol) and benzaldehyde **134** (0.124 g, 1 mmol) afforded **44** as an off-white solid (0.342 g, 76%). ¹H NMR (D₂O, 40 °C): δ 5.28 (s, 2 H, CH₂); 7.22 (t, *J* = 7.5, 1 H, CH-CH-C_q-C_q=O); 7.24-7.38 (m, 4 H, CH-C_q-O, CH-CH-C_q-F, C_q-CH-C_q-F and CH-CH-CH-C_q-F); 7.46 (d, *J* = 15.9, 1 H, CH-C_q=O); 7.50-7.59 (m, 4 H, CH=CH-C_q=O, 2x CH-C_q-O and CH-CH-C_q-F); 7.65 (dd, *J* = 7.7, 1.3, 1 H, CH-C_q-C_q=O); 7.67-7.72 (m, 3 H, 2x CH-C_q-S and CH-CH-C_q-O). ¹³C NMR (D₂O, 40 °C): δ 71.05 (t, 1 C, CH₂); 114.94 (d, 1 C, CH-C_q-O); 116.07 (dd, ²*J*_{19F-13C} = 21.1, 1 C, C_q-CH-C_q-F); 119.24 (dd, ²*J*_{19F-13C} = 21.6, 1 C, CH-CH-C_q-F); 122.99 (d, 1 C, CH-CH-C_q-C_q=O); 125.83 (d, 1 C, CH-C_q-CH-C_q-F); 127.13 (d, 2 C, 2x CH-C_q-S); 129.32 (d, 2 C, 2x CH-C_q-CH₂); 129.38 (s, 1 C, C_q-C_q=O); 129.48 (d, 1 C, CH-C_q=O); 131.59 (d, 1 C, CH-C_q-C_q=O); 132.51 (dd, ³*J*_{19F-13C} = 8.1, CH-CH-C_q-F); 135.88 (d, 1 C, CH-CH-C_q-O); 137.83 (d, ³*J*_{19F-13C} = 7.6, 1 C, C_q-CH-C_q-F); 140.78 (s, 1 C, C_q-CH₂); 144.15 (d, 1 C, CH=CH-C_q=O); 145.17 (s, 1 C, C_q-S); 158.42 (s, 1 C, C_q-O); 165.19 (d, ¹*J*_{19F-13C} = 244.7, 1 C, C_q-F); 196.02 (s, 1 C, C_q=O). HRMS: Calculated mass for C₂₂H₁₆O₅FS 411.0702; mass found 411.0706. Decomposes above 230 °C.

Potassium 4-(2-(2-[(2E)-3-(2-bromophenyl)prop-2-enoyl]phenoxy)methyl)benzenesulfonate (10)

Method H; sulfonate **125** (0.346 g, 1 mmol) and benzaldehyde **135** (0.185 g, 1 mmol) afforded **10** as an off-white solid (0.337 g, 66%). ¹H NMR (D₂O, 40 °C): δ 4.87 (br.s, 2 H, CH₂); 6.87 (t, *J* = 7.3, 1 H, CH-CH-C_q-C_q); 6.94 (d, *J* = 8.3, 1 H, CH-C_q-O); 6.99 (d, *J* = 7.9, 1 H, CH-C_q-C_q-Br); 7.01 (d, *J* = 15.1, 1 H, CH-C_q=O); 7.09 (m, 2 H, Br-C_q-C_q-CH-CH and CH-CH-C_q-Br); 7.29 (d, *J* = 8.1, 2 H, 2x CH-C_q-CH₂); 7.32-7.35 (m, 2 H, CH-C_q-Br and CH-CH-C_q-O); 7.40 (d, *J* = 7.7, 1 H, CH-C_q-C_q); 7.61 (d, *J* = 16.1, 1 H CH=CH-C_q); 7.62 (d, *J* = 8.2, 2 H, 2x CH-C_q-S). ¹³C NMR (D₂O, 40 °C): δ 71.17 (t, 1 C, CH₂); 114.61 (d, 1 C, CH-C_q-O); 122.74 (d, 1 C, CH-CH-C_q-C_q); 122.81 (s, 1 C, C_q-C_q=O); 126.79 (s, 1 C, C_q-Br); 127.28 (d, 2 C, 2x CH-C_q-S); 129.01 (d, 1 C, CH-C_q-C_q-Br); 129.46 (d, 2 C, 2x CH-C_q-CH₂); 129.66 (d, 1 C, CH-CH-C_q-C_q-Br or CH-CH-C_q-Br); 130.38 (d, 1 C, CH-C_q=O); 133.54 (d, 1 C, CH-CH-C_q-C_q-Br or CH-CH-C_q-Br); 134.22 (d, 1 C, CH-C_q-Br); 134.75 (s, 1 C, C_q-C_q-Br); 140.23 (s, 1 C, C_q-CH₂); 143.22 (d, 1 C, CH=CH-C_q=O); 144.89 (s, 1 C, C_q-S); 158.62 (s, 1 C, C_q-O); 194.60 (s, 1 C, C_q=O). HRMS: Calculated mass for C₂₂H₁₆O₅BrS 470.9902; mass found 470.9901. Decomposes above 220 °C.

Potassium 4-(2-(2-[(2E)-3-(2-chlorophenyl)prop-2-enoyl]phenoxy)methyl)benzenesulfonate (45)

Method H; sulfonate **125** (0.346 g, 1 mmol) and benzaldehyde **74** (0.148 g, 1 mmol) afforded **45** as an off-white solid (0.317 g, 68%). ¹H NMR (D₂O, 40 °C): δ 4.91 (s, 2 H, CH₂); 6.89 (t, *J* = 7.4, 1 H, CH-CH-C_q-C_q=O); 6.97 (d, *J* = 8.4, 1 H, CH-C_q-O); 7.03 (d, *J* = 8.4, 1 H, CH-C_q-Cl); 7.07-7.13 (m, 2 H, CH-C_q=O

and CH-CH-C_q-C_q-Cl); 7.19-7.22 (m, 2 H, CH-CH-C_q-Cl and CH-C_q-C_q-Cl); 7.31 (d, *J* = 8.1, 2 H, 2x CH-C_q-CH₂); 7.37 (t, *J* = 7.1, 1 H, CH-CH-C_q-O); 7.42 (d, *J* = 7.7, 1 H, CH-C_q-C_q=O); 7.63 (d, *J* = 8.2, 2 H, 2x CH-C_q-S); 7.68 (d, *J* = 15.8, 1 H, CH=CH-C_q=O). ¹³C NMR (D₂O, 40°C): δ 71.07 (t, 1 C, CH₂); 114.61 (d, 1 C, CH-C_q-O); 122.71 (d, 1 C, CH-CH-C_q-C_q=O); 127.24 (d, 2 C, 2x CH-C_q-S); 128.88 (d, 1 C, CH-CH-C_q-C_q=O); 128.96 (s, 1 C, C_q-C_q=O); 129.03 (d, 1 C, CH-CH-C_q-C_q-Cl); 129.41 (d, 2 C, 2x CH-C_q-CH₂); 130.34 (d, 1 C, CH-C_q=O); 131.40 (d, 1 C, CH-CH-C_q-Cl or CH-C_q-C_q-Cl); 131.82 (d, 1 C, CH-C_q-C_q=O); 133.33 (d, 1 C, CH-CH-C_q-Cl or CH-C_q-C_q-Cl); 135.83 (d, 1 C, CH-CH-C_q-O); 135.89 (s, 1 C, C_q-Cl); 140.07 (s, 1 C, C_q-CH₂); 140.24 (d, 1 C, CH=CH-C_q=O); 145.03 (s, 1 C, C_q-S); 158.61 (s, 1 C, C_q-O); 194.48 (s, 1 C, C_q=O). HRMS: Calculated mass for C₂₂H₁₆O₅ClS 427.0407; mass found 427.0413. Decomposes above 205 °C.

Potassium 4-(2-{2-[(2E)-3-(2-fluorophenyl)prop-2-enoyl]phenoxy)methyl}benzenesulfonate (46)

Method H; sulfonate **125** (0.344 g, 1 mmol) and benzaldehyde **136**(0.123 g, 1 mmol) afforded **46** as an off-white solid (0.320 g, 71%). ¹H NMR (D₂O, 40°C): δ 4.99 (s, 2 H, CH₂); 6.91 (t, *J* = 7.5, 1 H, CH-CH-C_q-C_q=O); 6.96 (dd, *J* = 8.6, 10.6, 1 H, CH-C_q-F); 7.01-7.04 (m, 2 H, CH-C_q-O and CH-CH-C_q-C_q-F); 7.13 (t, *J* = 7.6, 1 H, CH-CH-C_q-F); 7.19 (d, *J* = 16.1, 1 H, CH-C_q=O); 7.26-7.28 (m, 3 H, 2x CH-C_q-CH₂ and CH-C_q-C_q-F); 7.35 (d, *J* = 7.6, 1 H, CH-C_q-C_q=O); 7.37 (d, *J* = 16.0, 1 H, CH=CH-C_q=O); 7.39 (td, *J* = 7.8, 1.6, 1 H, CH-CH-C_q-O); 7.45 (d, *J* = 8.2, 2 H, 2x CH-C_q-S). ¹³C NMR (D₂O, 40°C): δ 71.03 (t, 1 C, CH₂); 114.83 (d, 1 C, CH-C_q-O); 117.59 (dd, ²*J*_{19F-13C} = 22.3, 1 C, CH-C_q-F); 122.93 (d, 1 C, CH-CH-C_q-C_q=O); 123.22 (d, ²*J*_{19F-13C} = 10.7, 1 C, C_q-C_q-F); 126.55 (d, 1 C, CH-CH-C_q-C_q-F); 127.12 (d, 2 C, 2x CH-C_q-S); 129.20 (s, 1 C, C_q-C_q=O); 129.31 (d, 2 C, 2x CH-C_q-CH₂); 130.18 (d, 1 C, CH-C_q=O or CH-CH-C_q-F); 130.20 (d, 1 C, CH-C_q=O or CH-CH-C_q-F); 131.64 (d, 1 C, CH-C_q-C_q=O); 134.42 (dd, ³*J*_{19F-13C} = 9.1, 1 C, CH-C_q-C_q-F); 135.92 (d, 1 C, CH-CH-C_q-O); 137.75 (d, 1 C, CH=CH-C_q=O); 140.12 (s, 1 C, C_q-CH₂); 145.15 (s, 1 C, C_q-S); 158.44 (s, 1 C, C_q-O); 162.40 (d, ¹*J*_{19F-13C} = 252.3, 1 C, C_q-F); 195.80 (s, 1 C, C_q=O). HRMS: Calculated mass for C₂₂H₁₆O₅FS 411.0702; mass found 411.0707. Decomposes above 210 °C.

Potassium 4-(2-{2-[(2E)-3-(2-methoxyphenyl)prop-2-enoyl]phenoxy)methyl}benzenesulfonate (47)

Method H; sulfonate **125** (0.345 g, 1 mmol) and benzaldehyde **100** (0.136g, 1 mmol) afforded **47** as an off-white solid (0.296 g, 64%). ¹H NMR (D₂O, 40°C): δ 3.83 (s, 3 H, CH₃); 5.12 (s, 2 H, CH₂); 7.07 (t, *J* = 7.5, 1 H, CH-CH-C_q-C_q-O-CH₃); 7.12 (d, *J* = 8.0, CH-C_q-O-CH₃); 7.19 (t, *J* = 7.5, 1 H, CH-CH-C_q-C_q=O); 7.29 (d, *J* = 8.5, CH-C_q-O-CH₂); 7.38-7.44 (m, 2 H, CH-C_q=O and CH-C_q-C_q-O-CH₃); 7.50-7.55 (m, 3 H, 2x CH-C_q-CH₂ and CH-CH-C_q-O-CH₃); 7.57 (d, *J* = 7.5, 1 H, CH-C_q-C_q=O); 7.64 (t, *J* = 7.3, 1 H, CH-CH-C_q-O-CH₂); 7.69 (d, *J* = 8.1, 2 H, 2x CH-C_q-S); 7.86 (d, *J* = 16.1, 1 H, CH=CH-C_q=O). ¹³C NMR (D₂O, 40°C): δ 56.90 (q, 1 C, CH₃); 70.86 (t,

1 C, CH₂); 113.29 (CH-C_q-O-CH₃); 114.74 (CH-C_q-O-CH₂); 122.55 (d, 1 C, CH-CH-C_q-C_q-O-CH₃); 122.85 (d, 1 C, CH-CH-C_q-C_q=O); 123.87 (s, 1 C, C_q-C_q=O); 127.06 (d, 2 C, 2x CH-C_q-S); 128.34 (d, 1 C, CH-C_q=O); 129.08 (d, 2 C, 2x CH-C_q-CH₂); 129.77 (s, 1 C, C_q-CH=CH-C_q=O); 129.92 (s, 1 C, CH-C_q-C_q-O-CH₃); 131.37 (d, 1 C, CH-C_q-C_q=O); 134.39 (d, 1 C, CH-CH-C_q-O-CH₃); 135.36 (d, 1 C, CH-CH-C_q-O-CH₂); 135.56 (d, 1 C, CH-CH-C_q-O-CH₂); 140.17 (s, 1 C, C_q-CH₂); 141.08 (d, 1 C, CH=CH-C_q=O); 145.16 (s, 1 C, C_q-S); 158.06 (s, 1 C, C_q-O-CH₂); 159.68 (s, 1 C, C_q-O-CH₃); 196.53 (s, 1 C, C_q=O). HRMS: Calculated mass for C₂₃H₁₉O₆S 423.0902; mass found 423.0913. Decomposes above 225 °C.

Potassium 4-((5-fluoro-2-[(2E)-3-phenylprop-2-enoyl]phenoxy)methyl)benzenesulfonate (11)

Method H; sulfonate **126** (0.362 g, 1 mmol) and benzaldehyde **67** (0.106 g, 1 mmol) afforded **11** as an off-white solid (0.387 g, 68%). ¹H NMR (D₂O, 40 °C): δ 5.44 (s, 2 H, CH₂); 7.14 (dd, *J* = 4.1, 2.2, 1 H, CH-C_q-O); 7.35 (dd, *J* = 11.1, 2.1, 1 H, CH-CH-C_q-F); 7.67-7.69 (m, 5 H, 2x CH-C_q-CH=CH, 2x CH-CH-C_q-CH=CH and CH-CH-CH-CH-CH); 7.69 (d, *J* = 15.5, 1 H, CH-C_q=O); 7.74 (d, *J* = 8.2, 2 H, 2x CH-C_q-S); 7.78 (d, *J* = 15.8 (1 H, CH=CH-C_q=O); 7.85 (d, *J* = 8.1, 2 H, 2x CH-C_q-CH₂); 7.92 (dd, *J* = 6.9, 8.6, 1 H, CH-CH-C_q-F). ¹³C NMR (D₂O, 40 °C): δ 71.44 (t, 1 C, CH₂); 102.71 (dd, ²*J*_{19F-13C} = 25.8, 1 C, CH-CH-C_q-F); 109.69 (dd, ²*J*_{19F-13C} = 22.3, 1 C, CH-C_q-O); 125.79 (s, 1 C, C_q-C_q=O); 127.10 (d, 2 C, 2x CH-C_q-S); 127.80 (d, 1 C, CH-C_q=O); 129.43 (d, 2 C, 2x CH-C_q-CH₂); 129.73 (d, 2 C, 2x CH-C_q-CH=CH); 130.63 (d, 2 C, 2x CH-CH-C_q-CH=CH); 132.56 (d, 1 C, CH-CH-CH-CH-CH); 133.79 (dd, ³*J*_{19F-13C} = 11.5, 1 C, CH-CH-C_q-F); 135.31 (s, 1 C, C_q-CH=CH-C_q=O); 139.14 (s, 1 C, C_q-CH₂); 145.49 (d, 1 C, CH=CH-C_q=O); 145.89 (s, 1 C, C_q-S); 160.77 (s, 1 C, C_q-O); 167.07 (d, ¹*J*_{19F-13C} = 252.1, 1 C, C_q-F); 193.64 (s, 1 C, C_q=O). HRMS: Calculated mass for C₂₂H₁₆O₅FS 411.0702; mass found 411.0707. Decomposes above 230 °C.

Potassium 4-((2-[(2E)-3-(4-bromophenyl)prop-2-enoyl]-5-fluorophenoxy)methyl)benzenesulfonate (48)

Method H; sulfonate **126** (0.361 g, 1 mmol) and benzaldehyde **63** (0.187 g, 1 mmol) afforded **48** as an off-white solid (0.369 g, 71%). ¹H NMR (D₂O, 40 °C): δ 5.52 (br.s, 2 H, CH₂); 7.22 (t, *J* = 7.5, 1 H, F-C_q-CH-CH-C_q); 7.44 (d, *J* = 10.7, 1 H, F-C_q-CH-C_q); 7.63 (d, *J* = 8.0, 2 H, 2x CH-C_q-Br); 7.76 (s, 1 H, CH-C_q=O); 7.77 (s, 1 H, CH=CH-C_q); 7.83 (d, *J* = 7.6, 2 H, 2x CH-C_q-CH₂); 7.91 (d, *J* = 7.9, 2x CH-C_q-CH=CH); 7.98 (d, *J* = 6.8, 2 H, 2x CH-C_q-S); 8.01 (d, *J* = 8.6, 1 H, CH-C_q-C_q). ¹³C NMR (D₂O, 40 °C): δ 71.43 (t, 1 C, CH₂); 102.56 (dd, ²*J*_{19F-13C} = 26.4, C_q-CH-C_q-F); 109.45 (dd, ²*J*_{19F-13C} = 22.5, 1 C, F-C_q-CH-CH); 125.54 (s, 1 C, C_q-C_q=O); 125.65 (s, 1 C, C_q-Br); 126.95 (d, 2 C, 2x CH-C_q-S); 128.17 (d, 1 C, CH-C_q=O), 129.22 (d, 2 C,

CH-C_q-CH₂); 131.18 (d, 2 C, 2x CH-C_q-Br); 133.32 (d, 2 C, 2x CH-C_q-CH=CH); 133.68 (dd, ³J_{19F-13C} = 10.8, 1 C, CH-C_q-C_q); 134.46 (s, 1 C, C_q-CH=CH); 138.66 (s, 1 C, C_q-CH₂); 143.46 (d, 1 C, CH=CH-C_q=O); 146.40 (s, 1 C, C_q-S); 160.20 (s, 1 C, C_q-O); 166.83 (d, ¹J_{19F-13C} = 251.3, 1 C, C_q-F); 192.49 (s, 1 C, C_q=O). HRMS: Calculated mass for C₂₂H₁₆O₅BrFS 488.9808; mass found 488.9809. Decomposes above 225 °C.

Potassium 4-((2-[(2E)-3-(4-chlorophenyl)prop-2-enoyl]-5-fluorophenoxy)methyl)benzenesulfonate (49)

Method H; sulfonate **126** (0.361 g, 1 mmol) and benzaldehyde **70** (0.145 g, 1 mmol) afforded **49** as an off-white solid (0.324 g, 67%). ¹H NMR (D₂O, 40°C): δ 5.23 (br.s, 2 H, CH₂); 6.94 (td, J = 8.3, 2.1, 1 H, CH-CH-C_q-F); 7.13 (dd, J = 11.1, 2.0, 1 H, CH-C_q-O); 7.32 (d, J = 8.2, 2 H, 2x CH-CH-C_q-Cl); 7.41 (d, J = 15.9, 1 H, CH-C_q=O); 7.49 (d, J = 8.5, 2 H, 2x CH-C_q-Cl); 7.52 (d, J = 15.8, 1 H, CH=CH-C_q=O); 7.59 (d, J = 8.3, 2 H, 2x CH-C_q-CH₂); 7.73-7.77 (m, 3 H, 2x CH-C_q-S and CH-C_q-C_q). ¹³C NMR (D₂O, 40°C): δ 71.73 (t, 1 C, CH₂); 102.86 (dd, ²J_{19F-13C} = 26.8, 1 C, CH-C_q-O); 109.96 (dd, ²J_{19F-13C} = 20.1, 1 H, CH-CH-C_q-F); 125.40 (s, 1 C, C_q-C_q=O); 127.37 (d, 1 C, 2x CH-C_q-S); 128.33 (d, 1 C, CH-C_q=O); 129.89 (d, 2 C, 2x CH-C_q-CH₂); 130.70 (d, 2 C, 2x CH-C_q-Cl); 131.19 d, 2 C, 2x CH-CH-C_q-Cl); 134.17 (s, 1 C, CH-C_q-CH=CH); 134.20 (dd, ³J_{19F-13C} = 11.2, 1 C, CH-C_q-C_q); 137.60 (s, 1 C, C_q-Cl); 139.60 (s, 1 C, C_q-CH₂); 144.22 (d, 1 C, CH=CH-C_q=O); 145.49 (s, 1 C, C_q-S); 160.81 (s, 1 C, C_q-O); 168.93 (d, ¹J_{19F-13C} = 256.7, 1 C, C_q-F); 193.66 (s, 1 C, C_q=O). HRMS: Calculated mass for C₂₂H₁₆O₅ClFS 445.0313; mass found 448.0308. Decomposes above 230 °C.

Potassium 4-((5-fluoro-2-[(2E)-3-(4-fluorophenyl)prop-2-enoyl]phenoxy)methyl)benzenesulfonate (17)

Method H; sulfonate **126** (0.365 g, 1 mmol) and benzaldehyde **72** (0.123 g, 1 mmol) afforded **17** as an off-white solid (0.323 g, 70%). ¹H NMR (D₂O, 40°C): δ 5.48 (br.s, 2 H, CH₂); 7.19 (td, J = 8.5, 2.5, 1 H, CH-C_q-F-CH-C_q); 7.40 (dd, J = 11.1, 2.0, 1 H, C_q-CH-C_q-F); 7.48 (t, J = 8.8, 2 H, 2x CH-C_q-F); 7.67 (d, J = 16.2, 1H, CH-C_q=O); 7.70-7.76 (m, 2 H, 2x CH-C_q-CH=CH); 7.78 (d, J = 16.0, CH=CH-C_q=O); 7.79 (d, J = 8.2, 2 H, 2x CH-C_q-CH₂); 7.92 (d, J = 8.1, 2 H, 2x CH-C_q-S); 7.95 (dd, J = 7.7, 2.6, CH-C_q-C_q). ¹³C NMR (D₂O, 40°C): δ 71.52 (t, 1 C, CH₂); 102.58 (dd, ²J_{19F-13C} = 24.9, C_q-F-CH-C_q); 109.55 (dd, ²J_{19F-13C} = 22.5, 1 C, CH-CH-C_q-C_q); 117.51 (dd, ²J_{19F-13C} = 19.9, 2 C, 2x CH-C_q-F); 125.64 (s, 1 C, C_q-C_q=O); 127.03 (d, 2 C, 2x CH-C_q-S); 127.55 (d, 1 C, CH-C_q=O); 129.37 (d, 2 C, 2x CH-C_q-CH₂); 131.72 (dd, ¹J_{19F-13C} = 251.7, 2 C, 2x CH-C_q-CH=CH); 133.74 (dd, ²J_{19F-13C} = 11.7, 1 C, CH-C_q-C_q); 138.86 (s, 1 C, C_q-CH₂); 143.87 (d, 1 C, CH=CH-C_q=O); 146.24 (s, 1 C, C_q-S); 146.33 (s, 1 C, C_q-CH=CH); 160.27 (s, 1 C, C_q-O); 163.49 (d, 1 C, ¹J_{19F-13C} = 249.8, CH-CH-C_q-F);

168.12 (d, $^1J_{19F-13C} = 251.1$, 1 C, O-C_q-CH-C_q-F); 192.98 (s, 1 C, C_q=O). HRMS: Calculated mass for C₂₂H₁₆O₅F₂S 429.0608; mass found 429.0598. Decomposes above 210 °C.

Potassium 4-((5-fluoro-2-[(2E)-3-(4-methoxyphenyl)prop-2-enoyl]phenoxy)methyl)benzenesulfonate (50)

Method H; sulfonate **126** (0.365 g, 1 mmol) and benzaldehyde **99** (0.136g, 1 mmol) afforded **50** as an off-white solid (0.259 g, 54%). ¹H NMR (D₂O, 40°C): δ 3.87 (s, 3 H, CH₃); 5.16 (s, 2 H, CH₂); 6.90 (t, $J = 8.4$, 1 H, CH-CH-C_q-F); 6.96 (d, $J = 8.6$, 2 H, 2x CH-C_q-O-CH₃); 7.06 (d, $J = 10.7$, 1 H, CH-C_q-O-CH₂); 7.28 (d, $J = 8.0$, 2 H, 2x CH-C_q-CH=CH); 7.29 (d, $J = 15.7$, 1 H, CH-C_q=O); 7.51 (d, $J = 15.7$, 1 H, CH=CH-C_q=O); 7.55 (d, $J = 8.0$, 2 H, 2x CH-C_q-CH₂); 7.70 (t, $J = 7.8$, CH-C_q-C_q=O); 7.75 (d, $J = 8.1$, 2 H, 2x CH-C_q-S). ¹³C NMR (D₂O, 40°C): δ 56.99 (q, 1 C, CH₃); 71.65 (t, 1 C, CH₂); 102.70 (dd, $^2J_{19F-13C} = 24.5$, 1 C, CH-C_q-O-CH₂); 109.83 (dd, $^2J_{19F-13C} = 21.6$, 1 C, CH-CH-C_q-F); 116.08 (d, 2 C, 2x CH-C_q-O-CH₃); 125.51 (d, 1 C, CH-C_q=O); 125.56 (s, 1 C, C_q-C_q=O); 127.30 (d, 2 C, 2x CH-C_q-S); 128.35 (s, 1 C, C_q-CH=CH-C_q=O); 129.82 (d, 2 C, 2x CH-C_q-CH₂); 131.88 (dd, $^3J_{19F-13C} = 10.1$, 2 C, 2x CH-C_q-CH=CH); 134.09 (d, 1 C, CH-C_q-C_q=O); 139.60 (s, 1 C, C_q-CH₂); 145.39 (s, 1 C, C_q-S); 145.80 (d, 1 C, CH=CH-C_q=O); 160.53 (d, $^3J_{19F-13C} = 11.0$, C_q-O-CH₂); 162.87 (s, 1 C, C_q-O-CH₃); 167.41 (d, $^1J_{19F-13C} = 251.0$; 1 C, C_q-F); 193.48 (s, 1 C, C_q=O). HRMS: Calculated mass for C₂₃H₁₈O₆FS 441.0808; mass found 441.0798. Decomposes above 230 °C.

Potassium 4-((2-[(2E)-3-(3-bromophenyl)prop-2-enoyl]-5-fluorophenoxy)methyl)benzenesulfonate (51)

Method H; sulfonate **126** (0.364 g, 1 mmol) and benzaldehyde **132** (0.187 g, 1 mmol) afforded **51** as an off-white solid (0.333 g, 63%). ¹H NMR (D₂O, 40°C): δ 5.10 (br.s, 2 H, CH₂); 6.85 (td, $J = 8.3, 2.1$, 1 H, CH-CH-C_q-F); 6.99 (dd, $J = 11.3, 2.1$, 1 H, CH-C_q-O); 7.16 (d, $J = 7.6$, 1 H, CH-CH-CH-C_q-Br); 7.26 (t, $J = 7.8$, 1 H, CH-CH-C_q-Br); 7.28 (d, $J = 15.9$, 1 H, CH-C_q=O); 7.36 (d, $J = 15.8$, 1 H, CH=CH-C_q=O); 7.48 (d, $J = 8.2$, 2 H, 2x CH-C_q-CH₂); 7.53 (s, 1 H, C_q-CH-C_q-Br); 7.54 (d, $J = 8.2$, 1 H, CH-CH-C_q-Br); 7.63 (dd, $J = 8.6, 1.6$, 1 H, CH-C_q-C_q); 7.69 (d, $J = 8.2$, 2 H, 2x CH-C_q-S). ¹³C NMR (D₂O, 40°C): δ 71.64 (t, 1 C, CH₂); 102.80 (dd, $^2J_{19F-13C} = 27.1$, 1 C, CH-C_q-O); 109.99 (dd, $^2J_{19F-13C} = 21.7$, 1 C, CH-CH-C_q-F); 124.00 (s, 1 C, C_q-CH-C_q-Br); 125.48 (s, 1 C, C_q-C_q=O); 127.39 (d, 2 C, 2x CH-C_q-S); 128.42 (d, 1 C, CH-CH-CH-C_q-Br); 129.04 (d, 1 C, CH-C_q=O); 129.58 (d, 2 C, 2x CH-C_q-CH₂); 132.35 (d, 1 C, CH-C_q-Br or CH-CH-C_q-Br); 132.37 (d, 1 C, CH-C_q-Br or CH-CH-C_q-Br); 134.34 (d, 1 C, CH-C_q-C_q); 135.02 (d, 1 C, CH-CH-C_q-Br); 137.76 (s, 1 C, C_q-Br);

139.73 (s, 1 C, C_q-CH₂); 143.45 (d, 1 C, CH=CH-C_q=O); 145.07 (s, 1 C, C_q-S); 160.64 (s, 1 C, C_q-O); 193.58 (s, 1 C, C_q=O); C_q-F not observed. HRMS: Calculated mass for C₂₂H₁₆O₅BrFS 488.9808; mass found 488.9803. Decomposes above 210 °C.

Potassium 4-((2-[(2E)-3-(3-chlorophenyl)prop-2-enoyl]-5-fluorophenoxy)methyl)benzenesulfonate (52)

Method H; sulfonate **126** (0.361 g, 1 mmol) and benzaldehyde **133** (0.144 g, 1 mmol) afforded **52** as an off-white solid (0.310 g, 64%). ¹H NMR (D₂O, 40°C): δ 5.21 (br.s, 2 H, CH₂); 6.94 (t, *J* = 7.9, 1 H, CH-CH-C_q-F); 7.12 (d, *J* = 10.5, 1 H, CH-C_q-O); 7.25 (d, *J* = 7.3, 1 H, CH-C_q-CH=CH); 7.39-7.53 (m, 5 H, 2x CH-C_q-Cl, CH-CH-C_q-Cl,); 7.58 (d, *J* = 7.3, 2 H, 2x CH-C_q-CH₂); 7.73 (dd, *J* = 7.8, 2.3, 1 H, CH-C_q-C_q); 7.77 (d, *J* = 7.3, 2 H, 2x CH-C_q-S). ¹³C NMR (D₂O, 40°C): δ 71.59 (t, 1 C, CH₂); 102.65 (dd, ²*J*_{19F-13C} = 26.9, 1 C, CH-C_q-O); 109.78 (dd, ²*J*_{19F-13C} = 20.8, 1 C, CH-C_q-F); 125.41 (s, 1 C, C_q-C_q=O); 127.22 (d, 2 C, 2x CH-C_q-S); 127.72 (d, 1 C, CH-C_q-CH=CH); 128.92 (d, 1 C, CH-C_q=O); 129.31 (d, 1 C, C_q-CH-C_q-Cl); 129.38 (d, 2 C, 2x CH-C_q-CH₂); 131.92 (s, 1 C, CH-CH-C_q-Cl or CH-CH-C_q-Cl); 132.15 (s, 1 C, CH-CH-C_q-Cl or CH-CH-C_q-Cl); 134.11 (dd, ³*J*_{19F-13C} = 11.4, 1 C, CH-C_q-C_q); 135.52 (s, 1 C, C_q-Cl); 137.40 (s, 1 C, C_q-CH=CH); 139.25 (s, 1 C, C_q-CH₂); 143.06 (d, 1 C, CH=CH-C_q=O); 145.62 (s, 1 C, C_q-S); 160.52 (d, ³*J*_{19F-13C} = 11.4, 1 C, C_q-O); 168.66 (d, ¹*J*_{19F-13C} = 253.6, 1 C, C_q-F); 192.80 (s, 1 C, C_q=O). HRMS: Calculated mass for C₂₂H₁₆O₅FCIS 445.0313; mass found 445.0314. Decomposes above 220 °C.

Potassium 4-((5-fluoro-2-[(2E)-3-(3-fluorophenyl)prop-2-enoyl]phenoxy)methyl)benzenesulfonate (53)

Method H; sulfonate **126** (0.361 g, 1 mmol) and benzaldehyde **134** (0.125 g, 1 mmol) afforded **53** as an off-white solid (0.323 g, 69%). ¹H NMR (D₂O, 40°C): δ 5.39 (br.s, 2 C, CH₂); 7.10 (td, *J* = 8.4, 2.3, 1 H, CH-CH-C_q-F); 7.30 (dd, *J* = 11.0, 2.3, 1 H, CH-C_q-O); 7.41 (d, *J* = 7.4, 1 H, CH-C_q-CH=CH); 7.42 (td, *J* = 8.5, 2.2, 1 H, CH-CH-C_q-F); 7.50 (d, *J* = 9.7, 1 C, C_q-CH-C_q-F); 7.61-7.73 (m, 3 H, CH=CH-C_q=O, CH-C_q=O and CH-CH-C_q-F); 7.71 (d, *J* = 7.9, 2 H, CH-C_q-CH₂); 7.82 (d, *J* = 8.3, 2 H, CH-C_q-S); 7.87 (dd, *J* = 7.9, 3.1, CH-C_q-C_q). ¹³C NMR (D₂O, 40°C): δ 71.42 (t, 1 C, CH₂); 102.75 (dd, ²*J*_{19F-13C} = 27.8, 1 C, CH-C_q-O); 109.76 (dd, ²*J*_{19F-13C} = 22.3, 1 C, CH-CH-C_q-C_q); 116.11 (dd, ²*J*_{19F-13C} = 22.4, 1 C, C_q-CH-C_q-F); 118.99 (dd, ²*J*_{19F-13C} = 22.1, 1 C, CH-CH-CH-C_q-F); 125.46 (d, 1 C, CH-C_q-CH=CH); 125.65 (2, 1 C, C_q-C_q=O); 127.07 (d, 2 C, 2x CH-C_q-S); 129.11 (d, 1 C, CH-C_q=O); 129.26 (d, 2 C, 2x CH-C_q-CH₂); 132.45 (dd, ³*J*_{19F-13C} = 8.2, 1 C, CH-CH-CH-C_q-F); 133.89 (dd, ³*J*_{19F-13C} = 12.3, 1 C, CH-C_q-C_q); 137.75 (d, ²*J*_{19F-13C} = 7.7, 1 C, C_q-CH=CH); 139.09 (s, 1 C, CH-C_q-CH₂); 143.39 (d, 1 C, CH=CH-C_q=O); 145.88 (s, 1 C, C_q-S); 160.34 (d, ³*J*_{19F-13C} = 11.6, 1 C, C_q-O); 164.92 (d, ¹*J*_{19F-13C} = 248.9, 1 C, F-C_q-CH-C_q-O); 167.73 (d, ¹*J*_{19F-13C} = 252.3, 1 C, F-C_q-CH-C_q);

193.21 (s, 1 C, C_q=O). HRMS: Calculated mass for C₂₂H₁₆O₅F₂S 429.0608; mass found 429.0602. Decomposes above 215 °C.

Potassium 4-((2-[(2E)-3-(2-bromophenyl)prop-2-enoyl]-5-fluorophenoxy)methyl)benzenesulfonate (23)

Method H; sulfonate **126** (0.363 g, 1 mmol) and benzaldehyde **135** (0.189 g, 1 mmol) afforded **23** as an off-white solid (0.328 g, 62%). ¹H NMR (D₂O, 40°C): δ 5.41 (br.s, 2 H, CH₂); 7.13 (t, J = 7.8, 1 H, CH-CH-C_q-F); 7.33 (d, J = 10.4, 1 H, CH-C_q-O), 7.48 (d, J = 7.3, 1 H, CH-C_q-C_q-Br); 7.52-7.63 (m, 3 H, CH-CH-C_q-C_q-Br, CH-CH-C_q-Br and CH-C_q=O), 7.73 (d, J = 7.8, 2 H, 2x CH-C_q-CH₂); 7.87 (d, J = 8.3, 2 H, 2x CH-C_q-S); 7.89 (d, J = 7.4, 1 H, CH-C_q-Br); 7.92 (d, J = 7.3, 1 H, CH-C_q-C_q=O); 8.01 (d, J = 16.1, 1 H, CH=CH-C_q-C_q-Br). ¹³C NMR (D₂O, 40°C): δ 71.50 (t, 1 C, CH₂); 102.58 (dd, ²J_{19F-13C} = 26.9, 1 C, CH-C_q-O); 109.70 (dd, ²J_{19F-13C} = 21.8, 1 C, CH-C_q-F); 125.32 (s, 1 C, C_q-C_q=O); 126.32 (s, 1 C, C_q-C_q-Br); 127.07 (d, 2 C, 2x CH-C_q-S); 128.98 (d, 1 C, CH-C_q-C_q-Br); 129.40 (d, 2 C, CH-C_q-CH₂); 129.77 (d, 1 C, CH-C_q=O); 130.27 (d, 1 C, CH-CH-C_q-C_q-Br or CH-CH-C_q-Br); 133.62 (d, 1 C, CH-CH-C_q-C_q-Br or CH-CH-C_q-Br); 133.99 (dd, ³J_{19F-13C} = 14.3, 1 C, CH-C_q-C_q); 134.62 (d, 1 C, CH-C_q-Br); 134.76 (s, 1 C, C_q-Br); 138.84 (s, 1 C, C_q-CH₂); 142.36 (d, 1 C, CH=CH-C_q=O); 146.09 (s, 1 C, C_q-S); 160.45 (s, 1 C, C_q-O); 167.27 (d, ¹J_{19F-13C} = 251.9, 1 C, C_q-F); 192.49 (s, 1 C, C_q=O). HRMS: Calculated mass for C₂₂H₁₆O₅BrFS 488.9808; mass found 488.9814. Decomposes above 240 °C.

Potassium 4-((2-[(2E)-3-(2-chlorophenyl)prop-2-enoyl]-5-fluorophenoxy)methyl)benzenesulfonate (54)

Method H; sulfonate **126** (0.364 g, 1 mmol) and benzaldehyde **74** (0.145 g, 1 mmol) afforded **54** as an off-white solid (0.324 g, 67%). ¹H NMR (D₂O, 40°C): δ 5.41 (br.s, 1 H, CH₂); 7.13 (t, J = 10.9, 1 H, CH-C_q-F); 7.33 (d, J = 6.8, 1 H, CH-C_q-O); 7.51 (t, J = 7.8, 1 H, CH-CH-C_q-C_q-Cl); 7.55 (t, J = 7.8, 1 H, CH-CH-C_q-Cl); 7.61-7.69 (m, 3 H, CH-C_q=O, CH-C_q-Cl and CH=C_q-C_q-Cl); 7.73 (d, J = 8.3; 2 H, 2x CH-C_q-CH₂); 7.87 (d, J = 8.7, 2 H, 2x CH-C_q-S); 7.92 (d, J = 8.3, 1 H, CH-C_q-C_q=O); 8.06 (d, J = 16.1, 1 H, CH=CH-C_q=O). ¹³C NMR (D₂O, 40°C): δ 71.49 (t, 1 C, CH₂); 102.59 (dd, ²J_{19F-13C} = 25.8, 1 C, CH-C_q-O); 109.70 (dd, ²J_{19F-13C} = 23.3, 1 C, CH-C_q-F); 125.31 (s, 1 C, C_q-C_q=O); 127.06 (d, 2 C, 2x CH-C_q-S); 128.81 (d, 1 C, CH-CH-C_q-C_q-Cl or CH-CH-C_q-Cl); 129.18 (d, 1 C, CH-CH-C_q-C_q-Cl or CH-CH-C_q-Cl); 129.40 (d, 2 C, 2x CH-C_q-CH₂); 130.12 (d, 1 C, CH-C_q=O); 131.35 (d, 1 C, CH-C_q-Cl); 133.07 (s, 1 C, C_q-Cl); 133.46 (d, 1 C, CH-C_q-C_q-Cl); 133.98 (dd, ³J_{19F-13C} = 10.4, 1 C, CH-C_q-C_q=O); 135.55 (s, 1 C, C_q-C_q-Cl); 138.85 (2, 1 C, C_q-CH₂); 139.66 (d, 1 C, CH=CH-C_q=O); 146.05 (s, 1 C, C_q-S); 160.44 (d, ³J_{19F-13C} = 11.9, 1 C, C_q-O); 167.26 (d, ¹J_{19F-13C} = 252.1, 1 C, C_q-F); 192.54 (s, 1 C, C_q=O). HRMS: Calculated mass for C₂₂H₁₆O₅FCIS 445.0313; mass found 445.0307. Decomposes above 230 °C.

Potassium 4-((5-fluoro-2-[(2E)-3-(2-fluorophenyl)prop-2-enoyl]phenoxy)methyl)benzenesulfonate (55)

Method H; sulfonate **126** (0.365 g, 1 mmol) and benzaldehyde **136** (0.125 g, 1 mmol) afforded **55** as an off-white solid (0.319 g, 68%). ¹H NMR (D₂O, 40°C): δ 5.19 (br.s, 2 H, CH₂); 6.92 (t, *J* = 8.3, 1 H, CH-C_q-F); 7.09 (d, *J* = 10.6, 1 H, CH-C_q-O); 7.24 (t, *J* = 9.2, 1 H, CH-C_q-C_q); 7.25-7.33 (m, 2 H, CH-C_q-C_q-F and CH-CH-C_q-C_q-F), 7.48 (d, *J* = 15.8, 1 H, CH-C_q=O); 7.55 (t, *J* = 7.1, 1 H, CH-CH-CH-C_q-F); 7.56 (d, *J* = 8.0, 2 H, CH-C_q-CH₂); 7.65 (d, *J* = 15.9, 1 H, CH=CH-C_q=O); 7.72 (t, *J* = 7.6, 1 H, CH-C_q-C_q=O); 7.75 (d, *J* = 7.7, 2 H, CH-C_q-S). ¹³C NMR (D₂O, 40°C): δ 71.54 (t, 1 C, CH₂); 102.61 (dd, ²*J*_{19F-13C} = 25.4, CH-C_q-O); 109.79 (dd, ²*J*_{19F-13C} = 22.0, 1 C, CH-C_q-F); 117.50 (dd, ²*J*_{19F-13C} = 22.1, 1 C, CH-C_q-C_q-CH=CH); 123.13 (d, ²*J*_{19F-13C} = 11.8, 1 C, C_q-C_q-F); 125.31 (s, 1 C, C_q-C_q=O); 126.45 (d, 1 C, CH-C_q-C_q-F or CH-CH-C_q-C_q-F); 127.14 (d, 2 C, 2x CH-C_q-S); 129.48 (d, 2 C, 2x CH-C_q-CH₂); 129.70 (d, 1 C, CH-C_q=O); 129.86 (d, 1 C, CH-C_q-C_q-F or CH-CH-C_q-C_q-F); 134.12 (dd, ³*J*_{19F-13C} = 9.8, 1 C, CH-CH-CH-C_q-F); 134.28 (dd, ³*J*_{19F-13C} = 8.7, 1 C, CH-C_q-C_q=O); 136.71 (s, 1 C, CH=CH-C_q=O); 139.22 (s, 1 C, C_q-CH₂); 145.57 (s, 1 C, C_q-S); 160.60 (s, 1 C, C_q-O); 162.16 (d, ¹*J*_{19F-13C} = 251.3, C_q-C_q-F); 167.36 (d, ¹*J*_{19F-13C} = 253.4, 1 C, C_q-CH-C_q-F); 192.89 (s, 1 C, C_q=O); HRMS: Calculated mass for C₂₂H₁₆O₅F₂S 429.0608; mass found 429.0599. Decomposes above 220 °C.

Potassium 4-((5-fluoro-2-[(2E)-3-(2-methoxyphenyl)prop-2-enoyl]phenoxy)methyl)benzenesulfonate (56)

Method H; sulfonate **126** (0.364 g, 1 mmol) and benzaldehyde **100** (0.136 g, 1 mmol) afforded **56** as an off-white solid (0.317 g, 66%). ¹H NMR (D₂O, 40°C): δ 3.70 (s, 3 H, CH₃); 5.11 (s, 2 H, CH₂); 6.82 (td, *J* = 8.3, 2.2, 1 H, CH-CH-C_q-F); 6.93 (t, *J* = 7.5, 1 H, CH-CH-C_q-C_q-O-CH₃); 6.99 (d, *J* = 8.6, 1 H, CH-C_q-O-CH₃); 7.01 (dd, *J* = 11.8, 2.8, 1 H, CH-C_q-O-CH₂); 7.29 (dd, *J* = 7.7, 1.4, 1 H, CH-CH-C_q-O-CH₃); 7.34-7.40 (m, 4 H, 2x CH-C_q-S, CH-C_q-C_q-O-CH₃ and CH-C_q=O); 7.51 (d, *J* = 8.2, 2 H, 2x CH-C_q-CH₂); 7.54 (dd, *J* = 6.9, 8.6, 1 H, CH-C_q-C_q=O); 7.72 (d, *J* = 16.0, 1 H, CH=CH-C_q=O). ¹³C NMR (D₂O, 40°C): δ 56.72 (d, 1 C, CH₃); 71.10 (t, 1 C, CH₂); 102.46 (dd, ²*J*_{19F-13C} = 27.2, 1 C, CH-C_q-O); 109.31 (dd, ²*J*_{19F-13C} = 21.6, 1 C, CH-CH-C_q-F); 113.00 (d, 1 C, CH-C_q-O-CH₃); 122.27 (d, 1 C, CH-CH-C_q-CH=CH); 123.56 (s, 1 C, C_q-C_q-O-CH₃); 126.11 (s, 1 C, C_q-C_q=O); 126.78 (d, 2 C, 2x CH-C_q-S); 127.80 (d, 1 C, CH-C_q=O); 128.68 (d, 2 C, 2x CH-C_q-CH₂); 128.79 (d, 1 C, CH-C_q-C_q-O-CH₃); 129.46 (d, 1 C, CH-CH-C_q-O-CH₃); 133.27 (dd, ²*J*_{19F-13C} = 11.9, 1 C, CH-CH-C_q-F); 138.65 (s, 1 C, C_q-CH₂); 139.94 (d, 1 C, CH=CH-C_q=O); 146.18 (s, 1 C, C_q-S); 159.30 (s, 1 C, C_q-O-CH₃);

159.67 (d, $^3J_{19F-13C} = 11.1$, 1 C, C_q-O-CH₂); 166.45 (d, $^1J_{19F-13C} = 250.8$, 1 C, C_q-F); 193.34 (s, 1 C, C_q=O). HRMS: Calculated mass for C₂₃H₁₈O₅FS 441.0808; mass found 441.0798. Decomposes above 220 °C.

Potassium 4-((5-chloro-2-[(2E)-3-phenylprop-2-enoyl]phenoxy)methyl)benzenesulfonate (12)

Method I: sulfonate **127** (0.379 g, 1 mmol) and benzaldehyde **67** (0.106 g, 1 mmol) afforded **12** as an off-white solid (0.322 g, 69%). ¹H NMR (D₂O, 40°C): δ 5.13 (s, 2 H, CH₂); 7.07 (dd, $J = 8.2, 1.6$, 1 H, CH-CH-C_q-Cl); 7.26 (d, $J = 1.5$, 1 H, C_q-CH-C_q-Cl); 7.33 (d, $J = 16.0$, 1 H, CH-C_q=O); 7.36-7.74 (m, 7 H, 2x CH-C_q-CH₂), 2x CH-C_q-CH=CH, 2 X CH-CH-C_q-CH=CH and CH-CH-CH-CH-CH); 7.44 (d, $J = 15.7$, 1 H, CH=CH-C_q=O); 7.51 (d, $J = 8.3$, 1 H, CH-C_q-C_q=O); 7.54 (d, $J = 8.1$, 2 H, 2x CH-C_q-S). ¹³C NMR (D₂O, 40°C): δ 71.22 (t, 1 C, CH₂); 114.93 (d, 1 C, CH-C_q-O); 122.57 (d, 1 C, CH-CH-C_q-Cl); 126.88 (d, 2 C, 2x CH-C_q-S); 128.04 (s, 1 C, C_q-C_q=O); 128.79 (d, 1 C, CH-C_q=O); 128.92 (d, 2 C, 2x CH-C_q-CH₂); 129.51 (d, 2 C, 2x CH-C_q-CH=CH) 130.39 (d, 2 C, 2x CH-CH-C_q-CH=CH); 132.31 (d, 1 C, CH-CH-CH-CH-CH); 135.06 (s, 1 C, C_q-CH=CH-C_q=O); 138.71 (s, 1 C, C_q-CH₂); 139.45 (s, 1 C, C_q-Cl); 145.42 (d, 1 C, CH=CH-C_q=O); 146.18 (s, 1 C, C_q-S); 158.67 (s, 1 C, C_q-O); 193.32 (s, 1 C, C_q=O). HRMS: Calculated mass for C₂₂H₁₆O₅ClS 427.0407; mass found 427.0410. Decomposes above 215 °C.

Potassium 4-((5-chloro-2-[(2E)-3-(4-methoxyphenyl)prop-2-enoyl]phenoxy)methyl)benzenesulfonate (57)

Method I: sulfonate **127** (0.377 g, 1 mmol) and benzaldehyde **99** (0.136 g, 1 mmol) afforded **57** as an off-white solid (0.323 g, 65%). ¹H NMR (D₂O, 40°C): δ 3.69 (s, 3 H, CH₃); 4.82 (br.s, 2 H, CH₂); 6.67 (d, $J = 8.5$, 2 H, 2x CH-C_q-CH=CH); 6.90 (d, $J = 8.1$, 2 H, 2x CH-C_q-O-CH₃); 6.97-7.01 (m, 3 H, 2x CH-C_q-Cl and CH-C_q=O), 7.25 (d, $J = 15.4$, 1 H, CH=CH-C_q=O); 7.31 (d, $J = 8.1$, 2 H, 2x CH-C_q-CH₂); 7.57 (d, $J = 8.1$, 1 H, CH-C_q-C_q=O); 7.67 (d, $J = 7.7$, 2 H, 2x CH-C_q-S). ¹³C NMR (D₂O, 40°C): δ 56.81 (q, 1 C, CH₃); 71.46 (t, 1 C, CH₂); 114.74 (d, 1 C, CH-C_q-O-CH₂); 115.7 (d, 2 C, 2x CH-C_q-CH=CH); 122.78 (d, 1 C, CH-CH-C_q-Cl); 125.27 (d, 1 C, CH-C_q=O); 127.28 (d, 2 C, 2x CH-C_q-S); 127.78 (s, 1 C, C_q-C_q=O or CH=CH-C_q-CH); 128.28 (s, 1 C, C_q-C_q=O or CH=CH-C_q-CH); 129.53 (d, 2 C, 2x CH-C_q-CH₂); 131.35 (d, 1 C, CH-C_q-O-CH₃); 133.43 (d, 1 C, CH-C_q-C_q=O); 139.36 (s, 1 C, C_q-CH₂); 140.46 (s, 1 C, C_q-Cl); 144.85 (d, 1 C, CH=CH-C_q=O); 145.24 (s, 1 C, C_q-S); 161.39 (s, 1 C, C_q-O-CH₃); 162.43 (s, 1 C, C_q-O-CH₂); 191.53 (s, 1 C, C_q=O). HRMS: Calculated mass for C₂₃H₁₈O₆ClS 457.0513; mass found 457.0518. Decomposes above 220 °C.

Potassium 4-((5-chloro-2-[(2E)-3-(3-chlorophenyl)prop-2-enoyl]phenoxy)methyl)benzenesulfonate (58)

Method I; sulfonate **127** (0.378 g, 1 mmol) and benzaldehyde **134** (0.124 g, 1 mmol) afforded **58** as an off-white solid (0.306 g, 61%). ¹H NMR (D₂O, 40°C): 5.10 (s, 2 H, CH₂); 7.06 (d, *J* = 8.3, 1 H, C_q-CH-CH-C_q-Cl); 7.17 (s, 1 H, C_q-CH-C_q-CH=CH); 7.24 (s, 1 H, CH-C_q-O); 7.31 (d, *J* = 15.9, 1 H, CH-C_q=O); 7.33-7.45 (m, 4 H, CH=CH-C_q=O, CH-CH-CH-C_q-Cl, CH-CH-CH-C_q-Cl and CH-CH-CH-C_q-Cl); 7.48 (d, *J* = 8.1, 2 H, 2x CH-C_q-CH₂); 7.53 (d, *J* = 8.3, 1 H, CH-C_q-C_q=O); 7.71 (d, *J* = 8.1, 2 H, 2x CH-C_q-S). ¹³C NMR (D₂O, 40°C): δ 70.36 (t, 1 C, CH₂); 115.15 (d, 1 C, CH-C_q-O); 122.95 (d, 1 C, C_q-CH-CH-C_q-Cl); 127.27 (d, 2 C, 2x CH-C_q-S); 127.74 (s, 1 C, C_q-C_q=O); 127.92 (d, 1 C, C_q-CH-C_q-CH=CH); 128.86 (d, 1 C, CH-C_q=O); 129.38 (d, 2 C, 2x CH-C_q-CH₂); 131.70 (d, 1 C, CH-C_q-CH=CH); 132.08 (d, 1 C, CH-CH-C_q-CH=CH or CH-CH-CH-C_q-Cl); 133.09 (d, 1 C, CH-C_q-C_q=O); 135.61 (s, 1 C, CH-CH-CH-C_q-Cl or O-C_q-CH-C_q-Cl); 137.37 (s, 1 C, CH-CH-CH-C_q-Cl or O-C_q-CH-C_q-Cl); 139.42 (s, 1 C, C_q-CH₂); 143.59 (d, 1 C, CH=CH-C_q=O); 145.44 (s, 1 C, C_q-S); 159.20 (s, 1 C, C_q-O); 193.34 (s, 1 C, C_q=O). HRMS: Calculated mass for C₂₂H₁₅O₅Cl₂FS 461.0017; mass found 461.0019. Decomposes above 210 °C.

Potassium 4-((5-chloro-2-[(2E)-3-(2-chlorophenyl)prop-2-enoyl]phenoxy)methyl)benzenesulfonate (59)

Method I; sulfonate **127** (0.380 g, 1 mmol) and benzaldehyde **74** (0.147 g, 1 mmol) afforded **59** as an off-white solid (0.301 g, 60%). ¹H NMR (D₂O, 40°C): δ 5.42 (s, 2 H, CH₂); 7.38 (d, *J* = 8.4, 1 H, CH-CH-C_q-Cl); 7.54-7.58 (m, 3 H, CH-C_q-O, CH-CH-CH-C_q-Cl and CH-CH-C_q-C_q-Cl); 7.59 (d, *J* = 16.0, 1 H, CH-C_q=O); 7.66 (td, *J* = 7.4, 1.7, 1 H, CH-CH-CH-C_q-Cl); 7.71 (d, *J* = 8.4, 1 H, CH-C_q-C_q-Cl); 7.73 (d, *J* = 8.3, 2 H, 2x CH-C_q-CH₂); 7.83 (d, *J* = 8.3, 1 H, CH-CH-C_q-C_q=O); 7.90 (d, *J* = 8.0, 2 H, 2x CH-C_q-S); 8.06 (d, *J* = 15.9, 1 H, CH=CH-C_q=O). ¹³C NMR (D₂O, 40°C): δ 71.49 (t, 1 C, CH₂); 115.05 (d, 1 C, CH-C_q-O); 122.86 (d, 1 C, CH-CH-C_q-C_q=O); 127.08 (d, 2 C, 2x CH-C_q-S); 127.57 (s, 1 C, C_q-C_q=O); 128.89 (d, 1 C, CH-CH-CH-C_q-Cl or CH-CH-CH-C_q-Cl); 129.17 (d, 1 C, CH-CH-CH-C_q-Cl or CH-CH-CH-C_q-Cl); 129.30 (d, 2 C, 2x CH-C_q-CH₂); 130.02 (d, 1 C, CH-C_q=O); 131.38 (d, 1 C, CH-C_q-C_q-Cl); 132.93 (d, 1 C, CH-C_q-C_q=O); 133.03 (s, 1 C, C_q-C_q-Cl); 133.54 (d, 1 C, CH-CH-CH-C_q-Cl); 135.63 (s, 1 C, C_q-CH=CH-C_q=O); 139.02 (s, 1 C, C_q-CH₂); 140.30 (d, 1 C, CH=CH-C_q=O); 140.54 (s, 1 C, O-C_q-CH-C_q-Cl); 145.84 (s, 1 C, C_q-S); 159.08 (s, 1 C, C_q-O); 193.25 (s, 1 C, C_q=O). HRMS: Calculated mass for C₂₂H₁₆O₅Cl₂S 461.0017; mass found 461.0014. Decomposes above 215 °C.

Potassium 4-((5-chloro-2-[(2E)-3-(2-fluorophenyl)prop-2-enoyl]phenoxy)methyl)benzenesulfonate (18)

Method I; sulfonate **127** (0.376 g, 1 mmol) and benzaldehyde **136** (0.123 g, 1 mmol) afforded **18** as an off-white solid (0.301 g, 62%). ¹H NMR (D₂O, 40 °C): δ 5.45 (s, 2 H, CH₂); 7.39 (dd, *J* = 8.3, 2.0, 1 H, CH-CH-C_q-Cl); 7.43-7.46 (m, 2 H, CH-C_q-F and CH-CH-CH-C_q-F); 7.49 (t, *J* = 7.3, 1 H, CH-CH-C_q-F); 7.57 (s, 1 H, CH-C_q-O); 7.65-7.72 (m, 4 H, 2x CH-C_q-CH₂, CH-C_q=O and CH-C_q-C_q-F); 7.81-7.84 (m, 3 H, 2x CH-C_q-S and CH-C_q-C_q=O); 7.85 (d, *J* = 16.3, 1 H, CH=CH-C_q=O). ¹³C NMR (D₂O, 40 °C): δ 71.29 (t, 1 C, CH₂); 115.09 (d, 1 C, CH-C_q-O); 117.50 (dd, ²*J*_{19F-13C} = 22.6, 1 C, CH-C_q-F); 122.87 (d, 1 C, CH-CH-C_q-Cl); 123.02 (s, 1 C, C_q-C_q-F); 126.55 (d, 1 C, CH-C_q-C_q-F or CH-CH-C_q-C_q-F); 127.01 (d, 2 C, 2x CH-C_q-S); 127.89 (s, 1 C, C_q-C_q=O); 129.14 (d, 2 C, 2x CH-C_q-CH₂); 129.83 (d, 1 C, CH-C_q=O); 130.10 (d, 1 C, CH-C_q-C_q-F or CH-CH-C_q-C_q-F); 132.85 (d, 1 C, CH-C_q-C_q=O); 134.41 (dd, ³*J*_{19F-13C} = 8.9, CH-CH-C_q-F); 137.25 (d, 1 C, CH=CH-C_q=O); 139.04 (s, 1 C, C_q-CH₂); 140.28 (s, 1 C, C_q-Cl); 145.92 (s, 1 C, C_q-S); 158.89 (s, 1 C, C_q-O); 163.20 (d, ¹*J*_{19F-13C} = 252.0, C_q-F); 193.78 (s, 1 C, C_q=O). HRMS: Calculated mass for C₂₂H₁₅O₅ClFS 445.0313; mass found 445.0305. Decomposes above 225 °C.

Potassium 4-((5-chloro-2-[(2E)-3-(2-methoxyphenyl)prop-2-enoyl]phenoxy)methyl)benzenesulfonate (24)

Method I; sulfonate **127** (0.379 g, 1 mmol) and benzaldehyde **100** (0.135 g, 1 mmol) afforded **24** as an off-white solid (0.298 g, 60%). ¹H NMR (D₂O, 40 °C): δ 3.68 (s, 3 H, CH₃); 5.09 (s, 2 H, CH₂); 6.92 (t, *J* = 7.4, 1 H, CH-CH-C_q-CH=CH); 6.97 (d, *J* = 8.3, 1 H, CH-C_q-O-CH₃); 7.04 (d, *J* = 7.8, 1 H, CH-CH-C_q-Cl); 7.20 (s, 1 H, C_q-CH-C_q-Cl); 7.26-7.31 (m, 2 H, CH-C_q=O and CH-CH-C_q-O); 7.32-7.39 (m, 3 H, 2x CH-C_q-CH₂ and CH-C_q-CH=CH); 7.43 (d, *J* = 7.9, 1 H, CH-CH-C_q-C_q=O); 7.51 (d, *J* = 7.6, 2 H, 2x CH-C_q-S); 7.69 (d, *J* = 16.0, 1 H, CH=CH-C_q=O). ¹³C NMR (D₂O, 40 °C): δ 56.82 (q, 1 C, CH₃); 71.16 (t, 1 C, CH₂); 113.15 (d, 1 C, CH-C_q-O-CH₃); 114.97 (d, 1 C, CH-C_q-O-CH₂); 122.41 (d, 1 C, CH-CH-C_q-CH=CH); 122.68 (d, 1 C, CH-CH-C_q-Cl); 126.90 (d, 2 C, 2x CH-C_q-S); 127.83 (d, 1 C, CH-C_q=O); 128.42 (s, 1 C, C_q-C_q=O); 128.80 (d, 2 C, 2x CH-C_q-CH₂); 129.71 (d, 1 C, CH-CH-C_q-O); 132.49 (d, 1 C, CH-C_q-C_q=O); 134.23 (d, 1 C, CH-C_q-CH=CH); 138.96 (s, 1 C, C_q-CH₂); 139.55 (s, 1 C, C_q-Cl); 140.77 (d, 1 C, CH=CH-C_q=O); 145.88 (s, 1 C, C_q-S); 158.85 (s, 1 C, C_q-O-CH₂); 159.49 (s, 1 C, C_q-O-CH₃); 194.26 (s, 1 C, C_q=O). HRMS: Calculated mass for C₂₃H₁₈O₆ClIS 457.0513; mass found 457.0507. Decomposes above 230 °C.

10. References

- (1) Dias, D.A.; Urban, S.; Roessner, U. *Metabolites* **2012**, 2, 303-336.
- (2) Cragg, G.M.; Newman, D.J. *Pure Appl. Chem.* **2005**, 77, 7-24.
- (3) Mesopotamian Cuneform Tablets.
http://www.academia.dk/MedHist/Biblioteket/mesopotamien_farmakope.php.
- (4) Ravina, E.; Kubinyi, H. *The Evolution of Drug Discovery: From Traditional Medicines to Modern Drugs*; John Wiley & Sons, 2011.
- (5) Yaniv, Z.; Bachrach, U. *Handbook of Medicinal Plants*; Taylor & Francis, 2005.
- (6) Ebers Papyrus. <http://www.crystalinks.com/egyptmedicine.html>.
- (7) Dwivedi, G.; Dwivedi, S. *Indian J. Chest Dis. Allied Sci.* **2007**, 49, 243-244.
- (8) Fallarino, M. *Herbalgram* **1994**, 31, 38-44.
- (9) Theophrastus' *Historia Plantarum*, 1644.
http://en.wikipedia.org/wiki/Historia_Plantarum_%28Theophrastus%29#mediaviewer/File:161Theophrastus_161_frontespizio.jpg.
- (10) McGinnis, J. *Avicenna*; Oxford University Press, 2010.
- (11) Osler, W. *The Evolution of Modern Medicine*; Kessinger Publishing, 2004.
- (12) Finger, S. *Origins of Neuroscience: A History of Explorations into Brain Function*; Oxford University Press, 2001.
- (13) Avicenna, Canon Medicinæ. http://en.wikipedia.org/wiki/File:Avicenna_canon_1597.jpg.
- (14) Boxer, C.R. *Two Pioneers of Tropical Medicine: Garcia D'orta and Nicolás Monardes*; Hispanic & Luso-Brazilian Councils, 1963.
- (15) Acuna-Soto, R.; Stahle, D.W.; Cleaveland, M.K.; Therrell, M.D. *Emerg. Infect. Dis.* **2002**, 8, 360-362.
- (16) De Sahagun Historia De Las Cosas. <http://ipce.mcu.es/conservacion/restauracion/conserv-rest-libr1-2.html>.
- (17) O'Malley, C.D. *Andreas Vesalius of Brussels, 1514-1564*; University of California Press, 1964.
- (18) Webster, C. *Paracelsus*; YALE University Press, 2008.
- (19) Borzelleca, J.F. *Toxicol. Sci.* **2000**, 53, 2-4.
- (20) Davenport-Hines, R. *The Pursuit of Oblivion: A Global History of Narcotics*; W.W. Norton, 2003.

- (21) Strathern, P. *A Brief History of Medicine: From Hippocrates to Gene Therapy*; Constable & Robinson, 2005.
- (22) Laudanum, 19th Cent. <http://drjenniferduffy.com/id6.html>.
- (23) Hodgson, B. *In the Arms of Morpheus: The Tragic History of Laudanum Morphine and Patent Medicines*; D&M Publishers Incorporated, 2008.
- (24) Musto, D.F. *The American Disease : Origins of Narcotic Control: Origins of Narcotic Control*; 3rd ed.; Oxford University Press, USA, 1999.
- (25) Victorian Heroin Bottle.
<http://slipintosomethingvictorian.wordpress.com/2011/01/20/laudanum-use-in-victorian-times/>
- (26) Victorian Cocaine Preparation.
<http://www.thetimes.co.uk/tto/arts/visualarts/article2905101.ece>.
- (27) Victorian Cannabis Preparation. <http://www.tiki-toki.com/timeline/entry/195245/Medicinal-Cannabis-Extracts-through-History/>.
- (28) A History of the Fda.
<http://www.fda.gov/AboutFDA/WhatWeDo/History/Origin/46.ucm054819.html>.
- (29) Original Text of the 1906 Food and Drugs Act and Amendments
<http://www.fda.gov/opacom/laws/wileyact.html>.
- (30) Hamowy, R. Medical Disasters and the Growth of Fda February 2010.
http://www.independent.org/pdf/policy_reports/2010-02-10-fda.pdf.
- (31) Temple, R. *Stat. Med.* **2002**, *21*, 2939-2948.
- (32) Thalidomide: A Promising Drug Promises Greater Protection for Consumers, 17 August, 1962.
<http://www.library.arizona.edu/exhibits/udall/congrept/87th/620817.html> (accessed 29 June 2014).
- (33) Dr Frances Kathleen Oldham Kelsey nlm.nih.gov.
http://www.nlm.nih.gov/changingthefaceofmedicine/physicians/biography_182.html.
- (34) "Expanded Access and Expedited Approval of New Therapies Related to Hiv/Aids" Fda.gov, 14 April 2009.
<http://www.fda.gov/ForConsumers/ByAudience/ForPatientAdvocates/SpeedingAccessToImportantNewTherapies/ucm134331.html>.
- (35) Boldrin, M.; Swamidass, S.J. "A New Bargain for Drug Approvals" Wsj.com, 25 July 2011.
<http://online.wsj.com/article/SB10001424052702303812104576441610360466984.html>.

- (36) Pandey, A. "Ebola Vaccine: First-Ever Human Trials for Experimental Drug to Begin Soon." Ibtimes.com, 2 September 2014. <http://www.ibtimes.com/ebola-vaccine-first-ever-human-trials-experimental-drug-begin-soon-1675440> (accessed 30 September 2014).
- (37) Green, T. "Zmapp Ebola Treatment: What to Know About the Experimental Drug Made from Tobacco" Ibtimes.com, 6 August 2014. <http://www.ibtimes.com/zmapp-ebola-treatment-what-know-about-experimental-drug-made-tobacco-1650870> (accessed 30 September 2014).
- (38) Sweeny, K. *Technology Trends in Drug Discovery and Development: Implications for the Development of the Pharmaceutical Industry in Australia*, Victoria University, 2002.
- (39) Evens, R. *Drug and Biological Development: From Molecule to Product and Beyond*; Springer, 2007.
- (40) Dalkas, G.A.; Vlachakis, D.; Tsagkrasoulis, D.; Kastania, A.; Kossida, S. *Briefings in bioinformatics* **2013**, *14*, 745-752.
- (41) Mucs, D.; Bryce, R.A. *Expert Opin Drug Discov* **2013**, *8*, 263-276.
- (42) Kapetanovic, I.M. *Chem. Biol. Interact.* **2008**, *171*, 165-176.
- (43) McRae, J.; Yang, Q.; Crawford, R.; Palombo, E. *The Environmentalist* **2007**, *27*, 165-174.
- (44) Fellows, L.; Scofield, A. In *Intellectual Property Rights and Biodiversity Conservation: An Interdisciplinary Analysis of the Values of Medicinal Plants*; Swanson, T., Ed.; Cambridge University Press: 1995.
- (45) Butler, M.S. *J. Nat. Prod.* **2004**, *67*, 2141-2153.
- (46) DerMarderosian, A.; Beutler, J.A. *The Review of Natural Products*; Lippincott Williams & Wilkins, 2012.
- (47) Holzman, R.S. *Anesthesiology* **1998**, *89*, 241-249.
- (48) Mein, H. *Annalen der Pharmacie* **1833**, *6*, 67-72.
- (49) Flückiger, F.A.; Hanbury, D. *Pharmacographia*; Macmillan, 1879.
- (50) "Quinine Sulfate Q&As" Fda.gov, 15 Dec 2006.
<http://www.google.co.za/url?sa=t&rct=j&q=&esrc=s&source=web&cd=1&cad=rja&uact=8&ved=0CBsQFjAA&url=http%3A%2F%2Fwww.fda.gov%2Fdownloads%2Fdrugs%2Fguidancecompliance%2Fregulatoryinformation%2Fenforcementactivitiesbyfda%2Fselectedenforcementactionsonunapproveddrugs%2Fucm119653.pdf&ei=jBjrU4zRA4WA7Qa9IYD4BQ&usq=AFOjCNEJjuXAEpdAlVnZ7YwzplV1FSq0dA&sig2=kAPHaEbzOnq8wRnW8YBEhw&bvm=bv.72938740,d.ZGU>.
- (51) Hicks, S. *Desert Plants and People*; Naylor Company, 1966.
- (52) Kinghorn, A.D.; Pan, L.; Fletcher, J.N.; Chai, H. *J. Nat. Prod.* **2011**, *74*, 1539-1555.

- (53) Mishra, B.B.; Tiwari, V.K. *Eur. J. Med. Chem.* **2011**, *46*, 4769-4807.
- (54) Haefner, B. *Drug Discov Today* **2003**, *8*, 536-544.
- (55) Rey-Ladino, J.; Ross, A.G.; Cripps, A.W.; McManus, D.P.; Quinn, R. *Vaccine* **2011**, *29*, 6464-6471.
- (56) Newman, D.J.; Cragg, G.M. *J. Nat. Prod.* **2012**, *75*, 311-335.
- (57) Jeffreys, D. *Aspirin: The Remarkable Story of a Wonder Drug*; Bloomsbury Publishing, 2008.
- (58) Stone, E. *Philosophical Transactions* **1763**, *53*, 195-200.
- (59) White Willow - Salix Alba.
http://commons.wikimedia.org/wiki/File:Salix_alba_%27Tristis%27_02_by_Line1.jpg.
- (60) Meadowsweet - Filipendula Ulmaria.
<http://en.wikipedia.org/wiki/Filipendula#mediaviewer/File:Filipendula-ulmaria.JPG>.
- (61) Gerhardt, C. *Justus Liebigs Ann. Chem.* **1853**, *87*, 57-84.
- (62) Von Gilm, H. *Justus Liebigs Ann. Chem.* **1859**, *112*, 180-185.
- (63) Schröder, A.; Prinzhorn, A.; Kraut, K. *Justus Liebigs Ann. Chem.* **1869**, *150*, 1-20.
- (64) Mann, C.C.; Plummer, M.L. *The Aspirin Wars: Money, Medicine, and 100 Years of Rampant Competition*; Knopf, 1991.
- (65) Aspirin Bottle Circa 1900. <http://www.deutsches-museum.de/en/information/young-people/inventors-trail/discovery/aspirin>.
- (66) Mann, J. *Murder, Magic, and Medicine*; Oxford University Press, 2000.
- (67) Williams, J.D. *Int. J. Antimicrob. Agents* **1999**, *12 Suppl 1*, S3-7; discussion S26-27.
- (68) Buss, A.D.; Waigh, R.D. In *Burger's Medicinal Chemistry and Drug Discovery: Drug Discovery*; Wolff, M. E., Ed.; Wiley: 1995; Vol. 1, p 1021-1028.
- (69) Fabbretti, A.; Gualerzi, C.O.; Brandi, L. *FEBS Lett.* **2011**, *585*, 1673-1681.
- (70) Cragg, G.M. *Med. Res. Rev.* **1998**, *18*, 315-331.
- (71) Dewick, P.M. *Medicinal Natural Products: A Biosynthetic Approach*; Wiley, 2011.
- (72) Weiss, R.B. *Semin. Oncol.* **1992**, *19*, 670-686.
- (73) Baker, D.D.; Chu, M.; Oza, U.; Rajgarhia, V. *Nat. Prod. Rep.* **2007**, *24*, 1225-1244.
- (74) Ojima, I. *J. Med. Chem.* **2008**, *51*, 2587-2588.
- (75) Von Nussbaum, F.; Brands, M.; Hinzen, B.; Weigand, S.; Habich, D. *Angew. Chem. Int. Ed. Engl.* **2006**, *45*, 5072-5129.
- (76) Luzhetskyy, A.; Pelzer, S.; Bechthold, A. *Current opinion in investigational drugs (London, England : 2000)* **2007**, *8*, 608-613.
- (77) Carr, R.; Jhoti, H. *Drug Discovery Today* **2002**, *7*, 522-527.

- (78) Davis, A.M.; Teague, S.J.; Kleywegt, G.J. *Angew. Chem. Int. Ed. Engl.* **2003**, *42*, 2718-2736.
- (79) Nowak, A.K.; Wilcken, N.R.C.; Stockler, M.R.; Hamilton, A.; Ghersi, D. *The Lancet Oncology* **2004**, *5*, 372-380.
- (80) Deprez-Poulain, R.; Deprez, B. *Curr. Top. Med. Chem.* **2004**, *4*, 569-580.
- (81) Keseru, G.M.; Makara, G.M. *Drug Discov Today* **2006**, *11*, 741-748.
- (82) Bleicher, K.H.; Bohm, H.J.; Muller, K.; Alanine, A.I. *Nature reviews. Drug discovery* **2003**, *2*, 369-378.
- (83) Harvey, A.L. *Trends Pharmacol. Sci.* **1999**, *20*, 196-198.
- (84) Rosenthal, J. *Nature* **2002**, *416*, 15.
- (85) Pethiyagoda, R. *Nature* **2004**, *429*, 129.
- (86) Dalton, R. *Nature* **2004**, *429*, 598-600.
- (87) Newman, D.J. *J. Med. Chem.* **2008**, *51*, 2589-2599.
- (88) Balkenhohl, F.; von dem Bussche-Hünnefeld, C.; Lansky, A.; Zechel, C. *Angewandte Chemie International Edition in English* **1996**, *35*, 2288-2337.
- (89) Myers, P.L. *Curr. Opin. Biotechnol.* **1997**, *8*, 701-707.
- (90) Rouhi, A.M. In *Chem. Eng. News* 2003; Vol. 81, p 77-91.
- (91) Hann, M.M.; Oprea, T.I. *Curr. Opin. Chem. Biol.* **2004**, *8*, 255-263.
- (92) Park, S.; Mann, J.; Li, N. *Chem Eng Process Tech* **2013**, *1*, 1004.
- (93) Henkel, T.; Brunne, R.M.; Müller, H.; Reichel, F. *Angew. Chem. Int. Ed.* **1999**, *38*, 643-647.
- (94) Stahura, F.L.; Godden, J.W.; Xue, L.; Bajorath, J. *J. Chem. Inf. Comput. Sci.* **2000**, *40*, 1245-1252.
- (95) Lee, M.L.; Schneider, G. *J. Comb. Chem.* **2001**, *3*, 284-289.
- (96) Feher, M.; Schmidt, J.M. *J. Chem. Inf. Comput. Sci.* **2003**, *43*, 218-227.
- (97) Burke, M.D.; Berger, E.M.; Schreiber, S.L. *Science* **2003**, *302*, 613-618.
- (98) Schreiber, S.L. *Science* **2000**, *287*, 1964-1969.
- (99) Arya, P.; Joseph, R.; Chou, D.T. *Chem. Biol.* **2002**, *9*, 145-156.
- (100) Duarte, C.D.; Barreiro, E.J.; Fraga, C.A. *Mini Rev. Med. Chem.* **2007**, *7*, 1108-1119.
- (101) Breinbauer, R.; Vetter, I.R.; Waldmann, H. *Angew. Chem. Int. Ed. Engl.* **2002**, *41*, 2879-2890.
- (102) Kingston, D.G.; Newman, D.J. *Current opinion in drug discovery & development* **2002**, *5*, 304-316.
- (103) Wessjohann, L.A. *Curr. Opin. Chem. Biol.* **2000**, *4*, 303-309.
- (104) Lee, A.; Breitenbucher, J.G. *Current opinion in drug discovery & development* **2003**, *6*, 494-508.
- (105) Horton, D.A.; Bourne, G.T.; Smythe, M.L. *Chem. Rev.* **2003**, *103*, 893-930.
- (106) Hall, D.G.; Manku, S.; Wang, F. *J. Comb. Chem.* **2001**, *3*, 125-150.

- (107) Rouhi, A.M. In *Chem. Eng. News* 2003; Vol. 81, p 104-107.
- (108) Abreu, P.M.; Branco, P.S. *J. Braz. Chem. Soc.* **2003**, *14*, 675-712.
- (109) Slee, A.M.; Wuonola, M.A.; McRipley, R.J.; Zajac, I.; Zawada, M.J.; Bartholomew, P.T.; Gregory, W.A.; Forbes, M. *Antimicrob. Agents Chemother.* **1987**, *31*, 1791-1797.
- (110) Daly, J.S.; Eliopoulos, G.M.; Reiszner, E.; Moellering, R.C., Jr. *J. Antimicrob. Chemother.* **1988**, *21*, 721-730.
- (111) Eustice, D.C.; Brittelli, D.R.; Feldman, P.A.; Brown, L.J.; Borkowski, J.J.; Slee, A.M. *Drugs Exp. Clin. Res.* **1990**, *16*, 149-155.
- (112) Eustice, D.C.; Feldman, P.A.; Zajac, I.; Slee, A.M. *Antimicrob. Agents Chemother.* **1988**, *32*, 1218-1222.
- (113) Gregory, W.A.; Brittelli, D.R.; Wang, C.L.; Wuonola, M.A.; McRipley, R.J.; Eustice, D.C.; Eberly, V.S.; Bartholomew, P.T.; Slee, A.M.; Forbes, M. *J. Med. Chem.* **1989**, *32*, 1673-1681.
- (114) Davidson, R.N.; den Boer, M.; Ritmeijer, K. *Trans. R. Soc. Trop. Med. Hyg.* **2009**, *103*, 653-660.
- (115) Kumar, A.; Voet, A.; Zhang, K.Y.J. *Curr. Med. Chem.* **2012**, *19*, 5128-5147.
- (116) Murray, C.W.; Rees, D.C. *Nat. Chem.* **2009**, *1*, 187-192.
- (117) Lipinski, C.A.; Lombardo, F.; Dominy, B.W.; Feeney, P.J. *Advanced drug delivery reviews* **2001**, *46*, 3-26.
- (118) Veber, D.F.; Johnson, S.R.; Cheng, H.Y.; Smith, B.R.; Ward, K.W.; Kopple, K.D. *J. Med. Chem.* **2002**, *45*, 2615-2623.
- (119) Park, S.Y.; Kim, D.S. *J. Nat. Prod.* **2002**, *65*, 1227-1231.
- (120) Geppert, T.; Bauer, S.; Hiss, J.A.; Conrad, E.; Reutlinger, M.; Schneider, P.; Weisel, M.; Pfeiffer, B.; Altmann, K.H.; Waibler, Z.; Schneider, G. *Angew. Chem. Int. Ed. Engl.* **2012**, *51*, 258-261.
- (121) Valkov, E.; Sharpe, T.; Marsh, M.; Greive, S.; Hyvonen, M. *Top. Curr. Chem.* **2012**, *317*, 145-179.
- (122) Bello, M.; Martínez-Archundia, M.; Correa-Basurto, J. *Expert Opinion on Drug Discovery* **2013**, *8*, 821-834.
- (123) Prull, C.R. *Med. Hist.* **2003**, *47*, 332-356.
- (124) Ehrlich, P. In *Gesammelte Arbeiten*; Himmelweit, F., Ed.; Springer-Verlag: Berlin, 1957.
- (125) Langley, J.N. *J. Physiol.* **1905**, *33*, 374-413.
- (126) Maehle, A.H.; Prull, C.R.; Halliwell, R.F. *Nature reviews. Drug discovery* **2002**, *1*, 637-641.
- (127) Campbell, S.F. *Clin. Sci. (Lond.)* **2000**, *99*, 255-260.
- (128) Oprea, T.I.; Davis, A.M.; Teague, S.J.; Leeson, P.D. *J. Chem. Inf. Comput. Sci.* **2001**, *41*, 1308-1315.
- (129) Blundell, T.L.; Jhoti, H.; Abell, C. *Nature reviews. Drug discovery* **2002**, *1*, 45-54.

- (130) Shuker, S.B.; Hajduk, P.J.; Meadows, R.P.; Fesik, S.W. *Science* **1996**, *274*, 1531-1534.
- (131) Hajduk, P.J.; Meadows, R.P.; Fesik, S.W. *Q. Rev. Biophys.* **1999**, *32*, 211-240.
- (132) Fejzo, J.; Lepre, C.A.; Peng, J.W.; Bemis, G.W.; Ajay, Murcko, M.A.; Moore, J.M. *Chem. Biol.* **1999**, *6*, 755-769.
- (133) Nienaber, V.L.; Richardson, P.L.; Klighofer, V.; Bouska, J.J.; Giranda, V.L.; Greer, J. *Nat. Biotechnol.* **2000**, *18*, 1105-1108.
- (134) Boehm, H.J.; Boehringer, M.; Bur, D.; Gmuender, H.; Huber, W.; Klaus, W.; Kostrewa, D.; Kuehne, H.; Luebbers, T.; Meunier-Keller, N.; Mueller, F. *J. Med. Chem.* **2000**, *43*, 2664-2674.
- (135) Verlinde, C.L.; Fan, E.; Shibata, S.; Zhang, Z.; Sun, Z.; Deng, W.; Ross, J.; Kim, J.; Xiao, L.; Arakaki, T.L.; Bosch, J.; Caruthers, J.M.; Larson, E.T.; Letrong, I.; Napuli, A.; Kelly, A.; Mueller, N.; Zucker, F.; Van Voorhis, W.C.; Buckner, F.S.; Merritt, E.A.; Hol, W.G. *Curr. Top. Med. Chem.* **2009**, *9*, 1678-1687.
- (136) de Kloe, G.E.; Bailey, D.; Leurs, R.; de Esch, I.J. *Drug Discov Today* **2009**, *14*, 630-646.
- (137) Erlanson, D.A. *Top. Curr. Chem.* **2012**, *317*, 1-32.
- (138) Bollag, G.; Tsai, J.; Zhang, J.; Zhang, C.; Ibrahim, P.; Nolop, K.; Hirth, P. *Nature reviews. Drug discovery* **2012**, *11*, 873-886.
- (139) Congreve, M.; Carr, R.; Murray, C.; Jhoti, H. *Drug Discov Today* **2003**, *8*, 876-877.
- (140) Card, G.L.; Blasdel, L.; England, B.P.; Zhang, C.; Suzuki, Y.; Gillette, S.; Fong, D.; Ibrahim, P.N.; Artis, D.R.; Bollag, G.; Milburn, M.V.; Kim, S.H.; Schlessinger, J.; Zhang, K.Y. *Nat. Biotechnol.* **2005**, *23*, 201-207.
- (141) Tsai, J.; Lee, J.T.; Wang, W.; Zhang, J.; Cho, H.; Mamo, S.; Bremer, R.; Gillette, S.; Kong, J.; Haass, N.K.; Sproesser, K.; Li, L.; Smalley, K.S.; Fong, D.; Zhu, Y.L.; Marimuthu, A.; Nguyen, H.; Lam, B.; Liu, J.; Cheung, I.; Rice, J.; Suzuki, Y.; Luu, C.; Settachatgul, C.; Shellooe, R.; Cantwell, J.; Kim, S.H.; Schlessinger, J.; Zhang, K.Y.; West, B.L.; Powell, B.; Habets, G.; Zhang, C.; Ibrahim, P.N.; Hirth, P.; Artis, D.R.; Herlyn, M.; Bollag, G. *Proc. Natl. Acad. Sci. U. S. A.* **2008**, *105*, 3041-3046.
- (142) Artis, D.R.; Lin, J.J.; Zhang, C.; Wang, W.; Mehra, U.; Perreault, M.; Erbe, D.; Krupka, H.I.; England, B.P.; Arnold, J.; Plotnikov, A.N.; Marimuthu, A.; Nguyen, H.; Will, S.; Signaevsky, M.; Kral, J.; Cantwell, J.; Settachatgull, C.; Yan, D.S.; Fong, D.; Oh, A.; Shi, S.; Womack, P.; Powell, B.; Habets, G.; West, B.L.; Zhang, K.Y.; Milburn, M.V.; Vlasuk, G.P.; Hirth, K.P.; Nolop, K.; Bollag, G.; Ibrahim, P.N.; Tobin, J.F. *Proc. Natl. Acad. Sci. U. S. A.* **2009**, *106*, 262-267.
- (143) Bollag, G.; Hirth, P.; Tsai, J.; Zhang, J.; Ibrahim, P.N.; Cho, H.; Spevak, W.; Zhang, C.; Zhang, Y.; Habets, G.; Burton, E.A.; Wong, B.; Tsang, G.; West, B.L.; Powell, B.; Shellooe, R.; Marimuthu, A.;

- Nguyen, H.; Zhang, K.Y.; Artis, D.R.; Schlessinger, J.; Su, F.; Higgins, B.; Iyer, R.; D'Andrea, K.; Koehler, A.; Stumm, M.; Lin, P.S.; Lee, R.J.; Grippo, J.; Puzanov, I.; Kim, K.B.; Ribas, A.; McArthur, G.A.; Sosman, J.A.; Chapman, P.B.; Flaherty, K.T.; Xu, X.; Nathanson, K.L.; Nolop, K. *Nature* **2010**, *467*, 596-599.
- (144) Scott, D.E.; Coyne, A.G.; Hudson, S.A.; Abell, C. *Biochemistry* **2012**, *51*, 4990-5003.
- (145) Joseph-McCarthy, D.; Campbell, A.J.; Kern, G.; Moustakas, D. *J. Chem. Inf. Model.* **2014**, *54*, 693-704.
- (146) Cheng, Y.; Judd, T.C.; Bartberger, M.D.; Brown, J.; Chen, K.; Fremeau, R.T., Jr.; Hickman, D.; Hitchcock, S.A.; Jordan, B.; Li, V.; Lopez, P.; Louie, S.W.; Luo, Y.; Michelsen, K.; Nixey, T.; Powers, T.S.; Rattan, C.; Sickmier, E.A.; St Jean, D.J., Jr.; Wahl, R.C.; Wen, P.H.; Wood, S. *J. Med. Chem.* **2011**, *54*, 5836-5857.
- (147) Taylor, S.J.; Abeywardane, A.; Liang, S.; Muegge, I.; Padyana, A.K.; Xiong, Z.; Hill-Drzewi, M.; Farmer, B.; Li, X.; Collins, B.; Li, J.X.; Heim-Riether, A.; Proudfoot, J.; Zhang, Q.; Goldberg, D.; Zuvela-Jelaska, L.; Zaher, H.; Li, J.; Farrow, N.A. *J. Med. Chem.* **2011**, *54*, 8174-8187.
- (148) Hughes, S.J.; Millan, D.S.; Kilty, I.C.; Lewthwaite, R.A.; Mathias, J.P.; O'Reilly, M.A.; Pannifer, A.; Phelan, A.; Stuhmeier, F.; Baldock, D.A.; Brown, D.G. *Bioorg. Med. Chem. Lett.* **2011**, *21*, 6586-6590.
- (149) Edink, E.; Rucktooa, P.; Retra, K.; Akdemir, A.; Nahar, T.; Zuiderveld, O.; van Elk, R.; Janssen, E.; van Nierop, P.; van Muijlwijk-Koezen, J.; Smit, A.B.; Sixma, T.K.; Leurs, R.; de Esch, I.J. *J. Am. Chem. Soc.* **2011**, *133*, 5363-5371.
- (150) Hung, A.W.; Silvestre, H.L.; Wen, S.; Ciulli, A.; Blundell, T.L.; Abell, C. *Angew. Chem. Int. Ed. Engl.* **2009**, *48*, 8452-8456.
- (151) Hajduk, P.J.; Sheppard, G.; Nettlesheim, D.G.; Olejniczak, E.T.; Shuker, S.B.; Meadows, R.P.; Steinman, D.H.; Carrera, G.M.; Marcotte, P.A.; Severin, J.; Walter, K.; Smith, H.; Gubbins, E.; Simmer, R.; Holzman, T.F.; Morgan, D.W.; Davidsen, S.K.; Summers, J.B.; Fesik, S.W. *J. Am. Chem. Soc.* **1997**, *119*, 5818-5827.
- (152) Maly, D.J.; Choong, I.C.; Ellman, J.A. *Proc. Natl. Acad. Sci. U. S. A.* **2000**, *97*, 2419-2424.
- (153) Swayze, E.E.; Jefferson, E.A.; Sannes-Lowery, K.A.; Blyn, L.B.; Risen, L.M.; Arakawa, S.; Osgood, S.A.; Hofstadler, S.A.; Griffey, R.H. *J. Med. Chem.* **2002**, *45*, 3816-3819.
- (154) Howard, N.; Abell, C.; Blakemore, W.; Chessari, G.; Congreve, M.; Howard, S.; Jhoti, H.; Murray, C.W.; Seavers, L.C.; van Montfort, R.L. *J. Med. Chem.* **2006**, *49*, 1346-1355.
- (155) Chung, S.; Parker, J.B.; Bianchet, M.; Amzel, L.M.; Stivers, J.T. *Nat. Chem. Biol.* **2009**, *5*, 407-413.

- (156) Petros, A.M.; Huth, J.R.; Oost, T.; Park, C.M.; Ding, H.; Wang, X.; Zhang, H.; Nimmer, P.; Mendoza, R.; Sun, C.; Mack, J.; Walter, K.; Dorwin, S.; Gramling, E.; Lador, U.; Rosenberg, S.H.; Elmore, S.W.; Fesik, S.W.; Hajduk, P.J. *Bioorg. Med. Chem. Lett.* **2010**, *20*, 6587-6591.
- (157) Barker, J.J.; Barker, O.; Courtney, S.M.; Gardiner, M.; Hestekamp, T.; Ichihara, O.; Mather, O.; Montalbetti, C.A.; Muller, A.; Varasi, M.; Whittaker, M.; Yarnold, C.J. *ChemMedChem* **2010**, *5*, 1697-1700.
- (158) Borsi, V.; Calderone, V.; Fragai, M.; Luchinat, C.; Sarti, N. *J. Med. Chem.* **2010**, *53*, 4285-4289.
- (159) Lewis, W.G.; Green, L.G.; Grynszpan, F.; Radic, Z.; Carlier, P.R.; Taylor, P.; Finn, M.G.; Sharpless, K.B. *Angew. Chem. Int. Ed. Engl.* **2002**, *41*, 1053-1057.
- (160) Hu, X.; Sun, J.; Wang, H.G.; Manetsch, R. *J. Am. Chem. Soc.* **2008**, *130*, 13820-13821.
- (161) Suzuki, T.; Ota, Y.; Kasuya, Y.; Mutsuga, M.; Kawamura, Y.; Tsumoto, H.; Nakagawa, H.; Finn, M.G.; Miyata, N. *Angew. Chem. Int. Ed. Engl.* **2010**, *49*, 6817-6820.
- (162) Hoffer, L.; Renaud, J.P.; Horvath, D. *Comb. Chem. High Throughput Screen.* **2011**, *14*, 500-520.
- (163) Fink, T.; Raymond, J.L. *J. Chem. Inf. Model.* **2007**, *47*, 342-353.
- (164) Blum, L.C.; Raymond, J.L. *J. Am. Chem. Soc.* **2009**, *131*, 8732-8733.
- (165) Jahnke, W.; Erlanson, D.A.; Mannhold, R.; Kubinyi, H.; Folkers, G. *Fragment-Based Approaches in Drug Discovery*; Wiley, 2006.
- (166) Shoichet, B.K. *Nat. Chem.* **2013**, *5*, 9-10.
- (167) Over, B.; Wetzels, S.; Grutter, C.; Nakai, Y.; Renner, S.; Rauh, D.; Waldmann, H. *Nat. Chem.* **2013**, *5*, 21-28.
- (168) ChemAxon Calculator Plugins, Marvin Version 14.8.11, 2014. www.chemaxon.com.
- (169) Steinbeck, C.; Han, Y.; Kuhn, S.; Horlacher, O.; Luttmann, E.; Willighagen, E. *J. Chem. Inf. Comput. Sci.* **2003**, *43*, 493-500.
- (170) Steinbeck, C.; Hoppe, C.; Kuhn, S.; Floris, M.; Guha, R.; Willighagen, E.L. *Curr. Pharm. Des.* **2006**, *12*, 2111-2120.
- (171) Inc, C.C.G. Molecular Operating Environment (Moe), Version 2013.08. <http://www.chemcomp.com/MOE2013.htm>.
- (172) Schrodinger. www.schrodinger.com.
- (173) Lewell, X.Q.; Judd, D.B.; Watson, S.P.; Hann, M.M. *J. Chem. Inf. Comput. Sci.* **1998**, *38*, 511-522.
- (174) Kolb, P.; Caflich, A. *J. Med. Chem.* **2006**, *49*, 7384-7392.
- (175) Degen, J.; Wegscheid-Gerlach, C.; Zaliani, A.; Rarey, M. *ChemMedChem* **2008**, *3*, 1503-1507.
- (176) GnbH, B. Colibri. www.biosolveit.de.

- (177) OpenEye Scientific Software, I. Chomp. www.eyesopen.com.
- (178) Joseph-McCarthy, D.; Baber, J.C.; Feyfant, E.; Thompson, D.C.; Humblet, C. *Current opinion in drug discovery & development* **2007**, *10*, 264-274.
- (179) Rester, U. *Current opinion in drug discovery & development* **2008**, *11*, 559-568.
- (180) Rollinger, J.M.; Stuppner, H.; Langer, T. *Prog. Drug Res.* **2008**, *65*, 211, 213-249.
- (181) Kroemer, R.T. *Current protein & peptide science* **2007**, *8*, 312-328.
- (182) Cavasotto, C.N.; Orry, A.J. *Curr. Top. Med. Chem.* **2007**, *7*, 1006-1014.
- (183) Lyne, P.D.; Lamb, M.L.; Saeh, J.C. *J. Med. Chem.* **2006**, *49*, 4805-4808.
- (184) Thompson, D.C.; Humblet, C.; Joseph-McCarthy, D. *J. Chem. Inf. Model.* **2008**, *48*, 1081-1091.
- (185) Goodford, P.J. *J. Med. Chem.* **1985**, *28*, 849-857.
- (186) Miranker, A.; Karplus, M. *Proteins* **1991**, *11*, 29-34.
- (187) Bohm, H.J. *J. Comput. Aided Mol. Des.* **1992**, *6*, 593-606.
- (188) Gillet, V.; Myatt, G.; Zsoldos, Z.; Johnson, A.P. *Perspect. Drug Discovery Des.* **1995**, *3*, 34-50.
- (189) Verdonk, M.L.; Cole, J.C.; Taylor, R. *J. Mol. Biol.* **1999**, *289*, 1093-1108.
- (190) Carlson, H.A.; Masukawa, K.M.; Rubins, K.; Bushman, F.D.; Jorgensen, W.L.; Lins, R.D.; Briggs, J.M.; McCammon, J.A. *J. Med. Chem.* **2000**, *43*, 2100-2114.
- (191) Evensen, E.; Joseph-McCarthy, D.; Weiss, G.A.; Schreiber, S.L.; Karplus, M. *J. Comput. Aided Mol. Des.* **2007**, *21*, 395-418.
- (192) Imai, T.; Oda, K.; Kovalenko, A.; Hirata, F.; Kidera, A. *J. Am. Chem. Soc.* **2009**, *131*, 12430-12440.
- (193) Brenke, R.; Kozakov, D.; Chuang, G.Y.; Beglov, D.; Hall, D.; Landon, M.R.; Mattos, C.; Vajda, S. *Bioinformatics* **2009**, *25*, 621-627.
- (194) Kolb, P.; Ferreira, R.S.; Irwin, J.J.; Shoichet, B.K. *Curr. Opin. Biotechnol.* **2009**, *20*, 429-436.
- (195) Chen, Y.; Shoichet, B.K. *Nat. Chem. Biol.* **2009**, *5*, 358-364.
- (196) Hubbard, R.E.; Chen, I.; Davis, B. *Current opinion in drug discovery & development* **2007**, *10*, 289-297.
- (197) Teotico, D.G.; Babaoglu, K.; Rocklin, G.J.; Ferreira, R.S.; Giannetti, A.M.; Shoichet, B.K. *Proc. Natl. Acad. Sci. U. S. A.* **2009**, *106*, 7455-7460.
- (198) Kawatkar, S.; Wang, H.; Czermanski, R.; Joseph-McCarthy, D. *J. Comput. Aided Mol. Des.* **2009**, *23*, 527-539.
- (199) Jencks, W.P. *Proc. Natl. Acad. Sci. U. S. A.* **1981**, *78*, 4046-4050.
- (200) Lauri, G.; Bartlett, P.A. *J. Comput. Aided Mol. Des.* **1994**, *8*, 51-66.
- (201) Eisen, M.B.; Wiley, D.C.; Karplus, M.; Hubbard, R.E. *Proteins* **1994**, *19*, 199-221.

- (202) Pearlman, D.A.; Murcko, M.A. *J. Med. Chem.* **1996**, *39*, 1651-1663.
- (203) Schneider, G.; Fechner, U. *Nature reviews. Drug discovery* **2005**, *4*, 649-663.
- (204) Loving, K.; Alberts, I.; Sherman, W. *Curr. Top. Med. Chem.* **2010**, *10*, 14-32.
- (205) Thompson, D.C.; Denny, R.A.; Nilakantan, R.; Humblet, C.; Joseph-McCarthy, D.; Feyfant, E. *J. Comput. Aided Mol. Des.* **2008**, *22*, 761-772.
- (206) Maass, P.; Schulz-Gasch, T.; Stahl, M.; Rarey, M. *J. Chem. Inf. Model.* **2007**, *47*, 390-399.
- (207) Pierce, A.C.; Rao, G.; Bemis, G.W. *J. Med. Chem.* **2004**, *47*, 2768-2775.
- (208) Dey, F.; Caflisch, A. *J. Chem. Inf. Model.* **2008**, *48*, 679-690.
- (209) Allegrow. www.bostondenovo.com.
- (210) OpenEye Scientific Software, I. Brood. www.eyesopen.com.
- (211) Bohacek, R.S.; McMartin, C. *J. Am. Chem. Soc.* **1994**, *116*, 5560-5571.
- (212) Kutchukian, P.S.; Lou, D.; Shakhnovich, E.I. *J. Chem. Inf. Model.* **2009**, *49*, 1630-1642.
- (213) Ni, S.; Yuan, Y.; Huang, J.; Mao, X.; Lv, M.; Zhu, J.; Shen, X.; Pei, J.; Lai, L.; Jiang, H.; Li, J. *J. Med. Chem.* **2009**, *52*, 5295-5298.
- (214) Li, H.; Liu, A.; Zhao, Z.; Xu, Y.; Lin, J.; Jou, D.; Li, C. *J. Med. Chem.* **2011**, *54*, 5592-5596.
- (215) Li, H.; Li, C. *J. Comput. Chem.* **2010**, *31*, 2014-2022.
- (216) Wishart, D.S.; Knox, C.; Guo, A.C.; Cheng, D.; Shrivastava, S.; Tzur, D.; Gautam, B.; Hassanali, M. *Nucleic Acids Res.* **2008**, *36*, D901-906.
- (217) Becker, O.M.; Dhanoa, D.S.; Marantz, Y.; Chen, D.; Shacham, S.; Cheruku, S.; Heifetz, A.; Mohanty, P.; Fichman, M.; Sharadendu, A.; Nudelman, R.; Kauffman, M.; Noiman, S. *J. Med. Chem.* **2006**, *49*, 3116-3135.
- (218) Wermuth, C.G.; Ganellin, C.R.; Lindberg, P.; Mitscher, L.A. *Pure Appl. Chem.* **1998**, *70*, 1129-1143.
- (219) Falchi, F.; Caporuscio, F.; Recanatini, M. *Future Med. Chem.* **2014**, *6*, 343-357.
- (220) Pandey, A.; Paliwal, S.K.; Paliwal, S.K. *Journal of Chemistry* **2014**, *2014*, 1-16.
- (221) Lakshmi, P.J.; Kumar, B.V.; Nayana, R.S.; Mohan, M.S.; Bolligarla, R.; Das, S.K.; Bhanu, M.U.; Kondapi, A.K.; Ravikumar, M. *Bioorg. Med. Chem.* **2009**, *17*, 6040-6047.
- (222) Sundriyal, S.; Sharma, R.K.; Jain, R.; Bharatam, P.V. *J. Mol. Model.* **2008**, *14*, 265-278.
- (223) Paliwal, S.; Pal, M.; Yadav, D.; Singh, S.; Yadav, R. *Med. Chem. Res.* **2012**, *21*, 2307-2315.
- (224) Lu, C.; Jin, F.; Li, C.; Li, W.; Liu, G.; Tang, Y. *J. Mol. Model.* **2011**, *17*, 2513-2523.
- (225) Sun, H. *Curr. Med. Chem.* **2008**, *15*, 1018-1024.

- (226) Ballester, P.J.; Westwood, I.; Laurieri, N.; Sim, E.; Richards, W.G. *Journal of the Royal Society, Interface / the Royal Society* **2010**, *7*, 335-342.
- (227) Roy, K.K.; Singh, S.; Saxena, A.K. *Mol. Divers.* **2011**, *15*, 477-489.
- (228) Yadav, D.; Paliwal, S.; Yadav, R.; Pal, M.; Pandey, A. *PLoS One* **2012**, *7*, e48942.
- (229) Leach, A.R.; Gillet, V.J.; Lewis, R.A.; Taylor, R. *J. Med. Chem.* **2010**, *53*, 539-558.
- (230) Fritzon, I.; Svensson, B.; Al-Karadaghi, S.; Walse, B.; Wellmar, U.; Nilsson, U.J.; da Graca Thrige, D.; Jonsson, S. *ChemMedChem* **2010**, *5*, 608-617.
- (231) Ji, H.; Stanton, B.Z.; Igarashi, J.; Li, H.; Martasek, P.; Roman, L.J.; Poulos, T.L.; Silverman, R.B. *J. Am. Chem. Soc.* **2008**, *130*, 3900-3914.
- (232) Sakkiah, S.; Thangapandian, S.; Lee, K. *J. Mol. Model.* **2012**, *18*, 3267-3282.
- (233) de Graaf, C.; Kooistra, A.J.; Vischer, H.F.; Katritch, V.; Kuijjer, M.; Shiroishi, M.; Iwata, S.; Shimamura, T.; Stevens, R.C.; de Esch, I.J.; Leurs, R. *J. Med. Chem.* **2011**, *54*, 8195-8206.
- (234) Evers, A.; Klabunde, T. *J. Med. Chem.* **2005**, *48*, 1088-1097.
- (235) Kumar, N.; Hendriks, B.S.; Janes, K.A.; de Graaf, D.; Lauffenburger, D.A. *Drug Discov Today* **2006**, *11*, 806-811.
- (236) Fischer, E. *Berichte der deutschen chemischen Gesellschaft* **1894**, *27*, 2985-2993.
- (237) Levinthal, C.; Wodak, S.J.; Kahn, P.; Dadvanian, A.K. *Proc. Natl. Acad. Sci. U. S. A.* **1975**, *72*, 1330-1334.
- (238) Salemme, F.R. *J. Mol. Biol.* **1976**, *102*, 563-568.
- (239) Wodak, S.J.; Janin, J. *J. Mol. Biol.* **1978**, *124*, 323-342.
- (240) Kuntz, I.D.; Blaney, J.M.; Oatley, S.J.; Langridge, R.; Ferrin, T.E. *J. Mol. Biol.* **1982**, *161*, 269-288.
- (241) Nicklaus, M.C.; Wang, S.; Driscoll, J.S.; Milne, G.W. *Bioorg. Med. Chem.* **1995**, *3*, 411-428.
- (242) Koshland, D.E. *Proc. Natl. Acad. Sci. U. S. A.* **1958**, *44*, 98-104.
- (243) DesJarlais, R.L.; Sheridan, R.P.; Dixon, J.S.; Kuntz, I.D.; Venkataraghavan, R. *J. Med. Chem.* **1986**, *29*, 2149-2153.
- (244) Busetta, B.; Tickle, I.J.; Blundell, T.L. *J. Appl. Crystallogr.* **1983**, *16*, 432-437.
- (245) Pattabiraman, N.; Levitt, M.; Ferrin, T.E.; Langridge, R. *J. Comput. Chem.* **1985**, *6*, 432-436.
- (246) Tomioka, N.; Itai, A.; Iitaka, Y. *J. Comput. Aided Mol. Des.* **1987**, *1*, 197-210.
- (247) Laurie, A.T.; Jackson, R.M. *Bioinformatics* **2005**, *21*, 1908-1916.
- (248) Liu, X.S.; Brutlag, D.L.; Liu, J.S. *Nat. Biotechnol.* **2002**, *20*, 835-839.
- (249) Singh, T.; Biswas, D.; Jayaram, B. *J. Chem. Inf. Model.* **2011**, *51*, 2515-2527.
- (250) Neuvirth, H.; Raz, R.; Schreiber, G. *J. Mol. Biol.* **2004**, *338*, 181-199.

- (251) Miller III, B., PhD, University of Florida, 2013, 224.
- (252) Jiang, F.; Kim, S.H. *J. Mol. Biol.* **1991**, *219*, 79-102.
- (253) Sherman, W.; Day, T.; Jacobson, M.P.; Friesner, R.A.; Farid, R. *J. Med. Chem.* **2006**, *49*, 534-553.
- (254) Ferrari, A.M.; Wei, B.Q.; Costantino, L.; Shoichet, B.K. *J. Med. Chem.* **2004**, *47*, 5076-5084.
- (255) Leach, A.R. *J. Mol. Biol.* **1994**, *235*, 345-356.
- (256) Anderson, A.C.; O'Neil, R.H.; Surti, T.S.; Stroud, R.M. *Chem. Biol.* **2001**, *8*, 445-457.
- (257) Yang, A.Y.; Kallblad, P.; Mancera, R.L. *J. Comput. Aided Mol. Des.* **2004**, *18*, 235-250.
- (258) Cavasotto, C.N.; Abagyan, R.A. *J. Mol. Biol.* **2004**, *337*, 209-225.
- (259) Meiler, J.; Baker, D. *Proteins* **2006**, *65*, 538-548.
- (260) Totrov, M.; Abagyan, R. *Proteins* **1997**, *Suppl 1*, 215-220.
- (261) Alonso, H.; Bliznyuk, A.A.; Gready, J.E. *Med. Res. Rev.* **2006**, *26*, 531-568.
- (262) Amaro, R.E.; Baron, R.; McCammon, J.A. *J. Comput. Aided Mol. Des.* **2008**, *22*, 693-705.
- (263) Lin, J.H.; Perryman, A.L.; Schames, J.R.; McCammon, J.A. *J. Am. Chem. Soc.* **2002**, *124*, 5632-5633.
- (264) Lin, J.H.; Perryman, A.L.; Schames, J.R.; McCammon, J.A. *Biopolymers* **2003**, *68*, 47-62.
- (265) Fernandez-Recio, J.; Totrov, M.; Abagyan, R. *Proteins* **2003**, *52*, 113-117.
- (266) Goodsell, D.S.; Morris, G.M.; Olson, A.J. *J. Mol. Recognit.* **1996**, *9*, 1-5.
- (267) Judson, R.S.; Jaeger, E.P.; Treasurywala, A.M. *Journal of Molecular Structure: THEOCHEM* **1994**, *308*, 191-206.
- (268) Taylor, J.S.; Burnett, R.M. *Proteins* **2000**, *41*, 173-191.
- (269) Jones, G.; Willett, P.; Glen, R.C.; Leach, A.R.; Taylor, R. *J. Mol. Biol.* **1997**, *267*, 727-748.
- (270) Morris, G.M.; Goodsell, D.S.; Halliday, R.S.; Huey, R.; Hart, W.E.; Belew, R.K.; Olson, A.J. *J. Comput. Chem.* **1998**, *19*, 1639-1662.
- (271) Hou, T.; Wang, J.; Chen, L.; Xu, X. *Protein Eng.* **1999**, *12*, 639-648.
- (272) Oshiro, C.M.; Kuntz, I.D.; Dixon, J.S. *J. Comput. Aided Mol. Des.* **1995**, *9*, 113-130.
- (273) Yang, J.M.; Kao, C.Y. *IEEE Trans. Inf. Technol. Biomed. Publ. IEEE Eng. Med. Biol. Soc* **2000**, *4*, 225-237.
- (274) Feher, M.; Williams, C.I. *J. Chem. Inf. Model.* **2009**, *49*, 1704-1714.
- (275) Goodsell, D.S.; Olson, A.J. *Proteins* **1990**, *8*, 195-202.
- (276) Metropolis, N.; Rosenbluth, A.W.; Rosenbluth, M.N.; Teller, A.H.; Teller, E. *The Journal of Chemical Physics* **1953**, *21*, 1087-1092.
- (277) Metropolis, N.; Ulam, S. *Journal of the American Statistical Association* **1949**, *44*, 335-341.

- (278) Trosset, J.Y.; Scheraga, H.A. *Proc. Natl. Acad. Sci. U. S. A.* **1998**, *95*, 8011-8015.
- (279) Pak, Y.; Wang, S. *The Journal of Physical Chemistry B* **1999**, *104*, 354-359.
- (280) Williams, C.I.; Feher, M. *J. Comput. Aided Mol. Des.* **2008**, *22*, 39-51.
- (281) Nakajima, N.; Higo, J.; Kidera, A.; Nakamura, H. *Chem. Phys. Lett.* **1997**, *278*, 297-301.
- (282) Nakajima, N.; Nakamura, H.; Kidera, A. *The Journal of Physical Chemistry B* **1997**, *101*, 817-824.
- (283) Di Nola, A.; Roccatano, D.; Berendsen, H.J. *Proteins* **1994**, *19*, 174-182.
- (284) Mangoni, M.; Roccatano, D.; Di Nola, A. *Proteins* **1999**, *35*, 153-162.
- (285) Friesner, R.A.; Banks, J.L.; Murphy, R.B.; Halgren, T.A.; Klicic, J.J.; Mainz, D.T.; Repasky, M.P.; Knoll, E.H.; Shelley, M.; Perry, J.K.; Shaw, D.E.; Francis, P.; Shenkin, P.S. *J. Med. Chem.* **2004**, *47*, 1739-1749.
- (286) Jorgensen, W.L.; Maxwell, D.S.; Tirado-Rives, J. *J. Am. Chem. Soc.* **1996**, *118*, 11225-11236.
- (287) Bash, P.A.; Field, M.J.; Karplus, M. *J. Am. Chem. Soc.* **1987**, *109*, 8092-8094.
- (288) Kollman, P. *Chem. Rev.* **1993**, *93*, 2395-2417.
- (289) Kitchen, D.B.; Decornez, H.; Furr, J.R.; Bajorath, J. *Nature reviews. Drug discovery* **2004**, *3*, 935-949.
- (290) Jones, J.E. *Proceedings of the Royal Society of London. Series A* **1924**, *106*, 463-477.
- (291) Verdonk, M.L.; Cole, J.C.; Hartshorn, M.J.; Murray, C.W.; Taylor, R.D. *Proteins* **2003**, *52*, 609-623.
- (292) Ewing, T.J.; Makino, S.; Skillman, A.G.; Kuntz, I.D. *J. Comput. Aided Mol. Des.* **2001**, *15*, 411-428.
- (293) Gohlke, H.; Hendlich, M.; Klebe, G. *J. Mol. Biol.* **2000**, *295*, 337-356.
- (294) Muegge, I.; Martin, Y.C. *J. Med. Chem.* **1999**, *42*, 791-804.
- (295) DeWitte, R.S.; Shakhnovich, E.I. *J. Am. Chem. Soc.* **1996**, *118*, 11733-11744.
- (296) Rarey, M.; Kramer, B.; Lengauer, T.; Klebe, G. *J. Mol. Biol.* **1996**, *261*, 470-489.
- (297) Eldridge, M.D.; Murray, C.W.; Auton, T.R.; Paolini, G.V.; Mee, R.P. *J. Comput. Aided Mol. Des.* **1997**, *11*, 425-445.
- (298) Friesner, R.A.; Murphy, R.B.; Repasky, M.P.; Frye, L.L.; Greenwood, J.R.; Halgren, T.A.; Sanschagrin, P.C.; Mainz, D.T. *J. Med. Chem.* **2006**, *49*, 6177-6196.
- (299) Halgren, T.A.; Murphy, R.B.; Friesner, R.A.; Beard, H.S.; Frye, L.L.; Pollard, W.T.; Banks, J.L. *J. Med. Chem.* **2004**, *47*, 1750-1759.
- (300) Plewczynski, D.; Lazniewski, M.; Augustyniak, R.; Ginalski, K. *J. Comput. Chem.* **2011**, *32*, 742-755.
- (301) Gilson, M.K.; Zhou, H.X. *Annu. Rev. Biophys. Biomol. Struct.* **2007**, *36*, 21-42.
- (302) Mobley, D.L.; Dill, K.A. *Structure* **2009**, *17*, 489-498.

- (303)Greenidge, P.A.; Kramer, C.; Mozziconacci, J.C.; Wolf, R.M. *J. Chem. Inf. Model.* **2013**, *53*, 201-209.
- (304)Massova, I.; Kollman, P.A. *Perspect. Drug Discovery Des.* **2000**, *18*, 113-135.
- (305)Kollman, P.A.; Massova, I.; Reyes, C.; Kuhn, B.; Huo, S.; Chong, L.; Lee, M.; Lee, T.; Duan, Y.; Wang, W.; Donini, O.; Cieplak, P.; Srinivasan, J.; Case, D.A.; Cheatham, T.E., 3rd *Acc. Chem. Res.* **2000**, *33*, 889-897.
- (306)Hou, T.; Wang, J.; Li, Y.; Wang, W. *J. Chem. Inf. Model.* **2011**, *51*, 69-82.
- (307)Hou, T.; Wang, J.; Li, Y.; Wang, W. *J. Comput. Chem.* **2011**, *32*, 866-877.
- (308)Rastelli, G.; Del Rio, A.; Degliesposti, G.; Sgobba, M. *J. Comput. Chem.* **2010**, *31*, 797-810.
- (309)Lafont, V.; Armstrong, A.A.; Ohtaka, H.; Kiso, Y.; Mario Amzel, L.; Freire, E. *Chem. Biol. Drug Des.* **2007**, *69*, 413-422.
- (310)Jacobson, M.P.; Friesner, R.A.; Xiang, Z.; Honig, B. *J. Mol. Biol.* **2002**, *320*, 597-608.
- (311)Jacobson, M.P.; Pincus, D.L.; Rapp, C.S.; Day, T.J.; Honig, B.; Shaw, D.E.; Friesner, R.A. *Proteins* **2004**, *55*, 351-367.
- (312)Li, J.; Abel, R.; Zhu, K.; Cao, Y.; Zhao, S.; Friesner, R.A. *Proteins* **2011**, *79*, 2794-2812.
- (313)Shivakumar, D.; Williams, J.; Wu, Y.; Damm, W.; Shelley, J.; Sherman, W. *J. Chem. Theory Comput.* **2010**, *6*, 1509-1519.
- (314)Kuhn, B.; Gerber, P.; Schulz-Gasch, T.; Stahl, M. *J. Med. Chem.* **2005**, *48*, 4040-4048.
- (315)Mooij, W.T.; Verdonk, M.L. *Proteins* **2005**, *61*, 272-287.
- (316)Cicero, D.O.; Barbato, G.; Bazzo, R. *J. Am. Chem. Soc.* **1995**, *117*, 1027-1033.
- (317)Jogalekar, A.S. *CHEMCOS* **2008**.
- (318)Torda, A.E.; Brunne, R.M.; Huber, T.; Kessler, H.; van Gunsteren, W.F. *J. Biomol. NMR* **1993**, *3*, 55-66.
- (319)Mierke, D.F.; Scheek, R.M.; Kessler, H. *Biopolymers* **1994**, *34*, 559-563.
- (320)Fesik, S.W.; O'Donnell, T.J.; Gampe, R.T.; Olejniczak, E.T. *J. Am. Chem. Soc.* **1986**, *108*, 3165-3170.
- (321)Kessler, H.; Griesinger, C.; Lautz, J.; Mueller, A.; Van Gunsteren, W.F.; Berendsen, H.J.C. *J. Am. Chem. Soc.* **1988**, *110*, 3393-3396.
- (322)Kim, Y.; Prestegard, J.H. *Biochemistry* **1989**, *28*, 8792-8797.
- (323)Torda, A.E.; Scheek, R.M.; van Gunsteren, W.F. *J. Mol. Biol.* **1990**, *214*, 223-235.
- (324)Mierke, D.F.; Kurz, M.; Kessler, H. *J. Am. Chem. Soc.* **1994**, *116*, 1042-1049.
- (325)Brüschweiler, R.; Blackledge, M.; Ernst, R.R. *J. Biomol. NMR* **1991**, *1*, 3-11.

- (326)Grimmer, C.; Moore, T.W.; Padwa, A.; Prussia, A.; Wells, G.; Wu, S.; Sun, A.; Snyder, J.P. *J. Chem. Inf. Model.* **2014**, *54*, 2214-2223.
- (327)Kingston, D.G. *J. Org. Chem.* **2008**, *73*, 3975-3984.
- (328)Snyder, J.P.; Lakdawala, A.S.; Kelso, M.J. *J. Am. Chem. Soc.* **2003**, *125*, 632-633.
- (329)Aggarwal, B.; Sundaram, C.; Malani, N.; Ichikawa, H. In *The Molecular Targets and Therapeutic Uses of Curcumin in Health and Disease*; Aggarwal, B. B., Surh, Y.-J., Shishodia, S., Eds.; Springer US: 2007; Vol. 595, p 1-75.
- (330)Biswas, T.K.; Mukherjee, B. *The Int. J. Of Low. Extremity Wounds* **2003**, *2*, 25-39.
- (331)Gupta, S.C.; Sung, B.; Kim, J.H.; Prasad, S.; Li, S.; Aggarwal, B.B. *Mol. Nutr. Food Res.* **2013**, *57*, 1510-1528.
- (332)Curcuma Longa. http://en.wikipedia.org/wiki/Turmeric#mediaviewer/File:Curcuma_longa_-_K%C3%B6hler%E2%80%93s_Medizinal-Pflanzen-199.jpg.
- (333)Aggarwal, B.B.; Kumar, A.; Bharti, A.C. *Anticancer Res.* **2003**, *23*, 363-398.
- (334)Chattopadhyay, I.; Biswas, K.; Bandyopadhyay, U.; Banerjee, R.K. *Curr Sci.* **2004**, *87*, 44-50.
- (335)Abas, F.; Lajis, N.H.; Shaari, K.; Israfi, D.A.; Stanslas, J.; Yusuf, U.K.; Raof, S.M. *J. Nat. Prod.* **2005**, *68*, 1090-1093.
- (336)Syu, W., Jr.; Shen, C.-C.; Don, M.-J.; Ou, J.-C.; Lee, G.-H.; Sun, C.-M. *J. Nat. Prod.* **1998**, *61*, 1531-1534.
- (337)Duke, J.A. *Crc Handbook of Medicinal Herbs* 2nd ed.; CRC Press, 2002.
- (338)Tohda, C.; Nakayama, N.; Hatanaka, F.; Komatsu, K. *Evid. Based Complement. Alternat. Med.* **2006**, *3*, 255-260.
- (339)Mohamad, H.; Lajis, N.H.; Abas, F.; Ali, A.M.; Sukari, M.A.; Kikuzaki, H.; Nakatani, N. *J. Nat. Prod.* **2005**, *68*, 285-288.
- (340)Dechatowongse, T. *Bull Dept Med Sci* **1976**, *18*, 75-79.
- (341)Ahsan, H.; Parveen, N.; Khan, N.U.; Hadi, S.M. *Chem. Biol. Interact.* **1999**, *121*, 161-175.
- (342)Sreejayan, N.; Rao, M.N. *Arzneimittelforschung* **1996**, *46*, 169-171.
- (343)Thapliyal, R.; Maru, G.B. *Food Chem. Toxicol.* **2001**, *39*, 541-547.
- (344)Huang, M.T.; Lou, Y.R.; Xie, J.G.; Ma, W.; Lu, Y.P.; Yen, P.; Zhu, B.T.; Newmark, H.; Ho, C.T. *Carcinogenesis* **1998**, *19*, 1697-1700.
- (345)Sreejayan, N.; Rao, M.N. *J. Pharm. Pharmacol.* **1997**, *49*, 105-107.
- (346)Nishiyama, T.; Mae, T.; Kishida, H.; Tsukagawa, M.; Mimaki, Y.; Kuroda, M.; Sashida, Y.; Takahashi, K.; Kawada, T.; Nakagawa, K.; Kitahara, M. *J. Agric. Food. Chem.* **2005**, *53*, 959-963.

- (347) Suryanarayana, P.; Saraswat, M.; Mrudula, T.; Krishna, T.P.; Krishnaswamy, K.; Reddy, G.B. *Invest. Ophthalmol. Vis. Sci.* **2005**, *46*, 2092-2099.
- (348) Deshpande, S.S.; Ingle, A.D.; Maru, G.B. *Cancer Lett.* **1997**, *118*, 79-85.
- (349) Deshpande, S.S.; Ingle, A.D.; Maru, G.B. *Cancer Lett.* **1998**, *123*, 35-40.
- (350) Li, S.; Yuan, W.; Deng, G.; Wang, P.; Yang, P.; Aggarwal, B.B. *Pharmaceutical Crops* **2011**, *2*, 28-54.
- (351) Prasad, S.; Gupta, S.C.; Tyagi, A.K.; Aggarwal, B.B. *Biotechnol. Adv.* **2014**, 1053-1064.
- (352) Sidhu, G.S.; Singh, A.K.; Thaloor, D.; Banaudha, K.K.; Patnaik, G.K.; Srimal, R.C.; Maheshwari, R.K. *Wound Repair Regen.* **1998**, *6*, 167-177.
- (353) Sidhu, G.S.; Mani, H.; Gaddipati, J.P.; Singh, A.K.; Seth, P.; Banaudha, K.K.; Patnaik, G.K.; Maheshwari, R.K. *Wound Repair Regen.* **1999**, *7*, 362-374.
- (354) Phan, T.-T.; See, P.; Lee, S.-T.; Chan, S.-Y. *Journal of Trauma and Acute Care Surgery* **2001**, *51*, 927-931.
- (355) Fray, T.R.; Watson, A.L.; Croft, J.M.; Baker, C.D.; Bailey, J.; Sirel, N.; Tobias, A.; Markwell, P.J. *J. Nutr.* **2004**, *134*, 2117s-2119s.
- (356) Gopinath, D.; Ahmed, M.R.; Gomathi, K.; Chitra, K.; Sehgal, P.K.; Jayakumar, R. *Biomaterials* **2004**, *25*, 1911-1917.
- (357) Jagetia, G.C.; Rajanikant, G.K. *Plast. Reconstr. Surg.* **2005**, *115*, 515-528.
- (358) Jagetia, G.C.; Rajanikant, G.K. *J Surg Res* **2004**, *120*, 127-138.
- (359) Jagetia, G.C.; Rajanikant, G.K. *J. Wound Care* **2004**, *13*, 107-109.
- (360) Sharma, O.P. *Biochem. Pharmacol.* **1976**, *25*, 1811-1812.
- (361) Sugiyama, Y.; Kawakishi, S.; Osawa, T. *Biochem. Pharmacol.* **1996**, *52*, 519-525.
- (362) Ruby, A.J.; Kuttan, G.; Babu, K.D.; Rajasekharan, K.N.; Kuttan, R. *Cancer Lett.* **1995**, *94*, 79-83.
- (363) Srimal, R.C.; Dhawan, B.N. *J. Pharm. Pharmacol.* **1973**, *25*, 447-452.
- (364) Gulcubuk, A.; Altunatmaz, K.; Sonmez, K.; Haktanir-Yatkin, D.; Uzun, H.; Gurel, A.; Aydin, S. *J. Vet. Med. A Physiol. Pathol. Clin. Med.* **2006**, *53*, 49-54.
- (365) Gülçubuk, A.; Sönmez, K.; Gürel, A.; Altunatmaz, K.; Gürler, N.; Aydın, S.; Öksüz, L.; Uzun, H.; Güzel, Ö. *Pancreatology* **2005**, *5*, 345-353.
- (366) Masamune, A.; Suzuki, N.; Kikuta, K.; Satoh, M.; Satoh, K.; Shimosegawa, T. *J. Cell. Biochem.* **2006**, *97*, 1080-1093.
- (367) Kim, D.-C.; Kim, S.-H.; Choi, B.-H.; Baek, N.-I.; Kim, D.; Kim, M.-J.; Kim, K.-T. *Biol. Pharm. Bull.* **2005**, *28*, 2220-2224.

- (368) Swarnakar, S.; Ganguly, K.; Kundu, P.; Banerjee, A.; Maity, P.; Sharma, A.V. *J. Biol. Chem.* **2005**, *280*, 9409-9415.
- (369) Sugimoto, K.; Hanai, H.; Tozawa, K.; Aoshi, T.; Uchijima, M.; Nagata, T.; Koide, Y. *Gastroenterology* **2002**, *123*, 1912-1922.
- (370) Salh, B.; Assi, K.; Templeman, V.; Parhar, K.; Owen, D.; Gómez-Muñoz, A.; Jacobson, K. *Am. J. Physiol. Gastrointest. Liver Physiol.* **2003**, *285*, G235-G243.
- (371) Jiang, Y.; Li, Z.S.; Jiang, F.S.; Deng, X.; Yao, C.S.; Nie, G. *World J. Gastroenterol.* **2005**, *11*, 6780-6786.
- (372) Holt, P.; Katz, S.; Kirshoff, R. *Dig. Dis. Sci.* **2005**, *50*, 2191-2193.
- (373) Joe, B.; Rao, U.J.; Lokesh, B.R. *Mol. Cell. Biochem.* **1997**, *169*, 125-134.
- (374) Liacini, A.; Sylvester, J.; Li, W.Q.; Zafarullah, M. *Matrix Biol.* **2002**, *21*, 251-262.
- (375) Liacini, A.; Sylvester, J.; Li, W.Q.; Huang, W.; Dehnade, F.; Ahmad, M.; Zafarullah, M. *Exp. Cell Res.* **2003**, *288*, 208-217.
- (376) Sylvester, J.; Liacini, A.; Li, W.Q.; Zafarullah, M. *Cell. Signal.* **2004**, *16*, 469-476.
- (377) Baek, O.-S.; Kang, O.-H.; Choi, Y.-A.; Choi, S.-C.; Kim, T.-H.; Nah, Y.-H.; Kwon, D.-Y.; Kim, Y.-K.; Kim, Y.-H.; Bae, K.-H.; Lim, J.-P.; Lee, Y.-M. *Clin. Chim. Acta* **2003**, *338*, 135-141.
- (378) Ram, A.; Das, M.; Ghosh, B. *Biol. Pharm. Bull.* **2003**, *26*, 1021-1024.
- (379) Lee, J.-J.; Huang, W.-T.; Shao, D.-Z.; Liao, J.-F.; Lin, M.-T. *The Japanese Journal of Physiology* **2003**, *53*, 367-375.
- (380) Shao, D.-Z.; Lee, J.-J.; Huang, W.-T.; Liao, J.-F.; Lin, M.-T. *Mol. Cell. Biochem.* **2004**, *262*, 177-185.
- (381) Verbeek, R.; van Tol, E.A.F.; van Noort, J.M. *Biochem. Pharmacol.* **2005**, *70*, 220-228.
- (382) Natarajan, C.; Bright, J.J. *The Journal of Immunology* **2002**, *168*, 6506-6513.
- (383) Babu, P.S.; Srinivasan, K. *Mol. Cell. Biochem.* **1997**, *166*, 169-175.
- (384) Babu, P.S.; Srinivasan, K. *Mol. Cell. Biochem.* **1995**, *152*, 13-21.
- (385) Sajithlal, G.B.; Chithra, P.; Chandrakasan, G. *Biochem. Pharmacol.* **1998**, *56*, 1607-1614.
- (386) Arun, N.; Nalini, N. *Plant Foods Hum. Nutr.* **2002**, *57*, 41-52.
- (387) Kempaiah, R.K.; Srinivasan, K. *Int. J. Vitam. Nutr. Res.* **2004**, *74*, 199-208.
- (388) Mahesh, T.; Sri Balasubashini, M.M.; Menon, V.P. *Therapie* **2004**, *59*, 639-644.
- (389) Kuroda, M.; Mimaki, Y.; Nishiyama, T.; Mae, T.; Kishida, H.; Tsukagawa, M.; Takahashi, K.; Kawada, T.; Nakagawa, K.; Kitahara, M. *Biol. Pharm. Bull.* **2005**, *28*, 937-939.
- (390) Majithiya, J.B.; Balaraman, R. *J. Cardiovasc. Pharmacol.* **2005**, *46*, 697-705.
- (391) Osawa, T.; Kato, Y. *Ann. N. Y. Acad. Sci.* **2005**, *1043*, 440-451.

- (392) Tourkina, E.; Gooz, P.; Oates, J.C.; Ludwicka-Bradley, A.; Silver, R.M.; Hoffman, S. *Am. J. Respir. Cell Mol. Biol.* **2004**, *31*, 28-35.
- (393) Bosman, B. *Skin Pharmacol.* **1994**, *7*, 324-334.
- (394) Qader, S.W.; Abdulla, M.A.; Chua, L.S.; Najim, N.; Zain, M.M.; Hamdan, S. *Molecules* **2011**, *16*, 3433-3443.
- (395) Cohly, H.H.; Taylor, A.; Angel, M.F.; Salahudeen, A.K. *Free Radic. Biol. Med.* **1998**, *24*, 49-54.
- (396) Mahady, G.B.; Pendland, S.L.; Yun, G.; Lu, Z.Z. *Anticancer Res.* **2002**, *22*, 4179-4181.
- (397) Kim, M.K.; Choi, G.J.; Lee, H.S. *J. Agric. Food. Chem.* **2003**, *51*, 1578-1581.
- (398) Reddy, R.C.; Vatsala, P.G.; Keshamouni, V.G.; Padmanaban, G.; Rangarajan, P.N. *Biochem. Biophys. Res. Commun.* **2005**, *326*, 472-474.
- (399) Jordan, W.C.; Drew, C.R. *J. Natl. Med. Assoc.* **1996**, 333.
- (400) Kuttan, R.; Bhanumathy, P.; Nirmala, K.; George, M.C. *Cancer Lett.* **1985**, *29*, 197-202.
- (401) Srivastava, R.; Dikshit, M.; Srimal, R.C.; Dhawan, B.N. *Thromb. Res.* **1985**, *40*, 413-417.
- (402) Dikshit, M.; Rastogi, L.; Shukla, R.; Srimal, R.C. *Indian J. Med. Res.* **1995**, *101*, 31-35.
- (403) Nirmala, C.; Puvanakrishnan, R. *Mol. Cell. Biochem.* **1996**, *159*, 85-93.
- (404) Nirmala, C.; Puvanakrishnan, R. *Biochem. Pharmacol.* **1996**, *51*, 47-51.
- (405) Sato, M.; Cordis, G.A.; Maulik, N.; Das, D.K. *Am. J. Physiol. Heart Circ. Physiol.* **2000**, *279*, H901-907.
- (406) Zhang, W.; Liu, D.; Wo, X.; Zhang, Y.; Jin, M.; Ding, Z. *Chin. Med. J. (Engl.)* **1999**, *112*, 308-311.
- (407) Chen, H.W.; Huang, H.C. *Br. J. Pharmacol.* **1998**, *124*, 1029-1040.
- (408) Manikandan, P.; Sumitra, M.; Aishwarya, S.; Manohar, B.M.; Lokanadam, B.; Puvanakrishnan, R. *Int. J. Biochem. Cell Biol.* **2004**, *36*, 1967-1980.
- (409) Ramaswami, G.; Chai, H.; Yao, Q.; Lin, P.H.; Lumsden, A.B.; Chen, C. *J. Vasc. Surg.* **2004**, *40*, 1216-1222.
- (410) Nguyen, K.T.; Shaikh, N.; Shukla, K.P.; Su, S.H.; Eberhart, R.C.; Tang, L. *Biomaterials* **2004**, *25*, 5333-5346.
- (411) Gupta, S.C.; Prasad, S.; Kim, J.H.; Patchva, S.; Webb, L.J.; Priyadarsini, I.K.; Aggarwal, B.B. *Nat. Prod. Rep.* **2011**, *28*, 1937-1955.
- (412) Jana, N.R.; Dikshit, P.; Goswami, A.; Nukina, N. *J. Biol. Chem.* **2004**, *279*, 11680-11685.
- (413) Liontas, A.; Yeger, H. *Anticancer Res.* **2004**, *24*, 987-998.
- (414) Chakravarti, N.; Myers, J.N.; Aggarwal, B.B. *Int. J. Cancer* **2006**, *119*, 1268-1275.
- (415) Aggarwal, S.; Takada, Y.; Singh, S.; Myers, J.N.; Aggarwal, B.B. *Int. J. Cancer* **2004**, *111*, 679-692.

- (416) Mehta, K.; Pantazis, P.; McQueen, T.; Aggarwal, B.B. *Anticancer Drugs* **1997**, *8*, 470-481.
- (417) Ramachandran, C.; You, W. *Breast Cancer Res. Treat.* **1999**, *54*, 269-278.
- (418) Choudhuri, T.; Pal, S.; Aggarwal, M.L.; Das, T.; Sa, G. *FEBS Lett.* **2002**, *512*, 334-340.
- (419) Holy, J.M. *Mutat. Res.* **2002**, *518*, 71-84.
- (420) Shao, Z.M.; Shen, Z.Z.; Liu, C.H.; Sartippour, M.R.; Go, V.L.; Heber, D.; Nguyen, M. *Int. J. Cancer* **2002**, *98*, 234-240.
- (421) Ramachandran, C.; Rodriguez, S.; Ramachandran, R.; Raveendran Nair, P.K.; Fonseca, H.; Khatib, Z.; Escalon, E.; Melnick, S.J. *Anticancer Res.* **2005**, *25*, 3293-3302.
- (422) Radhakrishna Pillai, G.; Srivastava, A.S.; Hassanein, T.I.; Chauhan, D.P.; Carrier, E. *Cancer Lett.* **2004**, *208*, 163-170.
- (423) Hecht, S.S.; Kenney, P.M.; Wang, M.; Trushin, N.; Agarwal, S.; Rao, A.V.; Upadhyaya, P. *Cancer Lett.* **1999**, *137*, 123-130.
- (424) Li, L.; Aggarwal, B.B.; Shishodia, S.; Abbruzzese, J.; Kurzrock, R. *Cancer* **2004**, *101*, 2351-2362.
- (425) Jiang, M.C.; Yang-Yen, H.F.; Lin, J.K.; Yen, J.J. *Oncogene* **1996**, *13*, 609-616.
- (426) Notarbartolo, M.; Poma, P.; Perri, D.; Dusonchet, L.; Cervello, M.; D'Alessandro, N. *Cancer Lett.* **2005**, *224*, 53-65.
- (427) Kuo, M.L.; Huang, T.S.; Lin, J.K. *Biochim. Biophys. Acta* **1996**, *1317*, 95-100.
- (428) Wu, Y.; Chen, Y.; Chen, W. *J. Tongji Med. Univ.* **1999**, *19*, 267-270.
- (429) Duvoix, A.; Morceau, F.; Schnekenburger, M.; Delhalle, S.; Galteau, M.M.; Dicato, M.; Diederich, M. *Ann. N. Y. Acad. Sci.* **2003**, *1010*, 389-392.
- (430) Bielak-Zmijewska, A.; Koronkiewicz, M.; Skierski, J.; Piwocka, K.; Radziszewska, E.; Sikora, E. *Nutr. Cancer* **2000**, *38*, 131-138.
- (431) Chen, Y.; Wu, Y.; He, J.; Chen, W. *J. Huazhong Univ. Sci. Technol. Med. Sci.* **2002**, *22*, 295-298.
- (432) Wu, L.X.; Xu, J.H.; Wu, G.H.; Chen, Y.Z. *Acta Pharmacol. Sin.* **2003**, *24*, 1155-1160.
- (433) Bielak-Mijewska, A.; Piwocka, K.; Magalska, A.; Sikora, E. *Cancer Chemother. Pharmacol.* **2004**, *53*, 179-185.
- (434) Shishodia, S.; Sethi, G.; Aggarwal, B.B. *Ann. N. Y. Acad. Sci.* **2005**, *1056*, 206-217.
- (435) Sun, C.; Liu, X.; Chen, Y.; Liu, F. *J. Huazhong Univ. Sci. Technol. Med. Sci.* **2005**, *25*, 404-407.
- (436) Bharti, A.C.; Shishodia, S.; Reuben, J.M.; Weber, D.; Alexanian, R.; Raj-Vadhan, S.; Estrov, Z.; Talpaz, M.; Aggarwal, B.B. *Blood* **2004**, *103*, 3175-3184.
- (437) Jee, S.H.; Shen, S.C.; Tseng, C.R.; Chiu, H.C.; Kuo, M.L. *J. Invest. Dermatol.* **1998**, *111*, 656-661.

- (438) Zheng, M.; Ekmekcioglu, S.; Walch, E.T.; Tang, C.H.; Grimm, E.A. *Melanoma Res.* **2004**, *14*, 165-171.
- (439) Siwak, D.R.; Shishodia, S.; Aggarwal, B.B.; Kurzrock, R. *Cancer* **2005**, *104*, 879-890.
- (440) Bush, J.A.; Cheung, K.J., Jr.; Li, G. *Exp. Cell Res.* **2001**, *271*, 305-314.
- (441) Kim, D.S.; Park, S.Y.; Kim, J.K. *Neurosci. Lett.* **2001**, *303*, 57-61.
- (442) Frautschy, S.A.; Hu, W.; Kim, P.; Miller, S.A.; Chu, T.; Harris-White, M.E.; Cole, G.M. *Neurobiol. Aging* **2001**, *22*, 993-1005.
- (443) Adlerz, L.; Beckman, M.; Holback, S.; Tehranian, R.; Cortes Toro, V.; Iverfeldt, K. *Brain Res. Mol. Brain Res.* **2003**, *119*, 62-72.
- (444) Lim, G.P.; Chu, T.; Yang, F.; Beech, W.; Frautschy, S.A.; Cole, G.M. *J. Neurosci.* **2001**, *21*, 8370-8377.
- (445) Giri, R.K.; Rajagopal, V.; Kalra, V.K. *J. Neurochem.* **2004**, *91*, 1199-1210.
- (446) Grundman, M.; Grundman, M.; Delaney, P. *Proc. Nutr. Soc.* **2002**, *61*, 191-202.
- (447) Gupta, S.C.; Patchva, S.; Koh, W.; Aggarwal, B.B. *Clin. Exp. Pharmacol. Physiol.* **2012**, *39*, 283-299.
- (448) Gupta, S.C.; Kim, J.H.; Prasad, S.; Aggarwal, B.B. *Cancer Metastasis Rev.* **2010**, *29*, 405-434.
- (449) Goel, A.; Aggarwal, B.B. *Nutr. Cancer* **2010**, *62*, 919-930.
- (450) Suresh, D.; Srinivasan, K. *Food Chem. Toxicol.* **2007**, *45*, 1437-1442.
- (451) Oppenheimer, A. *The Lancet* **1937**, *229*, 619-621.
- (452) Gupta, S.C.; Patchva, S.; Aggarwal, B.B. *The AAPS journal* **2013**, *15*, 195-218.
- (453) Bera, R.; Sahoo, B.K.; Ghosh, K.S.; Dasgupta, S. *Int. J. Biol. Macromol.* **2008**, *42*, 14-21.
- (454) Nafisi, S.; Adelzadeh, M.; Norouzi, Z.; Sarbolouki, M.N. *DNA Cell Biol.* **2009**, *28*, 201-208.
- (455) Pedersen, U.; Rasmussen, P.B.; Lawesson, S.-O. *Liebigs Ann. Chem.* **1985**, *1985*, 1557-1569.
- (456) Tonnesen, H.H.; Karlsten, J.; Mostad, A. *Acta Chem. Scand., Ser. B*, **1982**, *B36*, 475-479.
- (457) Baum, L.; Ng, A. *J. Alzheimers Dis.* **2004**, *6*, 367-377; discussion 443-369.
- (458) Marcu, M.G.; Jung, Y.J.; Lee, S.; Chung, E.J.; Lee, M.J.; Trepel, J.; Neckers, L. *Med. Chem.* **2006**, *2*, 169-174.
- (459) Fang, J.; Lu, J.; Holmgren, A. *J. Biol. Chem.* **2005**, *280*, 25284-25290.
- (460) Kumar, A.; Takada, Y.; Boriek, A.M.; Aggarwal, B.B. *J. Mol. Med. (Berl.)* **2004**, *82*, 434-448.
- (461) Aggarwal, B.B.; Takada, Y.; Shishodia, S.; Gutierrez, A.M.; Oommen, O.V.; Ichikawa, H.; Baba, Y.; Kumar, A. *Indian J. Exp. Biol.* **2004**, *42*, 341-353.
- (462) Ammon, H.P.T.; Safayhi, H.; Mack, T.; Sabieraj, J. *J. Ethnopharmacol.* **1993**, *38*, 105-112.
- (463) Ammon, H.P.; Anazodo, M.I.; Safayhi, H.; Dhawan, B.N.; Srimal, R.C. *Planta Med.* **1992**, *58*, 226.

- (464) Fujiyama-Fujiwara, Y.; Umeda, R.; Igarashi, O. *J Nutr Sci Vitaminol* **1992**, *38*, 353-363.
- (465) Srivastava, R. *Agents Actions* **1989**, *28*, 298-303.
- (466) Reddy, A.C.P.; Lokesh, B.R. *Ann. Nutr. Metab.* **1994**, *38*, 349-358.
- (467) Joe, B.; Lokesh, B. *Mol. Cell. Biochem.* **2000**, *203*, 153-161.
- (468) Joe, B.; Lokesh, B.R. *Lipids* **1997**, *32*, 1173-1180.
- (469) Jones, E.A.; Shahed, A.; Shoskes, D.A. *Urology* **2000**, *56*, 346-351.
- (470) Banerjee, M.; Tripathi, L.M.; Srivastava, V.M.L.; Puri, A.; Shukla, R. *Immunopharmacol. Immunotoxicol.* **2003**, *25*, 213-224.
- (471) Lantz, R.C.; Chen, G.J.; Solyom, A.M.; Jolad, S.D.; Timmermann, B.N. *Phytomedicine* **2005**, *12*, 445-452.
- (472) Xu, Y.X.; Pindolia, K.R.; Janakiraman, N.; Noth, C.J.; Chapman, R.A.; Gautam, S.C. *Exp. Hematol.* **1997**, *25*, 413-422.
- (473) Ireson, C.; Orr, S.; Jones, D.J.; Verschoyle, R.; Lim, C.K.; Luo, J.L.; Howells, L.; Plummer, S.; Jukes, R.; Williams, M.; Steward, W.P.; Gescher, A. *Cancer Res.* **2001**, *61*, 1058-1064.
- (474) Khopde, S.M.; Priyadarsini, K.I.; Guha, S.N.; Satav, J.G.; Venkatesan, P.; Rao, M.N. *Biosci. Biotechnol. Biochem.* **2000**, *64*, 503-509.
- (475) Okada, K.; Wangpoengtrakul, C.; Tanaka, T.; Toyokuni, S.; Uchida, K.; Osawa, T. *J. Nutr.* **2001**, *131*, 2090-2095.
- (476) Pari, L.; Amali, D.R. *J Pharm Pharmaceut Sci* **2005**, *8*, 115-123.
- (477) Pari, L.; Murugan, P. *Pharmacol. Res.* **2004**, *49*, 481-486.
- (478) Nakamura, Y.; Ohto, Y.; Murakami, A.; Osawa, T.; Ohigashi, H. *Cancer Sci.* **1998**, *89*, 361-370.
- (479) Shen, L.; Ji, H.F. *Clin. Cancer Res.* **2009**, *15*, 7108-7109.
- (480) Aggarwal, B.B.; Harikumar, K.B. *The International Journal of Biochemistry & Cell Biology* **2009**, *41*, 40-59.
- (481) Wua, S.; Sun, J.-C.; Lee, K.-J.; Sun, Y.-M. *Intl J Eng Sci Technol* **2010**, *2*, 4263-4277.
- (482) Gradisar, H.; Keber, M.M.; Pristovsek, P.; Jerala, R. *J. Leukoc. Biol.* **2007**, *82*, 968-974.
- (483) Padhye, S.; Banerjee, S.; Chavan, D.; Pandye, S.; Swamy, K.V.; Ali, S.; Li, J.; Dou, Q.P.; Sarkar, F.H. *Pharm. Res.* **2009**, *26*, 2438-2445.
- (484) Selvam, C.; Jachak, S.M.; Thilagavathi, R.; Chakraborti, A.K. *Bioorg. Med. Chem. Lett.* **2005**, *15*, 1793-1797.
- (485) Zsila, F.; Bikadi, Z.; Simonyi, M. *Bioorg. Med. Chem.* **2004**, *12*, 3239-3245.
- (486) Majhi, A.; Rahman, G.M.; Panchal, S.; Das, J. *Bioorg. Med. Chem.* **2010**, *18*, 1591-1598.

- (487) Reddy, S.; Aggarwal, B.B. *FEBS Lett.* **1994**, *341*, 19-22.
- (488) Leu, T.H.; Su, S.L.; Chuang, Y.C.; Maa, M.C. *Biochem. Pharmacol.* **2003**, *66*, 2323-2331.
- (489) Taha, M.O.; Bustanji, Y.; Al-Ghoussein, M.A.; Mohammad, M.; Zalloum, H.; Al-Masri, I.M.; Atallah, N. *J. Med. Chem.* **2008**, *51*, 2062-2077.
- (490) Jung, Y.; Xu, W.; Kim, H.; Ha, N.; Neckers, L. *Biochim. Biophys. Acta* **2007**, *1773*, 383-390.
- (491) Muthenna, P.; Suryanarayana, P.; Gunda, S.K.; Petrash, J.M.; Reddy, G.B. *FEBS Lett.* **2009**, *583*, 3637-3642.
- (492) Howard, E.I.; Sanishvili, R.; Cachau, R.E.; Mitschler, A.; Chevrier, B.; Barth, P.; Lamour, V.; Van Zandt, M.; Sibley, E.; Bon, C.; Moras, D.; Schneider, T.R.; Joachimiak, A.; Podjarny, A. *Proteins* **2004**, *55*, 792-804.
- (493) Matsunaga, T.; Endo, S.; Soda, M.; Zhao, H.T.; El-Kabbani, O.; Tajima, K.; Hara, A. *Biochem. Biophys. Res. Commun.* **2009**, *389*, 128-132.
- (494) Bora-Tatar, G.; Dayangac-Erden, D.; Demir, A.S.; Dalkara, S.; Yelekci, K.; Erdem-Yurter, H. *Bioorg. Med. Chem.* **2009**, *17*, 5219-5228.
- (495) Yuan, M.; Luo, M.; Song, Y.; Xu, Q.; Wang, X.; Cao, Y.; Bu, X.; Ren, Y.; Hu, X. *Bioorg. Med. Chem.* **2011**, *19*, 1189-1196.
- (496) Liu, M.; Yuan, M.; Luo, M.; Bu, X.; Luo, H.B.; Hu, X. *Biophys. Chem.* **2010**, *147*, 28-34.
- (497) Skrzypczak-Jankun, E.; McCabe, N.P.; Selman, S.H.; Jankun, J. *Int. J. Mol. Med.* **2000**, *6*, 521-526.
- (498) Skrzypczak-Jankun, E.; Zhou, K.; McCabe, N.P.; Selman, S.H.; Jankun, J. *Int. J. Mol. Med.* **2003**, *12*, 17-24.
- (499) Pauff, J.M.; Hille, R. *J. Nat. Prod.* **2009**, *72*, 725-731.
- (500) Shen, L.; Ji, H.F. *Bioorg. Med. Chem. Lett.* **2009**, *19*, 5990-5993.
- (501) Kapoor, S.; Priyadarsini, K.I. *Biophys. Chem.* **2001**, *92*, 119-126.
- (502) Wang, S.S.; Liu, K.N.; Lee, W.H. *Biophys. Chem.* **2009**, *144*, 78-87.
- (503) Girija, C.R.; Karunakar, P.; Poojari, C.S.; Begum, N.S.; Syed, A.A. *J. Proteomics Bioinf.* **2010**, *3*, 200-203.
- (504) Takeuchi, T.; Ishidoh, T.; Iijima, H.; Kuriyama, I.; Shimazaki, N.; Koiwai, O.; Kuramochi, K.; Kobayashi, S.; Sugawara, F.; Sakaguchi, K.; Yoshida, H.; Mizushima, Y. *Genes Cells* **2006**, *11*, 223-235.
- (505) Liu, Z.; Xie, Z.; Jones, W.; Pavlovicz, R.E.; Liu, S.; Yu, J.; Li, P.K.; Lin, J.; Fuchs, J.R.; Marcucci, G.; Li, C.; Chan, K.K. *Bioorg. Med. Chem. Lett.* **2009**, *19*, 706-709.
- (506) Sahoo, B.K.; Ghosh, K.S.; Dasgupta, S. *Protein and peptide letters* **2009**, *16*, 1485-1495.

- (507) Mazumder, A.; Raghavan, K.; Weinstein, J.; Kohn, K.W.; Pommier, Y. *Biochem. Pharmacol.* **1995**, *49*, 1165-1170.
- (508) Vajragupta, O.; Boonchoong, P.; Morris, G.M.; Olson, A.J. *Bioorg. Med. Chem. Lett.* **2005**, *15*, 3364-3368.
- (509) Bilmen, J.G.; Khan, S.Z.; Javed, M.H.; Michelangeli, F. *Eur. J. Biochem.* **2001**, *268*, 6318-6327.
- (510) Wang, L.; Wang, L.; Song, R.; Shen, Y.; Sun, Y.; Gu, Y.; Shu, Y.; Xu, Q. *Mol. Cancer Ther.* **2011**, *10*, 461-471.
- (511) Liu, Y.; Yang, Z.; Du, J.; Yao, X.; Lei, R.; Zheng, X.; Liu, J.; Hu, H.; Li, H. *Immunobiology* **2008**, *213*, 651-661.
- (512) Barik, A.; Mishra, B.; Kunwar, A.; Kadam, R.M.; Shen, L.; Dutta, S.; Padhye, S.; Satpati, A.K.; Zhang, H.Y.; Indira Priyadarsini, K. *Eur. J. Med. Chem.* **2007**, *42*, 431-439.
- (513) Mandeville, J.S.; Froehlich, E.; Tajmir-Riahi, H.A. *J. Pharm. Biomed. Anal.* **2009**, *49*, 468-474.
- (514) Pulla Reddy, A.C.; Sudharshan, E.; Appu Rao, A.G.; Lokesh, B.R. *Lipids* **1999**, *34*, 1025-1029.
- (515) Kunwar, A.; Barik, A.; Pandey, R.; Priyadarsini, K.I. *Biochim. Biophys. Acta* **2006**, *1760*, 1513-1520.
- (516) Leung, M.H.; Kee, T.W. *Langmuir* **2009**, *25*, 5773-5777.
- (517) Sahoo, B.K.; Ghosh, K.S.; Dasgupta, S. *Biopolymers* **2009**, *91*, 108-119.
- (518) Priyadarsini, K.I. *Journal of Photochemistry and Photobiology C: Photochemistry Reviews* **2009**, *10*, 81-95.
- (519) Zsila, F.; Bikádi, Z.; Simonyi, M. *Tetrahedron: Asymmetry* **2003**, *14*, 2433-2444.
- (520) Sneharani, A.H.; Karakkat, J.V.; Singh, S.A.; Rao, A.G. *J. Agric. Food. Chem.* **2010**, *58*, 11130-11139.
- (521) Mohammadi, F.; Bordbar, A.K.; Divsalar, A.; Mohammadi, K.; Saboury, A.A. *The protein journal* **2009**, *28*, 117-123.
- (522) Sahu, A.; Kasoju, N.; Bora, U. *Biomacromolecules* **2008**, *9*, 2905-2912.
- (523) Sneharani, A.H.; Singh, S.A.; Appu Rao, A.G. *J. Agric. Food. Chem.* **2009**, *57*, 10386-10391.
- (524) Luthra, P.M.; Kumar, R.; Prakash, A. *Biochem. Biophys. Res. Commun.* **2009**, *384*, 420-425.
- (525) Hafner-Bratkovic, I.; Gaspersic, J.; Smid, L.M.; Bresjanac, M.; Jerala, R. *J. Neurochem.* **2008**, *104*, 1553-1564.
- (526) Barik, A.; Mishra, B.; Shen, L.; Mohan, H.; Kadam, R.M.; Dutta, S.; Zhang, H.Y.; Priyadarsini, K.I. *Free Radic. Biol. Med.* **2005**, *39*, 811-822.
- (527) Shim, J.S.; Lee, J.; Park, H.J.; Park, S.J.; Kwon, H.J. *Chem. Biol.* **2004**, *11*, 1455-1463.

- (528) Koiram, P.R.; Veerapur, V.P.; Kunwar, A.; Mishra, B.; Barik, A.; Priyadarsini, I.K.; Mazhuvancherry, U.K. *J Radiat Res* **2007**, *48*, 241-245.
- (529) Kunwar, A.; Narang, H.; Priyadarsini, K.I.; Krishna, M.; Pandey, R.; Sainis, K.B. *J. Cell. Biochem.* **2007**, *102*, 1214-1224.
- (530) Gupta, K.K.; Bharne, S.S.; Rathinasamy, K.; Naik, N.R.; Panda, D. *The FEBS journal* **2006**, *273*, 5320-5332.
- (531) Shim, J.S.; Kim, J.H.; Cho, H.Y.; Yum, Y.N.; Kim, S.H.; Park, H.J.; Shim, B.S.; Choi, S.H.; Kwon, H.J. *Chem. Biol.* **2003**, *10*, 695-704.
- (532) Yang, F.; Lim, G.P.; Begum, A.N.; Ubeda, O.J.; Simmons, M.R.; Ambegaokar, S.S.; Chen, P.P.; Kaye, R.; Glabe, C.G.; Frautschi, S.A.; Cole, G.M. *J. Biol. Chem.* **2005**, *280*, 5892-5901.
- (533) Yanagisawa, D.; Shirai, N.; Amatsubo, T.; Taguchi, H.; Hirao, K.; Urushitani, M.; Morikawa, S.; Inubushi, T.; Kato, M.; Kato, F.; Morino, K.; Kimura, H.; Nakano, I.; Yoshida, C.; Okada, T.; Sano, M.; Wada, Y.; Wada, K.N.; Yamamoto, A.; Tooyama, I. *Biomaterials* **2010**, *31*, 4179-4185.
- (534) Pullakhandam, R.; Srinivas, P.N.; Nair, M.K.; Reddy, G.B. *Arch. Biochem. Biophys.* **2009**, *485*, 115-119.
- (535) Mathews, S.; Rao, M.N.A. *Int. J. Pharm.* **1991**, *76*, 257-259.
- (536) Awasthi, S.; Pandya, U.; Singhal, S.S.; Lin, J.T.; Thiviyanathan, V.; Seifert, W.E., Jr.; Awasthi, Y.C.; Ansari, G.A. *Chem. Biol. Interact.* **2000**, *128*, 19-38.
- (537) Lao, C.D.; Ruffin, M.T.t.; Normolle, D.; Heath, D.D.; Murray, S.I.; Bailey, J.M.; Boggs, M.E.; Crowell, J.; Rock, C.L.; Brenner, D.E. *BMC Complement. Altern. Med.* **2006**, *6*, 10.
- (538) Cheng, A.L.; Hsu, C.H.; Lin, J.K.; Hsu, M.M.; Ho, Y.F.; Shen, T.S.; Ko, J.Y.; Lin, J.T.; Lin, B.R.; Ming-Shiang, W.; Yu, H.S.; Jee, S.H.; Chen, G.S.; Chen, T.M.; Chen, C.A.; Lai, M.K.; Pu, Y.S.; Pan, M.H.; Wang, Y.J.; Tsai, C.C.; Hsieh, C.Y. *Anticancer Res.* **2001**, *21*, 2895-2900.
- (539) Shoba, G.; Joy, D.; Joseph, T.; Majeed, M.; Rajendran, R.; Srinivas, P.S. *Planta Med.* **1998**, *64*, 353-356.
- (540) Wahlstrom, B.; Blennow, G. *Acta Pharmacol. Toxicol. (Copenh.)* **1978**, *43*, 86-92.
- (541) Ravindranath, V.; Chandrasekhara, N. *Toxicology* **1980**, *16*, 259-265.
- (542) Ravindranath, V.; Chandrasekhara, N. *Toxicology* **1981**, *22*, 337-344.
- (543) Pan, M.H.; Huang, T.M.; Lin, J.K. *Drug Metab. Dispos.* **1999**, *27*, 486-494.
- (544) Yang, K.Y.; Lin, L.C.; Tseng, T.Y.; Wang, S.C.; Tsai, T.H. *J. Chromatogr. B Analyt. Technol. Biomed. Life Sci.* **2007**, *853*, 183-189.

- (545) Sharma, R.A.; Euden, S.A.; Platton, S.L.; Cooke, D.N.; Shafayat, A.; Hewitt, H.R.; Marczylo, T.H.; Morgan, B.; Hemingway, D.; Plummer, S.M.; Pirmohamed, M.; Gescher, A.J.; Steward, W.P. *Clin. Cancer Res.* **2004**, *10*, 6847-6854.
- (546) Perkins, S.; Verschoyle, R.D.; Hill, K.; Parveen, I.; Threadgill, M.D.; Sharma, R.A.; Williams, M.L.; Steward, W.P.; Gescher, A.J. *Cancer Epidemiol. Biomarkers Prev.* **2002**, *11*, 535-540.
- (547) Garcea, G.; Jones, D.J.; Singh, R.; Dennison, A.R.; Farmer, P.B.; Sharma, R.A.; Steward, W.P.; Gescher, A.J.; Berry, D.P. *Br. J. Cancer* **2004**, *90*, 1011-1015.
- (548) Hoehle, S.I.; Pfeiffer, E.; Solyom, A.M.; Metzler, M. *J. Agric. Food. Chem.* **2006**, *54*, 756-764.
- (549) Holder, G.M.; Plummer, J.L.; Ryan, A.J. *Xenobiotica* **1978**, *8*, 761-768.
- (550) Asai, A.; Miyazawa, T. *Life Sci.* **2000**, *67*, 2785-2793.
- (551) Hoehle, S.I.; Pfeiffer, E.; Metzler, M. *Mol. Nutr. Food Res.* **2007**, *51*, 932-938.
- (552) Pal, A.; Sung, B.; Bhanu Prasad, B.A.; Schuber, P.T., Jr.; Prasad, S.; Aggarwal, B.B.; Bornmann, W.G. *Bioorg. Med. Chem.* **2014**, *22*, 435-439.
- (553) Gupta, S.C.; Kismali, G.; Aggarwal, B.B. *Biofactors* **2013**, *39*, 2-13.
- (554) Sasaki, H.; Sunagawa, Y.; Takahashi, K.; Imaizumi, A.; Fukuda, H.; Hashimoto, T.; Wada, H.; Katanasaka, Y.; Kakeya, H.; Fujita, M.; Hasegawa, K.; Morimoto, T. *Biol. Pharm. Bull.* **2011**, *34*, 660-665.
- (555) Gota, V.S.; Maru, G.B.; Soni, T.G.; Gandhi, T.R.; Kochar, N.; Agarwal, M.G. *J. Agric. Food. Chem.* **2010**, *58*, 2095-2099.
- (556) Takahashi, M.; Uechi, S.; Takara, K.; Asikin, Y.; Wada, K. *J. Agric. Food. Chem.* **2009**, *57*, 9141-9146.
- (557) Chen, H.; Wu, J.; Sun, M.; Guo, C.; Yu, A.; Cao, F.; Zhao, L.; Tan, Q.; Zhai, G. *Journal of liposome research* **2012**, *22*, 100-109.
- (558) Liu, J.P.; Feng, L.; Zhu, M.M.; Wang, R.S.; Zhang, M.H.; Hu, S.Y.; Jia, X.B.; Wu, J.J. *Planta Med.* **2012**, *78*, 1757-1760.
- (559) Cuomo, J.; Appendino, G.; Dern, A.S.; Schneider, E.; McKinnon, T.P.; Brown, M.J.; Togni, S.; Dixon, B.M. *J. Nat. Prod.* **2011**, *74*, 664-669.
- (560) Cheng, K.K.; Yeung, C.F.; Ho, S.W.; Chow, S.F.; Chow, A.H.; Baum, L. *The AAPS journal* **2013**, *15*, 324-336.
- (561) Anand, P.; Nair, H.B.; Sung, B.; Kunnumakkara, A.B.; Yadav, V.R.; Tekmal, R.R.; Aggarwal, B.B. *Biochem. Pharmacol.* **2010**, *79*, 330-338.

- (562)Yadav, V.R.; Prasad, S.; Kannappan, R.; Ravindran, J.; Chaturvedi, M.M.; Vaahtera, L.; Parkkinen, J.; Aggarwal, B.B. *Biochem. Pharmacol.* **2010**, *80*, 1021-1032.
- (563)Oetari, S.; Sudibyo, M.; Commandeur, J.N.; Samhoedi, R.; Vermeulen, N.P. *Biochem. Pharmacol.* **1996**, *51*, 39-45.
- (564)Appiah-Opong, R.; Commandeur, J.N.; van Vugt-Lussenburg, B.; Vermeulen, N.P. *Toxicology* **2007**, *235*, 83-91.
- (565)Cao, J.; Jia, L.; Zhou, H.M.; Liu, Y.; Zhong, L.F. *Toxicol. Sci.* **2006**, *91*, 476-483.
- (566)Jiao, Y.; Wilkinson, J.t.; Di, X.; Wang, W.; Hatcher, H.; Kock, N.D.; D'Agostino, R., Jr.; Knovich, M.A.; Torti, F.M.; Torti, S.V. *Blood* **2009**, *113*, 462-469.
- (567)Gupta, S.C.; Hevia, D.; Patchva, S.; Park, B.; Koh, W.; Aggarwal, B.B. *Antioxidants & redox signaling* **2012**, *16*, 1295-1322.
- (568)Hatcher, H.; Planalp, R.; Cho, J.; Torti, F.M.; Torti, S.V. *Cell. Mol. Life Sci.* **2008**, *65*, 1631-1652.
- (569)Epelbaum, R.; Schaffer, M.; Vazel, B.; Badmaev, V.; Bar-Sela, G. *Nutr. Cancer* **2010**, *62*, 1137-1141.
- (570)Barthelemy, S.; Vergnes, L.; Moynier, M.; Guyot, D.; Labidalle, S.; Bahraoui, E. *Res. Virol.* **1998**, *149*, 43-52.
- (571)Kumar, S.; Dubey, K.K.; Tripathi, S.; Fujii, M.; Misra, K. *Nucleic Acids Symp. Ser.* **2000**, 75-76.
- (572)Mishra, S.; Karmodiya, K.; Surolia, N.; Surolia, A. *Bioorg. Med. Chem.* **2008**, *16*, 2894-2902.
- (573)Zheng, A.; Li, H.; Wang, X.; Feng, Z.; Xu, J.; Cao, K.; Zhou, B.; Wu, J.; Liu, J. *Curr. Cancer Drug Targets* **2014**, 156-166.
- (574)Zhou, G.Z.; Zhang, S.N.; Zhang, L.; Sun, G.C.; Chen, X.B. *Pharm. Biol.* **2014**, *52*, 111-116.
- (575)Basile, V.; Belluti, S.; Ferrari, E.; Gozzoli, C.; Ganassi, S.; Quaglino, D.; Saladini, M.; Imbriano, C. *PLoS One* **2013**, *8*, e53664.
- (576)Pan, Y.; Zhu, G.; Wang, Y.; Cai, L.; Cai, Y.; Hu, J.; Li, Y.; Yan, Y.; Wang, Z.; Li, X.; Wei, T.; Liang, G. *The Journal of nutritional biochemistry* **2013**, *24*, 146-155.
- (577)Al-Amiery, A.A.; Kadhum, A.A.; Obayes, H.R.; Mohamad, A.B. *Bioinorg. Chem. Appl.* **2013**, *2013*, 354982.
- (578)Dutta, S.; Padhye, S.; Priyadarsini, K.I.; Newton, C. *Bioorg. Med. Chem. Lett.* **2005**, *15*, 2738-2744.
- (579)Pandya, N.M.; Dhalla, N.S.; Santani, D.D. *Vascul. Pharmacol.* **2006**, *44*, 265-274.
- (580)Wan, S.B.; Yang, H.; Zhou, Z.; Cui, Q.C.; Chen, D.; Kanwar, J.; Mohammad, I.; Dou, Q.P.; Chan, T.H. *Int. J. Mol. Med.* **2010**, *26*, 447-455.

- (581) Omoigui, S. *Med. Hypotheses* **2007**, *69*, 70-82.
- (582) Tsu, S. *The Art of War*; Dover Publications: Mineola, New York, 2002.
- (583) Freudenrich, C. "How Pain Works" HowStuffWorks.com, 09 November 2007.
<<http://science.howstuffworks.com/life/inside-the-mind/human-brain/pain.htm>> (accessed 09 June 2014).
- (584) Besson, J.M. *Lancet* **1999**, *353*, 1610-1615.
- (585) Payne, R. *Cancer* **1989**, *63*, 2266-2274.
- (586) Buckwalter, J.A.; Saltzman, C.; Brown, T. *Clin. Orthop. Relat. Res.* **2004**, S6-15.
- (587) Felson, D.T. *Curr. Opin. Rheumatol.* **2005**, *17*, 624-628.
- (588) Belmonte, C.; Cervero, F. *Neurobiology of Nociceptors*; Oxford University Press: Oxford, 1996.
- (589) Meyer, R.A.; Campbell, J.N.; Raja, N. In *Wall and Melzack's Textbook of Pain*; 3rd ed.; Wall, P. P. D., McMahon, S. S. B., Koltzenburg, M., Eds.; Elsevier Science Health Science Division: 2006, p 13-44.
- (590) Lee, A.S.; Ellman, M.B.; Yan, D.; Kroin, J.S.; Cole, B.J.; van Wijnen, A.J.; Im, H.-J. *Gene* **2013**, *527*, 440-447.
- (591) Schweinhardt, P.; Bushnell, M.C. *The Journal of Clinical Investigation* **2010**, *120*, 3788-3797.
- (592) Tavares, I.; Martins, I. *Gene Therapy for Chronic Pain Management*, 2013.
- (593) Bingham, B.; Ajit, S.K.; Blake, D.R.; Samad, T.A. *Nat. Clin. Pract. Rheumatol.* **2009**, *5*, 28-37.
- (594) Ahrens, J.; Leffler, A. *Der Anaesthetist* **2014**, *63*, 376-386.
- (595) McDonald, J.; Lambert, D. *Continuing Education in Anaesthesia, Critical Care & Pain* **2005**, *5*, 22-25.
- (596) Treating Pain. <http://www.brainfacts.org/sensing-thinking-behaving/senses-and-perception/articles/2012/treating-pain/>.
- (597) Ricciotti, E.; FitzGerald, G.A. *Arterioscler. Thromb. Vasc. Biol.* **2011**, *31*, 986-1000.
- (598) Gomez, I.; Foudi, N.; Longrois, D.; Norel, X. *Prostaglandins, Leukotrienes and Essential Fatty Acids (PLEFA)* **2013**, *89*, 55-63.
- (599) Chen, L.; Yang, G.; Grosser, T. *Prostaglandins Other Lipid Mediat.* **2013**, *104-105*, 58-66.
- (600) Dray, A. *Can. J. Physiol. Pharmacol.* **1997**, *75*, 704-712.
- (601) Rosenbaum, T.; Simon, S.A. In *Trp Ion Channel Function in Sensory Transduction and Cellular Signaling Cascades*; Liedtke, W. B., Heller, S., Eds.; Taylor & Francis: Boca Raton, FL, 2007, p 69-84.

- (602) Nieto, F.R.; Cobos, E.J.; Tejada, M.A.; Sanchez-Fernandez, C.; Gonzalez-Cano, R.; Cendan, C.M. *Mar. Drugs* **2012**, *10*, 281-305.
- (603) Basbaum, A.I.; Bautista, D.M.; Scherrer, G.; Julius, D. *Cell* **2009**, *139*, 267-284.
- (604) Latremoliere, A.; Woolf, C.J. *J. Pain* **2009**, *10*, 895-926.
- (605) Costigan, M.; Woolf, C.J. *J. Pain* **2000**, *1*, 35-44.
- (606) Aoki, T.; Narumiya, S. *Trends Pharmacol. Sci.* **2012**, *33*, 304-311.
- (607) Nakanishi, M.; Rosenberg, D. *Semin. Immunopathol.* **2013**, *35*, 123-137.
- (608) Smith, W.L.; DeWitt, D.L.; Garavito, R.M. *Annu. Rev. Biochem* **2000**, *69*, 145-182.
- (609) Furuyashiki, T.; Narumiya, S. *Nat. Rev. Endocrinol.* **2011**, *7*, 163-175.
- (610) Narumiya, S.; FitzGerald, G.A. *J. Clin. Invest.* **2001**, *108*, 25-30.
- (611) Wallace, J.L. *Gastroenterol. Clin. North Am.* **2001**, *30*, 971-980.
- (612) Funk, C.D. *Science* **2001**, *294*, 1871-1875.
- (613) Iwakura, Y.; Ishigame, H.; Saijo, S.; Nakae, S. *Immunity* **2011**, *34*, 149-162.
- (614) Wilson, N.J.; Boniface, K.; Chan, J.R.; McKenzie, B.S.; Blumenschein, W.M.; Mattson, J.D.; Basham, B.; Smith, K.; Chen, T.; Morel, F.; Lecron, J.C.; Kastelein, R.A.; Cua, D.J.; McClanahan, T.K.; Bowman, E.P.; de Waal Malefyt, R. *Nat. Immunol.* **2007**, *8*, 950-957.
- (615) Rhen, T.; Cidlowski, J.A. *N. Engl. J. Med.* **2005**, *353*, 1711-1723.
- (616) Smoak, K.A.; Cidlowski, J.A. *Mech. Ageing Dev.* **2004**, *125*, 697-706.
- (617) Greaves, M.W. *Postgrad. Med. J.* **1976**, *52*, 631-633.
- (618) Peers, S.H.; Smillie, F.; Elderfield, A.J.; Flower, R.J. *Br. J. Pharmacol.* **1993**, *108*, 66-72.
- (619) Newton, R. *Thorax* **2000**, *55*, 603-613.
- (620) Klein, N.C.; Go, C.H.; Cunha, B.A. *Infect. Dis. Clin. North Am.* **2001**, *15*, 423-432.
- (621) Yuan, C.; Sidhu, R.S.; Kuklev, D.V.; Kado, Y.; Wada, M.; Song, I.; Smith, W.L. *J. Biol. Chem.* **2009**, *284*, 10046-10055.
- (622) Vane, J.R. *Nat. New Biol.* **1971**, *231*, 232-235.
- (623) Trelle, S.; Reichenbach, S.; Wandel, S.; Hildebrand, P.; Tschannen, B.; Villiger, P.M.; Egger, M.; Juni, P. *BMJ* **2011**, *342*, c7086.
- (624) Traversa, G.; Walker, A.M.; Ippolito, F.M.; Caffari, B.; Capurso, L.; Dezi, A.; Koch, M.; Maggini, M.; Alegiani, S.S.; Raschetti, R. *Epidemiology* **1995**, *6*, 49-54.
- (625) De Broe, M.E.; Elseviers, M.M. *N. Engl. J. Med.* **1998**, *338*, 446-452.
- (626) Shiri, R.; Koskimaki, J.; Hakkinen, J.; Tammela, T.L.; Auvinen, A.; Hakama, M. *J. Urol.* **2006**, *175*, 1812-1815; discussion 1815-1816.

- (627) Dubois, R.N.; Abramson, S.B.; Crofford, L.; Gupta, R.A.; Simon, L.S.; Van De Putte, L.B.; Lipsky, P.E. *FASEB J.* **1998**, *12*, 1063-1073.
- (628) Wang, D.; Dubois, R.N. *Gut* **2006**, *55*, 115-122.
- (629) Smyth, E.M.; Grosser, T.; Wang, M.; Yu, Y.; FitzGerald, G.A. *J. Lipid Res.* **2009**, *50 Suppl*, S423-428.
- (630) Mardini, I.A.; FitzGerald, G.A. *Mol Interv* **2001**, *1*, 30-38.
- (631) Dannhardt, G.; Kiefer, W. *Eur. J. Med. Chem.* **2001**, *36*, 109-126.
- (632) Flower, R.J. *Nature reviews. Drug discovery* **2003**, *2*, 179-191.
- (633) Gans, K.R.; Galbraith, W.; Roman, R.J.; Haber, S.B.; Kerr, J.S.; Schmidt, W.K.; Smith, C.; Hewes, W.E.; Ackerman, N.R. *J. Pharmacol. Exp. Ther.* **1990**, *254*, 180-187.
- (634) Futaki, N.; Takahashi, S.; Yokoyama, M.; Arai, I.; Higuchi, S.; Otomo, S. *Prostaglandins* **1994**, *47*, 55-59.
- (635) Tazawa, R.; Xu, X.M.; Wu, K.K.; Wang, L.H. *Biochem. Biophys. Res. Commun.* **1994**, *203*, 190-199.
- (636) Kosaka, T.; Miyata, A.; Ihara, H.; Hara, S.; Sugimoto, T.; Takeda, O.; Takahashi, E.; Tanabe, T. *Eur. J. Biochem.* **1994**, *221*, 889-897.
- (637) Garavito, R.M. *Nat. Struct. Biol.* **1996**, *3*, 897-901.
- (638) DeWitt, D.L.; Meade, E.A. *Arch. Biochem. Biophys.* **1993**, *306*, 94-102.
- (639) Kurumbail, R.G.; Stevens, A.M.; Gierse, J.K.; McDonald, J.J.; Stegeman, R.A.; Pak, J.Y.; Gildehaus, D.; Miyashiro, J.M.; Penning, T.D.; Seibert, K.; Isakson, P.C.; Stallings, W.C. *Nature* **1996**, *384*, 644-648.
- (640) Llorens, O.; Perez, J.J.; Palomer, A.; Mauleon, D. *Bioorg. Med. Chem. Lett.* **1999**, *9*, 2779-2784.
- (641) Michaux, C.; Charlier, C. *Mini Rev. Med. Chem.* **2004**, *4*, 603-615.
- (642) Grosser, T.; Fries, S.; FitzGerald, G.A. *The Journal of Clinical Investigation* **2006**, *116*, 4-15.
- (643) Penning, T.D.; Talley, J.J.; Bertenshaw, S.R.; Carter, J.S.; Collins, P.W.; Docter, S.; Graneto, M.J.; Lee, L.F.; Malecha, J.W.; Miyashiro, J.M.; Rogers, R.S.; Rogier, D.J.; Yu, S.S.; Anderson, G.D.; Burton, E.G.; Cogburn, J.N.; Gregory, S.A.; Koboldt, C.M.; Perkins, W.E.; Seibert, K.; Veenhuizen, A.W.; Zhang, Y.Y.; Isakson, P.C. *J. Med. Chem.* **1997**, *40*, 1347-1365.
- (644) Conaghan, P.G. *Rheumatol. Int.* **2012**, *32*, 1491-1502.
- (645) Prior, A.; Mason, E. "Pfizer Says Court Invalidates Celebrex Patent" *Wsj.com*, 13 Mar 2014.
<http://online.wsj.com/news/articles/SB10001424052702304185104579434792904590048>
(accessed 19/06/2014).

- (646) Bombardier, C.; Laine, L.; Reicin, A.; Shapiro, D.; Burgos-Vargas, R.; Davis, B.; Day, R.; Ferraz, M.B.; Hawkey, C.J.; Hochberg, M.C.; Kvien, T.K.; Schnitzer, T.J. *N. Engl. J. Med.* **2000**, *343*, 1520-1528, 1522 p following 1528.
- (647) Zhang, J.; Ding, E.L.; Song, Y. *JAMA* **2006**, *296*, 1619-1632.
- (648) Gajraj, N.M. *Curr. Top. Med. Chem.* **2007**, *7*, 235-249.
- (649) Clarke, R.; Derry, S.; Moore, R.A. *The Cochrane database of systematic reviews* **2014**, *5*, Cd004309.
- (650) "Merck Receives Non Approvable Letter from Fda for Arcoxia (Etoricoxib)" Drugs.com, 27 April 2007. http://www.drugs.com/nda/arcoxia_070427.html (accessed 19 June 2014).
- (651) Tacconelli, S.; Capone, M.L.; Patrignani, P. *Curr. Pharm. Des.* **2004**, *10*, 589-601.
- (652) "Medicines Regulator Cancels Registration of Anti Inflammatory Drug, Lumiracoxib (Prexige)" Tga.gov.au, 11 August 2007. <http://www.tga.gov.au/newsroom/media-2007-lumiracoxib-070811.htm#.U6LI5LEkTqx> (accessed 19 June 2014).
- (653) "Nz Regulators Ban Arthritis Drug" Nzherald.co.za, 21 August 2007. http://www.nzherald.co.nz/pharmaceuticals/news/article.cfm?c_id=278&objectid=10459030 (accessed 19 June 2014).
- (654) "Health Canada Pulls Osteoarthritis Drug Prexige" Cbc.ca, 04 October 2007. <http://www.cbc.ca/news/health-canada-pulls-osteoarthritis-drug-prexige-1.640285> (accessed 19 June 2014).
- (655) "European Medicines Agency Recommends Withdrawal of the Marketing Authorisations for Lumiracoxib-Containing Medicines)" Drugs.com, 14 December 2007. <http://www.drugs.com/news/european-medicines-agency-recommends-marketing-authorisations-lumiracoxib-containing-medicines-7403.html> (accessed 19 June 2014).
- (656) Pairet, M.; Van Ryn, J. *Cox-2 Inhibitors*; SPRINGER VERLAG NY, 2004.
- (657) Palomer, A.; Perez, J.J.; Navea, S.; Llorens, O.; Pascual, J.; Garcia, L.; Mauleon, D. *J. Med. Chem.* **2000**, *43*, 2280-2284.
- (658) Peskar, B.M.; Maricic, N.; Gretzera, B.; Schuligoi, R.; Schmassmann, A. *Life Sci.* **2001**, *69*, 2993-3003.
- (659) Harris, R.C.; Breyer, M.D. *Am. J. Physiol. Renal Physiol.* **2001**, *281*, F1-11.
- (660) Rouzer, C.A.; Kingsley, P.J.; Wang, H.; Zhang, H.; Morrow, J.D.; Dey, S.K.; Marnett, L.J. *J. Biol. Chem.* **2004**, *279*, 34256-34268.

- (661)Chen, M.; Boilard, E.; Nigrovic, P.A.; Clark, P.; Xu, D.; Fitzgerald, G.A.; Audoly, L.P.; Lee, D.M. *Arthritis Rheum.* **2008**, *58*, 1354-1365.
- (662)McAdam, B.F.; Mardini, I.A.; Habib, A.; Burke, A.; Lawson, J.A.; Kapoor, S.; FitzGerald, G.A. *J. Clin. Invest.* **2000**, *105*, 1473-1482.
- (663)Takada, Y.; Bhardwaj, A.; Potdar, P.; Aggarwal, B.B. *Oncogene* **2004**, *23*, 9247-9258.
- (664)Dogne, J.M.; Hanson, J.; Supuran, C.; Pratico, D. *Curr. Pharm. Des.* **2006**, *12*, 971-975.
- (665)Chan, A.T.; Manson, J.E.; Albert, C.M.; Chae, C.U.; Rexrode, K.M.; Curhan, G.C.; Rimm, E.B.; Willett, W.C.; Fuchs, C.S. *Circulation* **2006**, *113*, 1578-1587.
- (666)Hermann, M.; Ruschitzka, F. *Intern. Med. J.* **2006**, *36*, 308-319.
- (667)Grosser, T.; Yu, Y.; Fitzgerald, G.A. *Annu. Rev. Med.* **2010**, *61*, 17-33.
- (668)Dannenber, A.J.; Subbaramaiah, K. *Cancer Cell* **2003**, *4*, 431-436.
- (669)Farooqui, M.; Li, Y.; Rogers, T.; Poonawala, T.; Griffin, R.J.; Song, C.W.; Gupta, K. *Br. J. Cancer* **2007**, *97*, 1523-1531.
- (670)Chow, L.W.; Loo, W.T.; Toi, M. *Biomed. Pharmacother.* **2005**, *59 Suppl 2*, S281-284.
- (671)Legan, M. *Bosn. J. Basic Med. Sci.* **2010**, *10*, 192-196.
- (672)Menter, D.G.; Schilsky, R.L.; DuBois, R.N. *Clin. Cancer Res.* **2010**, *16*, 1384-1390.
- (673)Johnsen, J.I.; Lindskog, M.; Ponthan, F.; Pettersen, I.; Elfman, L.; Orrego, A.; Sveinbjornsson, B.; Kogner, P. *Cancer Res.* **2004**, *64*, 7210-7215.
- (674)Lau, L.; Hansford, L.M.; Cheng, L.S.; Hang, M.; Baruchel, S.; Kaplan, D.R.; Irwin, M.S. *Oncogene* **2007**, *26*, 1920-1931.
- (675)Schonthal, A.H. *Br. J. Cancer* **2007**, *97*, 1465-1468.
- (676)Schonthal, A.H. *Neurosurg. Focus* **2006**, *20*, E21.
- (677)Schonthal, A.H.; Chen, T.C.; Hofman, F.M.; Louie, S.G.; Petasis, N.A. *Expert Opin Investig Drug* **2008**, *17*, 197-208.
- (678)Zhu, J.; Song, X.; Lin, H.P.; Young, D.C.; Yan, S.; Marquez, V.E.; Chen, C.S. *J. Natl. Cancer Inst.* **2002**, *94*, 1745-1757.
- (679)Chuang, H.C.; Kardosh, A.; Gaffney, K.J.; Petasis, N.A.; Schonthal, A.H. *Mol. Cancer* **2008**, *7*, 38.
- (680)Meyer, E.F.; Swanson, S.M.; Williams, J.A. *Pharmacol. Ther.* **2000**, *85*, 113-121.
- (681)Stone, K. "Top-Selling OTC Drugs by Category, 2012" Pharma.about.com.
<http://pharma.about.com/od/Over-the-Counter-Medicine/a/Top-selling-Otc-Drugs-By-Category-2012.htm> (accessed 21 July 2014).

- (682) Bernstein, J.; Davis, R.E.; Shimoni, L.; Chang, N.-L. *Angewandte Chemie International Edition in English* **1995**, *34*, 1555-1573.
- (683) Hawkey, C.J. *Best Practice & Research Clinical Gastroenterology* **2001**, *15*, 801-820.
- (684) Wang, J.L.; Limburg, D.; Graneto, M.J.; Springer, J.; Hamper, J.R.; Liao, S.; Pawlitz, J.L.; Kurumbail, R.G.; Maziasz, T.; Talley, J.J.; Kiefer, J.R.; Carter, J. *Bioorg. Med. Chem. Lett.* **2010**, *20*, 7159-7163.
- (685) Vecchio, A.J.; Simmons, D.M.; Malkowski, M.G. *J. Biol. Chem.* **2010**, *285*, 22152-22163.
- (686) Ligprep, Version 3.0, Schrödinger, LLC, New York, NY, 2014
- (687) Glide, Version 6.3, Schrödinger, LLC, New York, NY, 2014
- (688) Epik, Version 2.8, Schrödinger, LLC, New York, NY, 2014
- (689) Maestro, Version 9.8, Schrödinger, LLC, New York, NY, 2014
- (690) Rimon, G.; Sidhu, R.S.; Lauver, D.A.; Lee, J.Y.; Sharma, N.P.; Yuan, C.; Frieler, R.A.; Trievel, R.C.; Lucchesi, B.R.; Smith, W.L. *Proceedings of the National Academy of Sciences* **2010**, *107*, 28-33.
- (691) Okimoto, N.; Futatsugi, N.; Fuji, H.; Suenaga, A.; Morimoto, G.; Yanai, R.; Ohno, Y.; Narumi, T.; Taiji, M. *PLoS Comput. Biol.* **2009**, *5*, e1000528.
- (692) Payton, F.; Sandusky, P.; Alworth, W.L. *J. Nat. Prod.* **2007**, *70*, 143-146.
- (693) Hunter, L. *Bellstein J. Org. Chem.* **2010**, *6*, 38.
- (694) Filler, R.; Saha, R. *Future Med. Chem.* **2009**, *1*, 777-791.
- (695) Witiak, D.T.; Kim, S.K.; Tehim, A.K.; Sternitzke, K.D.; McCreery, R.L.; Kim, S.U.; Feller, D.R.; Romstedt, K.J.; Kamanna, V.S.; Newman, H.A. *J. Med. Chem.* **1988**, *31*, 1437-1445.
- (696) Murata, T.; Shimada, M.; Kadono, H.; Sakakibara, S.; Yoshino, T.; Masuda, T.; Shimazaki, M.; Shintani, T.; Fuchikami, K.; Bacon, K.B.; Ziegelbauer, K.B.; Lowinger, T.B. *Bioorg. Med. Chem. Lett.* **2004**, *14*, 4013-4017.
- (697) Kim, J.; Kim, K.S.; Lee, H.S.; Park, K.S.; Park, S.Y.; Kang, S.Y.; Lee, S.J.; Park, H.S.; Kim, D.E.; Chong, Y. *Bioorg. Med. Chem. Lett.* **2008**, *18*, 4661-4665.
- (698) Chang, C.-Y.; Kuo, S.-C.; Lin, Y.-L.; Wang, J.-P.; Huang, L.-J. *Bioorg. Med. Chem. Lett.* **2001**, *11*, 1971-1974.
- (699) Zhao, P.-L.; Liu, C.-L.; Huang, W.; Wang, Y.-Z.; Yang, G.-F. *J. Agric. Food. Chem.* **2007**, *55*, 5697-5700.
- (700) Zhang, Y.-L.; Wang, Y.-Q. *Tetrahedron Lett.* **2014**, *55*, 3255-3258.
- (701) Bible, R.H. *Interpretation of NMR Spectra : An Empirical Approach*; Plenum Press: New York, 1966.

- (702)Perjéssy, A.; Kolehmainen, E.; Fabian, W.M.F.; Ludwig, M.; Laihia, K.; Kulhánek, J.; Šusteková, Z. *Sulfur Letters* **2002**, *25*, 71-78.
- (703)Corominas, A.; Montaña, Á.M. *Synth. Commun.* **2013**, *43*, 2062-2072.
- (704)Barros, A.I.R.N.A.; Silva, A.M.S.; Alkorta, I.; Elguero, J. *Tetrahedron* **2004**, *60*, 6513-6521.
- (705)Khlebnikova, T.S.; Piven', Y.A.; Khripach, N.B.; Lakhvich, F.A. *Chem. Nat. Compd.* **2011**, *47*, 33-37.
- (706)Periasamy, M.; Anwar, S.; Reddy, M.N. *Indian Journal of Chemistry -Section B (IJC-B)* **2009**, *48*, 1261-1273.
- (707)Chang, C.T.; Chen, F.C. *J. Chem Soc* **1961**, 3155-3156.
- (708)Chimenti, F.; Fioravanti, R.; Bolasco, A.; Chimenti, P.; Secci, D.; Rossi, F.; Yáñez, M.; Orallo, F.; Ortuso, F.; Alcaro, S. *J. Med. Chem.* **2009**, *52*, 2818-2824.
- (709)Ohkatsu, Y.; Satoh, T. *Journal of the Japan Petroleum Institute* **2008**, *51*, 298-308.
- (710)De Meyer, N.; Haemers, A.; Mishra, L.; Pandey, H.K.; Pieters, L.A.; Vanden Berghe, D.A.; Vlietinck, A.J. *J. Med. Chem.* **1991**, *34*, 736-746.
- (711)Hasan, A.; Rasheed, L.; Malik, A. *Asian J. Chem* **2007**, *19*.
- (712)Nie, A.; Wang, J.; Huang, Z. *J. Comb. Chem.* **2006**, *8*, 646-648.
- (713)Thornton, M.T.; Henderson, L.C.; Byrne, N.; Pfeffer, F.M. *Curr. Org. Chem.* **2012**, *16*.
- (714)Jadhav, K.P.; Ingle, D.B. *Indian Journal of Chemistry, Section B: Organic Chemistry Including Medicinal Chemistry* **1983**, *22B*, 180-182.
- (715)Sagrera, G.; Bertucci, A.; Vazquez, A.; Seoane, G. *Biorg. Med. Chem.* **2011**, *19*, 3060-3073.
- (716)Chimenti, F.; Bolasco, A.; Manna, F.; Secci, D.; Chimenti, P.; Granese, A.; Befani, O.; Turini, P.; Cirilli, R.; La Torre, F.; Alcaro, S.; Ortuso, F.; Langer, T. *Curr. Med. Chem.* **2006**, *13*, 1411-1428.
- (717)Chimenti, F.; Fioravanti, R.; Bolasco, A.; Chimenti, P.; Secci, D.; Rossi, F.; Yanez, M.; Orallo, F.; Ortuso, F.; Alcaro, S.; Cirilli, R.; Ferretti, R.; Sanna, M.L. *Bioorg. Med. Chem.* **2010**, *18*, 1273-1279.
- (718)Biradar, N.S.; Patil, B.R.; Kulkarni, V.H. *Journal of the Karnatak University, Science* **1975**, *20*, 27-39.
- (719)Khupse, R.S.; Erhardt, P.W. *J. Nat. Prod.* **2008**, *71*, 275-277.
- (720)Nibbs, A.E.; Scheidt, K.A. *European J. Org. Chem.* **2012**, *2012*, 449-462.
- (721)Guo, L.; Yang, C.; Zheng, L.; Xia, W. *Org. Biomol. Chem.* **2013**, *11*, 5787-5792.
- (722)Talley, J.J.; Brown, D.L.; Carter, J.S.; Graneto, M.J.; Koboldt, C.M.; Masferrer, J.L.; Perkins, W.E.; Rogers, R.S.; Shaffer, A.F.; Zhang, Y.Y.; Zweifel, B.S.; Seibert, K. *J. Med. Chem.* **2000**, *43*, 775-777.
- (723)Silva, A.M.G.; Tomé, A.C.; Silva, A.M.S.; Cavaleiro, J.A.S. *Phosphorus, Sulfur, and Silicon and the Related Elements* **1998**, *140*, 113-124.

- (724)Drewes, S.E., Personal Communication,2014.
- (725)Houmam, A.; Hamed, E.M. *Chem. Commun.* **2012**, *48*, 11328-11330.
- (726)Xu, G.; Lv, B.; Roberge, J.Y.; Xu, B.; Du, J.; Dong, J.; Chen, Y.; Peng, K.; Zhang, L.; Tang, X.; Feng, Y.; Xu, M.; Fu, W.; Zhang, W.; Zhu, L.; Deng, Z.; Sheng, Z.; Welihinda, A.; Sun, X. *J. Med. Chem.* **2014**, *57*, 1236-1251.
- (727)Zhao, N.; Li, Y.; Wang, Y.; Wang, J. *Journal of Sulfur Chemistry* **2006**, *27*, 427-432.
- (728)Gibson, M.S.; Bradshaw, R.W. *Angewandte Chemie International Edition in English* **1968**, *7*, 919-930.
- (729)Gatta, F.; Settimj, G. *J. Heterocycl. Chem.* **1984**, *21*, 937-943.
- (730)Liu, X.; Pan, D.; Guo, Q.; Zhao, Y.; Wang, Z. *J. Appl. Polym. Sci.* **2013**, *129*, 748-755.
- (731)Gao, F.; Carr, J.L.; Hoveyda, A.H. *J. Am. Chem. Soc.* **2014**, *136*, 2149-2161.
- (732)Mao, X.; Ma, X.; Zhang, S.; Hu, H.; Zhu, C.; Cheng, Y. *Eur. J. Org. Chem.* **2013**, *2013*, 4245-4248.
- (733)Yoshida, S.; Igawa, K.; Tomooka, K. *J. Am. Chem. Soc.* **2012**, *134*, 19358-19361.
- (734)Palakurthy, N.B.; Dev, D.; Rana, S.; Nadimpally, K.C.; Mandal, B. *Eur. J. Org. Chem.* **2013**, *2013*, 2627-2633.
- (735)Gompper, R.; Stetter, J. *Tetrahedron Lett.* **1973**, 233-236.
- (736)Kundu, S.; Choi, J.; Wang, D.Y.; Choliy, Y.; Emge, T.J.; Krogh-Jespersen, K.; Goldman, A.S. *J. Am. Chem. Soc.* **2013**, *135*, 5127-5143.
- (737)Laha, J.K.; Jethava, K.P.; Dayal, N. *The Journal of Organic Chemistry* **2014**, *79*, 8010-8019.
- (738)Guan, Z.; Chai, X.; Yu, S.; Hu, H.; Jiang, Y.; Meng, Q.; Wu, Q. *Chem. Biol. Drug Des.* **2010**, *76*, 496-504.
- (739)Ozturk, S.; Kutuk, H. *International Journal of Organic Chemistry* **2011**, *1*, 202-206.
- (740)Asteriscus Aquaticus. http://www.stridvall.se/flowers/gallery/Asteraceae_3/NIK3078.
- (741)San Feliciano, A.; Medarde, M.; Miguel del Corral, J.M.; Aramburu, A.; Gordaliza, M.; Barrero, A.F. *Tetrahedron Lett.* **1989**, *30*, 2851-2854.
- (742)Lodewyk, M.W.; Soldi, C.; Jones, P.B.; Olmstead, M.M.; Rita, J.; Shaw, J.T.; Tantillo, D.J. *J. Am. Chem. Soc.* **2012**, *134*, 18550-18553.
- (743)E. Garcia-Rubino, M.; Mahfoudh, N.; M. Campos, J. *Curr. Org. Chem.* **2014**, *18*, 1513-1519.
- (744)Yang, H.-M.; Shin, H.-R.; Cho, S.-H.; Bang, S.-C.; Song, G.-Y.; Ju, J.-H.; Kim, M.-K.; Lee, S.-H.; Ryu, J.-C.; Kim, Y.; Jung, S.-H. *Biorg. Med. Chem.* **2007**, *15*, 104-111.
- (745)Shrot, Y.; Frydman, L. *J. Magn. Reson.* **2008**, *195*, 226-231.

- (746) Cobas, C. "Dosy NMR" Nmr-analysis.blogspot.com/2008/07/dosy-nmr.html, 20 July 2008.
<http://nmr-analysis.blogspot.com/2008/07/dosy-nmr.html> (accessed 17 September 2014).
- (747) Barjat, H.; Morris, G.A.; Smart, S.; Swanson, A.G.; Williams, S.C.R. *Journal of Magnetic Resonance, Series B* **1995**, *108*, 170-172.
- (748) Dosy Diffusion Effect. <http://chem.ch.huji.ac.il/nmr/techniques/other/diff/diff.html>.
- (749) Hoffman, R.E.; Shabtai, E.; Rabinovitz, M.; Iyer, V.S.; Mullen, K.; Rai, A.K.; Bayrd, E.; Scott, L.T. *Journal of the Chemical Society, Perkin Transactions 2* **1998**, 1659-1664.
- (750) "Automatic Dosy Processing" Mestrelab.com, 8 October 2013.
<http://mestrelab.com/resources/dosy/> (accessed 19 September 2014).
- (751) Stejskal, E.O.; Tanner, J.E. *The Journal of Chemical Physics* **1965**, *42*, 288-292.
- (752) Einstein, A. *Annalen der Physik* **1905**, *322*, 549-560.
- (753) Holz, M.; Heil, S.R.; Sacco, A. *Phys. Chem. Chem. Phys.* **2000**, *2*, 4740-4742.
- (754) Butts, C.P.; Jones, C.R.; Harvey, J.N. *Chem. Commun. (Camb.)* **2011**, *47*, 1193-1195.
- (755) Butts, C.P.; Jones, C.R.; Towers, E.C.; Flynn, J.L.; Appleby, L.; Barron, N.J. *Org. Biomol. Chem.* **2011**, *9*, 177-184.
- (756) Chini, M.G.; Jones, C.R.; Zampella, A.; D'Auria, M.V.; Renga, B.; Fiorucci, S.; Butts, C.P.; Bifulco, G. *J. Org. Chem.* **2012**, *77*, 1489-1496.
- (757) Jones, C.R.; Butts, C.P.; Harvey, J.N. *Beilstein J. Org. Chem.* **2011**, *7*, 145-150.
- (758) Gaurrand, S.; Desjardins, S.; Meyer, C.; Bonnet, P.; Argouillon, J.M.; Oulyadi, H.; Guillemont, J. *Chem. Biol. Drug Des.* **2006**, *68*, 77-84.
- (759) Nikiforovich, G.V.; Prakash, O.; Gehrig, C.A.; Hruby, V.J. *J. Am. Chem. Soc.* **1993**, *115*, 3399-3406.
- (760) Ali, S.M.; Khan, S.; Crowyn, G. *Magn. Reson. Chem.* **2012**, *50*, 299-304.
- (761) Mackeen, M.; Almond, A.; Cumpstey, I.; Enis, S.C.; Kupce, E.; Butters, T.D.; Fairbanks, A.J.; Dwek, R.A.; Wormald, M.R. *Org. Biomol. Chem.* **2006**, *4*, 2241-2246.
- (762) Borgias, B.A.; Gochin, M.; Kerwood, D.J.; James, T.L. *Prog. Nucl. Magn. Reson. Spectrosc.* **1990**, *22*, 83-100.
- (763) Atasoylu, O.; Smith, A.B. Sourceforge.net, DISCON. <http://discon.sourceforge.net/> (accessed 20 October 2014).
- (764) Evans, D.; Sharman, G. Janocchio Sourceforge.net. <http://janocchio.sourceforge.net/> (accessed 20 October 2014).
- (765) Nugteren, D.H.; Hazelhof, E. *Biochim. Biophys. Acta* **1973**, *326*, 448-461.
- (766) Hamberg, M.; Samuelsson, B. *Proc. Natl. Acad. Sci. U. S. A.* **1973**, *70*, 899-903.

- (767) Blobaum, A.L.; Marnett, L.J. *J. Biol. Chem.* **2007**, *282*, 16379-16390.
- (768) Peek, R.M., Jr. *Cancer Chemother. Pharmacol.* **2004**, *54 Suppl 1*, S50-56.
- (769) Koshland, D.E., Jr.; Nemethy, G.; Filmer, D. *Biochemistry* **1966**, *5*, 365-385.
- (770) Levy, J.A. *AIDS* **2009**, *23*, 147-160.
- (771) Zou, H.; Yuan, C.; Dong, L.; Sidhu, R.S.; Hong, Y.H.; Kuklev, D.V.; Smith, W.L. *J. Lipid Res.* **2012**, *53*, 1336-1347.
- (772) Sharma, N.P.; Dong, L.; Yuan, C.; Noon, K.R.; Smith, W.L. *Mol. Pharmacol.* **2010**, *77*, 979-986.
- (773) Dong, L.; Vecchio, A.J.; Sharma, N.P.; Jurban, B.J.; Malkowski, M.G.; Smith, W.L. *J. Biol. Chem.* **2011**, *286*, 19035-19046.
- (774) Yuan, C.; Rieke, C.J.; Rimon, G.; Wingerd, B.A.; Smith, W.L. *Proc. Natl. Acad. Sci. U. S. A.* **2006**, *103*, 6142-6147.
- (775) Non-Competitive Inhibition. <http://www.quia.com/jg/1197721list.html>.
- (776) Kulmacz, R.J.; Lands, W.E. *J. Biol. Chem.* **1984**, *259*, 6358-6363.
- (777) Kulmacz, R.J.; Lands, W.E. *J. Biol. Chem.* **1985**, *260*, 12572-12578.
- (778) Sidhu, R.S.; Lee, J.Y.; Yuan, C.; Smith, W.L. *Biochemistry* **2010**, *49*, 7069-7079.
- (779) Wallace, J.L.; Bak, A.; McKnight, W.; Asfaha, S.; Sharkey, K.A.; MacNaughton, W.K. *Gastroenterology* **1998**, *115*, 101-109.
- (780) Gordon, S.M.; Brahim, J.S.; Rowan, J.; Kent, A.; Dionne, R.A. *Clin. Pharmacol. Ther.* **2002**, *72*, 175-183.
- (781) Noguchi, K.; Shitashige, M.; Endo, H.; Kondo, H.; Yotsumoto, Y.; Izumi, Y.; Nitta, H.; Ishikawa, I. *J. Periodontal Res.* **2001**, *36*, 124-130.
- (782) Gilroy, D.W.; Tomlinson, A.; Willoughby, D.A. *Inflamm. Res.* **1998**, *47*, 79-85.
- (783) Gilroy, D.W.; Tomlinson, A.; Willoughby, D.A. *Eur. J. Pharmacol.* **1998**, *355*, 211-217.
- (784) Langenbach, R.; Morham, S.G.; Tiano, H.F.; Loftin, C.D.; Ghanayem, B.I.; Chulada, P.C.; Mahler, J.F.; Lee, C.A.; Goulding, E.H.; Kluckman, K.D.; Kim, H.S.; Smithies, O. *Cell* **1995**, *83*, 483-492.
- (785) Noguchi, K.; Shitashige, M.; Yanai, M.; Morita, I.; Nishihara, T.; Murota, S.; Ishikawa, I. *Inflammation* **1996**, *20*, 555-568.
- (786) Tilley, S.L.; Coffman, T.M.; Koller, B.H. *J. Clin. Invest.* **2001**, *108*, 15-23.
- (787) Retsky, M.; Rogers, R.; Demicheli, R.; Hrushesky, W.J.; Gukas, I.; Vaidya, J.S.; Baum, M.; Forget, P.; Dekock, M.; Pachmann, K. *Breast Cancer Res. Treat.* **2012**, *134*, 881-888.
- (788) Harris, R.E.; Beebe, J.; Alshaie, G.A. *J. Exp. Pharmacol.* **2012**, *4*, 91-96.
- (789) Zhu, X.; Eisenach, J.C. *Anesthesiology* **2003**, *99*, 1175-1179.

- (790)Zhu, X.; Conklin, D.; Eisenach, J.C. *Pain* **2003**, *104*, 15-23.
- (791)Zhu, X.; Conklin, D.R.; Eisenach, J.C. *Anesth. Analg.* **2005**, *100*, 1390-1393, table of contents.
- (792)Goto, K.; Ochi, H.; Yasunaga, Y.; Matsuyuki, H.; Imayoshi, T.; Kusuhara, H.; Okumoto, T.
Prostaglandins Other Lipid Mediat. **1998**, *56*, 245-254.
- (793)Perrone, M.G.; Scilimati, A.; Simone, L.; Vitale, P. *Curr. Med. Chem.* **2010**, *17*, 3769-3805.
- (794)Belton, O.; Byrne, D.; Kearney, D.; Leahy, A.; Fitzgerald, D.J. *Circulation* **2000**, *102*, 840-845.
- (795)Gupta, R.A.; Tejada, L.V.; Tong, B.J.; Das, S.K.; Morrow, J.D.; Dey, S.K.; DuBois, R.N. *Cancer Res.* **2003**, *63*, 906-911.
- (796)Hwang, D.; Scollard, D.; Byrne, J.; Levine, E. *J. Natl. Cancer Inst.* **1998**, *90*, 455-460.
- (797)Kirschenbaum, A.; Klausner, A.P.; Lee, R.; Unger, P.; Yao, S.; Liu, X.H.; Levine, A.C. *Urology* **2000**, *56*, 671-676.
- (798)Bauer, A.K.; Dwyer-Nield, L.D.; Malkinson, A.M. *Carcinogenesis* **2000**, *21*, 543-550.
- (799)Sales, K.J.; Katz, A.A.; Howard, B.; Soeters, R.P.; Millar, R.P.; Jabbour, H.N. *Cancer Res.* **2002**, *62*, 424-432.
- (800)Choi, S.H.; Aid, S.; Bosetti, F. *Trends Pharmacol. Sci.* **2009**, *30*, 174-181.
- (801)Rodrigues, T.; da Cruz, F.P.; Lafuente-Monasterio, M.J.; Gonçalves, D.; Ressurreição, A.S.; Siteo, A.R.; Bronze, M.R.; Gut, J.; Schneider, G.; Mota, M.M.; Rosenthal, P.J.; Prudêncio, M.; Gamo, F.-J.; Lopes, F.; Moreira, R. *J. Med. Chem.* **2013**, *56*, 4811-4815.
- (802)Rosenkranz, B.; Winkelmann, B.R.; Parnham, M.J. *Clin. Pharmacokinet.* **1996**, *30*, 372-384.
- (803)Lomonosova, E.E.; Kirsch, M.; Rauen, U.; de Groot, H. *Free Radic. Biol. Med.* **1998**, *24*, 522-528.
- (804)Nishikawa, M.; Kanamori, M.; Hidaka, H. *J. Pharmacol. Exp. Ther.* **1982**, *220*, 183-190.
- (805)Braden, M.R.; Parrish, J.C.; Naylor, J.C.; Nichols, D.E. *Mol. Pharmacol.* **2006**, *70*, 1956-1964.
- (806)Ettrup, A.; Palner, M.; Gillings, N.; Santini, M.A.; Hansen, M.; Kornum, B.R.; Rasmussen, L.K.; Nagren, K.; Madsen, J.; Begtrup, M.; Knudsen, G.M. *J. Nucl. Med.* **2010**, *51*, 1763-1770.
- (807)Moya, P.R.; Berg, K.A.; Gutierrez-Hernandez, M.A.; Saez-Briones, P.; Reyes-Parada, M.; Cassels, B.K.; Clarke, W.P. *J. Pharmacol. Exp. Ther.* **2007**, *321*, 1054-1061.
- (808)Wu, D.H.; Chen, A.D.; Johnson, C.S. *Journal of Magnetic Resonance, Series A* **1995**, *115*, 260-264.
- (809)Lin, C.-F.; Yang, J.-S.; Chang, C.-Y.; Kuo, S.-C.; Lee, M.-R.; Huang, L.-J. *Biorg. Med. Chem.* **2005**, *13*, 1537-1544.
- (810)Gregg, D.C.; Blood, C.A. *The Journal of Organic Chemistry* **1951**, *16*, 1255-1258.
- (811)Matsushima, R.; Kishimoto, T.; Suzuki, M.; Morioka, M.; Mizuno, H. *Bull. Chem. Soc. Jpn.* **1980**, *53*, 2938-2942.

- (812)Roethlisberger, A. *Helv. Chim. Acta* **1925**, *8*, 112-117.
- (813)Kagawa, H.; Takahashi, T.; Uno, M.; Ohta, S.; Harigaya, Y. *Chem. Pharm. Bull. (Tokyo)* **2004**, *52*, 953-956.
- (814)Detsi, A.; Majdalani, M.; Kontogiorgis, C.A.; Hadjipavlou-Litina, D.; Kefalas, P. *Bioorg. Med. Chem.* **2009**, *17*, 8073-8085.
- (815)Jung, S.H.; Park, S.Y.; Kim-Pak, Y.; Lee, H.K.; Park, K.S.; Shin, K.H.; Ohuchi, K.; Shin, H.K.; Keum, S.R.; Lim, S.S. *Chem. Pharm. Bull. (Tokyo)* **2006**, *54*, 368-371.
- (816)Colescott, R.L.; Herr, R.R.; Dailey, J.P. *J. Am. Chem. Soc.* **1957**, *79*, 4232-4235.
- (817)Nishikawa, M.; Inaba, Y.; Furukawa, M. *Chem. Pharm. Bull. (Tokyo)* **1983**, *31*, 1374-1377.
- (818)Soai, K.; Ookawa, A.; Kato, K. *Bull. Chem. Soc. Jpn.* **1982**, *55*, 1671-1672.
- (819)Freiman, A.; Sugden, S. *Journal of the Chemical Society (Resumed)* **1928**, 263-269.
- (820)Shimao, I.; Fujimori, K.; Oae, S. *Bull. Chem. Soc. Jpn.* **1982**, *55*, 1538-1542.